DESIGN AND APPLICATION OF BISPHOSPHITE LIGANDS WITH A DISTAL REGULATION SITE FOR ASYMMETRIC CATALYSIS

Laura Rovira González

Laura Rovira González

Design and Application of Bisphosphite Ligands with a Distal Regulation Site for Asymmetric Catalysis

Doctoral Thesis

Supervised by Prof. Dr. Anton Vidal i Ferran

Institute of Chemical Research of Catalonia (ICIQ)

UNIVERSITAT ROVIRA I VIRGILI

Tarragona

2016

Institut Català d'Investigació Química

UNIVERSITAT ROVIRA I VIRGILI

DEPARTAMENT DE QUIMICA ANALITICA I QUIMICA ORGANICA

C/ Marcel.lí Domingo s/n
Campus Sescelades
43007 Tarragona
Tel. 34 977 55 97 69
Fax 34 977 55 84 46
e-mail: secqaqo@urv.net

Prof. Dr. Anton Vidal i Ferran, Group leader of the Institute of Chemical Research of Catalonia (ICIQ) and Research Professor of the Catalan Institution for Research and Advanced Studies (ICREA),

CERTIFIED that the present research work entitled "Design and Application of Bisphosphite Ligands with a Distal Regulation Site for Asymmetric Catalysis", that Laura Rovira González presented to obtain the PhD degree in Chemistry, has been carried out under his supervision, in the corresponding research group at the Institute of Chemical Research of Catalonia (ICIQ).

Tarragona 17 June 2016

Prof. Dr. Anton Vidal i Ferran

Als meus pares, i a Salva

Agraïments

Fa tres anys i un poc més de mig que vaig fer les maletes, unes maletes plenes d'il·lusió i metes perseguint un somni, que a dia de hui ja és una realitat. En tot aquest temps de formació, on hi ha hagut dies satisfactoris i altres no tant, a la fi t´adones que tot l´esforç es veu reflectit. Pares i mires enrere i veus tot el camí recorregut i ara, en quatre línies, no pots expressar tot el que has anat experimentant en tot aquest temps. Així que intentaré fer un resum.

En primer lloc vull donar les gràcies al Prof. Anton Vidal, per donar-me l´oportunitat de fer la tesi en aquest grup i aquest gran institut que es l´ICIQ. Gràcies per confiar en mi, pel temps que m´has dedicat, per les explicacions, pels consells, per la paciència que has tingut, per tot el que m´has ensenyat i per tota l´ajuda que m´has donat en tots aquests anys, moltes gràcies.

Gràcies també a totes les unitats de suport (RMN, CromTAE, CRTU, Masses, Espectroscòpia, Raigs-X) per ajudar-me amb tots els experiments durant la tesi. Especialment, vull agrair a Eddy per les mesures dels cristalls, i a Jordi Benet per aconsellar-me i guiar-me amb el capítol de les sals de BArF.

I want to say thank to all my old lunch mates: Aurelio, John, and Vijay. In their funny and great company, I had a nice relief of my hard time at the beginning of my incorporation. To my lab neighbor, Sam, with his constant visits with a big smile, he was always welcome. Thank you very much for your help and friendship.

Agradecer a todo mi grupo: a Paula per tota la seva ajuda en temes burocràtics, a Nacho por abrirme el camino al mundo supramolecular, a Héctor por todas sus explicaciones y ayuda desde el primer día, a José Luis por sus explicaciones, ayuda y consejos de moda, a Mónica por sus consejos y gran ayuda en todo lo que ha estado a su alcance, a Bala for being my first lab mate, and after a cup of water, my confidant, my trustworthy Indian friend and for showing me his culture, a Joan per les seues correccions detallades, a Lucas per la seva ajuda amb l'anglès i les seues correccions amb "pilot roig" per tot arreu, a los recién llegados Rajesh, Alicia, Núria, y a mis ex-compañeros de vitrina: Alaric i Dominik. A todos vosotros os quiero dar las gracias por ser grandes compañeros, por ayudarme en todo, por enseñarme algo nuevo, por vuestra paciencia en mis momentos de agobio, por las correcciones al milímetro, por tantas explicaciones y discusiones, por vuestras risas y momentos inolvidables en el laboratorio y fuera de él. Formáis el mejor equipo, de todos vosotros he aprendido tanto a nivel personal como profesional.

No quiero olvidarme de Cris, compañera de comidas, quien junto con Mónica también compartió esas cenas de terapia, días de diversión hasta la madrugada, fiestas de Santa Tecla, baños de agua, sol y bronceador que hicieron más llevaderos los días de química. Gracias a todos por formar parte de esta etapa de mi vida.

No vull oblidar-me de tots els meus, amigues i amics, sempre amb paraules d'ànim. A Meryt per ajudar-me a plasmar la idea en la portada i a José Luis per editar el lligand en 3D. Vull agrair també a Sara Goberna, la meua amiga i companya de facultat, per ella el meu descobriment del ICIQ. A la meva família al complet, germà/nes, nebots/des i família política pel seu afecte i recolzament incondicional, en especial a la meua neboda Paula, tot un exemple de superació dia a dia i valentia davant la vida.

Gran menció la que he de fer al meus pares, sempre amb mi, sempre constants per inculcar-me els valors, per l´educació que m'han donat, pel seu esforç, afecte i confiança. Tot el que sóc es gràcies a ells i sense ells no hagués sigut possible arribar fins on estic.

Deixem per el final, i no per ser menys important a Salva, el meu company de vida, la meva mitat. Sense el teu continu recolzament, les teues paraules sempre positives, la teua ajuda constant, el teu recolzament en totes i cada una de les meves decisions, per estar ací sempre sense estar-ho i perquè la vida al teu costat serà meravellosa, mil GRÀCIES!

Moltes gràcies a TOTS els que m'haveu ajudat a fer possible aquest somni!

El treball realitzat a la present tesi doctoral ha sigut possible gràcies al finançament rebut per l´Institut Català d´Investigació Química (ICIQ) amb la beca pre-doctoral amb referència ICIQ-01/13 i s´ha desenvolupat en el marc dels projectes del MINECO amb referències CTQ 2011-28512/BQU, CTQ 2014-60256-P i Excel·lència Severo Ochoa 2014-2018 SEV-2013-0319.

UNIVERSITAT ROVIRA I VIRGILI

List of Publications

Some of the results presented in this thesis have already been published:

- **Asymmetric Hydroformylation of Heterocyclic Olefins Mediated by Supramolecularly Regulated Rhodium-Bisphosphite Complexes**.
  Laura Rovira, Mónica Vaquero and Anton Vidal-Ferran, *J.Org.Chem*. **2015**, *80*, 10397−10403.
- **Supramoleculary regulated Ligands for Asymmetric Hydroformylations and Hydrogenations.**
  Anton Vidal-Ferran, Ignasi Mon, Antonio Bauzá, Antonio Frontera and Laura Rovira,
  Chem. Eur. J. **2015**, *21*, 11417−11426.
- **Palladium-Based Supramolecularly Regulated Catalyst for Asymmetric Allylic Substitutions.**
  Laura Rovira, Héctor Fernandez-Pérez and Anton Vidal-Ferran, *Organometallics* **2016**, *35*, 528−533.

Furthermore two manuscripts are under preparation. First, the report on supramolecularly fine-regulated enantioselective catalysts presented in Chapter 1, which will be submitted as a review in due time. Secondly, the discussion on the solid state structure of alkali metal BArF salts presented in Chapter 4, which will be submitted as a research article in a suitable journal in due time.

Acronyms and Abbreviations

In the present thesis the abbreviations and acronyms most commonly used in organic chemistry have been used, according to the recommendations of the ACS "Guidelines for authors" (http://pubs.acs.org/paragonplus/submission/joceah/joceah_authguide.pdf).

AAS	Asymmetric allylic substitution
acac	Acetylacetonate
ACN	Acetonitrile
AHF	Asymmetric hydroformylation
API	Active pharmaceutical ingredient
BArF	Tetra[3,5-bis(trifluoromethyl)phenyl]borate
Conv.	Conversion
DCM	Dichloromethane
ee	Enantiomeric excess
equiv.	Equivalents
EtOAc	Ethyl acetate
ESI	Electrospray ionization
FID	Flame ionization detector
GC	Gas chromatography
HMBC	Heteronuclear multiple-bond correlation spectroscopy
HPLC	High performance liquid chromatography
IPA	Isopropanol
IR	Infra-red
nbd	norbornadiene
n.d	Not determined
NMR	Nuclear magnetic resonance
ORTEP	Oak ridge thermal ellipsoid plot program
rt	Room temperature
SPS	Solvent purification system
THF	Tetrahydrofurane
t_R	Retention time
UV-vis	Ultraviolet-visible

Table of Contents

Chapter 1

Introduction:

Supramolecularly Fine-Regulated Enantioselective Catalysts

Chapter 1.

Chapter 1

Introduction

Supramolecularly Fine-Regulated Enantioselective Catalysts

Laura Rovira[†], and Anton Vidal-Ferran[†‡*]

[†]Institute of Chemical Research of Catalonia (ICIQ) & The Barcelona Institute of Science and Technology, Avgda. Països Catalans 16, 43007 Tarragona, Spain.

[‡]Catalan Institution for Research and Advanced Studies (ICREA), Passeig Lluís Companys 23, 08010 Barcelona, Spain.

1.1. Abstract

The use of supramolecular interactions in catalysis has undergone a major growth in the last decade and has contributed to the major advances achieved in the field of enantioselective catalysis. Amongst the approaches involving use of supramolecular interactions in enantioselective catalysis, this manuscript highlights different supramolecular strategies to generate a set of enantiopure ligands (or enantioselective catalysts) that retain the majority of the backbone's structural features, yet at the same time incorporate subtle changes at its active site that depend on the structural characteristics of the regulation agent (RA) employed.

1.2. Introduction

Enantioselective catalysis enables unique and selective pathways for the conversion of simple compounds into enantiomerically pure complex molecules, often with significant advantages over non-catalytic methods. It has evolved greatly since the early 1970s to now encompass nearly any transformation subject to three-dimensional bias.[1] The critical step in most enantioselective processes is the assembly of a supramolecular system around the catalytic site. This supramolecular system involves the substrate, the metal precursor, if present, and an enantiopure molecule (the *chiral ligand*). In metal-mediated transformations, the metal center provides a low-energy reaction pathway that enables catalysis, whereas the enantiomerically pure ligand activates and creates an asymmetric environment around the metal ultimately enabling preferential recognition of one of the enantiotopic elements in the prochiral substrate (the source of enantioselectivity). Albeit in metal-mediated asymmetric transformations the metal center is responsible for providing a low energy reaction pathway, whereas the chiral ligand is at the origin of the symmetry-breaking that provides the enantiomeric enrichment, in organocatalysis, these two roles are played by an enantiopure organic molecule.[2]

The first chiral ligands that were employed in enantioselective catalysis mostly derived from the "*chiral pool*".[3] The practitioners in enantioselective catalysis soon realized that because of the limited structural diversity among the ligands derived from natural products, it was unlikely that they could provide a satisfactory response to all conceivable selectivity demands in catalysis (reactions, substrates, reagents, etc.). Thus, researchers soon realized that asymmetric synthesis had to be harnessed to broaden the repertoire of ligand scaffolds, to incorporate all types of stereogenic elements in the ligand, and to functionalize ligands with a myriad of functional groups that bind the desired metal center (in transition metal-based transformations) or interact with the substrates/reagents (in organocatalyzed processes). Not surprisingly, enantiopure C–, N–, O–, P– and S–containing ligands of synthetic origin have enabled major advances in enantioselective catalysis.[4]

The use of supramolecular interactions in catalysis has undergone a major growth in the last decade and has also contributed to the major advances achieved in the field of enantioselective catalysis. Beyond the situations in which supramolecular interactions do exclusively participate in the catalytic event,[5] the use of supramolecular chemistry in enantioselective catalysis can be categorized as follows:

First and foremost, supramolecular interactions have been widely used in the construction of the backbone of the chiral ligand *via* attachment of suitably designed building blocks by non-covalent and metal-ligand interactions. The building blocks contain the binding groups required for the desired catalysis as well as the motifs necessary for the supramolecular assembly. This synthetic methodology has enabled the synthesis of libraries of structurally diverse chiral ligands or catalysts with greater ease than for standard covalent chemistry. The use of supramolecular interactions for the construction of ligands for enantioselective catalysis, or catalysts themselves, has been widely reviewed[6] and is outside the scope of this text.

Second, the use of supramolecular interactions in enantioselective catalysis has also been exploited by placing in the ligand or catalyst well-designed functional groups capable of supramolecularly interacting with the substrate. Substrate-, chemo-, diastereo- and/or enantio-selectivities have been dramatically improved with this strategy, which relies on the precise positioning of the substrate relative to the catalytic site. Reported examples encompass both transition-metal or metal-free catalyzed enantioselective transformations and will not be discussed in this text, as these have been recently reviewed.[7]

Encapsulation of the catalytic species in a molecular container constitutes the third supramolecular strategy that has been applied in catalysis. Amongst other advantages, the rate enhancement due to an increase in the effective concentration of the reagents within a confined space, the achievement of unusual selectivity within the molecular container or the stabilization within the cavity of otherwise unstable molecules have been achieved by encapsulating the catalytic system. Many of these applications refer to achiral transformations and examples of enantioselective transformations within a confined space are scarce in the literature. This topic has been object of recent reviews and is also outside the scope of this text.[8]

The fourth and last supramolecular strategy that has been implemented in enantioselective catalysis has sought to override one of the intrinsic limitations of enantioselective catalysts: their lack of generality. It is well known for the practitioners of the field that structural changes to the substrate(s) and/or reagent(s) often translate to a loss of enantioselectivity. Early strategies to improve the generality of a catalyst were based on standard covalent chemistry. *Modular ligand design* and *ligand tuning*[9] have been employed to develop efficient catalytic systems for diverse substrates/reagents in a given transformation. Libraries of structurally related ligands have also been assembled through parallel synthesis[10] and subsequently assessed by automated high-throughput screening to rapidly identify high-performing catalysts for a specific transformation and substrate.[10,11] With the aim of reducing the synthetic efforts associated with the above mentioned strategies, supramolecular chemistry has also been harnessed to produce libraries of enantioselective catalysts, whose members preserve the main structural characteristics of the whole set but also incorporate subtle geometrical differences at the catalytic site. Hence, the members of these libraries of related catalysts are capable of geometric adaptation to the requirements of a given substrate for high enantioselectivity.

Two strategies have been developed to achieve these goals:

"Supramolecular regulation onto an already formed enantioselective catalysts"

This approach resembles allosteric modulation or "*allosterism*", which is one of the most exquisite mechanisms of action in enzymic catalysis in Nature.[12] Allosteric modulation of a biocatalyst refers to modification of its active site upon binding of an effector molecule at a distinct site on it (known as the *allosteric site* or *regulation site*). Supramolecularly fine-regulated enantioselective catalysts belonging to this category possess a catalytic site with a well-defined three-dimensional structure suitable for enantioselective catalysis and a distal regulation site containing a supramolecular motif capable of interacting with a regulation agent (RA). In this way, the members of the library of enantioselective catalysts arising upon the binding of an array of geometrically diverse RAs to the regulation site preserve most of the structural characteristics but also incorporate structural peculiarities that depend on the size and shape of the RA employed.

"Supramolecular regulation onto a pro-chiral catalysts"

The principle of this approach is similar to that summarized above with one crucial exception. The three-dimensional structure of the catalytic site is not well-defined in the absence of the regulation agent. Upon addition of an enantiopure regulation agent, chirality is created in the catalytic site and the geometry of the catalytic site also depends on the size and shape of the RA employed.

It should be recalled at this point that this section focus only on the progress in developing supramolecular catalysts that fall within the two above mentioned categories (supramolecular regulation of enantioselective catalysts that implies major alterations of the principal structural features of the catalyst has been object of recent reviews[13] and is outside the scope of this text). Furthermore, it should be noted that this section highlights published pieces of work only when the authors demonstrate the regulation ability of a set of RAs onto an array of substrates. Examples describing the use of only one external molecule for the whole array of substrates have not been mentioned herein, as the authors of the present section have considered that these examples refer to the construction of the catalyst[13] and not to the regulation effects induced by the external molecule. Analogously, examples describing an array of external molecules or RAs for only one substrate have not been highlighted either.

1.3. Discussion

The discussion is divided into two sections corresponding to the two different strategies that have been already mentioned.

1.3.1. Supramolecular regulation onto an already formed enantioselective catalysts

In this strategy, regulation consists of the modification of a catalytic site by interaction of an external unit (regulation agent; RA) with a distinct specific regulation site. The following discussion is divided in different sections corresponding to the different supramolecular motifs that have been employed as regulation sites. Examples on fine-regulated enantioselective catalysts that share the same supramolecular motif are then presented in chronological order of publication.

1.3.1.1. Catalytic systems regulated by interactions of a regulation agent with (aza-)crown-ether motifs

Cyclic crown-ethers and their nitrogenated analogues form very stable complexes with charged species (*i.e.* metal ions, halide anions, carboxylates, etc.).[14] Furthermore, with the possibility to easily vary the crown-ether size, shape, and topology together with well-established synthetic strategies for their preparation, crown-ethers have become popular supramolecular motifs.[14] Ito and coworkers[15] pioneered the field of supramolecularly fine-regulated enantioselective catalysts for asymmetric allylic substitutions (AASs) incorporating an aza-crown-ether motif as a regulation site in their bisphosphine ligand design. The underlying principle in the design of the catalyst consisted in introducing a secondary interaction[16] between the reacting nucleophile (enolates generated from **S1** or **S2** by using alkali metal salts as bases) and the aza-crown-ether motif. It was envisaged that the enolate and the anionic carbon of the enolate would form an inclusion complex with the aza-crown-ether. In doing so, it was expected that the reacting nucleophile would be placed in close proximity to the allyl group bound to the palladium center with an overall improvement in the reaction rate as well as in the stereocontrol of the reaction by reducing the degrees of freedom in the intervening transition states (TSs). Reactions of the enolates derived from **S1** or **S2** with allyl acetate were carried out in the presence of *in situ* formed palladium catalyst (equimolar amounts of $Pd_2(dba)_3{\cdot}CHCl_3$ and the corresponding ligand) and an array of alkali metal fluorides (*i.e.* KF, RbF or CsF) as bases. The authors used an array of bases, as they considered that the size of the cation could have an influence in the relative arrangement of the attacking nucleophile and the allyl group: the possibility to modify the arrangement of reactants through supramolecular interactions constitutes the regulation mechanism in this catalytic system. After an optimization process, ligand **L1** was found to be the optimal one for high enantioselectivities in the AASs of allyl acetate with the nucleophiles derived from **S1** and **S2**. The authors also found that the combined use of RbF with ligand **L1** provided the highest conversions and enantioselectivities in both cases. The authors reported that the affinity between RbF and the aza-crown-ether motif in ligand **L1** was higher than those for KF and CsF. The better complementarity between RbF and the aza-crown-ether motif translated into more efficient regulation effects in terms of enantioselectivity

than those observed for KF (compare entries 2 with 1 for **S1** and 5 with 4 for **S2**, in the table in Figure 1) or CsF (compare entries 2, 3, 5 and 6 in the table in Figure 1).

a) Ligand structure

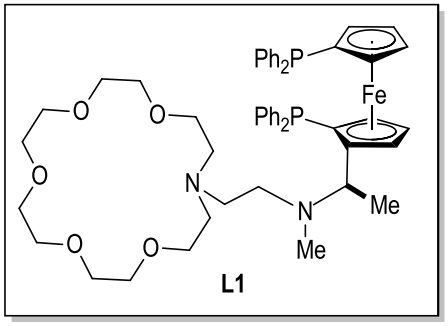

b) Allylic substitutions studied

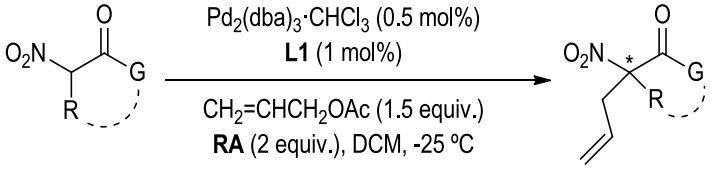

S1 G = –CH_2–, R = (–CH_2–)$_3$ **P1** G = –CH_2–, R = (–CH_2–)$_3$
S2 G = O-*t*Bu, R = Me **P2** G = O-*t*Bu, R = Me

c) Catalytic results

Entry	Carbanion derived from	RA	Yield (%)	ee (%) (config.)	Regulation effects in ee (%)[a]
1	**S1**	KF	33	25 (*R*)	–
2	**S1**	RbF	57	38 (*R*)	+13
3	**S1**	CsF	31	31 (*R*)	+6
4	**S2**	KF	95	51 (*R*)	+17
5	**S2**	RbF	95	60 (*R*)	+26
6	**S2**	CsF	91	34 (*R*)	–

[a] Calculated with respect to the lowest ee described.

Figure 1. Supramolecularly regulated catalyst for AAS from Ito *et al.*

More recently, Vidal-Ferran *et al.* reported the preparation of supramolecularly regulated bisphosphine ligand **L2**, which incorporates a crown-ether motif as a distal regulation site, and its use in rhodium-mediated asymmetric hydrogenations (AHs).[17] The authors envisaged that binding of a regulation agent to the crown-ether motif could modulate the catalyst performance by modifying the dihedral angle θ of the biaryl unit (see Figure 2 for a general representation of the regulation principle). The importance of the geometrical parameter θ in the performance of a transition-metal-based catalyst is well precedented in the literature, as it is associated to the natural bite-angle β of a ligand to the metal center (see Figure 2).[18] Rhodium complexes derived from enantiopure bisphosphine **L2** performed as efficient catalysts in the AH of **S3** in terms of activity, though enantioselectivities remained moderate (ee's ranging from 56 to 62% in favor of the (*S*)-configured hydrogenation product of **S3** and from 26 to 30% ee for the hydrogenation product of **S4**). As regards the AH of **S3** in the presence of a set of regulation agents, small but noticeable regulation effects on the enantioselectivity were observed. The maximal increment in the ee (up to 2% ee) was observed with the enantiomerically pure ammonium salt **RA1** as the regulation agent. On the contrary, the best enantioselectivity for **S4** was obtained in the absence of RA. These results indicate that even for the same combination of ligand and RA, the sign and magnitude of the regulation effects depend on the substrate. Though regulation effects were small in magnitude, the authors demonstrated that a library of bisphosphines could be easily generated with this strategy by supramolecularly modifying the catalytic site upon variation of the regulation agent.

1.3.1.2. Catalytic systems containing a polyether linear chain as the regulation site

Metallacrown-ethers are formed by combination of a metal precursor with a linear polyether chain containing functional groups at the α and ω positions capable of coordinating to the metal center. Fan *et al.*[19] identified metallacrown-ethers[20] as ideal scaffolds for developing supramolecularly regulated enantioselective catalysts: metallacrown derivatives simultaneously contain a plausible catalytic group (the metal center) and a supramolecular motif capable of acting as a regulation site (polyether motif) by binding a complementary external unit (RA). It should be noted at this point that, like cyclic crown-ethers, linear polyether groups are also capable of binding charged species such as metal ions, carboxylates, etc.[21] Fan *et al.* pioneered the use of supramolecularly regulated polyether-based ligands for rhodium-mediated asymmetric hydrogenations (AHs).[19] These authors reported the first example on the use of rhodium complexes derived from bisphosphite-polyether ligands, whose catalytic performance in terms of enantioselectivity in AH was enhanced by the addition of a RA. Fan *et al.* first investigated the effect of the linker length in the catalytic performance of the metallacrown-ether catalyst. Ligands with five, six or seven ethyleneoxy units in the polyether chain provided the best results in the absence of RA in terms of enantioselectivity (whilst the results for ligand **L3**, which contains six ethyleneoxy units, are indicated in Figure 3, the reader is referred to the original work[19] for the results of the other two ligands). The efficiency of the ligand with six ethyleneoxy units (**L3**) could be enhanced by addition of a RA (*i.e.* LiBArF, NaBArF or

KBArF; $[BArF]^-$ = $[B(3,5\text{-}(CF_3)_2C_6H_3)_4]^-$) capable of interacting with the polyether chain through ion-dipole interactions.

a) Ligand structure and regulation principle

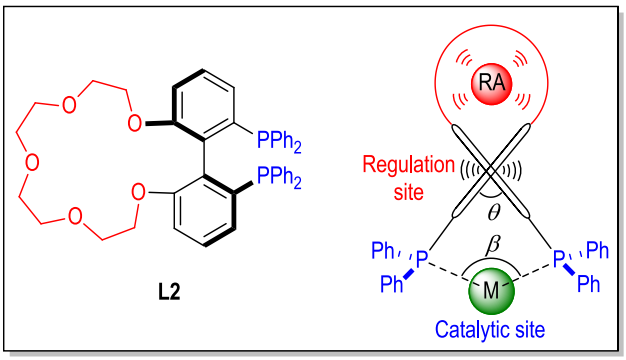

b) Structures of RAs

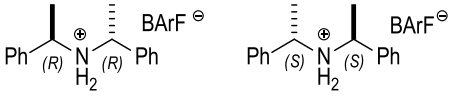

RA1 **RA2**

c) Asymmetric hydrogenations studied

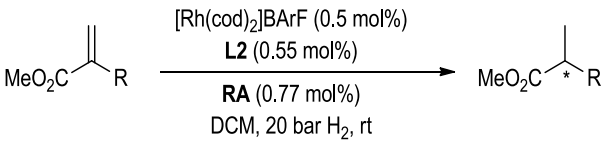

S3 R = CH_2CO_2Me
S4 R = NHAc

P3 R = CH_2CO_2Me
P4 R = NHAc

d) Catalytic results

Entry	Substrate	RA	ee (%) (config.)	Regulation effects in ee (%) [a]
1	**S3**	–	60 (*S*)	–
2	**S3**	NaBArF	56 (*S*)	–4
3	**S3**	CsBArF	60 (*S*)	0
4	**S3**	**RA1**	62 (*S*)	+2
5	**S3**	**RA2**	61 (*S*)	+1
6	**S4**	–	30 (*S*)	–
7	**S4**	NaBArF	27 (*S*)	–3
8	**S4**	CsBArF	26 (*S*)	–4

[a] Calculated for each substrate with respect to the experiment in absence of RA.

Figure 2. Supramolecularly regulated catalyst for AH from Vidal-Ferran *et al.*

a) Ligand structure

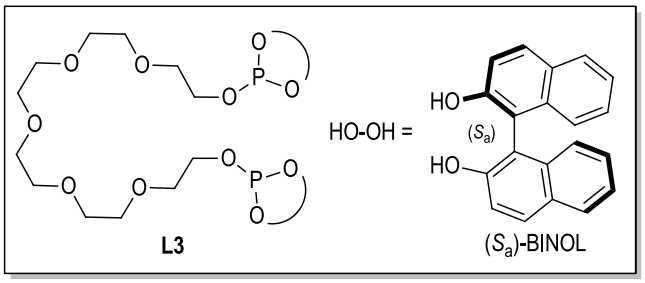

b) Asymmetric hydrogenations studied

S5 R = G–C_6H_4–
S4 R = H

P5 R = G–C_6H_4–
P4 R = H

c) Catalytic results

Entry	Substrate	RA	ee (%) (config.)	Regulation effects in ee (%) [a]
1	**S5**, G=H	–	84 (*R*)	–
2	**S5**, G=H	LiBArF	87 (*R*)	+3
3	**S5**, G=H	NaBArF	95 (*R*)	+11
4	**S5**, G=H	KBArF	94 (*R*)	+10
5	**S5**, G=4-F	–	83 (*R*)	–
6	**S5**, G=4-F	NaBArF	95 (*R*)	+12
7	**S5**, G=4-Cl	–	84 (*R*)	–
8	**S5**, G=4-Cl	NaBArF	96 (*R*)	+12
9	**S5**, G=3-Cl	–	82 (*R*)	–
10	**S5**, G=3-Cl	NaBArF	95 (*R*)	+13
11	**S5**, G=2-Cl	–	84 (*R*)	–
12	**S5**, G=2-Cl	NaBArF	94 (*R*)	+10
13	**S5**, G=4-Me	–	86 (*R*)	–
14	**S5**, G=4-Me	NaBArF	94 (*R*)	+8
15	**S5**, G=4-NO_2	–	79 (*R*)	–
16	**S5**, G=4-NO_2	NaBArF	96 (*R*)	+17
17	**S4**	–	93 (*R*)	–
18	**S4**	NaBArF	98 (*R*)	+5

[a] Calculated for each substrate with respect to the experiment in absence of RA.

Figure 3. Supramolecularly regulated catalyst for AH from Fan *et al.*

The highest increase in the enantioselectivity of the AH of model substrate **S5** (G=H) was achieved with NaBArF, up to 11% ee (see entry 3 in the table in Figure 3c). The authors suggested that the difference in the abilities of ligand **L3** to bind LiBArF, NaBArF or KBArF stayed at the origin in the regulation effects provoked by these polyether binders to the enantioselectivity of the reaction. A binding competition experiment between 18-crown-6 ether (*i.e.* 1,4,7,10,13,16-hexaoxacyclooctadecane), KBArF and **L3** helped determining the role of the alkali-metal salts in the regulation event. Due to the higher affinity of 18-crown-6 ether for KBArF with respect to **L3**, addition of 18-crown-6 ether to the catalytic system derived from **L3** and KBArF led to a similar enantioselectivity than that obtained in the absence of RA. Once the optimal catalytic system had been identified, a series of α-dehydroaminoacids was hydrogenated employing cationic rhodium complexes derived from **L3** as catalyst and NaBArF as RA. As shown in the table in Figure 3c, AHs proceeded efficiently with full conversions, excellent enantioselectivities (ee's ranged from 94 to 98% ee; see entries 5 to 18 in the table in Figure 3c) as well as with positive regulation effects that ranged from an increase of 5% to 17% in the ee when NaBArF was used as the RA.

More recently, Fan, He *et al.* have reported the preparation of supramolecularly regulated phosphine-phosphite ligand **L4** and its assessment in rhodium-mediated AHs.[22] The design principle was the same than for **L3**, though metallacrown-ether derivatives bearing different coordinating groups at the α and ω positions of the polyether group were unknown in the literature before the work of Fan, He *et. al*. The catalytic system that provided higher enantioselectivities in the AH of model α-arylenamide **S6** derived from ligand **L4**. The use of KBArF as RA provided the highest enhancements in enantioselectivity within all RAs assayed (ee enhancement up to 9% ee; see entry 4 in the table in Figure 4c for all RAs studied).

Fan, He *et al.* also described that the addition of KBArF had a rate accelerating effect on the AH, which indicated that the addition of alkali metal salts also improved the activity of the metallacrown catalyst.[22] The authors attributed the differences in regulation effects (or enhancements) on the ee of the hydrogenated product to the differences in match of the RAs (*i.e.* LiBArF, NaBArF, KBArF or CsBArF) to the metallacrown motif. A series of α-arylenamides (**S6** and **S7**) were hydrogenated employing the rhodium catalyst derived from **L4** and KBArF as the RA. In general terms, the AHs of *para*-substituted arylenamides proceeded with full conversions and high enantioselectivities (from 94 to 99% ee). Lower ee's were obtained for the *ortho*- and *meta*-substituted analogues, though considerable regulation effects (enhancements up to +6 % in the ee; see entry 17 in the table in Figure 4c) were observed for these substrates.

a) Ligand structure

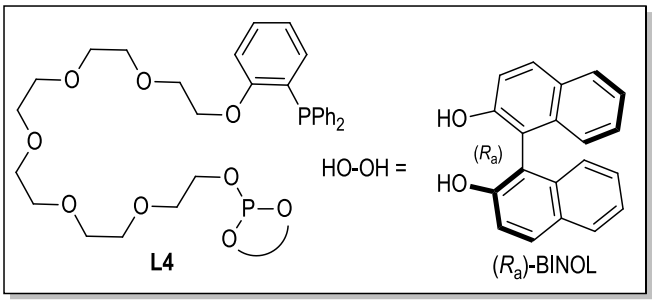

b) Asymmetric hydrogenations studied

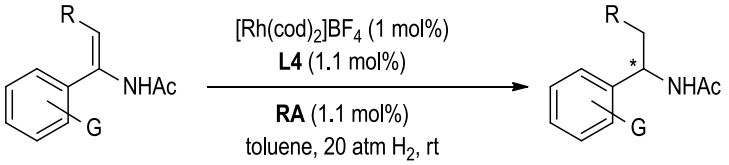

S6 R = H,
G = H, Me, F, CF_3, Cl, Br
S7 G = H, R = Me

P6 R = H,
G = H, Me, F, CF_3, Cl, Br
P7 G = H, R = Me

c) Catalytic results

Entry	Substrate	RA	ee (%)	Regulation effects in ee (%)[a]
1	**S6**, G = H	–	84	–
2	**S6**, G = H	LiBArF	89	+5
3	**S6**, G = H	NaBArF	91	+7
4	**S6**, G = H	KBArF	93	+9
5	**S6**, G = H	CsBArF	92	+8
6	**S6**, G = 4-Me	–	84	–
7	**S6**, G = 4-Me	KBArF	96	+12
8	**S6**, G = 4-F	–	85	–
9	**S6**, G = 4-F	KBArF	94	+9
10	**S6**, G = 4-CF_3	–	92	–
11	**S6**, G = 4-CF_3	KBArF	99	+7
12	**S6**, G = 4-Cl	–	94	–
13	**S6**, G = 4-Cl	KBArF	99	+5
14	**S6**, G = 4-Br	–	93	–
15	**S6**, G = 4-Br	KBArF	98	+5
16	**S6**, G = 3-Cl	–	81	–
17	**S6**, G = 3-Cl	KBArF	87	+6
18	**S6**, G = 2-Cl	–	66	–
19	**S6**, G = 2-Cl	KBArF	70	+4
20	**S7**	–	50	–
21	**S7**	KBArF	58	+8

[a] Calculated for each substrate with respect to the experiment in absence of RA.

Figure 4. Supramolecularly regulated phosphine-phosphite-derived catalysts for AH from Fan, He *et al.*

In between the publication dates of these two contributions on supramolecularly regulated metallacrown-based enantioselective catalysts from Fan and He *et al.*,[19,22] Vidal-Ferran *et al.* reported a first generation of supramolecularly regulated α,ω-bisphosphites for asymmetric hydroformylations (AHFs).[23] The design of the ligand was similar to that of **L3** but incorporated a conformationally labile [1,1'-biphenyl]-2,2'-diol motif in the regulation site. The supramolecularly regulated α,ω-bisphosphite was successfully applied in the AHF of terminal alkenes with remarkably high positive regulation effects in the enantioselectivity (increases of up to 62% ee for vinyl acetate).[23] Further optimization studies towards the optimal supramolecularly regulated ligand for this chemistry (*i.e.* optimal bisphosphite motif, optimal length of the polyether chain, necessity or not of having a conformationally labile [1,1'-biaryl]-2,2'-diol motif in the regulation site and nature of the anionic component of the RA) led to an improved supramolecularly regulated catalytic system for the AHF of terminal alkenes (see ligand **L5** in Figure 5).[24] These studies revealed that ligands with longer polyether chains led to lower conversions in the AHF of the chosen model substrate (*i.e.* vinyl acetate) and that phosphite groups derived from 3,3'-bis(trimethylsilyl)-[1,1'-binaphthalene]-2,2'-diol provided the highest ee's in the already mentioned transformation.[25] As regards the nature of the anionic component of the RA, the non-coordinating BArF anion provided higher branched to linear (b:l) ratios for the studied model substrate than those observed with other RAs containing the $[BF_4]^-$ or $[ClO_4]^-$ anionic components.[24] Furthermore, BArF salts were an attractive option, given their adequate solubility profile in solvents that are suitable for hydroformylations (*e.g.* toluene containing a small amount of THF). As a continuation of the catalytic studies, Vidal-Ferran *et al.* became interested in evaluating the design principle-namely, whether the addition of a RA in the reaction medium would affect the catalytic activity of the rhodium complexes derived from **L5**. The effects produced by different alkali metal and ammonium salts on the catalytic activity have been summarized in the table in Figure 5c. Of all the RAs tested for the AHF of vinyl acetate employing **L5**, RbBArF gave the best results: Full conversion, complete regioselectivity (> 99:1 in favor of the branched product) and perfect enantioselectivity (99% ee) were observed (see entry 4 in the table in Figure 5c). It should be noted that the addition RbBArF to the reaction mixture provoked the highest positive regulation effect in the enantioselectivity (enhancement of 64% in the ee). Interestingly, the use of KBArF or CsBArF rather than RbBArF also provided very high ee's (98 and 96% ee, respectively; see entries 3 and 5 in the table in Figure 5c). In contrast, when enantiomerically pure ammonium salts **RA1** and **RA2** were used, the activity of catalysts derived from **L5** worsened (see entries 6 and 7 in the table in Figure 5c).

For all the assays summarized in the table in Figure 5c, 1 mol% of catalyst (substrate-to-catalyst [S/C] ratio of 100:1) was used. However, the amount of rhodium catalyst derived from RbBArF•**L5** could be reduced to 0.1 mol% (S/C = 1000) without almost no decrease in the catalytic activity (99% conv., b:l ratio > 99:1, and 97% ee in favor of (*S*)-**P8**).[25] Furthermore, addition of RbBArF enhanced the catalytic activity of the catalyst as evidenced by *ca.* four-fold increase in the reaction rate (TOF value with a S/C ratio = 1000 at 50% conversion (*i.e.* $TOF_{½}$) = 40 h^{-1} in the absence of RbBArF; $TOF_{½}$ = 177 h^{-1} in the presence of RA).

As regards the AHF of a wider array of terminal alkenes, addition of RbBArF also provoked important enhancements in the ee's of the AHFs of substrates **S9**, **S10** and **S12** (entries 9, 11 and 15 in the table in Figure 5c) and also turned out be the ideal RA for these substrates. Unfortunately, the use of RAs led to lower regio- and enantio-selectivity for styrene (compare entries 12 and 13 in the table in Figure 5c).

With the aim of gaining insight into structural changes induced by the RA in the geometry of the catalytic site, computational studies on the geometry of the hydrido-dicarbonyl Rh(I) complexes derived from **L5** were performed. These computational studies revealed that the RA had an important effect in the P–Rh–P bond angle of the rhodium complexes (see Figure 6). The trend observed was that the size of the ionic radius in the RA cation correlated to the width of the P–Rh–P angle (from 113 º, when no RA is present, to *ca.* 122 º for K^+, Rb^+ and Cs^+). Most interestingly, a plot of the ee in the AHF of vinyl acetate as a function of the P–Rh–P bond angle revealed a maximum in the ee value around the P–Rh–P bond induced by RbBArF, which indicates that the significant increase in the enantiomeric excess resulted from adaptation of the P–Rh–P bond angle (see Figure 6).

Encouraged by the good levels of regulation and overall performance achieved with polyether-based ligands in AHF, the same research group shifted their attention to developing supramolecular ligands for AH.[24] After a ligand screening process, Vidal-Ferran *et al.* identified the rhodium(I) complexes derived from **L6** without using a RA (for substrate **S3** and **S5**; see entries 1 and 3 in the table of Figure 7c), or in combination with ammonium derivative **RA1** (for substrates **S4**, **S6** and **S13**; see entries 2, 4 and 5 in the table of Figure 7c) or with CsBArF (for substrate **S14**; see entry 6 in the table of Figure 7c), as efficient AH catalysts. As indicated in the table of Figure 7c, regulation effects in AH were minor (enhancements of up to 5% in the ee were observed), as ligand **L6** already provided very high enantioselectivities. However, the use of RAs served to slightly improve enantioselectivities by adapting the catalysts derived from **L6** to the geometry of the different substrates: enantioselectivity in the studied AHs could be maximized by the choice of whether or not to use a RA (and if so, employing **RA1** or CsBArF as the regulation agent).

a) Ligand structure

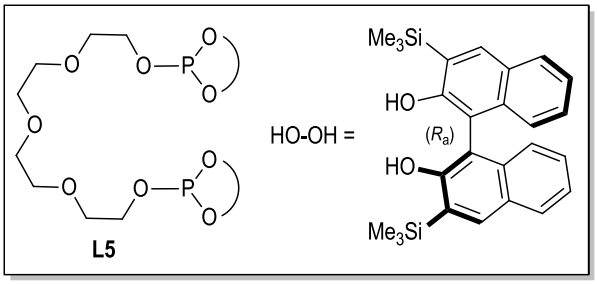

b) Asymmetric hydroformylations studied

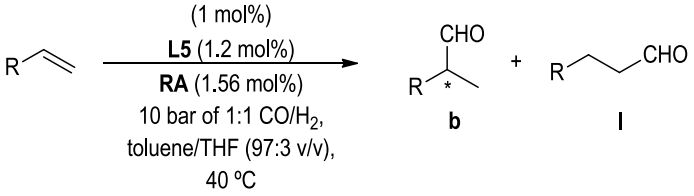

S8 R = OCOMe
S9 R = OCOEt
S10 R = OCOPh
S11 R = Ph
S12 R = CH_2OSiMe_3

P8 **P9**
P10 **P11**
P12 **P13**
P14 **P15**
P16 **P17**

c) Catalytic results

Entry	Substrate	RA	b:l ratio	ee (%) (config.)	Regulation effects in ee (%) [a]
1	**S8**	–	90:10	35 (*S*)	–
2	**S8**	NaBArF	>99:1	74 (*S*)	+39
3	**S8**	KBArF	>99:1	98 (*S*)	+63
4	**S8**	RbBArF	>99:1	99 (*S*)	+64
5	**S8**	CsBArF	>99:1	96 (*S*)	+61
6	**S8**	**RA1**	>99:1	40 (*S*)	+5
7	**S8**	**RA2**	>99:1	40 (*S*)	+5
8	**S9**	–	96:4	36 (*S*)	–
9	**S9**	RbBArF	>99:1	99 (*S*)	+63
10	**S10**	–	98:2	14 (*S*)	–
11	**S10**	RbBArF	>99:1	96 (*S*)	+82
12	**S11**	–	95:5	12 (*S*)	–
13	**S11**	RbBArF	80:20	5 (*S*)	–7
14	**S12**	–	59:41	7 (*S*)	–
15	**S12**	RbBArF	18:82	25 (*S*)	+18

[a] Calculated for each substrate with respect to the experiment in absence of RA.

Figure 5. Supramolecularly regulated catalyst for AHF from Vidal-Ferran *et al.*

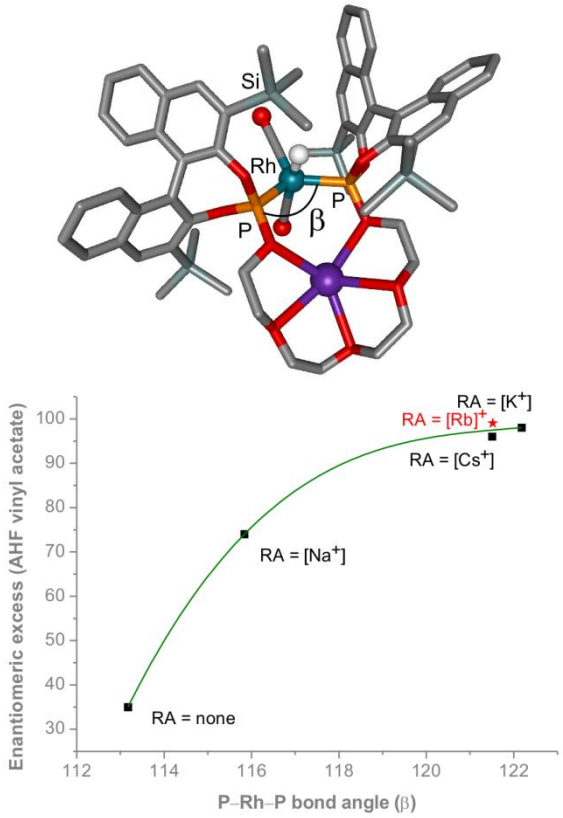

Figure 6. Rhodium-derived supramolecular complex and representation of the ee values *versus* calculated P–Rh–P bond angle value.

It has been described in this section, that combinations of regulation agents and polyether based-ligands have been used to supramolecularly regulate the outcome of AHs and AHFs. Positive increments in the regio- and/or enantio-selectivity for a given substrate in the aforementioned transformations have been achieved by the careful choice of whether or not to use an RA (and if so, which one). The achievements that have been summarized in this section demonstrate that libraries of enantiopure supramolecular ligands (or catalytic systems) have been easily prepared with this strategy. Furthermore, appropriated combinations of ligands plus the corresponding regulation agents have provided adaptive enantioselective catalysts to the specific geometry of the substrate of interest in a given transformation.

a) Ligand structure

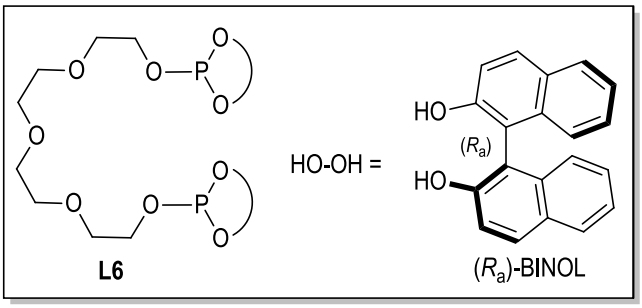

b) Asymmetric hydrogenations studied

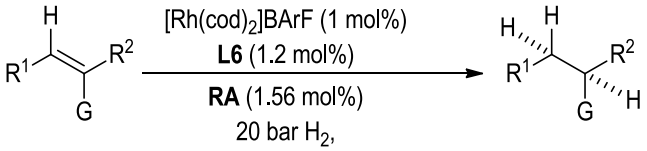

	R^1	R^2	G	
S3	H	COOMe	CH_2COOMe	**P3**
S4	H	COOMe	NHAc	**P4**
S5	Ph	COOMe	NHAc	**P5**
S6	H	Ph	NHAc	**P6**
S13	Ph	COOMe	CH_2NHAc	**P18**
S14	H	1-Naphth	NHAc	**P19**

c) Catalytic results

Entry	Substrate	RA	ee (%) (config.)	Regulation effects in ee (%) [a]
1	**S3**	–	97 (*R*) [b]	–
2	**S4**	**RA1**	96 (*S*)	+2
3	**S5**	–	92 (*S*) [b]	–
4	**S6**	**RA1**	93 (*S*)	+3
5	**S13**	**RA1**	95 (*S*)	+2
6	**S14**	CsBArF	78 (*R*)	+5

[a] Calculated for each substrate with respect to the experiment in absence of RA.
[b] The highest ee's were obtained in the absence of RA.

Figure 7. Supramolecularly regulated catalyst for AH from Vidal-Ferran *et al.*

1.3.1.3. Catalytic systems containing complementary hydrogen-bonding motifs

Clarke and co-workers designed a supramolecularly regulated enantioselective catalyst formed by complementary hydrogen bonding between a first unit, containing a substituted pyrrolidine ring responsible for enantioselective catalysis (see **L7** and **L8** in Figure 8a), and a second unit bearing an achiral additive to influence the steric environment at the catalytic site (see the 1-(1*H*-imidazol-2-yl)urea-containing structures **RA3** and **RA4** in Figure 8a). Furthermore, this example is highly interesting in illustrating that supramolecular regulation strategies are not only limited to transition-metal catalyzed reactions but also to organocatalyzed processes, such as the asymmetric Michael addition of ketones to nitroalkenes.[26]

Clarke *et al.* envisaged that amidonaphtyridine motifs (present in structures **L7** and **L8**) and 3-substituted 1-(1*H*-imidazol-2-yl)urea structures (present in **RA3** and **RA4**) would be highly complementary recognition motifs through hydrogen-bonding interactions. Thus, they were chosen as the complementary units for achieving precise self-assembly by hydrogen bonding towards the target supramolecular catalysts (Figure 8a).[26] Clarke *et al.* observed that supramolecular assemblies arising from the combination of ligands **L7** or **L8** and regulation agents **RA3** and **RA4** were more efficient in mediating asymmetric Michael reactions than catalysts **L7** or **L8** alone (compare entries 1 with 2 and 5 with 6 in the table of Figure 8c). For asymmetric Michael additions of cyclohexanone **S15** to nitroalkene **S17**, an important enhancement in the diastereoselectivity (from a 26:1 to a 65:1 ratio in favor of the *syn* diastereoisomer) and enantioselectivity (from 6 to 68% ee) of the reaction was observed when the hydrogen-bonding complementary regulation agent **RA3** was used. Interestingly, a slightly modified regulation agent (the 4-substituted 1-(1*H*-imidazol-2-yl)urea **RA4**) was used for achieving the highest diastereo- and enantio-selectivties in the asymmetric Michael additions of cyclohexanone **S15** to (*E*)-(2-nitrovinyl)benzenes with substituents at the phenyl ring (**S18** and **S19**; see entries 3 and 4 in the table of Figure 8c). As regards asymmetric Michael additions of the acyclic aliphatic aldehyde **S16** to nitroalkene **S17**, the combination of a new amino-containing unit (**(*S*)-L8**), with respect to the original pyrrolidine-containing one (**(*R*)-L7**), and the regulation agent **RA3** was required (see structures in Figure 8a). Acceptable diastereoselectivity levels were obtained with the catalyst derived from the aforementioned self-complementary units for hydrogen bonding. Unfortunately, the final product was obtained as a racemic mixture (see entries 5 and 6 in the table of Figure 8c).

a) Catalyst structure

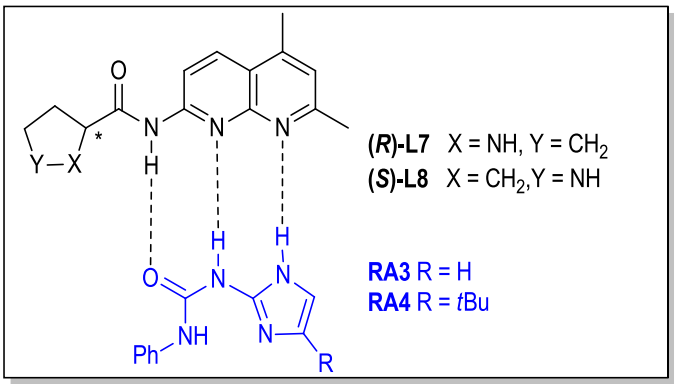

b) Asymmetric Michael reactions studied

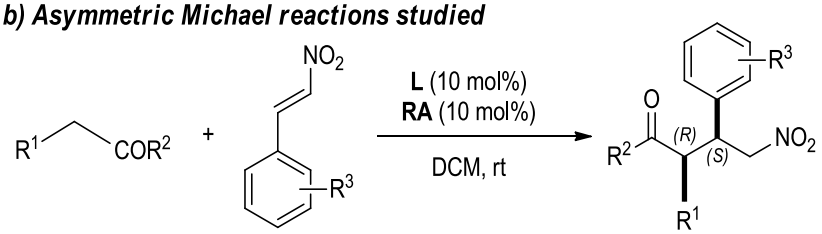

(major (*syn*) stereoisomer formed)

S15 R^1, R^2 = $(–CH_2–)_4$
S16 R^1 = *n*Bu, R^2 = H
S17 R^3 = H
S18 R^3 = *p*-MeO
S19 R^3 = *m*-NO_2
P20 R^1, R^2 = $(–CH_2–)_4$, R^3 = H
P21 R^1, R^2 = $(–CH_2–)_4$, R^3 = *p*-MeO
P22 R^1, R^2 = $(–CH_2–)_4$, R^3 = *m*-NO_2
P23 R^1 = *n*Bu, R^2 = H, R^3 = H

c) Catalytic results

Entry	Substrates	Catalyst	Conv. (%)	dr[a]	ee (%) (config.)[b]	Regulation effects in ee (%)[c]
1	**S15, S17**	**(*R*)-L7**, –	87	26:1	6 (*R*,*S*)	–
2	**S15, S17**	**(*R*)-L7, RA3**	99	65:1	68 (*R*,*S*)	+62
3	**S15, S18**	**(*R*)-L7, RA4**	47	36:1	74 (*R*,*S*)	–
4	**S15, S19**	**(*R*)-L7, RA4**	41	7:1	81 (*R*,*S*)	–
5	**S16, S17**	**(*S*)-L8**, –	6	n.d.	n.d.	–
6	**S16, S17**	**(*S*)-L8, RA3**	95	12:1	*rac*	n.d.

[a] *syn*:*anti* ratio. [b] ee of the *syn* product. The first stereochemical descriptor refers to the carbon alpha to the C=O group and the second to the aryl-substituted one. [c] Calculated for each substrate with respect to the experiment in absence of RA.

Figure 8. Supramolecularly regulated catalyst for asymmetric Michael additions from Clarke *et al.*

1.3.2. Supramolecular regulation onto a pro-chiral catalysts

The principle of this approach is similar to that detailed in the previous section: a regulation agent is employed to modify the geometry of the catalytic site. However, the three-dimensional structure of the catalytic site is not well defined in the absence of the regulation agent and, upon addition of an enantiopure regulation agent, chirogenesis processes mediated by the RA lead to an asymmetric supramolecular assembly with a well-defined three-dimensional structure.

Reek *et al.* have published the only example of this elegant approach for generating libraries of enantioselective supramolecular catalysts.[27] These authors have shown that the interaction of an enantiopure regulation agent (called "*cofactor"* by the authors) with an achiral bisphosphine rhodium complex, which was equipped with a binding site for the recognition of the regulation agent, efficiently led to the formation of an asymmetric supramolecular assembly that was used as pre-catalyst in rhodium-mediated asymmetric hydrogenations (AHs). First studies aimed to identify a suitable strategy that would facilitate the straightforward preparation of libraries of enantioselective catalysts from ligand **L9** (see Figure 9a). This ligand contained the diamidodiindolylmethane motif (as the binding site for the regulation agent) and phosphine binding groups for the generation of rhodium catalysts for AH. Reek *et al.* demonstrated that cationic ligand-rhodium complexes [Rh(nbd)(**L9**)]$^+$ were straightforwardly formed by mixing stoichiometric amounts of ligand **L9** and the standard cationic rhodium precursor for hydrogenations (*i.e.* $[Rh(nbd)_2]BF_4$).[27] Interestingly, the X-ray structure of the resulting complexes $[Rh(nbd)(\mathbf{L9})]BF_4$ showed that in the solid state the $[BF_4]^-$ anion was bound to the ligand's diamidodiindolylmethane motif, which acted as an efficient receptor for this anion. Binding studies in solution demonstrated that the $[BF_4]^-$ anion was easily displaced by regulation agents (or *cofactors*) with carboxylate groups, as these proved to have a much higher affinity for the diamidodiindolylmethane motif than did the $[BF_4]^-$ anion. The authors exploited the high affinity of carboxylate anions to the diamidodiindolylmethane motif in ligand **L9** ($K > 10^5$ M^{-1} in CD_2Cl_2) and the wide availability of enantiomerically pure compounds containing a carboxylate group to easily generate libraries of supramolecular enantioselective catalysts with this strategy.[27] Detailed NMR studies confirmed chirogenesis in the supramolecular binding event (*i.e.* chirality transfer from the regulation agent to the carbon backbone of the rhodium complex through supramolecular interactions).

Subsequent studies aimed to identify the optimal regulation agent that mediated the highest enantioselectivity in the AH of functionalized alkenes. The authors studied[27] a wide variety of enantiopure carboxylate-containing derivatives in the AH of α-acylaminoacrylate **S4** (see entry 1 in the table in Figure 9d), with amino acid derivatives as RAs providing the best results in terms of enantioselectivity. Reek *et al.* identified the substituents at the nitrogen group of the amino acid derivative as the structural motif of the regulation agent that provoked the highest effects on the enantioselectivity of the hydrogenation, whilst variation of the side chain of the amino acid derivative had a smaller influence.[27] The valine-derived regulation agent **RA5**, which incorporates a *tert*-butyl thiourea group, was identified after an iterative deconvolution catalyst screening strategy as the optimal RA that provided the highest enantioselectivities in the AH of α-acylaminoacrylate **S4** (full conversion, 98% ee; entry 1 in the table of Figure 9d). In an analogous manner, the same regulation agent mediated the hydrogenation of α-acylaminoacrylate derivative **S20**, arylenamide **S6**, itaconic acid derivative **S3** and 2-methylenepentanedioic acid derivative **S23** (ee's ranging from 39 to 91% ee; see entries 2, 3, 6, and 7 in the table of Figure 9d, respectively) with the highest enantioselectivities. Alternatively, pivaloyl valine derivative **RA6**, was the regulation agent of choice for the hydrogenation of dihydronaphthalenyl acetamides **S21** and **S22** (see entries 4 and 5 in the table of Figure 9d). In conclusion, Reek's most elegant approach for supramolecularly regulating the catalyst's activity and stereoselectivity demonstrates that efficient AH catalysts can be easily obtained by the optimal choice of an enantiomerically pure regulation agent and the achiral ligand **L9**.

a) Ligand structure

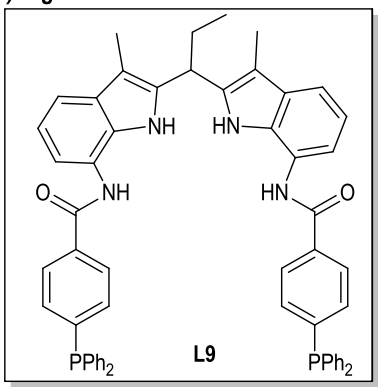

b) Structures of RA

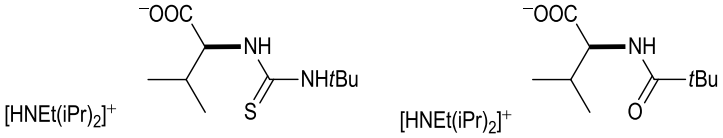

RA5 **RA6**

c) Asymmetric hydrogenations studied

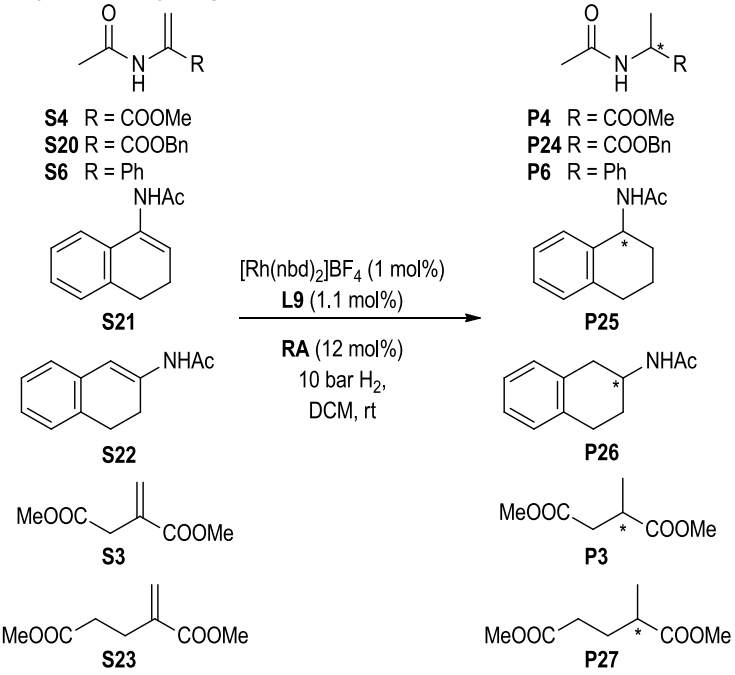

d) Catalytic results

Entry	Substrate	RA	Yield (%)	ee (%) (config.)
1	**S4**	**RA5**	93	98 (*R*)
2	**S20**	**RA5**	92	91[a]
3	**S6**	**RA5**	84	82[a]
4	**S21**	**RA6**	95	79[a]
5	**S22**	**RA6**	89	43[a]
6	**S3**	**RA5**	58	39[a]
7	**S23**	**RA5**	69	50[a]

[a] Configuration not provided

Figure 9. Supramolecularly regulated catalyst for AH from Reek *et al.*

1.4. Conclusions and outlook

This section highlights different supramolecular strategies to generate a set of enantioselective catalysts that retain the majority of the backbone's structural features yet at the same time incorporate subtle changes at their active site that depend on the structural characteristics of the external molecule (or regulation agent) that is employed. Two different categories of supramolecularly fine-regulated enantioselective catalytic systems have been developed.

The first type of catalytic systems possesses a catalytic site with a well-defined three-dimensional structure suitable for enantioselective catalysis and a distal regulation site containing a supramolecular motif capable of interacting with the regulation agent. The interaction of cyclic (aza)-crown-ether, metallacrown-ether and polyether supramolecular motifs with metal salts or ammonium derivatives have been exploited by a number of research groups for generating libraries of enantioselective catalysts that preserve most of the structural characteristics but also incorporate structural peculiarities at the active site that depend on the RA employed. The results summarized in this section for this first type of supramolecularly fine-regulated enantioselective catalysts demonstrate that the generated libraries of related catalysts are capable of geometric adaptation to the requirements of a given substrate for high enantioselectivity in asymmetric hydrogenations and hydroformylations on an array of structurally diverse substrates. This regulation concept on the active site of the enantioselective catalyst has not been restricted to transition-metal based transformations, such as those previously mentioned. Researchers have also developed supramolecularly regulated enantioselective organocatalysts for asymmetric Michael addition reactions. In this case, the regulation agent is attached to the unit that contains the catalytic site by a highly efficient and precise hydrogen-bonding-mediated assembly process.

The second type of supramolecularly fine-regulated catalytic systems is directly generated from a pro-chiral unit containing the catalytic site. The three-dimensional structure of the catalytic site is not well-defined in the absence of a regulation agent, and in this most elegant approach, addition of an enantiopure regulation agent triggers chirogenesis processes from the regulation agent to the carbon backbone containing the catalytic site. In this case, the authors demonstrate that highly efficient asymmetric hydrogenation catalysts could be obtained with unprecedented ease just by the optimal choice of an enantiopure regulation agent (or "*cofactor*" as referred to by the authors).

The approaches herein reported for fine-regulation of the activity of an enantioselective catalyst combine concepts from supramolecular and physical organic chemistry with traditional approaches from enantioselective catalysis. The potential for research and innovation is almost unlimited, with ample scope for development of practical applications. Thus, one can only imagine that the near future will witness new examples of successful application of fine-regulation strategies to new enantioselective catalysts for transformations of interest.

1.5. Objectives

As summarized in the previous sections of this chapter, linear polyether chains containing functional groups at the α and ω positions are capable of coordinating to metal centers. The corresponding metal complexes simultaneously contain a plausible catalytic group (the metal center) and a supramolecular motif capable of acting as a regulation site (polyether motif) by binding a complementary external unit (RA). It has been demonstrated by others and us that conformationally transformable α,ω-bisphosphites behave as supramolecularly regulated ligands in rhodium-mediated asymmetric hydrogenations (AHs) of functionalized alkenes and in the asymmetric hydroformylation (AHFs) of linear alkenes.

The conformationally transformable ligands already reported incorporate a wide range of regulation centers (purely linear polyether chains of variable length and the combination of polyether chains with conformationally labile [1,1'-biphenyl]-2,2'-diol groups as linkers). The enantioselective catalytic groups already reported for polyether-based ligands have been exclusively restricted to configurationally stable [1,1'-binaphthalene]-2,2'-diol-derived (or BINOL-derived) phosphite groups. In terms of the reported regulation agents (RA), alkali metal and ammonium salts have been employed in combination with polyether-based ligands.

No reports on the effects of additional stereogenic elements in the regulation site of the enantioselective catalysts had been published by the commencement of the research work presented in this Thesis. The catalytic properties of supramolecularly regulated bisphosphites ligands with enantiopure TADDOL-derived phosphite groups at the α and ω positions of the polyether chain were unknown [TADDOL = (2,2-dimethyl-1,3-dioxolane-4,5-diyl)bis(diphenylmethanol)]. Furthermore, supramolecularly regulated enantioselective catalysts incorporating a polyether-based regulation site had not been employed in the asymmetric hydroformylation (AHF) of cyclic alkenes and in palladium–mediated asymmetric allylic substitutions (AASs).

Therefore, the general aims of this thesis are:

- Design and development of supramolecularly regulated, polyether-based and enantiopure bisphosphite ligands containing an stereogenic axis in the regulation site. Preparation of supramolecular ligands with TADDOL-derived phosphite groups at the α and ω positions of the polyether chain.

- Evaluation of the catalytic properties of the newly developed and previously prepared supramolecularly regulated bisphosphite ligands in palladium–mediated asymmetric allylic substitutions (AAS's).

- Evaluation of the catalytic properties of the newly developed and previously prepared supramolecularly regulated bisphosphite ligands in the rhodium-mediated asymmetric hydroformylation (AHF) of cyclic alkenes.

- Study of the solid state structure of alkali metal BArF salts (BArF anion = $[B(3,5\text{-}(CF_3)_2C_6H_3)_4]^-$), since these derivatives have proved to be efficient regulation agents in asymmetric hydroformylations and hydrogenations.

1.6. References and notes

1) For general references on this topic, see for example: (a) *Catalytic Asymmetric Synthesis*; Ojima, I. Ed.; VCH Publishers: Cambridge, 1993. (b) *Comprehensive Asymmetric Catalysis*; 1st ed.; Jacobsen, E. N.; Pfaltz, A.; Yamamoto, H., Eds.; Springer-Verlag: Heidelberg, 1999; Vol. I-III. (c) Noyori, R. *Asymmetric Catalysis in Organic Synthesis*, John Wiley and Sons: New York, 1999. (d) Walsh, P. J.; Kozlowski, M. C.; *Fundamentals of Asymmetric Catalysis*, University Science Books, 2009. (e) *Comprehensive Chirality*; Carreira, E. M.; Yamamoto, H., Eds.; Elsevier Science: Oxford, 2012; Vol 1–9.

2) In biocatalysis these two roles are played by the biocatalyst (*i.e.* enzyme).

3) Chiral pool refers to the stock of readily available enantiopure natural products.

4) In *Privileged Chiral Ligands and Catalysts*; Zhou, Q.-L., Ed.; Wiley-VCH: Weinheim, Germany, 2011.

5) Any catalytic event involves supramolecular interactions, as the catalytic system recognizes substrates and reagents, and organizes them in a certain arrangement. Within this section, the concept supramolecular catalysis does not refer to those situations but is employed when the supramolecular interactions do not form part of the catalytic event.

6) See, for example: (a) Breit, B. *Angew. Chem., Int. Ed.* **2005**, *44*, 6816–6825. (b) Kraemer, R. *Angew. Chem., Int. Ed.* **2006**, *45*, 858–860. (c) Letondor, C.; Ward, T. R. *ChemBioChem* **2006**, *7*, 1845–1852. (d) Goudriaan, P. E.; van Leeuwen, P. W. N. M.; Birkholz, M.-N.; Reek, J. N. H. *Eur. J. Inorg. Chem.* **2008**, 2939–2958. (e) Boersma, A. J.; Megens, R. P.; Feringa, B. L.; Roelfes, G. *Chem. Soc. Rev.* **2010**, *39*, 2083–2092. (f) Haak, R. M.; Wezenberg, S. J.; Kleij, A. W. *Chem. Commun.* **2010**, *46*, 2713–2723. (g) Joyce, L. A.; Shabbir, S. H.; Anslyn, E. V. *Chem. Soc. Rev.* **2010**, *39*, 3621–3632. (h) Meeuwissen, J.; Reek, J. N. H. *Nat. Chem.* **2010**, *2*, 615–621. (i) Rosati, F.; Roelfes, G. *ChemCatChem* **2010**, *2*, 916–927. (j) Carboni, S.; Gennari, C.; Pignataro, L.; Piarulli, U. *Dalton Trans.* **2011**, *40*, 4355–4373. (k) Deuss, P. J.; den Heeten, R.; Laan, W.; Kamer, P. C. J. *Chem. –Eur. J.* **2011**, *17*, 4680–4698. (l) Reetz, M. T. *Chem. Rec.* **2012**, *12*, 391-406. (m) Raynal, M.; Ballester, P.; Vidal-Ferran, A.; van Leeuwen, P. W. N. M. *Chem. Soc. Rev.* **2014**, *43*, 1660–1733. (n) Raynal, M.; Ballester, P.; Vidal-Ferran, A.; van Leeuwen, P. W. N. M. *Chem. Soc. Rev.* **2014**, *43*, 1734–1787.

7) See, for example references 6j,m,n and: (a) Crabtree, R. H. *New J. Chem.* **2011**, *35*, 18–23. (b) Lindbäck, E.; Dawaigher, S.; Wärnmark, K. *Chem. –Eur. J.* **2014**, *20*, 13432-13481. (c) Dydio, P.; Reek, J. N. H. *Chem. Sci.* **2014**, *5*, 2135–2145.

8) See, for example: (a) Koblenz, T. S.; Wassenaar, J.; Reek, J. N. H. *Chem. Soc. Rev.* **2008**, *37*, 247–262. (b) Yoshizawa, M.; Klosterman, J. K.; Fujita, M. *Angew. Chem., Int. Ed.* **2009**, *48*, 3418–3438. (c) Leenders, S. H. A. M.; Gramage-Doria, R.; de Bruin, B.; Reek, J. N. H. *Chem. Soc. Rev.* **2015**, *44*, 433–448.

9) The underlying principle is to design enantiopure ligands that incorporate several independent modules or molecular fragments. Such modules are designed to influence the catalytic site, whereby their sterics and electronics are considered *input parameters* for catalyst optimization. Selective modification of these parameters (based on mechanistic insight, molecular recognition principles, or even by the intuition of chemists themselves) has generally yielded higher-performing catalytic systems in terms of conversion, enantioselectivity and substrate scope. For some early examples of this methodology, see for example: (a) Trost, B. M.; Van Vranken, D. L.; Bingel, C. *J. Am. Chem. Soc.* **1992**, *114*, 9327–9343. (b) Rajanbabu, T. V.; Casalnuovo, A. L.; Ayers, T. A. *Adv. Catal. Processes* **1997**, *2*, 1–41. (c) Vidal-Ferran, A.; Moyano, A.; Pericàs, M. A.; Riera, A. *J. Org. Chem.* **1997**, *62*, 4970–4982.

10) See, for example reference 6d and: (a) Wennemers, H. *Comb. Chem. High Throughput Screening* **2001**, *4*, 273–285. (b) Hoveyda, A. H.; Murphy, K. E. Combinatorial Approaches. In *Compr. Asymmetric Catal., Suppl.*, 2004; Vol. 1, pp 171. (c) Jäkel, C.; Paciello, R. *Chem. Rev.* **2006**, *106*, 2912–2942. (d) Busacca, C. A.; Fandrick, D. R.; Song, J. J.; Senanayake, C. H. *Adv. Synth. Catal.* **2011**, *353*, 1825–1864. (e) Leung, D.; Kang, S. O.; Anslyn, E. V. *Chem. Soc. Rev.* **2012**, *41*, 448–479.

11) See, for example: (a) Traverse, J. F.; Snapper, M. L. *Drug Discovery Today* **2002**, *7*, 1002–1012. (b) Markert, C.; Roesel, P.; Pfaltz, A. *J. Am. Chem. Soc.* **2008**, *130*, 3234–3235.

12) See, for example: (a) Perutz, M. F.; Fermi, G.; Luisi, B.; Shaanan, B.; Liddington, R. C. *Acc. Chem. Res.* **1987**, *20*, 309–321. (b) Grandori, R.; Lavoie, T. A.; Pflumm, M.; Tian, G.; Niersbach, H.; Maas, W. K.; Fairman, R.; Carey, J. *J. Mol. Biol.* **1995**, *254*, 150–162.

13) Progress has been made by using a regulation agent in regulating the size and shape of an enantioselective catalyst, in changing the first-sphere coordination geometry of the active metal in enantioselective catalysis, or even in switching on and off the activity of the enantioselective catalyst. For general reviews which contain examples of major regulation effects in catalysis of achiral and enantioselective transformations, see: (a) Kovbasyuk, L.; Kraemer, R. *Chem. Rev.* **2004**, *104*, 3161–3187. (b) Gianneschi, N. C.; Masar, M. S., III; Mirkin, C. A. *Acc. Chem. Res.* **2005**, *38*, 825–837. (c) Kubo, Y.; Ishii, Y. *J. Nanosci. Nanotechnol.* **2006**, *6*, 1489–1509. (d) Zhu, L.; Anslyn, E. V. *Angew. Chem., Int. Ed. Engl.* **2006**, *45*, 1190–1196. (e) Lee, S. J.; Lin, W. *Acc. Chem. Res.* **2008**, *41*, 521–537. (f) Wiester, M. J.; Ulmann, P. A.; Mirkin, C. A. *Angew. Chem., Int. Ed.* **2011**, *50*, 114–137. (g) Kremer, C.; Luetzen, A. *Chem. –Eur. J.* **2013**, *19*, 6162–6196. (h) Kumagai, N.; Shibasaki, M. *Catal. Sci. Technol.* **2013**, *3*, 41–57. (i) Blanco, V.; Leigh, D. A.; Marcos, V. *Chem. Soc. Rev.* **2015**, *44*, 5341–5370.

14) For example, see: (a) Cram, D. J. *Angew. Chem. Int. Ed. Engl.* **1988**, *100*, 1009–1020. (b) Pedersen, C. J. *Angew. Chem. Int. Ed. Engl.* **1988**, *100*, 1021–1027. (c) Bajaj, A. V.; Poonia, N. S. *Coord. Chem.*

Rev. **1988**, *87*, 55–213. (d) van Veggel, F. C. J. M.; Verboom, W.; Reinhoudt, D. N. *Chem. Rev.* **1994**, *94*, 279–299.

15) Sawamura, M.; Nakayama, Y.; Tang, W.-M.; Ito, Y. *J. Org. Chem.* **1996**, *61*, 9090–9096.

16) Sawamura, M.; Ito, Y. *Chem. Rev.* **1992**, *92*, 857–871

17) Fernández-Pérez, H.; Mon, I.; Frontera, A.; Vidal-Ferran, A. *Tetrahedron* **2015**, *71*, 4490–4494.

18) For selected reviews on the concept of natural bite-angle and their effects, see: (a) van Leeuwen, P. W. N. M.; Kamer, P. C. J.; Reek, J. N. H.; Dierkes, P. *Chem. Rev.* **2000**, *100*, 2741–2769. (b) Shimizu, H.; Nagasaki, I.; Saito, T. *Tetrahedron* **2005**, *61*, 5405–5432 and the references cited therein.

19) Li, Y.; Ma, B.; He, Y.; Zhang, F.; Fan, Q.-H. *Chem. Asian J.* **2010**, *5*, 2454–2458.

20) For seminal examples of applications of metallacrown-ethers in catalysis, see: (a) Owens, S. B., Jr.; Gray, G. M. *Organometallics* **2008**, *27*, 4282–4287. (b) Zhang, X.; Qiu, Y.; Rao, B.; Luo, M. *Organometallics* **2009**, *28*, 3093–3099. Effects of the metallacrown-ether binders on the enantioselectivity of the reaction are not mentioned in ref 20a. The transformation detailed in ref. 20b is achiral.

21) For selected reviews, ref 14d and the following references: (a) Gray, G. M. *Comments Inorg. Chem.* **1995**, *17*, 95–114. (b) Mezei, G.; Zaleski, C. M.; Pecoraro, V. L. *Chem. Rev.* **2007**, *107*, 4933–5003.

22) Song, F.-T.; Ouyang, G.-H.; Li, Y.; He, Y.-M.; Fan, Q.-H. *Eur. J. Org. Chem.* **2014**, 6713–6719.

23) Mon, I.; Jose, D. A.; Vidal-Ferran, A. *Chem. –Eur. J.* **2013**, *19*, 2720–2725.

24) Vidal-Ferran, A.; Mon, I.; Bauza, A.; Frontera, A.; Rovira, L. *Chem. –Eur. J.* **2015**, *21*, 11417–11426.

25) The reader is referred to the original publication for further details.

26) Fuentes, J. A.; Lebl, T.; Slawin, A. M. Z.; Clarke, M. L. *Chem. Sci.* **2011**, *2*, 1997–2005.

27) Dydio, P.; Rubay, C.; Gadzikwa, T.; Lutz, M.; Reek, J. N. H. *J. Am. Chem. Soc.* **2011**, *133*, 17176–17179.

Chapter 2

Palladium-Based Supramolecularly Regulated Catalysts for Asymmetric Allylic Substitutions

Chapter 2.

Palladium-Based Supramolecularly Regulated Catalysts for Asymmetric Allylic Substitutions

Organometallics **2016**, *35*, 528–533

Laura Rovira†, Héctor Fernández-Pérez†, and Anton Vidal-Ferran†‡*

†Institute of Chemical Research of Catalonia (ICIQ) & The Barcelona Institute of Science and Technology, Avgda. Països Catalans 16, 43007 Tarragona, Spain.

‡Catalan Institution for Research and Advanced Studies (ICREA), Passeig Lluís Companys 23, 08010 Barcelona, Spain.

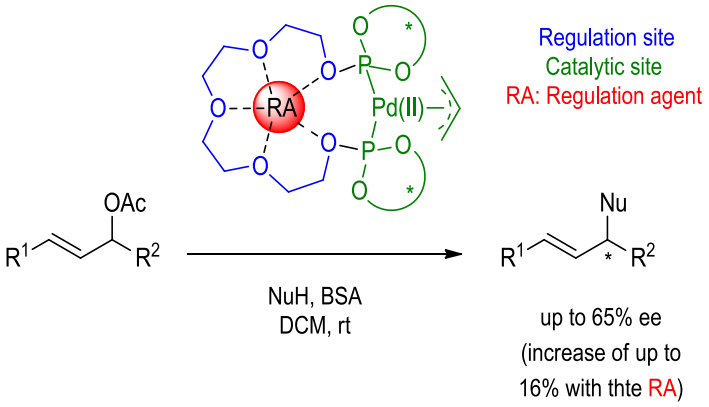

2.1. Abstract

Herein is reported the effect of different polyether binders (alkali metal, alkaline earth metal, and lanthanide salts) as regulation agents to enhance the catalytic properties of palladium complexes derived from enantiopure bisphosphite ligands in allylic substitutions. The addition of RbOAc or $M(OTf)_x$ ($M = Mg^{2+}$, La^{3+}, or Ho^{3+}) led to positive effects in enantioselectivity (by up to 16% ee) for the allylic substitution reactions. These ligands coordinated in the usual *cis*-fashion or in an unprecedented *trans*-fashion to the palladium center, depending on the phosphite group, and presented different reactivity in the allylic substitutions.

2.2. Introduction

The search for efficient chiral catalysts for the broadest possible substrate scope in a given transformation is still a cutting-edge research goal, as structural changes to the substrate(s) and or reagent(s) often translate into a loss of enantioselectivity. Within the supramolecular enantioselective catalysis arena,[1] progress has been made in regulating the size and shape of the chiral catalyst,[2] or in modifying the first-sphere coordination geometry of the active metal.[3] However, there are few examples of fine modification of the geometry of the active site that do not imply major alteration of the principal structural features of the enantioselective catalyst.[4,5]

Fan *et al.* pioneered the use of supramolecularly regulated polyether-based ligands for rhodium-mediated hydrogenations.[5b] These authors reported the first example on the use of rhodium complexes derived from bisphosphite-polyether ligands in asymmetric hydrogenation, whose catalytic performance in terms of enantioselectivity was enhanced by the addition of a regulation agent (RA, Figure 1).[5b] Later, we also demonstrated that conformationally transformable bisphosphite ligands[4a-c] incorporating polyether groups behaved as supramolecularly regulated ligands in asymmetric hydroformylations[4a-c] and hydrogenations[4b] (Figure 1). We showed that enantioselectivities in the transformation of interest can be maximized by the choice of whether or not to use an RA (and if so, which one).[4a-c] Computational studies revealed that the significant increase in enantiomeric excess provided by the RAs in hydroformylation reactions resulted from adaptation of the P–Rh–P bond angle (β).[4b]

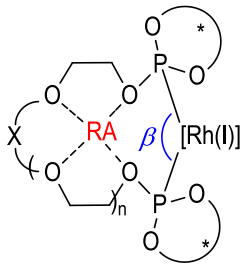

Fan *et al.*:[5b] X = -$(CH_2)_2$-; n = 0 and 3-5; O-O = BINOL
RA = alkali metal BArF salts as RAs for Rh-mediated hydrogenations

Vidal-Ferran *et al.*:[4a-c] X = O, BIPOL and BINOL; n = 2, 5 and 7
O-O = BIPOL, BINOL and substituted BINOLs
RA = alkali metal or ammonium BArF salts as RAs for Rh-mediated hydroformylations and hydrogenations

Previous work

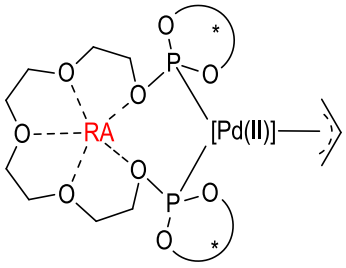

RA = metal salt as base and regulation agent for Pd-mediated allylic substitutions

This work

Figure 1. Supramolecularly regulated bisphosphite ligands in enantioselective catalysis (BIPOL = [1,1'-biphenyl]-2,2'-diol, BINOL = [1,1'-binaphthalene]-2,2'-diol).

Pd-mediated allylic substitutions represent an efficient transformation to stereoselectively form C–C and C–X bonds.[6] Palladium complexes derived from *P* ligands are efficient catalysts for the reaction between allylic alcohol derivatives and nucleophiles,[7] which have often been generated *in situ* from the protonated nucleophile (*i.e.*, a malonic ester) in the presence of *N*,*O*-bis(trimethylsilyl)-acetamide (BSA) and catalytic amounts of an alkali metal salt.[8]

Herein, we report our efforts in expanding our supramolecular regulation strategy to allylic substitutions. We envisaged that the combination of ligands **1a**–**c** with Pd(II) precursors suitable for this chemistry and an array of metal salts (for both generating the required nucleophile and triggering the regulation mechanism in our ligands) could function as supramolecularly regulated catalysts in allylic substitutions.

2.3. Results and discussion

We initially designed ligands **1a**–**c** by combining the linker group that showed the highest regulation ability in our hydroformylation studies[4b] (see blue fragment in Figure 2) and an array of stereogenic phosphite groups (see green fragment in Figure 2). Bisphosphites **1a** and **1b** had already been described[9,4b,c] and compound **1c** was prepared in an analogous manner to **1a** and **1b**: reaction of tetraethylene glycol with 2 equivalents of the corresponding chlorophosphite in the presence of a base (NEt_3).

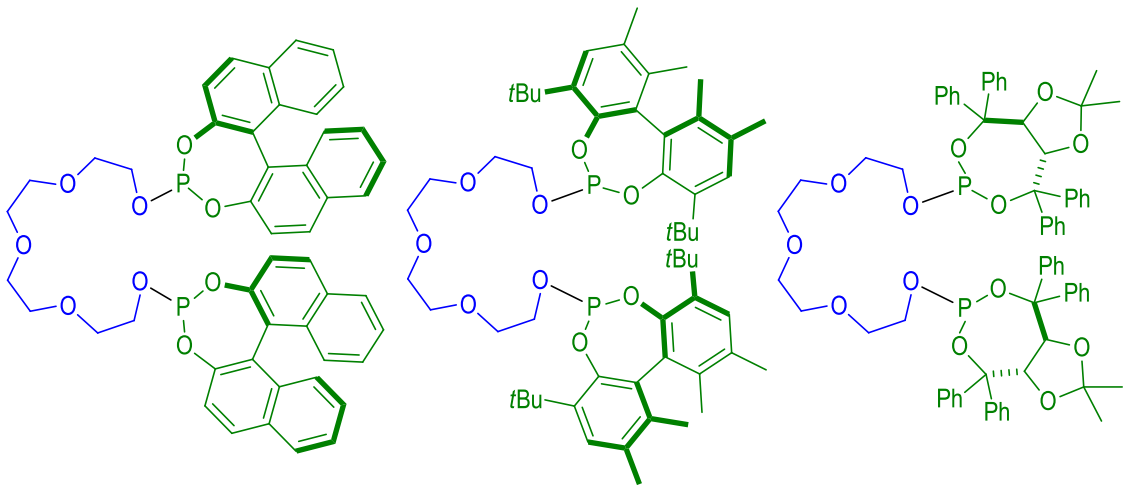

1a **1b** **1c**

Figure 2. Set of supramolecular bisphosphite ligands **1a**–**c**.

With ligands **1a**–**c** in hand, we then assessed their catalytic activity in combination with an array of RAs in allylic substitutions. Initially, we chose 1,3-diphenylallyl acetate **2** as the substrate and dimethyl malonate (DMM) as the nucleophile. The precatalysts were generated *in situ* from $[Pd(\mu\text{-Cl})(\eta^3\text{-}C_3H_5)]_2$, the ligands

1a–**c**, and the RA. The reactions were conducted in dichloromethane (DCM) as we considered that this solvent would provide a compromise between the solubility of the RA and its binding strength with the polyether fragment.[4b,10]

As illustrated in Table 1, the palladium complexes derived from bisphosphites **1a**–**c** provided active catalysts displaying full conversion in almost all cases (see Table 1). Enantioselectivity in the absence of regulation agents was moderate and highly dependent on the nature of the phosphite fragment.

Table 1. Pd-mediated asymmetric allylic alkylation of **2** with ligands **1a**–**c** and different regulation agents (RAs).[a]

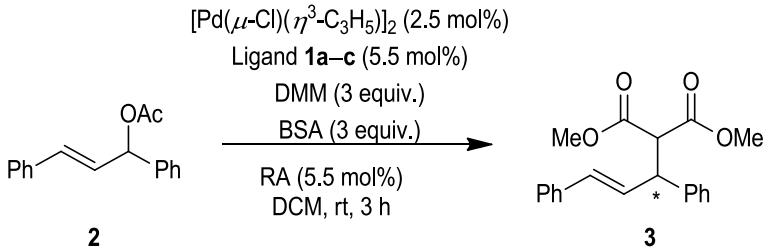

2 **3**

Entry	Ligand	RA	Conv. (%)[b]	ee of **3** (%) config.[c]
1	**1a**	-	>99	44 (*R*)
2	**1a**	LiOAc	>99	21 (*R*)
3	**1a**	CsOAc	>99	54 (*R*)
4	**1b**	-	>99	20 (*R*)
5	**1b**	LiOAc	>99	26 (*R*)
6	**1b**	CsOAc	>99	26 (*R*)
7[d]	**1c**	-	60	43 (*S*)
8	**1c**	LiOAc	>99	24 (*S*)
9[d]	**1c**	CsOAc	90	39 (*S*)

[a] Reaction conditions are indicated in the above scheme unless otherwise stated. [b] Determined by ^{1}H NMR spectroscopy. [c] Determined by HPLC on chiral stationary phases. [d] Reaction performed at rt for 24 h.

The palladium complex of ligand **1a** incorporating an (S_a)-BINOL-derived phosphite fragment provided the best enantioselectivity (up to 44% ee, entry 1 in Table 1). A similar ee was observed for ligand **1c**, although reactivity was lower (see entry 7 in Table 1). Finally, the sterically more demanding phosphite groups in ligand **1b** led to a decrease in ee (see entry 4 in Table 1). As our regulation design allows new catalytic systems to be generated by employing a set of RAs, subsequent attempts to improve enantioselectivity following this strategy (addition of LiOAc or CsOAc) resulted in some cases in higher ee's for ligands **1a** and **1b** (increase of up to 10% ee, compare entry 1 with 3 in Table 1).

We then studied the influence of the Pd precursor on the outcome of the allylic substitutions by incorporating [$PdCl_2$(cod)] to our studies (Table 2). Interestingly, [$PdCl_2$(cod)] performed better than [Pd(μ-Cl)(η^3-C_3H_5)]$_2$ in terms of enantioselectivity (for instance, compare entries 1–3 in Table 1 with

entries 1, 2 and 9 in Table 2). Of all the RA/ligand combinations tested, RbOAc•**1a** gave the best results: full conversion and 65% ee (increase of 6% ee with respect to when no RA was used, compare entry 1 with 6 in Table 2). Higher amounts of RbOAc did not bring any advantage in the result of the reaction, and lower temperatures (0 ºC) resulted in no conversion (see entries 7 and 8 in Table 2, respectively).

Two different potassium salts with different counterions (*i.e.,* KOAc and KF) were used as RAs, and no differences in reactivity were observed (compare entry 4 with 5 in Table 2).

Table 2. Allylic alkylations of **2** with bisphosphite ligand **1a** or **1c** and different RAs.[a]

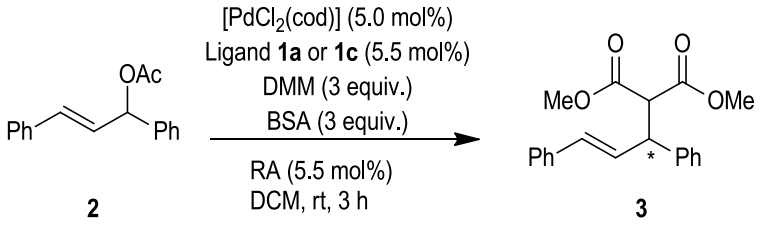

2 **3**

Entry	Ligand	RA	Conv. (%)[b]	ee of **3** (%) config.[c]
1	**1a**	-	>99	59 (*R*)
2	**1a**	LiOAc	>99	46 (*R*)
3	**1a**	NaOAc	>99	62 (*R*)
4	**1a**	KOAc	>99	63 (*R*)
5	**1a**	KF	>99	62 (*R*)
6	**1a**	RbOAc	>99	65 (*R*)
7[d]	**1a**	RbOAc	>99	65 (*R*)
8[e]	**1a**	RbOAc	0	n.d.
9	**1a**	CsOAc	>99	56 (*R*)
10[f]	**1a**	$Mg(OTf)_2$	15	56 (*R*)
11[f]	**1a**	$Ba(OTf)_2$	>99	4 (*R*)
12	**1a**	$La(OTf)_3$	>99	3 (*R*)
13	**1a**	$Ho(OTf)_3$	>99	*rac*
14[f]	**1c**	-	0	n.d.
15[f]	**1c**	LiOAc	0	n.d.
16[f]	**1c**	CsOAc	0	n.d.

[a] See footnote a in Table 1. [b] See footnote b in Table 1. [c] See footnote c in Table 1. [d] 1.7 equiv. of RA relative to Pd precursor was used. [e] Reaction performed at 0 ºC for 24 h. [f] Reaction performed at rt for 24 h.

It should be noted that the use of alkaline earth metal or lanthanide triflates as RAs led to detrimental effects for both reactivity and selectivity (see entries 10–13 in Table 2). The palladium complex derived from bisphosphite **1c** led to inactive catalysts in this chemistry since no reactivity for the allylic alkylation of **2** was observed even in the presence of different RAs (see entries 14–16 in Table 2).

We then assessed the supramolecularly regulated catalysts derived from the lead bisphosphite **1a** in allylic substitutions using benzylamine (BZA) as a nitrogen nucleophile. Standard screening conditions

were used, and the results of this study are shown in Table 3. Complexes derived from **1a** performed as efficient catalysts in the allylic amination of **2** in terms of conversion (see Table 3). When no RAs were used, a low ee was achieved (30% ee, see entry 1 in Table 3).

Interestingly, and in sharp contrast with the results using a *C*-nucleophile, an improvement in ee was obtained by using group II or lanthanides triflates as RAs (increase of up to 16% ee with $Mg(OTf)_2$, $La(OTf)_3$, or $Ho(OTf)_3$; see entries 4, 7, and 8 in Table 3) and $[Pd(\mu\text{-}Cl)(\eta^3\text{-}C_3H_5)]_2$ as palladium precursor (compare entry 4 with 5 in Table 3).

Table 3. Allylic amination of **2** with bisphosphite ligand **1a** and different RAs.[a]

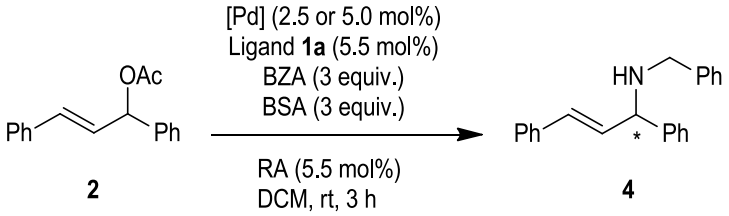

Entry	Ligand, Pd-precursor	RA	Conv. (%)[b]	ee of **4** (%) config.[c]
1	**1a**, $[Pd(\mu\text{-}Cl)(\eta^3\text{-}C_3H_5)]_2$	-	>99	30 (*S*)
2[d]	**1a**, $[Pd(\mu\text{-}Cl)(\eta^3\text{-}C_3H_5)]_2$	LiOAc	>99	33 (*S*)
3	**1a**, $[Pd(\mu\text{-}Cl)(\eta^3\text{-}C_3H_5)]_2$	CsOAc	0	n.d.
4	**1a**, $[Pd(\mu\text{-}Cl)(\eta^3\text{-}C_3H_5)]_2$	$Mg(OTf)_2$	>99	46 (*S*)
5	**1a**, $[PdCl_2(cod)]$	$Mg(OTf)_2$	35	29 (*S*)
6	**1a**, $[Pd(\mu\text{-}Cl)(\eta^3\text{-}C_3H_5)]_2$	$Ba(OTf)_2$	>99	45 (*S*)
7	**1a**, $[Pd(\mu\text{-}Cl)(\eta^3\text{-}C_3H_5)]_2$	$La(OTf)_3$	>99	46 (*S*)
8	**1a**, $[Pd(\mu\text{-}Cl)(\eta^3\text{-}C_3H_5)]_2$	$Ho(OTf)_3$	>99	46 (*S*)

[a] See footnote a in Table 1. [b] See footnote b in Table 1. [c] See footnote c in Table 1. [d] Reaction performed at rt for 72 h.

Finally, we tested our set of supramolecular bisphosphite ligands in the Pd-mediated allylic substitution of cinnamyl acetate **5** using DMM as nucleophile under standard screening conditions (Table 4). In general terms, palladium complexes derived from bisphosphites **1** were efficient catalysts in the alkylation of substrate **5** in terms of conversion (see Table 4). As expected for palladium-based catalysts,[7d,e] and in the absence of regulation agents, either low branched-to-linear ratios (b:l ratio, see entries 1 and 4 in Table 4) or exclusively the linear product **7** (see entries 5 and 12 in Table 4) were achieved depending on both the bisphosphite and the palladium precursor (see results for ligand **1b**, compare entry 4 with 5 in Table 4). In terms of enantioselectivity, a respectable value of 60% ee at a b:l ratio of 12:88 was achieved by using the palladium complex derived from **1b** and $[Pd(\mu\text{-}Cl)(\eta^3\text{-}C_3H_5)]_2$ (see entry 4 in Table 4). Interestingly, the use of LiOAc or CsOAc as RAs led to an increase in the regioselectivity of the reaction for the palladium complex derived of **1a** (b:l ratio up to 17:83; entries 2 and

3 in Table 4).[7] Unfortunately, the enantioselectivity could not be further improved for those catalytic systems leading to the highest ratio of branched product.

Table 4. Allylic alkylation of **5** with bisphosphite ligands **1a**–**c** and different RAs.[a]

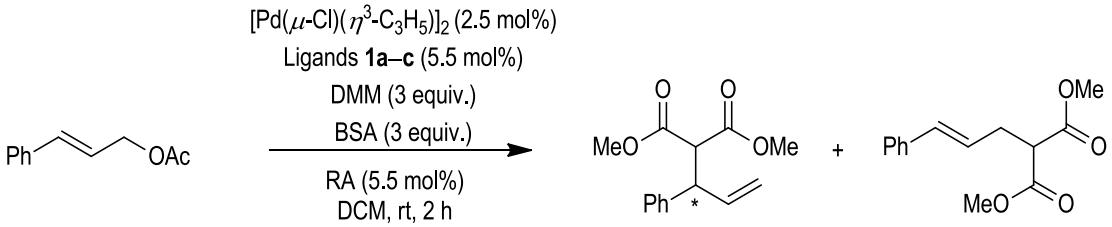

5 **6** **7**

Entry	Ligand	RA	Conv. (%)[b]	ratio[b] **6**:**7**	ee of **6** (%) config.[c]
1	**1a**	-	>99	14:86	28 (*R*)
2	**1a**	LiOAc	>99	17:83	19 (*R*)
3	**1a**	CsOAc	>99	17:83	32 (*R*)
4	**1b**	-	>99	12:88	60 (*R*)
5[d]	**1b**	-	75	>1:99	n.d.
6	**1b**	LiOAc	>99	14:86	57 (*R*)
7	**1b**	CsOAc	>99	11:89	55 (*R*)
8	**1b**	$Mg(OTf)_2$	>99	15:85	50 (*R*)
9	**1b**	$Ba(OTf)_2$	0	n.d.	n.d.
10	**1b**	$La(OTf)_3$	>99	12:88	42 (*R*)
11	**1b**	$Ho(OTf)_3$	0	n.d.	n.d.
12	**1c**	-	>99	>1:99	n.d.
13	**1c**	LiOAc	>99	>1:99	n.d.
14	**1c**	CsOAc	>99	>1:99	n.d.

[a] See footnote a in Table 1. [b] See footnote b in Table 1. [c] See footnote c in Table 1. [d] $[PdCl_2(cod)]$ (5.0 mol%) was used as metal precursor and the reaction was performed at rt for 6 h.

After having studied bisphosphite ligands **1a**–**c** in Pd-mediated allylic substitutions, we carried out coordination studies in order to gain insight into the reactivity of the palladium precatalysts derived from **1a** and **1c** (see Table 2) as well as into the regulation mechanism. The reaction of bisphosphites **1a** and **1c** with $[PdCl_2(cod)]$ proceeded smoothly to provide the corresponding palladium complexes $[PdCl_2(\mathbf{1a})]$ (**8a**) and $[PdCl_2(\mathbf{1c})]$ (**8c**), which were isolated and characterized. The $^{31}P\{^1H\}$ NMR spectra for compounds **8a** and **8c** showed single resonances at 109.8 and 90.2 ppm, respectively.[11] It is interesting to note that the signal of TADDOL-based bisphosphite **8c** was shielded upfield with respect to the signal of **8a** ($\Delta\delta \approx 20$ ppm), which might hint at important structural differences between palladium complexes **8a** and **8c**. Interestingly, compounds **8a** and **8c** could be crystallized and X-ray analysis unambiguously established their structures.[12] For **8a**, the palladium center had a distorted square-planar geometry in which the two

phosphorus groups of ligand **1a** were coordinated in a *cis*-fashion (see Figure 3 and Table 5). Meanwhile in complex **8c**, the palladium center also displayed a square-planar geometry but with the phosphorus groups of ligand **1c** occupying *trans*-binding sites (see Figure 3 and Table 5). To the best of our knowledge, this is the first reported example of a *trans*-chelating bisphosphite in Pd-complexes, which appears to be bound to a lack of reactivity in this chemistry (see entries 14–16 in Table 2).

Finally, to support our hypothesis on the regulation mechanism, we studied the interaction of RbOAc with the regulation site of the highest-performing palladium complex **8a**. NMR analysis qualitatively demonstrated the binding of RbOAc within the polyethyleneoxy moieties: the addition of incremental amounts of RbOAc to a solution of **8a** (up to 1.7 equiv.) caused significant changes to the chemical shift, multiplicity, and signal width of the polyethyleneoxy fragments.[12] These results suggest that binding of RbOAc within the polyethyleneoxy moieties is involved in the regulation effects mediated by the RA in the described allylic substitutions.

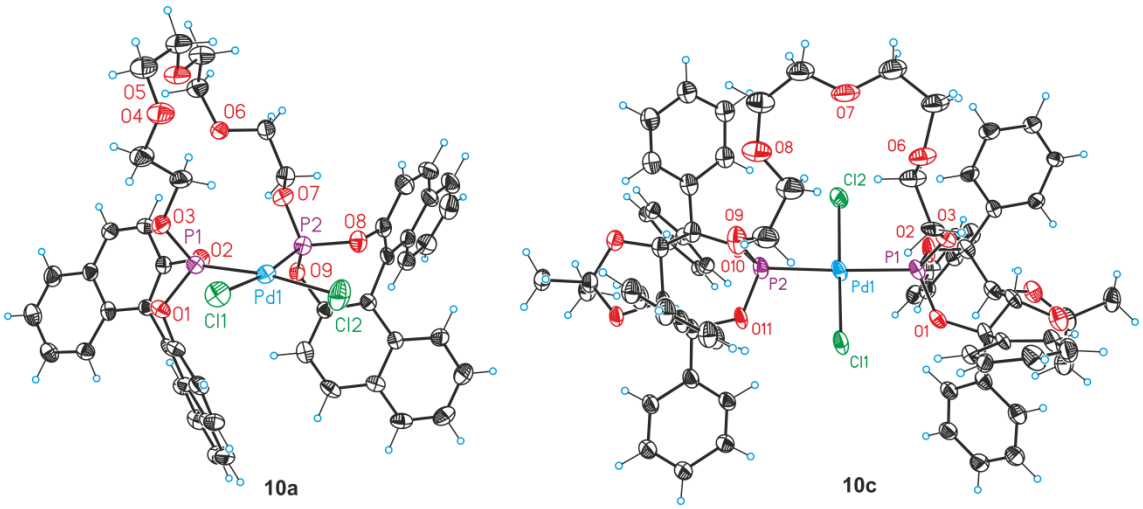

Figure 3. Crystal structures of **8a** and **8c** (ORTEP drawings showing in both cases thermal ellipsoids at 30% probability).

Table 5. Selected bond lengths (Å) and angles (°) for palladium complexes **8a** and **8c**.

Compound **8a**		Compound **8c**	
Atoms	Lengths (Å) or Angles (°)	Atoms	Lengths (Å) or Angles (°)
Pd1–P1	2.2141(17)	Pd1–P1	2.287(2)
Pd1–P2	2.2191(16)	Pd1–Cl1	2.291(2)
Pd1–Cl2	2.3113(17)	Pd1–Cl2	2.291(2)
Pd1–Cl1	2.3450(16)	Pd1–P2	2.301(2)
P1–Pd1–P2	92.45(6)	P1–Pd1–Cl1	91.30(7)
P1–Pd1–Cl2	172.10(6)	P1–Pd1–Cl2	88.36(8)
P2–Pd1–Cl2	93.27(6)	Cl1–Pd1–Cl2	174.58(10)
P1–Pd1–Cl1	83.41(6)	P1–Pd1–P2	177.39(8)
P2–Pd1–Cl1	171.04(5)	Cl1–Pd1–P2	91.30(7)
Cl2–Pd1–Cl1	91.66(6)	Cl2–Pd1–P2	89.07(8)

2.4. Conclusions

In summary, we have designed and prepared supramolecularly regulated ligands for Pd-mediated asymmetric allylic substitutions. The selectivity (both regio- and stereo-selectivity) of the allylic substitutions mediated by bisphosphites **1** could be regulated by using several alkali metal, alkaline earth metal or lanthanide salts as regulation agents. Positive increments in the regio- and enantio-selectivity were achieved in the allylic substitutions of benchmark substrates using carbon and nitrogen nucleophiles. The distinct reactivity between **8a** and **8c** in allylic substitution reactions may be attributed to the different coordination mode of bisphosphite ligands **1a** and **1c** with [$PdCl_2$(cod)] (in a *cis*- or *trans*-fashion, respectively), as demonstrated by X-ray single crystal analysis.

2.5. Experimental section

General information: All syntheses were carried out using chemicals as purchased from commercial sources unless otherwise cited. All manipulations and reactions were performed under inert atmosphere. Glassware was dried *in vacuo* before use with a hot air gun. All solvents were dried and deoxygenated by using a Solvent Purification System (SPS). Silica gel 60 (230 – 400 mesh) or C18–SiO_2 (200 – 400 mesh) was used for column chromatography. NMR spectra were recorded in $CDCl_3$ unless otherwise cited. ^{1}H NMR and ^{13}C NMR chemical shifts were quoted in ppm relative to residual solvent peaks, whereas ^{31}P{1H} NMR chemical shifts were quoted in ppm relative to 85% phosphoric acid in water. High-resolution mass spectra (HRMS) were recorded by using an electrospray ionization (ESI) method in positive mode or matrix-assisted laser desorption/ionization (MALDI) method, respectively. Melting points were determined in open capillaries and are uncorrected. Enantiomeric excesses were determined by HPLC equipped with a diode array detector using chiral stationary phases.

General synthetic procedure for bisphosphite ligands (1a–c)

Under an inert atmosphere, the chlorophosphites (1 equiv.) were dissolved in anhydrous toluene (25 mL per mmol of the chlorophosphites) and NEt_3 (3 equiv.). A solution of tetraethylene glycol (0.46 equiv., in 50 mL of toluene per mmol of tetraethylene glycol) was slowly added to the previous solution and allowed to react overnight at rt. The reaction mixture was filtered and the solvent was evaporated *in vacuo*. The resulting crude mixtures were purified by column chromatography on C18–SiO_2 using acetonitrile/ethyl acetate 1:1 as elution solvent to provide the expected bisphosphites **1** as white solids.

Compound 1c: Compound **1c** was synthesised from TADDOL-derived chlorophosphite[13] (1.44 g, 2.71 mmol) and a slow addition of tetraethylene glycol (243.0 mg, 1.25 mmol) with NEt_3 (0.52 mL, 3.75 mmol) as base. Purification by C18–SiO_2 column chromatography afforded the expected bisphosphite ligand **1c** as a white solid. Isolated 1.05 g, 71% yield. ^{1}H NMR ($CDCl_3$, 400 MHz): δ 7.50–7.60 (m, 12H), 7.42–7.45 (m, 4H), 7.19–7.36 (m, 24H), 5.19 (d, J = 8.3 Hz, 2H), 5.06 (dd, $J_{H,H}$ = 8.3 Hz, $J_{H,P}$ = 1.8 Hz, 2H,), 3.85–4.02 (m, 4H), 3.53–3.61 (m, 8H), 3.40–3.48 (m, 4H), 0.91 (s, 6H), 0.57 (s, 6H). ^{13}C{^{1}H,^{31}P} NMR ($CDCl_3$, 125 MHz): δ 146.3, 146.2, 141.7, 141.5, 129.2, 128.9, 128.3, 128.0, 127.8, 127.5, 127.4, 127.33, 127.29, 127.2, 112.8, 85.0, 82.9, 82.3, 81.2, 70.8, 70.7, 61.9, 27.0, 26.3. ^{31}P{^{1}H} NMR ($CDCl_3$, 162 MHz): δ 134.6 (s). HRMS–ESI–TOF (*m/z*): $[M + Na]^+$ calcd for $C_{70}H_{72}O_{13}P_2Na$ 1205.4340; found 1205.4339. Anal. calcd for $C_{70}H_{72}O_{13}P_2$: C, 71.05; H, 6.13. Found: C, 71.85; H, 6.25. $[\alpha]_D^{24}$= +162.4 (*c* 0.39, DCM). mp 90.3–95.3 °C.

General synthetic procedure for Pd-complexes based on bisphosphite ligands (8a and 8c)

A solution of enantiomerically pure bisphosphite ligand **1a** or **1c** (0.059 mmol) in dry DCM (1.8 mL) was slowly added to a solution of [$PdCl_2$(cod)] (0.054 mmol) in DCM (0.2 mL) at room temperature under an inert atmosphere. The reaction mixture was stirred for 2 h, after which the DCM solvent was evaporated off until the mixture had one fourth of its original volume. Hexane (15.0 mL) was added, leading to the formation of a precipitate, which was filtered off and then washed with a small quantity of hexane (1 x 5.0 mL) to give the desired Pd(II) complexes [$PdCl_2$(**1**)] as yellowish powders.

Synthesis of compound 8a: Palladium complex **8a** was prepared following the general procedure, starting from ligand **1a** (117 mg, 0.142 mmol) and [$PdCl_2$(cod)] (37 mg, 0.129 mmol). It was obtained as a yellowish powder. Isolated 27 mg, 20% yield. ^{1}H NMR (C_4D_8O, 500 MHz): δ 8.06–8.08 (m, 4H), 7.97 (d, J = 8.2 Hz, 2H), 7.77 (d, J = 8.9 Hz, 2H), 7.63 (d, J = 8.8 Hz, 2H,), 7.52–7.55 (m, 2H), 7.44–7.47 (m, 2H), 7.25–7.35 (m, 8H), 6.75 (d, J = 8.8 Hz, 2H), 4.65–4.70 (m, 2H), 4.23–4.26 (m, 2H), 3.65–3.85 (m, 12H). ^{13}C{^{1}H} NMR (C_4D_8O, 125 MHz,): δ 147.1, 133.4, 133.2, 133.1, 132.8, 132.1, 131.9, 129.6, 129.4, 127.9, 127.7, 127.6, 126.8, 126.6, 123.6, 122.6, 122.0, 121.8, 72.0, 71.7, 71.5, 70.8. ^{31}P{^{1}H} NMR (C_4D_8O, 202 MHz,): δ 109.8 (s). HRMS–MALDI–TOF (*m/z*): $[M - Cl]^+$ calcd for $C_{48}H_{40}O_9P_2ClPd$, 963.0865, found

963.0839. Anal. calcd. for $C_{48}H_{40}O_9P_2Cl_2Pd$: C, 57.65; H, 4.03. Found: C, 57.33; H, 4.44. $[\alpha]_D^{25}$= –40.4 (*c* 0.10, DCM). mp 187.0–190.0 °C.

Synthesis of compound 8c: Palladium complex **8c** was prepared following the general procedure, starting from ligand **1c** (70 mg, 0.059 mmol) and [$PdCl_2$(cod)] (15 mg, 0.053 mmol). It was obtained as a yellowish powder. Isolated 47 mg, 65% yield. ^{1}H NMR (C_4D_8O, 500 MHz): δ 7.83–7.85 (m, 8H), 7.72–7.74 (m, 4H), 7.51–7.52 (m, 4H), 7.24–7.40 (m, 24H), 5.74 (d, J = 8.4 Hz, 2H), 5.07 (d, J = 8.4 Hz, 2H), 3.75–3.81 (m, 2H), 3.54–3.60 (m, 2H), 3.35–3.39 (m, 6H), 3.20–3.25 (m, 2H), 2.86–2.91 (m, 2H), 2.76–2.80 (m, 2H), 1.25 (s, 6H), 0.41 (s, 6H). ^{13}C{^{1}H} NMR (C_4D_8O, 125 MHz): δ 143.5, 142.7, 139.2, 138.4, 127.5, 126.5, 125.9, 125.7, 125.6, 125.4, 125.3, 125.1, 111.1, 87.0, 86.92, 86.87, 86.71, 86.67, 86.6, 80.1, 77.6, 68.9, 68.6, 66.7, 24.8, 23.1. ^{31}P{^{1}H} NMR (C_4D_8O, 202 MHz) δ 90.2 (s). HRMS–ESI–TOF (*m*/*z*): $[M + OH - Cl]^+$ calcd for $C_{70}H_{73}O_{14}P_2ClPd$ 1340.3213, found 1340.3233. Anal. Calcd. for $C_{70}H_{72}O_{13}P_2Cl_2Pd \cdot 0.5CH_2Cl_2$: C, 60.35; H, 5.24. Found: C, 60.78; H, 5.68. $[\alpha]_D^{27}$= +160.6 (*c* 0.04, DCM). mp 210.2–214.9 °C.

General procedure for Pd-mediated allylic alkylation of *rac*-1,3-diphenylallyl acetate (2)

A solution of [Pd(μ-Cl)(η^3-C_3H_5)]$_2$ (2.50 μmol) or [$PdCl_2$(cod)] (5.00 μmol), enantiopure bisphosphite **1** (5.50 μmol) in DCM (0.30 mL) and regulation agent (RA, 5.50 μmol; if appropriate) was stirred for 15 min. Subsequently, a solution of 1,3-diphenylallyl acetate **2** (0.1 mmol) in DCM (0.10 mL), dimethyl malonate (0.3 mmol) and *N*,*O*-bis(trimethylsilyl)-acetamide (0.3 mmol) were added. The reaction mixture was stirred at room temperature for the appropriate reaction time. The reaction mixture was then diluted with Et_2O (4.0 mL) and washed with water (2 x 2.0 mL). The organic phase was dried over $MgSO_4$, filtered and concentrated *in vacuo*. The conversion was determined by ^{1}H NMR spectroscopy and the enantiomeric excess was determined by HPLC on chiral stationary phases (Daicel Chiralcel OD–H, 99:1 *n*-hexane/2-propanol, 0.5 mL/min, 216 nm).[14]

General procedure for Pd-mediated allylic amination of *rac*-1,3-diphenylallyl acetate (2)

A solution of [Pd(μ-Cl)(η^3-C_3H_5)]$_2$ (2.50 μmol), enantiopure bisphosphite **1** (5.50 μmol) in DCM (0.30 mL) and regulation agent (RA, 5.50 μmol; if appropriate) was stirred for 15 min. Subsequently, a solution of 1,3-diphenylallyl acetate **2** (0.1 mmol) in DCM (0.10 mL), benzylamine (0.3 mmol) and *N*,*O*-bis(trimethylsilyl)-acetamide (0.3 mmol) were added. The reaction mixture was stirred at rt for the appropriate reaction time. The reaction mixture was then diluted with Et_2O (4.0 mL) and washed with water (2 x 2.0 mL). The organic phase was dried over $MgSO_4$, filtered and concentrated *in vacuo*. The conversion was determined by ^{1}H NMR spectroscopy and the enantiomeric excess was determined by

HPLC on chiral stationary phases (Daicel Chiralcel OD–H, 99:1 *n*-hexane/2-propanol, 0.6 mL/min, 254 nm).[15]

General procedure for Pd-mediated allylic alkylation of cinnamyl acetate (5)

A solution of [Pd(μ-Cl)(η^3-C_3H_5)]$_2$ (2.50 μmol), enantiopure bisphosphite **1** (5.50 μmol) in DCM (0.30 mL) and regulation agent (RA, 5.50 μmol; if appropriate) was stirred for 15 min. Subsequently, a solution of cinnamyl acetate **5** (0.1 mmol) in DCM (0.10 mL), dimethyl malonate (0.3 mmol) and *N*,*O*-bis(trimethylsilyl)-acetamide (0.3 mmol) were added. The reaction mixture was stirred at rt for the appropriate reaction time. The reaction mixture was then diluted with Et_2O (4.0 mL) and washed with water (2 x 2.0 mL). The organic phase was dried over $MgSO_4$, filtered and concentrated *in vacuo*. The conversion was determined by ^{1}H NMR spectroscopy and the enantiomeric excess was determined by HPLC on chiral stationary phases (Daicel Chiralcel OJ–H, 97:3 *n*-hexane/2-propanol, 0.7 mL/min, 220 nm).[14]

2.6. Supporting information

2.6.1. *In situ* coordination studies of ligand 1a with [$PdCl_2$(cod)] and RbOAc as regulation agent

A mixture of the bisphosphite ligand **1a**, [$PdCl_2$(cod)], and RbOAc in different ratios was prepared in CD_2Cl_2 (*ca.* 2.5 mM) in a glass vessel, and the solution was stirred for 2 h at room temperature. After that, the content was transferred to a NMR Young tube and the *in situ* formed palladium complexes were investigated by ^{1}H NMR and ^{31}P{^{1}H} NMR spectroscopy (see Figure S1 and Figure S2).

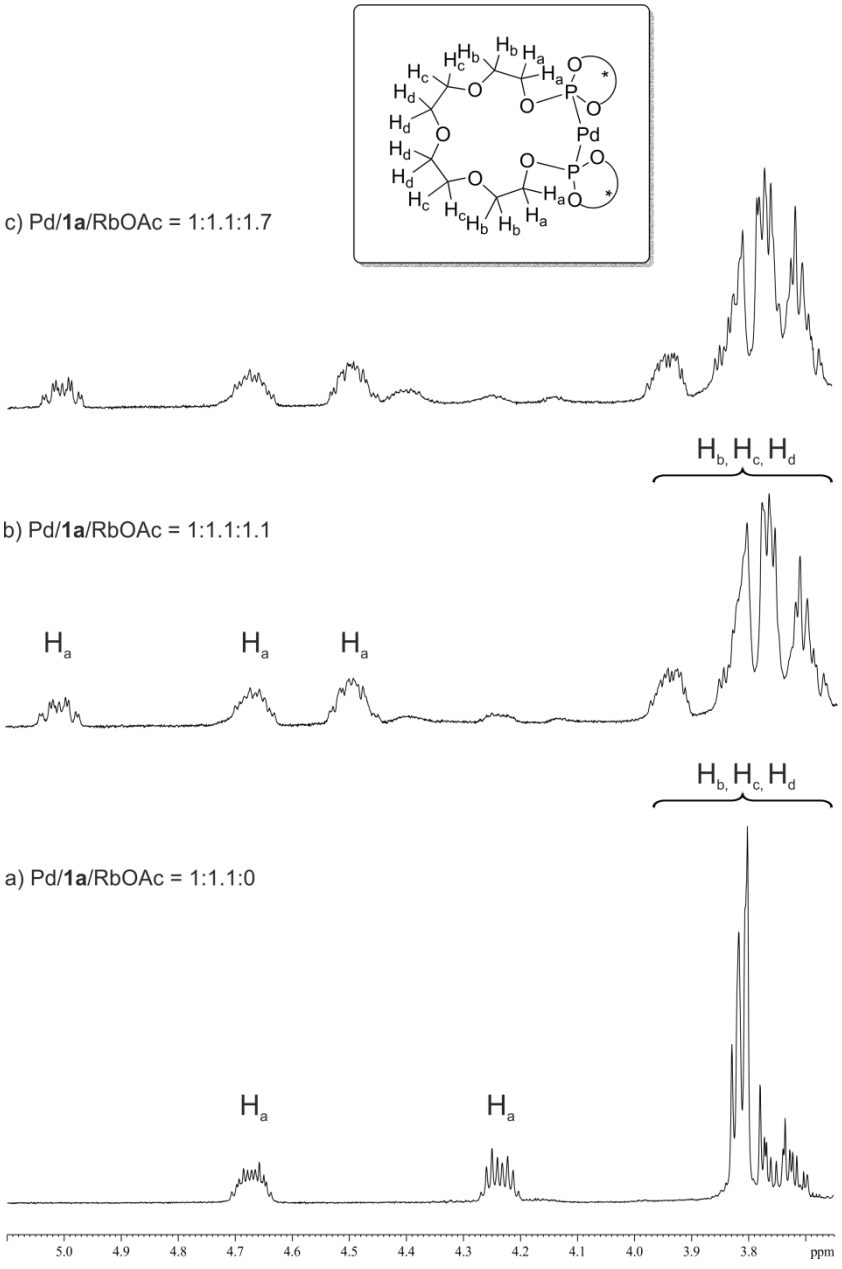

Figure S1. Stacked plot of ^{1}H NMR spectra for a zoom view of the polyether chain (400MHz, CD_2Cl_2, 25 ºC): a) [$PdCl_2$(cod)]/**1a**/RbOAc = 1:1.1:0; b) [$PdCl_2$(cod)]/**1a**/RbOAc = 1:1.1:1.1; c) [$PdCl_2$(cod)]/**1a**/RbOAc = 1:1.1:1.7.

As indicated in the text, addition of RbOAc as RA caused significant changes to the chemical shift, multiplicity and width of the signals of the polyethyleneoxy moieties in ^{1}H NMR (See Figure S1). Similar effects are observed in the phosphorus signals in $^{31}P\{^{1}H\}$ NMR (chemical shift: phosphorus signals are deshielded upon addition of incremental amounts of RbOAc; multiplicity: a coupling between the two phosphorus groups is observed upon addition of RbOAc, see Figure S2).

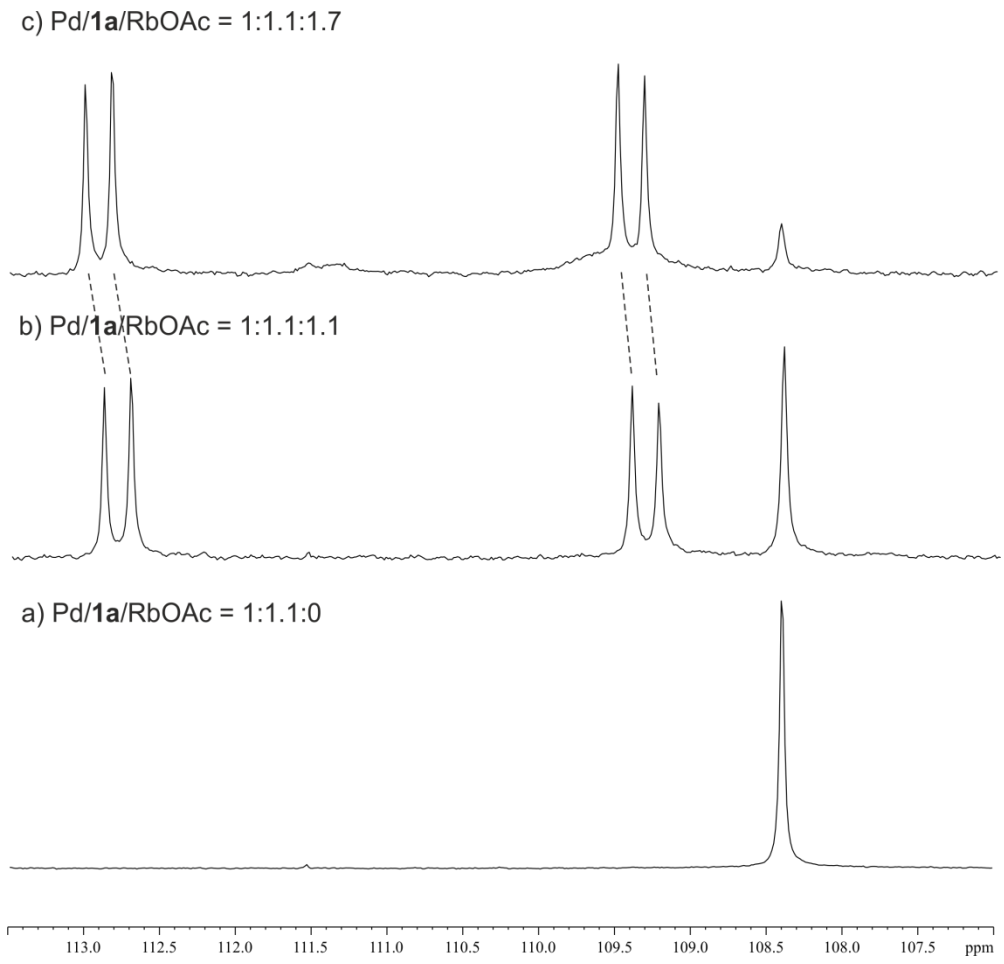

Figure S2. Stacked plot for a zoom view of $^{31}P\{^{1}H\}$ NMR spectra (162MHz, CD_2Cl_2, 25 ºC): a) $[PdCl_2(cod)]$/**1a**/RbOAc = 1:1.1:0; b) $[PdCl_2(cod)]$/**1a**/RbOAc = 1:1.1:1.1; c) $[PdCl_2(cod)]$/**1a**/RbOAc = 1:1.1:1.7.

2.6.2. Single crystal X-ray structure determination

X-Ray crystal structure determination: Crystals of **8a** and **8c** were obtained under inert conditions after carefully layering hexane to a solution of the palladium complex in dichloromethane [the final solvent composition was a mixture of DCM:Hexane 1/2 (v/v)]. The mixture was kept at −24 ºC. Pale yellow needles were obtained after 3 days. The measured crystals were prepared under inert conditions immersed in perfluoropolyether as protecting oil for manipulation.

Data collection: Crystal structure determination for **8a** and **8c** was carried out using a Apex DUO diffractometer equipped with a Kappa 4-axis goniometer, an APEX II 4K CCD area detector, a Microfocus Source E025 IuS using MoK_α radiation, Quazar MX multilayer Optics as monochromator and an Oxford Cryosystems low temperature device Cryostream 700 plus (T = −173 ˚C). Full-sphere data collection was used with ω and φ scans. *Programs used:* Data collection APEX-2,[16] data reduction Bruker Saint[17] V/.60A and absorption correction SADABS.[18]

Structure solution and refinement: Crystal structure solution was achieved using direct methods as implemented in SHELXTL[19] and visualized using the program XP. Missing atoms were subsequently located from difference Fourier synthesis and added to the atom list. Least-squares refinement on F^2 using all measured intensities was carried out using the program SHELXTL. All non-hydrogen atoms were refined including anisotropic displacement parameters.

Comments to the structures: The asymmetric unit of compound **8a** is formed by one molecule of the metal complex and three molecules of dichloromethane. The polyether ring contained in the main molecule is disordered in two orientations (ratio: 70:30).

Compound **8c** crystallized with one molecule of the metal complex and highly disordered solvent molecules in the asymmetric unit. The main molecule is disordered in two orientations with a ratio in the range of 60:40 to 50:50. In order to avoid the highly disordered solvent molecules (probably dichloromethane) the program SQUEEZE was applied leading to a refined model with a R1 value of 6.57 % in which all the solvent molecules were removed.[20]

Table S1. Crystal data for compounds **8a** and **8c**.

Compound	8a	8c
Formula	$C_{51}H_{46}Cl_8O_9P_2Pd$	$C_{70}H_{72}Cl_2O_{13}P_2Pd$
Solvents	3 x CH_2Cl_2	Disordered CH_2Cl_2
Formula weight	1254.82	1360.51
Crystal size (mm^3)	0.12 x 0.12 x 0.04	0.30 x 0.06 x 0.04
Crystal color	colourless	yellow
Temp (K)	100	100
Crystal system	Orthorhombic	Orthorhombic
Space group	$P2_12_12_1$	$P2_12_12_1$
A (Å)	11.752(3)	12.5154(8)
B (Å)	13.584(4)	22.1406(12)
C (Å)	32.731(9)	26.2373(17)
α (deg)	90	90
β (deg)	90	90
γ (deg)	90	90
V ($Å^3$)	5225(2)	7270.3(8)
Z	4	4
ρ (g/cm^3)	1.595	Squeeze
μ (mm^{-1})	0.881	0.430
θ_{max} (°)	30.97	28.35
Reflec. measured	45367	72166
Unique reflections	9638 [R_{int} = 0.0914]	9510 [R_{int} = 0.0781]
Absorpt. correct.	SADABS	SADABS
Trans. min/max	0.966/0.806	0.983/0.756
Parameters/Restrains	739/182	1458/3010
R1/wR2 [I > 2σ(I)]	0.0512/0.0913	0.0657/0.1466
R1/wR2 [all data]	0.0990/0.1099	0.1336/0.1675
Goodness-of-fit (F^2)	0.935	0.982
Peak/hole ($e/Å^3$)	0.529/–0.873	0.681/–0.865

CCDC 1415397 and CCDC 1415398 contain the supplementary crystallographic data for this paper. These data can be obtained free of charge from The Cambridge Crystallographic Data Centre via www.ccdc.cam.ac.uk/data_request/cif.

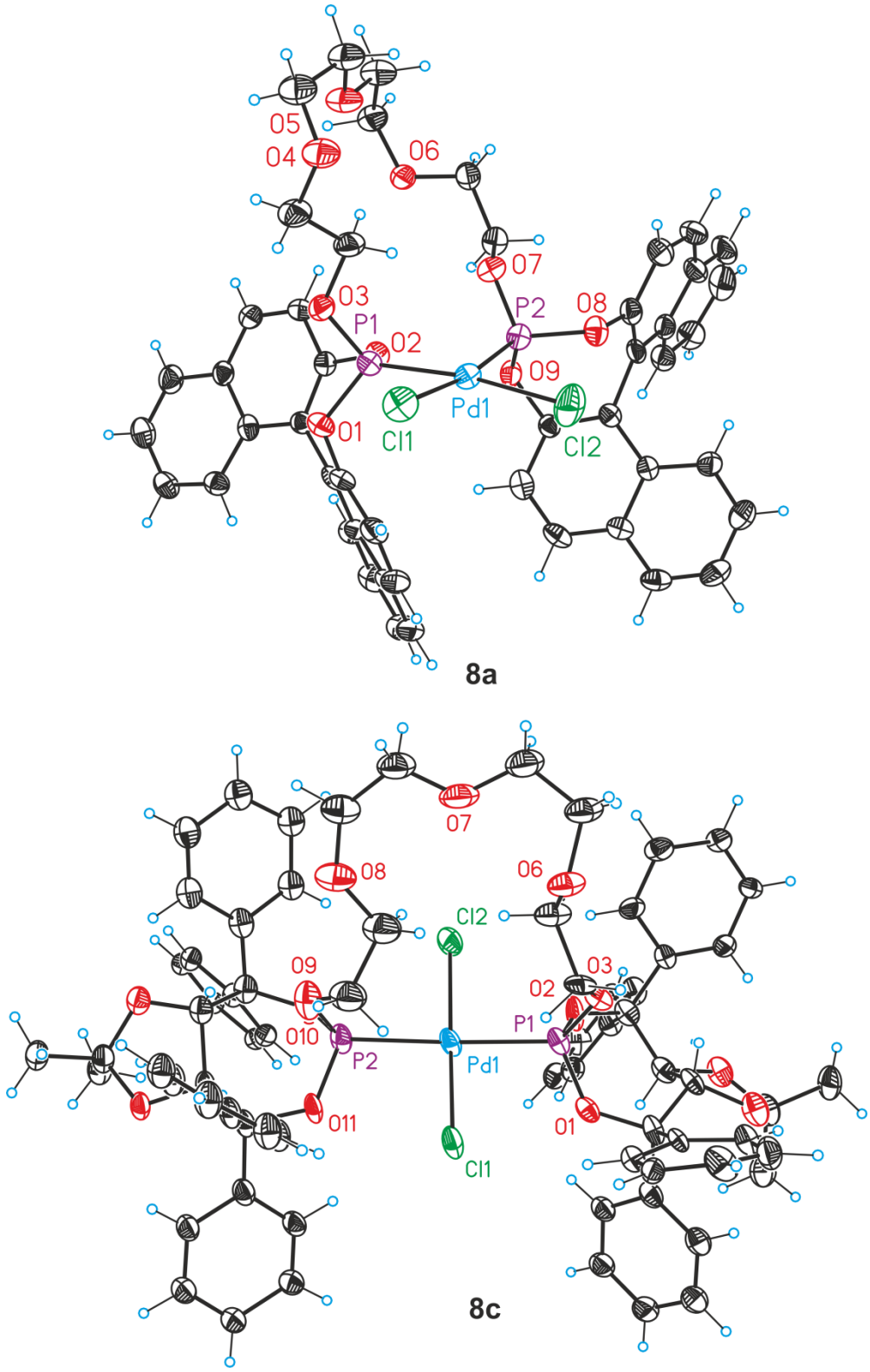

Figure S3. Crystal structures of **8a** and **8c** (ORTEP drawing showing thermal ellipsoids at 50% and 30% probability, respectively).

2.6.3. NMR spectra of new compounds

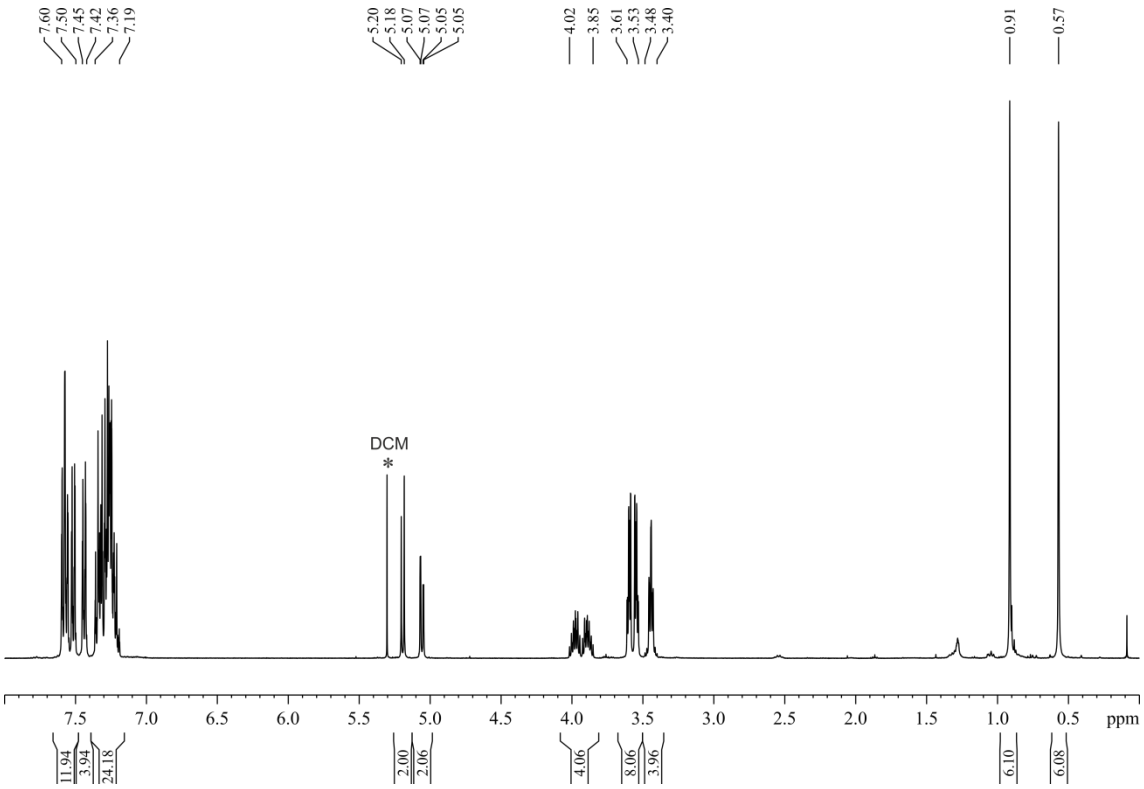

Figure S4. ^{1}H NMR spectrum for compound **1c**.

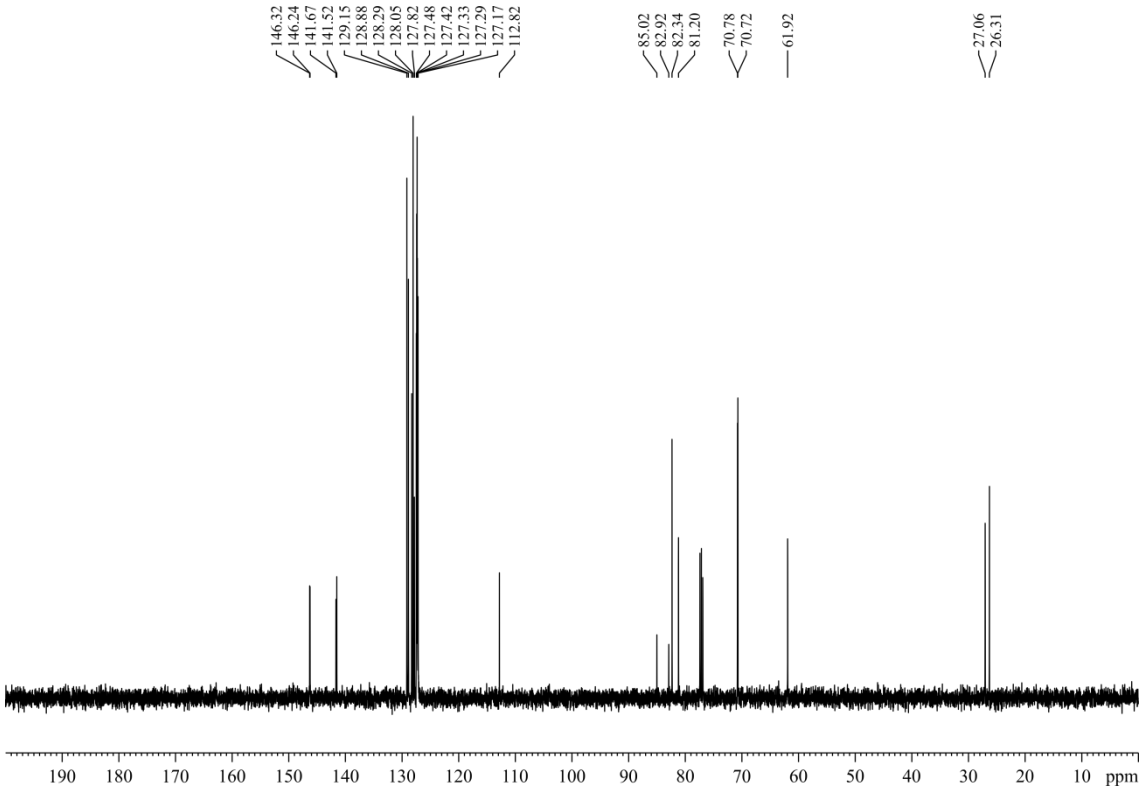

Figure S5. $^{13}C\{^{1}H,^{31}P\}$ NMR spectrum for compound **1c**.

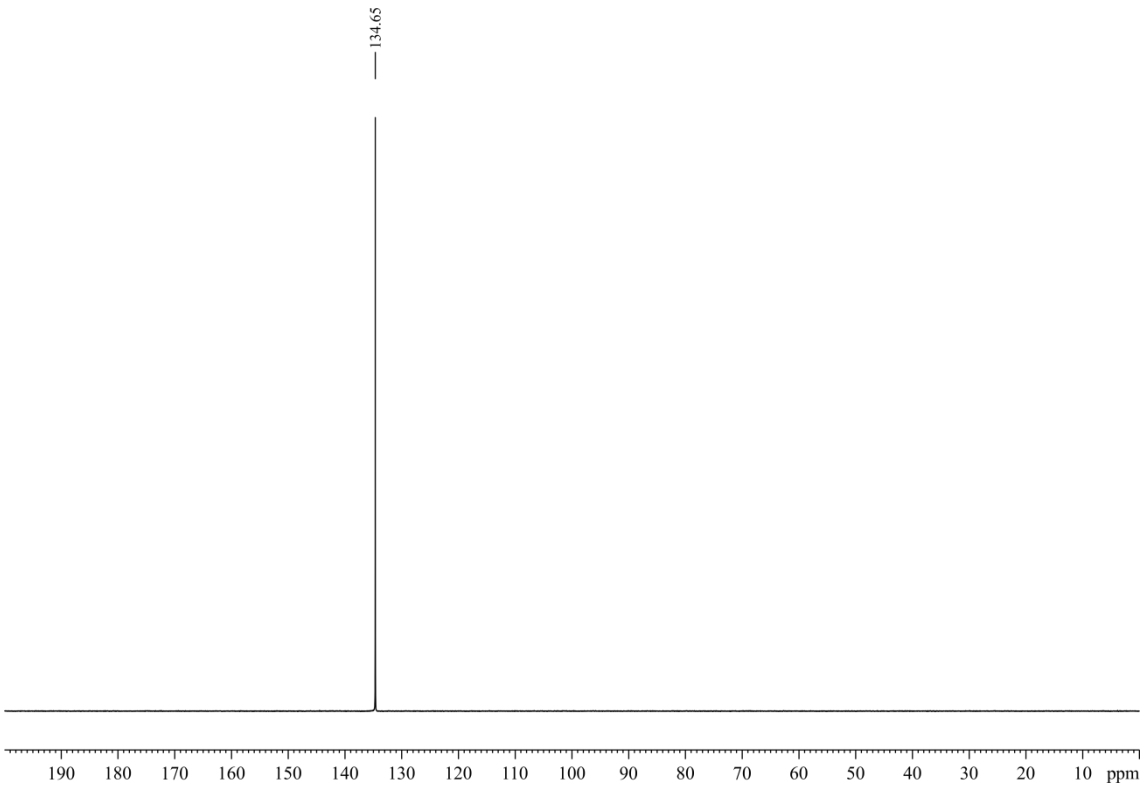

Figure S6. $^{31}P\{^{1}H\}$ NMR spectrum for compound **1c**.

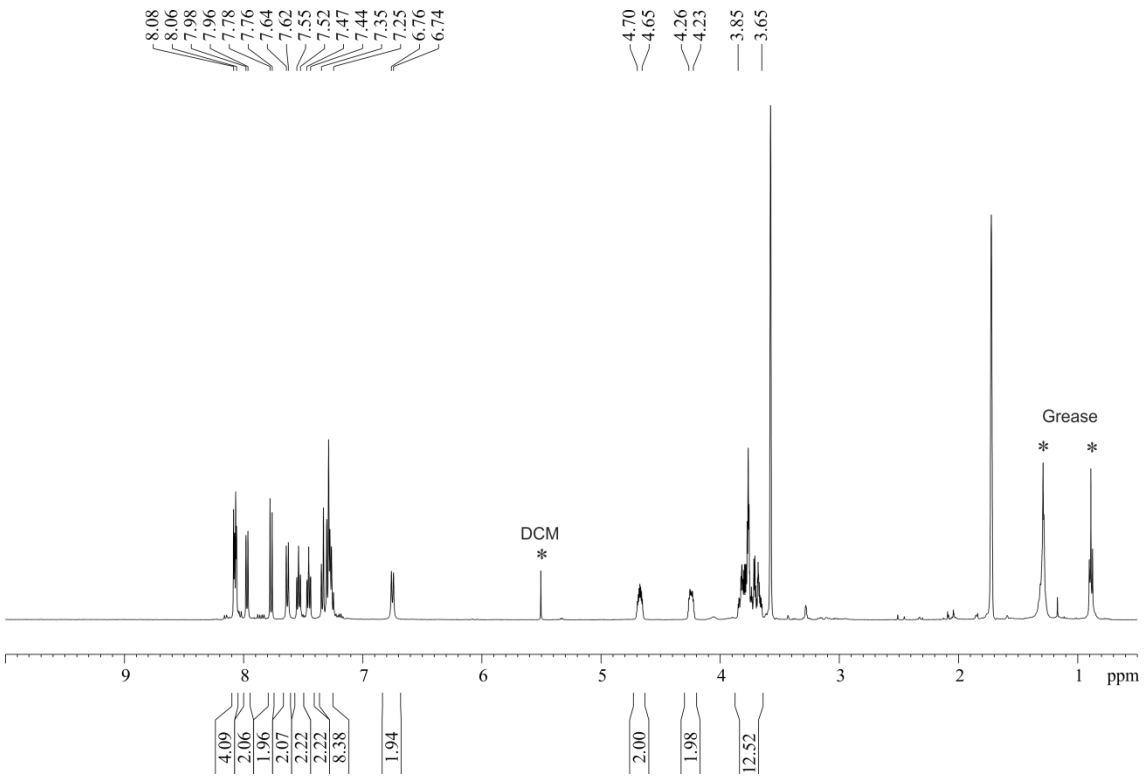

Figure S7. ^{1}H NMR spectrum for compound **8a**.

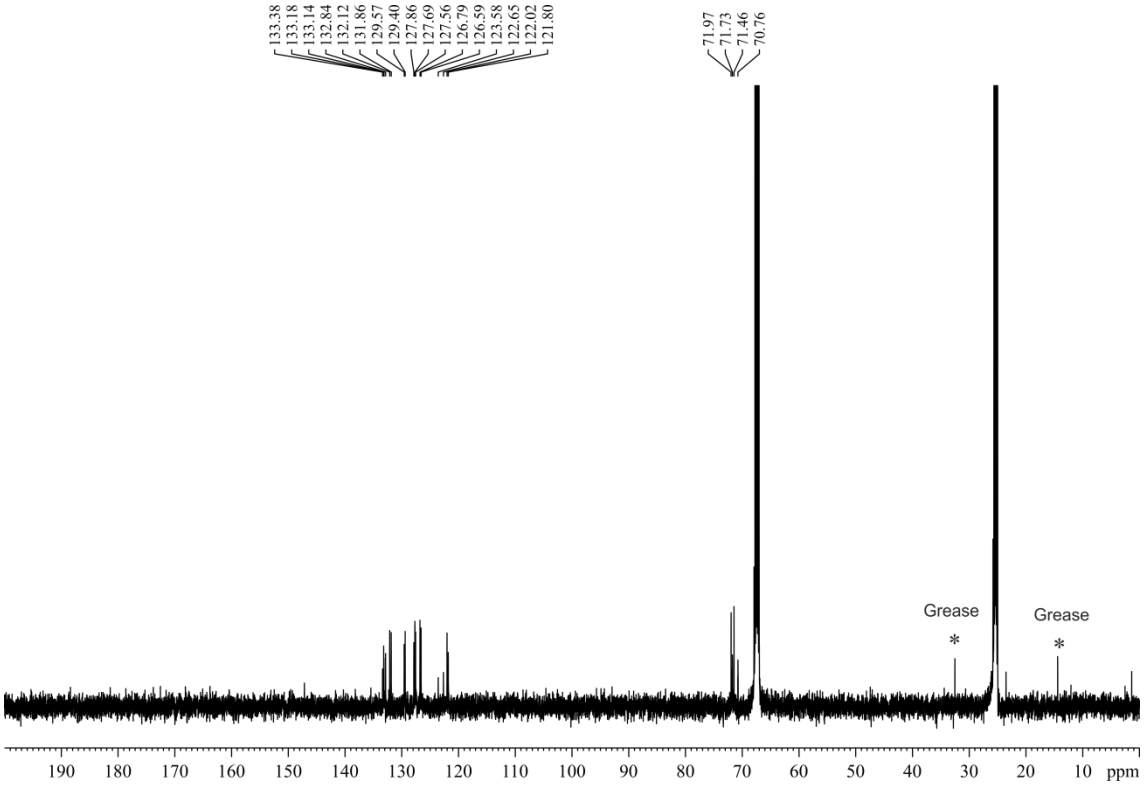

Figure S8. $^{13}C\{^{1}H\}$ NMR spectrum for compound **8a**.

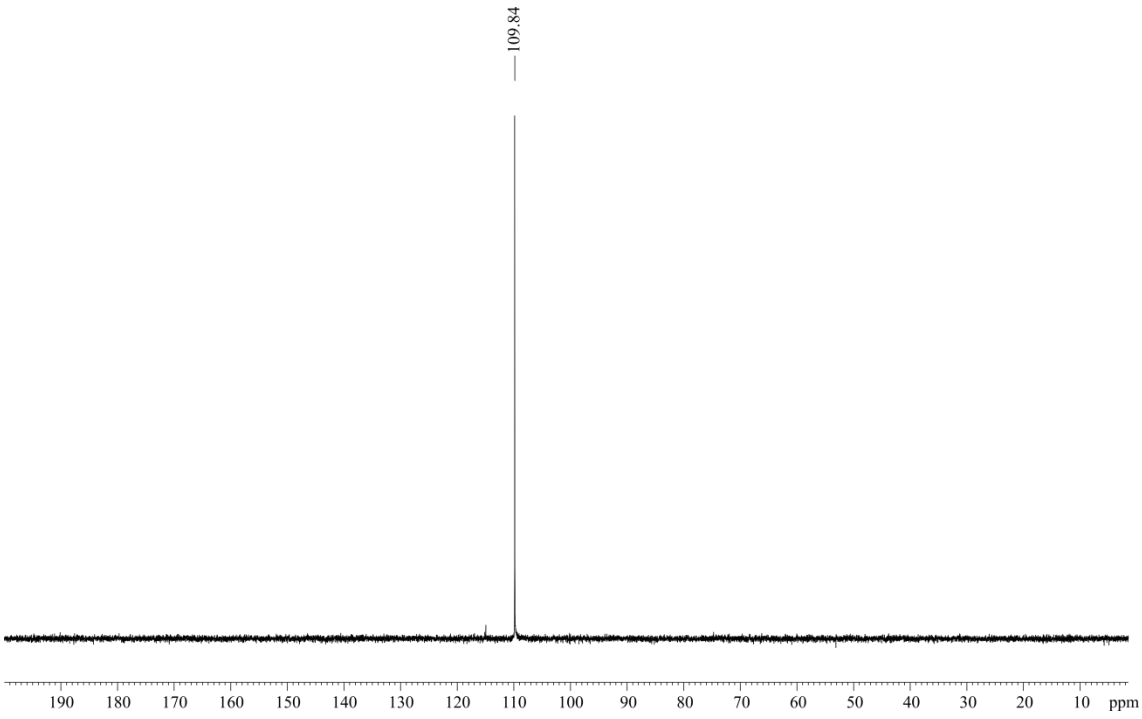

Figure S9. $^{31}P\{^{1}H\}$ NMR spectrum for compound **8a**.

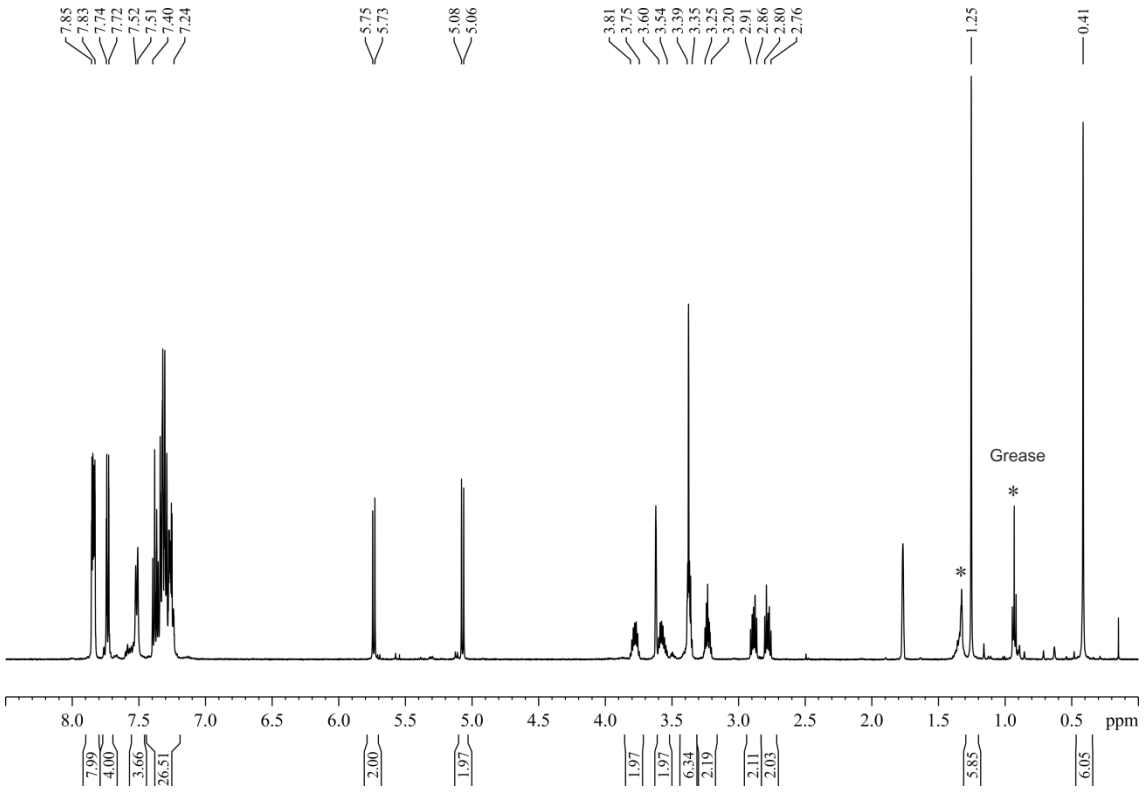

Figure S10. ^{1}H NMR spectrum for compound **8c**.

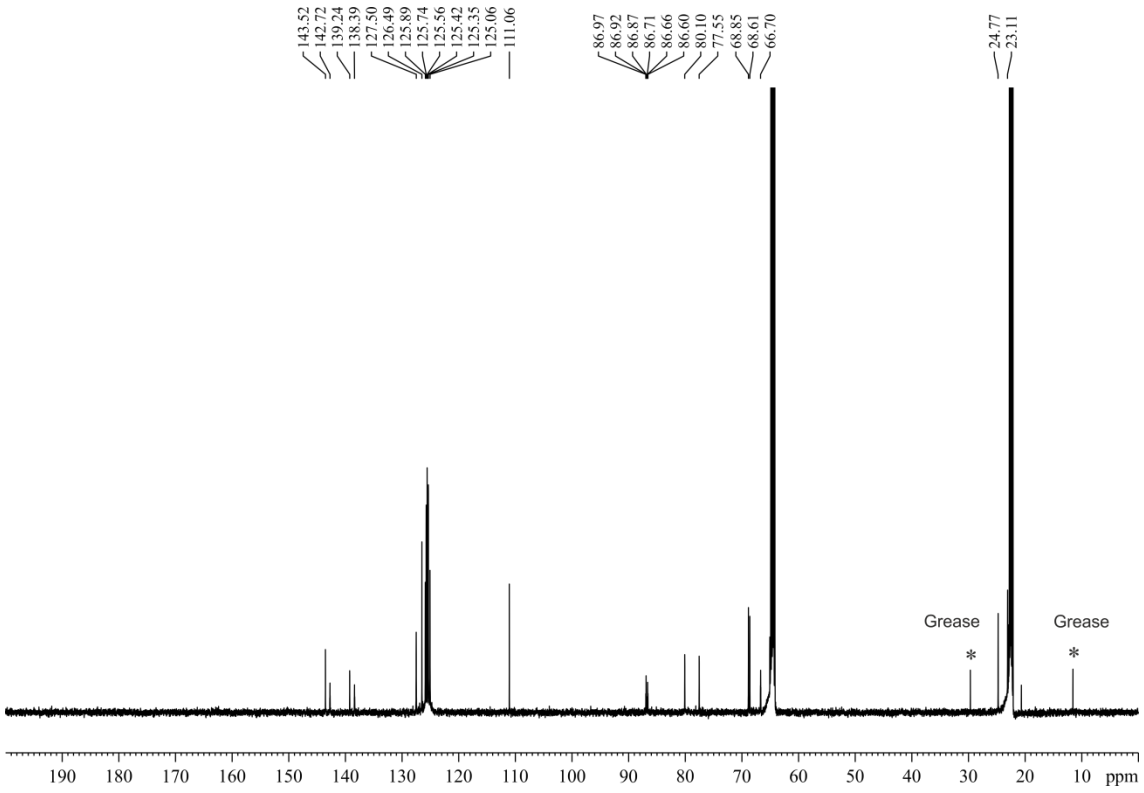

Figure S11. $^{13}C\{^{1}H\}$ NMR spectrum for compound **8c**.

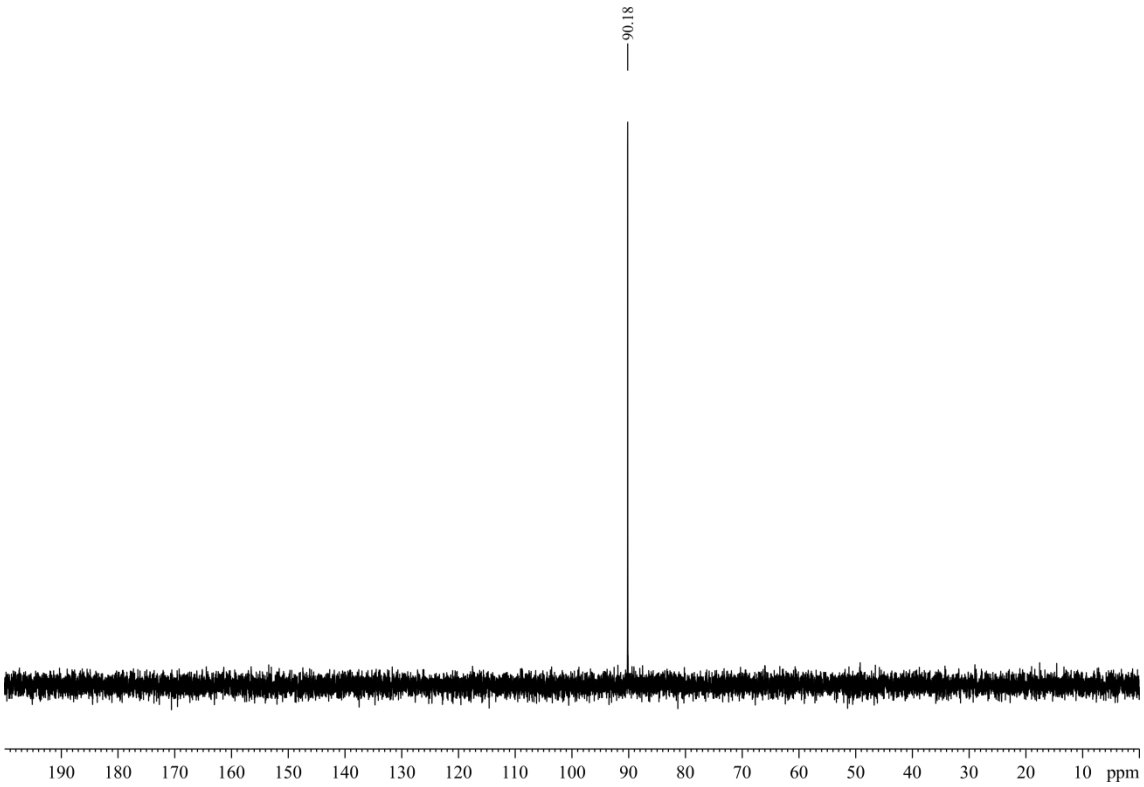

Figure S12. $^{31}P\{^{1}H\}$ NMR spectrum for compound **8c**.

2.7. References

1) For selected reviews, see: (a) Raynal, M.; Ballester, P.; Vidal-Ferran, A.; van Leeuwen, P. W. N. M. *Chem. Soc. Rev.* **2014**, *43*, 1660–1733. (b) Raynal, M.; Ballester, P.; Vidal-Ferran, A.; van Leeuwen, P. W. N. M. *Chem. Soc. Rev.* **2014**, *43*, 1734–1787.

2) (a) Gianneschi, N. C.; Bertin, P. A.; Nguyen, S. T.; Mirkin, C. A.; Zakharov, L. N.; Rheingold, A. L. *J. Am. Chem. Soc.* **2003**, *125*, 10508–10509. (b) Gianneschi, N. C.; Cho, S.-H.; Nguyen, S. B. T.; Mirkin, C. A. *Angew. Chem. Int. Ed. Engl.* **2004**, *43*, 5503–5507. (c) Sud, D.; Norsten, T. B.; Branda, N. R. *Angew. Chem. Int. Ed.* **2005**, *44*, 2019–2021. (d) Wang, J.; Feringa, B. L. *Science* **2011**, *331*, 1429–1432.

3) (a) Bellini, R.; Chikkali, S. H.; Berthon-Gelloz, G.; Reek, J. N. H. *Angew. Chem., Int. Ed.* **2011**, *50*, 7342–7345. (b) Bellini, R.; Reek, J. N. H. *Chem. –Eur. J.* **2012**, *18*, 7091–7099. (c) Bellini, R.; Reek, J. N. H. *Chem.-Eur. J.* **2012**, *18*, 13510–13519.

4) (a) Mon, I.; Jose, D. A.; Vidal-Ferran, A. *Chem. –Eur. J.* **2013**, *19*, 2720–2725. (b) Vidal-Ferran, A.; Mon, I.; Bauza, A.; Frontera, A.; Rovira, L. *Chem. –Eur. J.* **2015**, *21*, 11417–11426. (c) Rovira, L.; Vaquero, M.; Vidal-Ferran, A. *J. Org. Chem.* **2015**, *80*, 10397–10403. (d) Fernández-Pérez, H.; Mon, I.; Frontera, A.; Vidal-Ferran, A. *Tetrahedron* **2015**, *71*, 4490–4494.

5) (a) Clarke, M. L.; Fuentes, J. A. *Angew. Chem. Int. Ed.* **2007**, *46*, 930–933. (b) Li, Y.; Ma, B.; He, Y.; Zhang, F.; Fan, Q.-H. *Chem. Asian J.* **2010**, *5*, 2454–2458. (c) van Leeuwen, P. W. N. M.; Rivillo, D.; Raynal, M.; Freixa, Z. *J. Am. Chem. Soc.* **2011**, *133*, 18562–18565. (d) Dydio, P.; Rubay, C.; Gadzikwa, T.; Lutz, M.; Reek, J. N. H. *J. Am. Chem. Soc.* **2011**, *133*, 17176–17179. (e) Song, F.-T.; Ouyang, G.-H.; Li, Y.; He, Y.-M.; Fan, Q.-H. *Eur. J. Org. Chem.* **2014**, 6713–6719. f) Ouyang, G.-H.; He, Y.-M.; Fan, Q.-H. *Chem. –Eur. J.* **2014**, *20*, 16454–16457.

6) For selected contributions, see: (a) Trost, B. M.; Lee. C. Asymmetric Carbon-Carbon Bond-Forming Reactions: Asymmetric Allylic Alkylation Reactions. In *Catalytic Asymmetric Synthesis*; Ojiwa, I., Ed.; Wiley-VCH: New York, 2000, Vol. 8e, pp 593–649. (b) Trost, B. M.; Zhang, T.; Sieber, J. D. *Chem. Sci.* **2010**, *1*, 427–440.

7) For selected contributions see: (a) Trost, B. M.; Crawley, M. L. *Chem. Rev.* **2003**, *103*, 2921–2944. (b) Gavrilov, K. N.; Bondarev, O. G.; Polosukhin, A. I. *Russ. Chem. Rev.* **2004**, *73*, 671–699. (c) Takacs, J. M.; Reddy, D. S.; Moteki, S. A.; Wu, D.; Palencia, H. *J. Am. Chem. Soc.* **2004**, *126*, 4494–4495. (d) Lu, Z.; Ma, S. *Angew. Chem., Int. Ed.* **2008**, *47*, 258–297. (e) Diéguez, M.; Pàmies, O. *Acc. Chem. Res.* **2010**, *43*, 312–322. (f) Grabulosa, A.; Doran, S.; Brandariz, G.; Muller, G.; Benet-Buchholz, J.; Riera, A.; Verdaguer, X. *Organometallics* **2014**, *33*, 692–701.

8) (a) El Gihani, M. T.; Heaney, H. *Synthesis* **1998**, 357–375. (b) Trost, B. M.; Murphy, D. J. *Organometallics* **1985**, *4*, 1143–1145.

9) Reetz, M. T.; Mehler, G.; Bondarev, O. *Chem. Commun.* **2006**, 2292–2294.

10) Jose, D. A.; Mon, I.; Fernández-Pérez, H.; Escudero-Adan, E. C.; Benet-Buchholz, J.; Vidal-Ferran, A. *Org. Lett.* **2011**, *13*, 3632–3635.

11) The $^{31}P\{^{1}H\}$ NMR chemical shift for **8a** is similar to that previously reported for a related Pd-complex. See: Sheff, J. T.; Lucius, A. L.; Owens, S. B.; Gray, G. M. *Organometallics* **2011**, *30*, 5695–5709.

12) See Section 2.6 for details.

13) Wassenaar, J.; de Bruin, B.; Reek, J. N. H. *Organometallics* **2010**, *29*, 2767–2776.

14) Popa, D.; Puigjaner, C.; Gómez, M.; Benet-Buchholz, J.; Vidal-Ferran, A.; Pericàs, M. A. *Adv. Synth. Catal.* **2007**, *349*, 2265–2278.

15) Popa, D.; Marcos, R.; Sayalero, S.; Vidal-Ferran, A.; Pericàs, M. A. *Adv. Synth. Catal.* **2009**, *351*, 1539–1556.

16) Data collection with: *APEX II* versions v1.0-22, v2009.1–0 and v2009.1–02, Bruker AXS Inc., Madison, Wisconsin, USA, 2007.

17) Data reduction with: *SAINT* versions V.2.10, V/.60A and V7.60A, Bruker AXS Inc., Madison, Wisconsin, USA, 2003/2007.

18) *SADABS*, V.2.10, V2008 and V2008/1, Bruker AXS Inc., Madison, Wisconsin, USA, 2003/2001, see: Blessing, R. H. *Acta Crystallogr., Sect. A: Found. Crystallogr.* **1995**, *A51*, 33–38.

19) *SHELXTL*, versions V6.12 and 6.14, see: Sheldrick, G. M. *Acta Crystallogr., Sect. A: Found. Crystallogr.* **2008**, *64*, 112–122.

20) *SQUEEZE* implemented in Platon. Platon: (a) Spek, A. L. *J. Appl. Crystallogr.* **2003**, *36*, 7–13; *SQUEEZE*: (b) Van der Sluis, P.; Spek, A. L. *Acta Crystallogr., Sect. A: Found. Crystallogr.* **1990**, *A46*, 194–201.

Chapter 3

Asymmetric Hydroformylation of Heterocyclic Olefins Mediated by Supramolecularly Regulated Rhodium-Bisphosphite Complexes

Chapter 3.

Asymmetric Hydroformylation of Heterocyclic Olefins Mediated by Supramolecularly Regulated Rhodium-Bisphosphite Complexes

J.Org.Chem. **2015**, *80*, 10397−10403

Laura Rovira†, Mónica Vaquero†, and Anton Vidal-Ferran †‡*

†Institute of Chemical Research of Catalonia (ICIQ) & The Barcelona Institute of Science and Technology, Avgda. Països Catalans 16, 43007 Tarragona, Spain.

‡Catalan Institution for Research and Advanced Studies (ICREA), Passeig Lluís Companys 23, 08010 Barcelona, Spain.

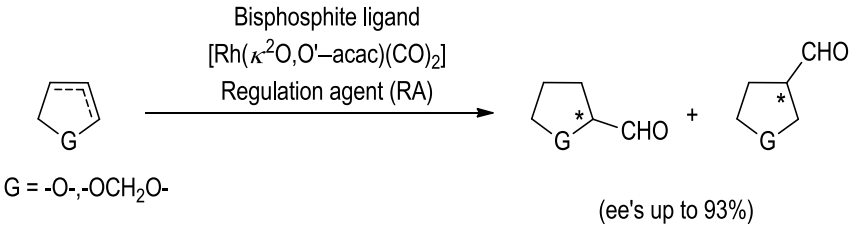

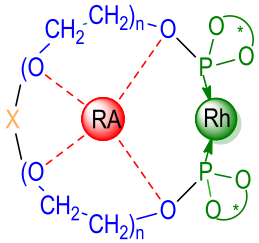

Linker & Regulation site
Catalytic site
RA: Regulation agent

3.1. Abstract

Rhodium complexes derived from conformationally transformable α,ω–bisphosphite ligands combined with a suitable alkali metal BArF salt as a regulation agent (RA) provide high regio- and enantio-selectivities in the asymmetric hydroformylation (AHF) of three heterocyclic olefins. The outcome of the AHF could be exquisitely regulated by choosing the appropriate RA with an increase in the ee, the reversal of the regioselectivity, or the complete suppression of one byproduct.

3.2. Introduction

The development of efficient strategies for generating libraries of enantioselective catalysts with minimal synthetic efforts remains an appealing challenge. Supramolecular interactions have been used to regulate the size, shape and first coordination sphere of a chiral catalyst.[1] However, there are few examples of the fine modification of the geometry of the active site.[2,3] Our group has developed supramolecularly regulated bisphosphite ligands possessing two different structural features: a catalytic site consisting of two identical phosphite fragments and a distal regulation site containing a polyether chain. Ion–dipole interactions between the polyether chain and the regulation agent (RA; *e.g.* alkali metal salts; see Scheme 1) bring the ligating groups together at the metal center.[2] Furthermore, the library of catalysts arising upon the binding of an array of RAs to the regulation site not only preserves most of the structural characteristics but also incorporates structural peculiarities that depend on the size and shape of the RA employed. Hydroformylation is an attractive industrial process requiring transition metal catalysts,[4] from which rhodium complexes derived from bisphosphite ligands have been used with variable success in the hydroformylation of heterocyclic alkenes.[5] Herein, we describe the design and synthesis of new supramolecularly regulated ligands (*R*,*S*)-**L2** and (*S*,*S*)-**L3** (Scheme 1), which incorporate a BINOL motif in the regulation site (BINOL = [1,1'-binaphthalene]-2,2'-diol). We also show that the inclusion of this motif reinforces the regulation ability of the catalysts and leads to efficient AHF catalysts for a number of heterocyclic olefins.

3.3. Results and discussion

The new ligands, (*R*,*S*)-**L2** and (*S*,*S*)-**L3**, were synthesized by *O*-phosphorylation[6] of the corresponding diol derivatives. Ligand (*S*)-**L1**, which lacks a stereogenic element in the regulation site, was also considered in order to aid comparison and was synthesized in an analogous manner (see section 3.5. for the experimental details, synthesis of the ligands and the characterization data).

We first tested the activity of these new ligands in the AHF of benchmark substrates comprising vinyl esters **1a–c**, styrene **1d** and (allyloxy)trimethylsilane **1e** (Scheme 2 and Table 1). Initial studies were performed with [Rh(κ^2O,O´–acac)$(CO)_2$] and the corresponding ligand at 40 °C under 10 bar of syngas in toluene, with the minimum amount of THF to solubilize the RA.[2a-c] The results on AHF are partially summarized in Table 1, which summarizes the results for the catalysts that show the highest positive regulation effects.[7] In the case of vinyl ester derivatives **1a–c**, the reactions performed in the absence of RAs yielded aldehydes with lower conversions than those in which an RA was used. Rhodium complexes derived from ligands (*S*)-**L1** and (*R*,*S*)-**L2** provided highly active catalysts and remarkable enhancements in the enantioselectivity of the hydroformylation of **1a–c** (with increases ranging from 69 to 77% ee; see entries 1–6 in Table 1). The combined use of (*S*,*S*)-**L3** and NaBArF provided the highest enantioselectivity for styrene (b:l ratio = 96:4; 54% ee; see entry 8 in Table 1), whereas the highest enantioselectivities were achieved for compound **1e** with (*S*,*S*)-**L3** and CsBArF (b:l ratio = 18:82; 23% ee; see entry 10 in Table 1).

The principal steric directors in our catalysts are the bisphosphite units, which favor the formation of (*R*)-configured products, although the configuration of the [1,1'-binaphthalene]-2,2'-diol motif in the regulation site is also decisive in obtaining the highest performing ligands.

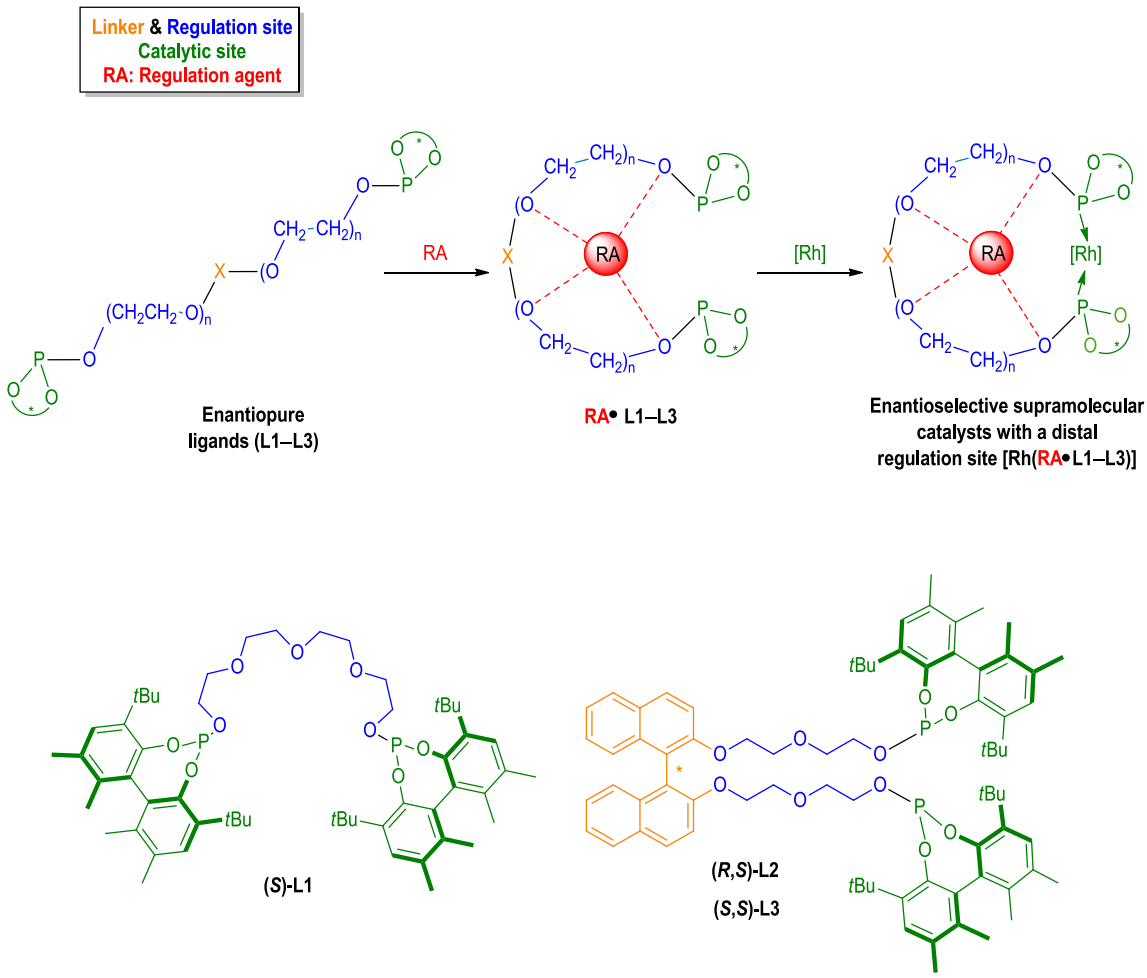

Scheme 1. Supramolecularly regulated bisphosphite ligands with a distal regulation site.

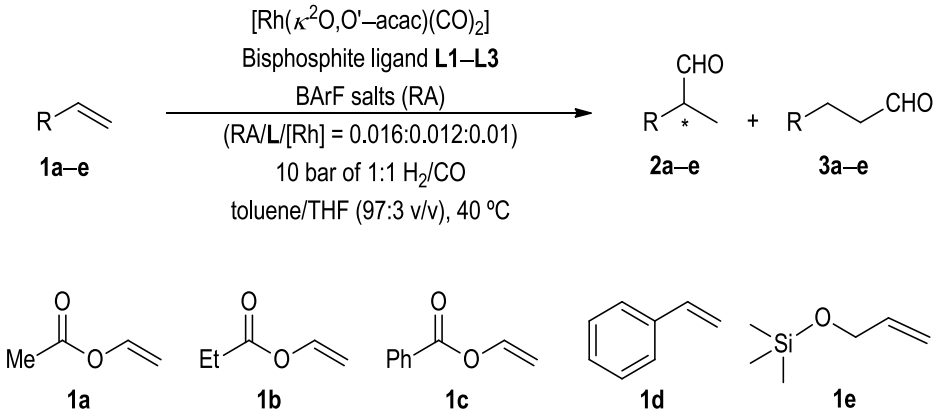

Scheme 2. AHF of compounds **1a**–**e** mediated by supramolecularly regulated ligands **L1**–**L3**.

After testing the AHF of linear substrates with our catalysts, we moved on to the AHF of heterocyclic olefins, given the applicability of enantiopure heterocyclic aldehydes in the synthesis of biologically relevant products.[8] Our group[9] and others have studied the AHF of five-,[5b,8a,10] six-,[10d] and seven-[5b,10a,c] membered heterocyclic olefins and reported problems in the control of chemo- and regio-selectivity.

Table 1. AHF of **1a**–**e** using the catalysts that lead to the highest regulation effects.[a]

Entry	Ligand	Substrate	RA	Conv. (%)	b:l ratio	ee of **2** (%) config.
1	(*R*,*S*)-**L2**	**1a**	-	92	>99:1	23 (*R*)
2			RbBArF	>99	>99:1	92 (*R*)
3	(*R*,*S*)-**L2**	**1b**	-	94	>99:1	15 (*R*)
4			KBArF	>99	>99:1	92 (*R*)
5	(*S*)-**L1**	**1c**	-	90	>99:1	7 (*S*)
6			NaBArF	78	98:2	76 (*R*)
7	(*S*,*S*)-**L3**	**1d**	-	>99	95:5	42 (*R*)
8			NaBArF	>99	96:4	54 (*R*)
9	(*S*,*S*)-**L3**	**1e**	-	>99[b]	61:39[b]	17 (*R*)
10			CsBArF	>99[b]	18:82[b]	23 (*R*)

[a] Reaction conditions are shown in Scheme 2. Conversion was determined by GC chromatography (*β*-Dex 225) using *n*-dodecane as internal standard unless otherwise stated. The ratio of the regioisomers and ee values were determined by GC analysis on a chiral stationary phase (*β*-Dex 225) unless otherwise stated. Absolute configurations were assigned by comparing the elution order in GC analysis with reported data (for details, see section 3.5). [b] Conversion and regioselectivity were determined by ^{1}H NMR.

In the AHF of 2,5-dihydrofuran, the expected tetrahydrofuran-3-carbaldehyde (**6**), the regioisomeric aldehyde **5**, and 2,3-dihydrofuran (**7**) can be formed (Scheme 3 and Table 2). The latter compound arises from a C=C bond isomerization that occurs simultaneously with the hydroformylation.[11]

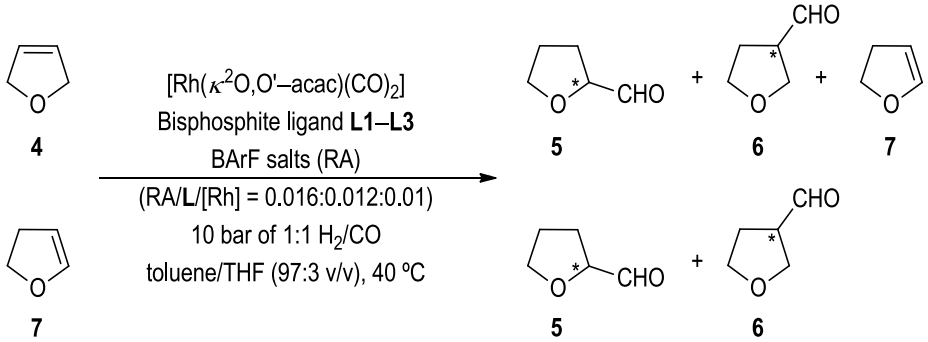

Scheme 3. AHF of **4** and **7** mediated by supramolecularly regulated ligands **L1**–**L3**.

Supramolecularly regulated ligands **L1**–**L3** proved to be very active in the AHF of 2,5-dihydrofuran (with conversions ranging from 92 to >99%; Table 2). In the reactions performed without an RA, carbaldehyde **6** was obtained as the major product, although in poor enantioselectivities (from 36 to 38% ee; Table 2), together with small amounts of isomerization product **7** (from 5 to 9%; see entries 1, 6 and 11 in Table 2). The combined use of (*R*,*S*)-**L2** with KBArF as the RA had several major effects in the outcome of the reaction. First, the use of ligand (*R*,*S*)-**L2** and KBArF brought about a reversal of regioselectivity in favor of tetrahydrofuran-2-carbaldehyde (**5**:**6** ratio from 1:92 to 35:39; compare entries 6 and 8 in Table 2); second, they induced a change in the configuration of the final product and an increase in the ee (from 11% ee in favor of (*S*)-**5** to 82% ee in favor of (*R*)-**5**; compare entries 6 and 8 in Table 2). It is interesting that the reversal of regioselectivity was associated with major amounts of isomerization product **7** (from 7 to 26%; compare entries 6 and 8 in Table 2).

Table 2. AHF of **4** using Rh-complexes of ligands **L1**–**L3** and a set of BArF salts as RAs.[a]

Entry	Ligand	RA	Conv. (%)	ratio **5**:**6**:**7**	ee of **5** (%) config.	ee of **6** (%) config.
1	(*S*)-**L1**	-	>99	2:93:5	23 (*S*)	38 (*R*)
2		NaBArF	92	5:73:22	60 (*R*)	61 (*S*)
3		KBArF	>99	21:15:64	74 (*R*)	60 (*S*)
4		RbBArF	>99	25:31:44	77 (*R*)	21 (*S*)
5		CsBArF	>99	13:72:15	52 (*R*)	15 (*R*)
6	(*R*,*S*)-**L2**	-	>99	1:92:7	11 (*S*)	36 (*R*)
7		NaBArF	98	1:91:8	2 (*S*)	25 (*R*)
8		KBArF	>99	35:39:26	82 (*R*)	56 (*S*)
9		RbBArF	>99	34:26:40	81 (*R*)	52 (*S*)
10		CsBArF	>99	19:38:43	76 (*R*)	14 (*S*)
11	(*S*,*S*)-**L3**	-	98	1:90:9	10 (*S*)	38 (*R*)
12		NaBArF	>99	1:97:2	34 (*S*)	42 (*R*)
13		KBArF	96	3:85:12	18 (*R*)	2 (*S*)
14		RbBArF	93	4:69:27	45 (*R*)	13 (*S*)
15		CsBArF	97	5:70:25	43 (*R*)	18 (*R*)

[a] See footnote a in Table 1 for details, with the following remarks: Reaction conditions are shown in Scheme 3, and the amount of **7** was determined by ^{1}H NMR.

To gain more information about this complex transformation, the hydroformylation of 2,3-dihydrofuran under the same conditions was also studied (see Scheme 3 and Table 3). Substrate **7** reacted more slowly than compound **4** under the same reaction conditions, with or without an RA (conversion from 7 to 89%; Table 3). The use of an RA increased activity in almost all the examples tested. The major product of the hydroformylation of **7** was tetrahydrofuran-2-carbaldehyde (**5**) in moderate to high enantioselectivities (*e.g.*, (*R*,*S*)-**L2** and KBArF led to 81% ee in favor of (*R*)-**5**; entry 8 in Table 3).

Table 3. AHF of **7** using Rh-complexes of ligands **L1**–**L3** and a set of BArF salts as RAs.[a]

Entry	Ligand	RA	Conv. (%)	ratio **5**:**6**:**7**	ee of **5** (%) config.	ee of **6** (%) config.
1	(*S*)-**L1**	-	7	2:5:93	5 (*S*)	26 (*S*)
2		NaBArF	31	18:13:69	62 (*R*)	44 (*R*)
3		KBArF	23	21:2:77	76 (*R*)	8 (*S*)
4		RbBArF	39	34:5:61	79 (*R*)	2 (*S*)
5		CsBArF	89	57:32:11	56 (*R*)	6 (*S*)
6	(*R*,*S*)-**L2**	-	32	12:20:68	13 (*S*)	16 (*S*)
7		NaBArF	40	17:23:60	3 (*S*)	8 (*R*)
8		KBArF	65	52:13:35	81 (*R*)	20 (*R*)
9		RbBArF	57	48:9:43	79 (*R*)	10 (*R*)
10		CsBArF	40	33:7:60	75 (*R*)	*rac*
11	(*S*,*S*)-**L3**	-	29	10:19:71	11 (*S*)	14 (*S*)
12		NaBArF	31	11:20:69	24 (*S*)	15 (*S*)
13		KBArF	50	30:20:50	19 (*R*)	*rac*
14		RbBArF	32	22:10:68	44 (*R*)	13 (*S*)
15		CsBArF	28	19:9:72	44 (*R*)	16 (*S*)

[a] See footnote a in Table 1 for details, with the following remarks: Reaction conditions are shown in Scheme 3, and the amount of **7** was determined by ^{1}H NMR.

To minimize the formation of isomerization product **7** and enhance regioselectivity toward carbaldehyde **5**, we decided to study the effect of variable amounts of H_2 and CO in the syngas mixture on the outcome of the AHF of **4**. We also hoped to be able to identify the AHF conditions that leading to carbaldehyde **5** as the most abundant product. These studies were performed with ligand (*R*,*S*)-**L2** and KBArF, as their combined use provided the best results in terms of enantioselectivity for product **5** (see entry 8 in Table 2).

The AHF of **4** at 10 bar employing a 1:1 H_2/CO mixture led to **5** in a selectivity of 35% with 82% ee, together with the formation of **7** with a selectivity of 26%. Independently of the total pressure employed in the AHF, increasing the amount of H_2 with respect to CO led to an increase in selectivity toward **5** and a reduction in the amount of isomerization product **7** (see Table S6 and Figure S22 in section 3.6.3).[12] One of the most attractive AHF conditions was obtained at 5 bar with a 4:1 H_2/CO mixture, under which **7** was not detected and carbaldehyde **5** was formed with a selectivity of 71% with 69% ee (Figure 1).

Ligands **L1**–**L3** were also tested in the AHF of six-membered heterocyclic olefins (see section 3.6.3) for the substrates studied and results obtained). Unfortunately our catalysts were not active in the AHF of these types of compounds. It has already been reported in the literature that these substrates normally require harsh reaction conditions in AHF, which reduce control of regio- and enantio-selectivity.[11]

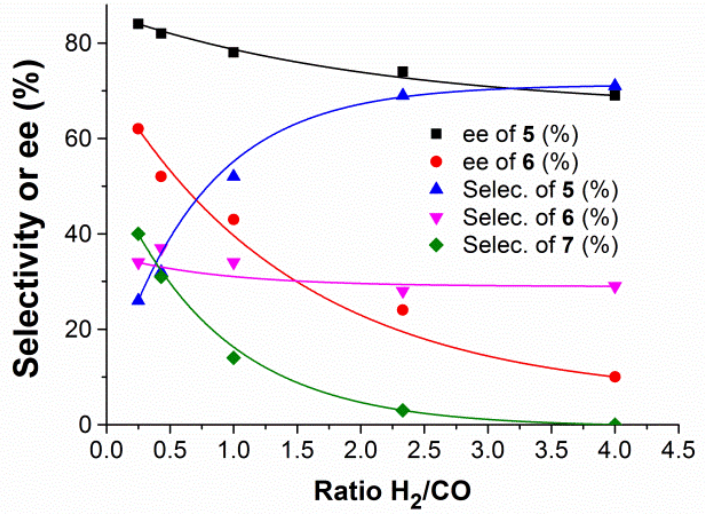

Figure 1. AHF of **4** at 5 bar with different syngas mixtures.

Finally, ligands (*S*)-**L1**, (*R*,*S*)-**L2** and (*S*,*S*)-**L3** were tested in the AHF of *cis*-4,7-dihydro-1,3-dioxepin (**8**) with a set of alkali BArF salts as RAs (see Scheme 4 and Table 4).

The reactions showed complete regioselectivity toward product **9** (see Table 4 and Table S8). The use of RAs led to a great improvement in the conversion (up to 82%) and enantioselectivity (up to 79%). The highest enantioselectivities were obtained with combinations (*S*)-**L1**/NaBArF (85% ee), (*R*,S)-**L2**/KBArF (83% ee), and (*S*,*S*)-**L3**/RbBArF (74% ee) (entries 2, 5, and 8, respectively, in Table 4). In order to increase the enantioselectivity, these reactions were performed at room temperature (entries 3, 6, and 9 in Table 4). Improvements ranging from 7 to 15% in the ee were observed, with the combination (*R*,*S*)-**L2**/KBArF being the best for this transformation. Carbaldehyde **9** was obtained with an excellent enantioselectivity (93% ee), which, to the best of our knowledge, is the highest reported for this substrate.[10a]

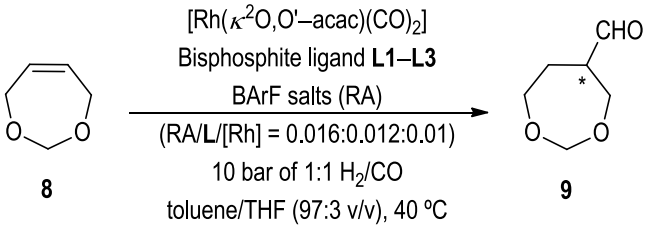

Scheme 4. AHF of **8** mediated by supramolecularly regulated ligands **L1**–**L3**.

Table 4. AHF of **8** using Rh-complexes of ligands **L1**–**L3** and a set of BArF salts as RAs.[a]

Entry	Ligand	RA	Conv. (%)	ee of **9** (%) config.[b]
1	(*S*)-**L1**	-	28	6 (+)
2		NaBArF	>99	85 (+)
3[c]		NaBArF	95	92 (+)
4	(*R*,*S*)-**L2**	-	23	10 (–)
5		KBArF	>99	83 (+)
6[c]		KBArF	>99	93 (+)
7	(*S*,*S*)-**L3**	-	17	*rac*
8		RbBArF	>99	74 (+)
9[c]		RbBArF	93	89 (+)

[a] See footnote a in Table 1 for details, with the following remarks: Reaction conditions are shown in Scheme 4. [b] Absolute configuration is unknown, and the sign of the optical rotation is provided. [c] Reaction performed at 25°C.

To elucidate the structure of the catalytic species, complexation experiments between [Rh(κ^2O,O´–acac)(CO_2)], ligand (*R*,*S*)-**L2**, and one representative RA (KBArF) were performed. These compounds were reacted at 40 °C under 10 bar of 1:1 H_2/CO. Interestingly, the expected hydrido-dicarbonyl chelate [Rh(H)$(CO)_2$(κ^2P,P´–KBArF•(*R*,*S*)-**L2**)] was efficiently formed.[13] NMR analysis showed the hydrido signal as a broad and partially resolved multiplet centered at –10.38 ppm ($^2J_{PH}$ = 22 Hz). The value of this coupling constant indicates that the system undergoes an equilibrium between hydrido–dicarbonyl rhodium complexes with the two P-ligating groups coordinated in an equatorial–equatorial or apical–equatorial fashion to a trigonal–bipyramidal rhodium center (Scheme 5).[14] The complexation behavior of ligand (*R*,*S*)-**L2** is different from that of ligand (*S*)-**L1**, which lacks the biaryl core in the regulation site. NMR analysis on the hydrido-dicarbonyl chelate derived from (*S*)-**L1** indicated that the two P-ligating groups coordinated in an equatorial–equatorial fashion[14] (see section 3.5 for experimental details and section 3.6.2 for NMR spectra). This difference in coordination behavior between ligands with or without the [1,1'-binaphthalene]-2,2'-diol motif in the regulation site could account for the higher activity of ligand (*R*,*S*)-**L2** in the AHF of heterocyclic alkenes.

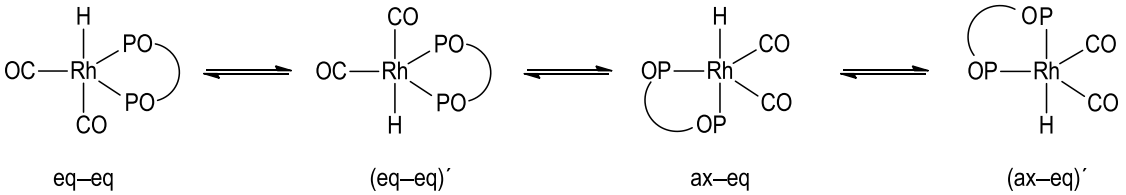

Scheme 5. Coordination modes of bisphosphite ligands in hydrido-dicarbonyl rhodium complexes.

3.4. Conclusions

In summary, challenging heterocyclic olefins were efficiently hydroformylated in terms of high regio- and enantio-selectivities with supramolecularly regulated rhodium complexes derived from bisphosphite ligands **L1**–**L3**. Small amounts of polyether-binder RAs were shown to regulate the activity of the AHF catalysts. The distribution of the enantiomers was biased in some examples (rhodium complexes of a ligand and an RA enabled up to 86% higher enantioselectivities compared with those obtained in the reactions of the corresponding complexes without an RA). In the AHF of 2,5-dihydrofuran, we have demonstrated the potential of our supramolecularly regulated catalysts, as the use of an alkali metal BArF salt as RA increased enantioselectivity (up to 33% ee), reversed the regioselectivity of the reaction, or completely suppressed the formation of the side-product.

3.5. Experimental section

General information: All syntheses were carried out using chemicals as purchased from commercial sources unless otherwise cited. All manipulations and reactions were performed under an inert atmosphere. Glassware was dried *in vacuo* before use with a hot air gun. All solvents were dried and deoxygenated by using a solvent purification system (SPS). Silica gel 60 (230–400 mesh) or Silica-C18 (200–400 mesh) were used for column chromatography. NMR spectra were recorded in $CDCl_3$ unless otherwise cited. ^{1}H and ^{13}C NMR chemical shifts are quoted in ppm relative to residual solvent peaks, whereas ^{31}P NMR chemical shifts are quoted in ppm relative to 85% phosphoric acid in water. IR spectra were recorded using attenuated total reflection (ATR) unless otherwise cited. High-resolution mass spectra (HRMS) were recorded using an electrospray ionization (ESI) method in positive mode for the ligands (**L1**–**L3**) and matrix-assisted laser desorption ionization (MALDI) in positive mode for [Rh(H)(CO)$_2$(κ^2P,P′–KBArF•(*S*)-**L1**)] and [Rh(H)(CO)$_2$(κ^2P,P′–KBArF•(*R*,*S*)-**L2**)], using, in all cases, a time-of-flight (TOF) detector. Melting points were determined in open capillaries and are uncorrected. Enantiomeric excesses were determined by GC equipped with a FID detector using chiral stationary phases.

Synthesis of ligand (*S*)-L1: (*S*)-5,5'-6,6′-Tetramethyl-3,3′-di-*tert*-butyl-1,1'-biphenyl-2,2'-diol (265 mg, 0.75 mmol) was azeotropically dried with toluene (3 × 2 mL), dissolved in anhydrous toluene (*ca.* 10 mL), and slowly added to a stirred solution of PCl_3 (82.4 μL, 0.94 mmol) and NEt_3 (297 μL, 2.14 mmol) in dry toluene (*ca.* 10 mL) at 0 °C. The solution was allowed to reach room temperature and was stirred overnight. The turbid reaction mixture was filtered, and the solvent was evaporated under reduced pressure. The resulting residue was dissolved in *ca*. 10 mL of dry toluene and NEt_3 (297 μL, 2.14 mmol). A solution of the tetraethylenglycol (66.8 mg, 0.34 mmol in *ca*. 10 mL of toluene) was slowly added to the previous solution, and the mixture was allowed to react overnight at room temperature. The reaction mixture was filtered, and the solvent was evaporated under reduced pressure. The resulting crude mixture was purified by column chromatography on silica gel C18 using acetonitrile/EtOAc 1:1 as the elution

solvent to obtain the expected bisphosphite ligand (*S*)-**L1** as a white solid. Isolated 312 mg, 83% yield. ^{1}H NMR ($CDCl_3$, 500 MHz): δ 7.15 (s, 2H), 7.11 (s, 2H), 3.96–3.91 (m, 2H), 3.60–3.55 (m, 8H), 3.54–3.48 (m, 6H), 2.25 (s, 6H), 2.24 (s, 6H), 1.85 (s, 6H), 1.78 (s, 6H), 1.45 (s, 18H), 1.42 (s, 18H). ^{13}C{^{1}H,^{31}P} NMR ($CDCl_3$, 125 MHz): δ 145.5, 145.5, 138.2, 138.2, 137.0, 135.1, 134.5, 132.5, 131.9, 131.8, 131.7, 130.8, 130.8, 128.2, 127.9, 71.0, 70.9, 70.7, 63.6, 63.6, 34.8, 34.8, 31.5, 31.5, 31.3, 20.6, 16.9, 16.7. ^{31}P{^{1}H} NMR ($CDCl_3$, 202 MHz): δ 132.6 (s). HRMS–ESI–TOF (*m/z*): $[M + Na]^+$ calcd for $C_{56}H_{80}O_9P_2Na$, 981.5170; found, 981.5191. $[\alpha]_D^{25}$= +371.8 (*c* 0.1, DCM). IR (neat, cm^{-1}) $\tilde{\upsilon}$ 2963, 2867, 1254, 1027, 870. mp 71.2–72.6 °C.

Synthesis of ligand (*R,S*)-L2: A mixture of (*R*)-[1,1'-binaphthalene]-2,2'-diol (1.75 g, 6.13 mmol), 2-(2-hydroxyethoxy)ethyl-4-methylbenzenesulfonate[15] (3.19 g, 12.3 mmol), and K_2CO_3 (3.64 g, 26.3 mmol) in dry acetonitrile (53 mL) was refluxed for 72 h. The reaction mixture was filtered and then concentrated under reduced pressure. The crude product was purified by column chromatography over silica gel (EtOAc/MeOH 95:5 as eluent) to afford the desired product, (*R*)-2,2'-((([1,1'-binaphthalene]-2,2'-diylbis(oxy))bis(ethane-2,1-diyl))bis(oxy))diethanol ((*R*)-**D1**; see section 3.6.1 for the spectra) as a clear brown oil. Isolated 1.33 g, 46% yield. ^{1}H NMR ($CDCl_3$, 500 MHz,): δ 7.95 (d, *J* = 9.1 Hz, 2H), 7.87 (d, *J* = 8.1 Hz, 2H), 7.43 (d, *J* = 9.1 Hz, 2H), 7.35–7.32 (m, 2H), 7.24–7.21 (m, 2H), 7.16 (s, 1H), 7.14 (s, 1H), 4.17–4.13(m, 2H), 4.03–3.99 (m, 2H), 3.53–3.49 (m, 2H), 3.45–3.38 (m, 6H), 3.22–3.15 (m, 4H), 2.56 (t, *J* = 6.6 Hz, 2H). ^{13}C{^{1}H} NMR ($CDCl_3$, 125 MHz): δ 154.4, 134.2, 129.6, 129.5, 128.0, 126.5, 125.6, 123.9, 120.8, 116.1, 72.5, 70.0, 69.7, 61.7. HRMS–ESI–TOF (*m/z*): $[M + Na]^+$ calcd for $C_{28}H_{30}NaO_6$, 485.1935; found, 485.1923. $[\alpha]_D^{25}$= +43.1 (*c* 0.1, DCM). IR (neat, cm^{-1}) $\tilde{\upsilon}$ 3414, 2927, 2869, 1240, 1054. Ligand (*R,S*)-**L2** was synthesized from (*S*)-5,5'-6,6´-Tetramethyl-3,3´-di-*tert*-butyl-1,1'-biphenyl-2,2'-diol (424 mg, 1.2 mmol), which was azeotropically dried with toluene (3 × 2 mL) under argon atmosphere. The remaining solid was dissolved in anhydrous toluene (*ca.* 20 mL) and slowly added to a stirred solution of PCl_3 (132 μL, 1.51 mmol) and NEt_3 (476 μL, 3.42 mmol) in dry toluene (*ca.* 20 mL) at 0 °C. The solution was allowed to reach room temperature and was stirred overnight. The turbid reaction mixture was filtered, and the solvent was evaporated under reduced pressure. The resulting residue was dissolved in *ca.* 20 mL of dry toluene and NEt_3 (476 μL, 3.42 mmol). A solution of the diol (*R*)-**D1** (255 mg, 0.55 mmol in *ca.* 20 mL of toluene) was slowly added to the previous solution, and the mixture was allowed to react overnight at room temperature. The reaction mixture was filtered, and the solvent was evaporated under reduced pressure. The resulting crude mixture was purified by column chromatography on silica gel C18 using acetonitrile/EtOAc 1:1 as the elution solvent to obtain the expected bisphosphite ligand (*R,S*)-**L2** as a white solid. Isolated 554 mg, 82% yield, quantitatively pure by ^{31}P NMR. ^{1}H NMR ($CDCl_3$, 400 MHz): δ 7.82 (s, 1H), 7.80 (s, 1H), 7.76 (s, 1H), 7.74 (s, 1H), 7.32 (s, 1H), 7.29 (s, 1H), 7.25–7.24 (m, 1H), 7.23–7.22 (m, 1H), 7.18–7.09 (m, 8H), 4.01–3.99 (m, 4H), 3.56–3.52 (m, 2H), 3.39–3.36 (m, 4H), 3.20–3.14 (m, 2H), 2.94–2.91 (m, 4H), 2.26 (s, 6H), 2.26 (s, 6H), 1.87 (s, 6H), 1.79 (s, 6H), 1.43 (s, 18H), 1.40 (s, 18H).

$^{13}C\{^{1}H,^{31}P\}$ NMR ($CDCl_3$, 125 MHz): δ 154.3, 145.6, 138.2, 137.1, 135.1, 134.4, 134.2, 132.5, 131.9, 131.6, 130.9, 129.5, 129.4, 128.1, 127.9, 127.9, 126.4, 125.6, 123.8, 120.7, 115.8, 70.9, 70.1, 69.5, 63.6, 34.8, 34.8, 31.4, 31.3, 20.6, 20.6, 16.9, 16.7. $^{31}P\{^{1}H\}$ NMR: ($CDCl_3$, 202 MHz) δ 133.8 (s). HRMS–ESI–TOF (*m/z*): [M + Na]$^+$ calcd for $C_{76}H_{92}NaO_{10}P_2$, 1249.6058; found, 1249.6037. $[\alpha]_D^{25}$ = +331.2 (*c* 0.1, DCM). IR (neat, cm^{-1}) $\tilde{\upsilon}$ 2953, 2868, 1227, 1023. mp 89.3– 90.7 °C.

Synthesis of ligand (*S,S*)-L3: A mixture of (*S*)-[1,1'-binaphthalene]-2,2'-diol (2 g, 6.93 mmol), 2-(2-hydroxyethoxy)ethyl-4-methylbenzenesulfonate[15] (3.68 g, 13.9 mmol) and K_2CO_3 (4.12 g, 29.8 mmol) in dry acetonitrile (60 mL) was refluxed for 72 h. The reaction mixture was filtered and then concentrated under reduced pressure. The crude product was purified by column chromatography over silica gel (EtOAc/MeOH 95:5 as eluent) to afford (*S*)-2,2'-((([1,1'-binaphthalene]-2,2'-diylbis(oxy))bis(ethane-2,1-diyl))bis(oxy))diethanol ((*S*)-**D1**, see section 3.6.1 for the spectra) as a clear brown oil. Isolated 1.5 g, 47% yield. ^{1}H NMR ($CDCl_3$, 500 MHz): δ 7.95 (d, *J* = 9.1 Hz, 2H), 7.87 (d, *J* = 8.1 Hz, 2H), 7.43 (d, *J* = 9.1 Hz, 2H), 7.35–7.32 (m, 2H), 7.24–7.21 (m, 2H), 7.15 (s, 1H), 7.14 (s, 1H), 4.17–4.13 (m, 2H), 4.03–3.99 (m, 2H), 3.53–3.49 (m, 2H), 3.45–3.40 (m, 6H), 3.22–3.15 (m, 4H), 2.53 (br s, 2H). $^{13}C\{^{1}H\}$ NMR ($CDCl_3$, 125 MHz): δ 154.4, 134.2, 129.6, 129.5, 128.0, 126.5, 125.6, 124.0, 120.8, 116.1, 72.5, 70.0, 69.7, 61.7. HRMS–ESI–TOF (*m/z*): [M + Na]$^+$ calcd for $C_{28}H_{30}NaO_6$, 485.1935; found, 485.1927. $[\alpha]_D^{25}$= –25.5 (*c* 0.1, DCM). IR (neat, cm^{-1}) $\tilde{\upsilon}$ 3419, 2927, 2869, 1240, 1055. Ligand (*S*,*S*)-**L3** was synthesized following the general strategy. (*S*)-5,5'-6,6´-Tetramethyl-3,3´-di-*tert*-butyl-1,1'-biphenyl-2,2'-diol (600 mg, 1.7 mmol) was azeotropically dried with toluene (3 × 2 mL) under an argon atmosphere, dissolved in anhydrous toluene (*ca*. 23 mL), and slowly added to a stirred solution of PCl_3 (186 μL, 2.13 mmol) and NEt_3 (673 μL, 4.84 mmol) in dry toluene (*ca*. 23 mL) at 0 °C. The solution was allowed to reach room temperature and was stirred overnight. The turbid reaction mixture was filtered, and the solvent was evaporated under reduced pressure. The resulting residue was dissolved in *ca*. 23 mL of dry toluene and NEt_3 (673 μL, 4.84 mmol). A solution of the diol (*S*)-**D1** (360 mg, 0.78 mmol in *ca*. 23 mL of toluene) was slowly added to the previous solution and allowed to react overnight at room temperature. The reaction mixture was filtered, and the solvent was evaporated under reduced pressure. The resulting crude mixture was purified by column chromatography on silica gel C18 using acetonitrile/EtOAc 1:1 as the elution solvent to provide the expected bisphosphite ligand (*S*,*S*)-**L3** as a white solid. Isolated 589 mg, 62% yield, quantitatively pure by ^{31}P NMR. ^{1}H NMR ($CDCl_3$, 500 MHz,): δ 7.83 (s, 1H), 7.81 (s, 1H), 7.77 (s, 1H), 7.75 (s, 1H), 7.30 (s, 1H), 7.28 (s, 1H), 7.27–7.24 (m, 2H), 7.17–7.14 (m, 6H), 7.11 (s, 1H), 7.10 (m, 1H), 4.02–3.97 (m, 4H), 3.52–3.46 (m, 2H), 3.43–3.39 (m, 2H), 3.36–3.31 (m, 2H), 3.20–3.14 (m, 2H), 2.94– 2.90 (m, 2H), 2.84– 2.81 (m, 2H), 2.26 (s, 12H), 1.86 (s, 6H), 1.79 (s, 6H), 1.42 (s, 18H), 1.39 (s, 18H). $^{13}C\{^{1}H,^{31}P\}$ NMR ($CDCl_3$, 125 MHz): δ 154.3, 145.5, 138.2, 137.1, 135.1, 134.4, 134.2, 132.5, 131.9, 131.6, 130.9, 129.5, 129.4, 128.1, 127.9, 127.9, 126.4, 125.6, 123.8, 120.6, 115.7, 70.9, 70.1, 69.5, 63.8, 34.8, 34.8, 31.4, 31.3, 20.6, 17.0, 16.7. $^{31}P\{^{1}H\}$ NMR ($CDCl_3$, 202 MHz): δ 134.7 (s). HRMS–ESI–TOF

(*m/z*): [M + Na]$^+$ calcd for $C_{76}H_{92}NaO_{10}P_2$, 1249.6058; found, 1249.6032. $[\alpha]_D^{25}$ = +279.5 (*c* 0.1, DCM). IR (neat, cm^{-1}) $\tilde{\upsilon}$ 2954, 2867, 1227, 1022. mp 107.9–109.3 °C.

General procedure for Rh-mediated asymmetric hydroformylations

To a 2 mL vial equipped with a magnetic bar in a glovebox filled with nitrogen were added ligand **L1**–**L3** (*ca*. 2.7 μmol in 360 μL of toluene), alkali BArF salt (*ca*. 3.6 μmol in 27 μL of THF), and [Rh(κ^2O,O'-acac)(CO)$_2$] (*ca.* 2.3 μmol in 65 μL of toluene). Substrate (*ca*. 230 μmol) and additional toluene were charged, obtaining the mixture toluene/THF (97:3 v/v) and providing the desired final concentration of substrate, 0.26 M. In the cases of vinyl derivatives (**1a**–**c**) and styrene (**1d**), *n*-dodecane (*ca*. 69 μmol) was added as an internal standard. The vial was transferred into an autoclave and taken out of the glovebox. The autoclave was purged three times with syngas (at a pressure not higher than that required for the reaction) and, finally, the autoclave was pressurized with the corresponding pressure of syngas. The reaction mixture was stirred at 40 °C (water bath) for 18 h. The reaction was cooled, and the pressure was carefully released in a well-ventilated hood.

Determination of enantiomeric excesses and configuration of hydroformylated products

Characterization of hydroformylation products of **1a**–**e**, **4**, **7** and **8** have been described previously in the literature and spectroscopic data were in agreement with those reported.[16] Conversion, regioselectivity and enantiomeric excesses of hydroformylated products of vinyl derivatives (**1a**–**c**) and styrene (**1d**) were determined by GC from the crude mixtures, using *n*-dodecane as an internal standard, with a β-Dex 225 column (30 m × 0.25 mm × 0.25 μm). Conversion and regioselectivity for (allyloxy)trimethylsilane (**1e**) were determined by ^{1}H NMR, and the enantiomeric excesses, by GC analysis with β-Dex 225 column (30 m × 0.25 mm × 0.25 µm) from the crude reaction mixture. Conversion and isomerization of 2,5-dihydrofuran (**4**) and 2,3-dihydrofuran (**7**) were determined by ^{1}H NMR, and the enantiomeric excesses, by GC analysis with β-Dex 225 column (30 m × 0.25 mm × 0.25 µm) from the crude reaction mixture. Conversion and regioselectivity of *cis*-4,7-dihydro-1,3-dioxepin (**8**) were determined by ^{1}H NMR, and enantiomeric excesses, by GC from the crude mixture with a β-Dex 225 column (30 m × 0.25 mm × 0.25 µm).

Optical rotation of aldehyde **9** ($[\alpha]_D^{25}$ = +70.2 (*c* 0.1, THF)) was determined from the reaction mixture with a 93% ee (entry 6 in Table 4) distilling in a Kugelrohr apparatus (40 °C, 5 × 10^{-2} mbar), obtaining aldehyde **9** with a final enantiomeric excess of 91% (^{1}H NMR spectrum and GC chromatogram are available in section 3.6.5).

Vinyl acetate (**1a**):[17] Temperature program: 100 °C for 5 min then 4 °C/min to 160 °C. Retention times: 2.5 min for **1a**, 7.2 min for (*R*)-**2a,** 9.1 min for (*S*)-**2a**, and 12.2 min for **3a**.

Vinyl propionate (**1b**):[16a] Temperature program: Isothermal 100 °C. Retention times: 2.8 min for **1b**, 9.1 min for (*R*)-**2b**, 10.5 min for (*S*)-**2b**, and 21.1 min for **3b**.

Vinyl benzoate (**1c**):[16a] Temperature program: Isothermal 135 °C. Retention times: 6.6 min for **1c**, 25.3 min for (*R*)-**2c**, 27.6 min for (*S*)-**2c**, and 57.3 min for **3c**.

Styrene (**1d**):[17] Temperature program: 100 °C for 5 min then 4 °C/min to 160 °C. Retention times: 4.6 min for **1d**, 12.5 min for (*R*)-**2d**, 12.8 min for (*S*)-**2d**, and 16.3 min for **3d**.

(Allyloxy)trimethylsilane (**1e**):[16d] Temperature program: Isothermal 70 °C. Retention times: 24.5 min for (*R*)-**2e**, and 25.6 min for (*S*)-**2e**.

2,5-dihydrofuran (**4**) and **2,3-dihydrofuran** (**7**):[9] Temperature program: 40 °C for 5 min, 5 °C/min to 150 °C, hold for 1 min, and then 10 °C/min to 210 °C. Retention times: 22.7 min for (*R*)-**5,** and 23.3 min for (*S*)-**5**, 24.7 min for (*S*)-**6**, and 25.6 min for (*R*)-**6**.

***cis*-4,7-dihydro-1,3-dioxepin** (**8**): Temperature program: 40 °C, hold for 5 min, 2 °C/min to 150 °C, hold for 1 min, and then 10 °C/min to 210 °C. Retention times: 48.1 min for (+)-**9** and 49.1 min for (–)-**9**.[18]

Direct formation of [Rh(H)(CO)$_2$(κ^2P,P'–KBArF•(*S*)-L1)]

A 0.03 M solution of (*S*)-**L1** (12.2 mg, 12.7 μmol), [Rh(κ^2O,O'–acac)(CO)$_2$] (3.31 mg, 12.7 μmol) and KBArF (14.2 mg, 16.5 μmol) in C_7D_8/C_4D_8O (97:3 v/v) were transferred to a 25 mL autoclave reactor, which was pressurized to 10 bar of syngas (1:1 H_2/CO) and warmed to 40 °C. The mixture was allowed to stir for 2 h. The reactor was cooled to room temperature and depressurized in a well-ventilated fume hood, and the reaction mixture was transferred to 5 mm HP-NMR sapphire tube. The tube was pressurized with syngas (1:1 H_2/CO, 10 bar) and the HP-NMR spectra were collected at 25 °C (see section 3.6.2). MS samples were immediately recorded under N_2 after depressurizing the autoclave. Spectroscopic data obtained from this solution was in agreement with the quantitative formation of the [Rh(H)(CO)$_2$(κ^2P,P´–KBArF•(*S*)-**L1**)] complex: ^{1}H NMR (C_7D_8/C_4D_8O (97:3 v/v), 500 MHz): δ 7.23 (s, 2H), 7.16 (s, 2H), 3.90–3.88 (m, 2H), 3.37–3.34 (m, 2H), 2.95–2.85 (m, 10H), 2.67–2.64 (m, 2H), 2.11 (s, 6H), 1.98 (s, 6H), 1.65 (s, 6H), 1.58 (s, 6H), 1.52 (s, 18H), 1.48 (s, 18H), –10.83 (d, J_{Rh-H} = 4.8 Hz, 1H). ^{13}C{^{1}H} NMR (C_7D_8/C_4D_8O (97:3 v/v), 125 MHz): δ 191.2, 147.6, 144.5, 136.1, 136.0, 135.7, 134.9, 133.7, 133.5, 130.6, 130.3, 130.0, 129.8, 129.6, 129.1, 126.4, 118.7, 69.6, 69.5, 69.4, 67.0, 35.6, 34.9, 33.0, 31.2, 20.2, 20.0, 16.3, 16.3. ^{31}P NMR (C_7D_8/C_4D_8O (97:3 v/v), 202 MHz): δ 142.6 (d, J_{Rh-P} = 242.9 Hz). HMRS–MALDI–TOF (*m/z*): [M–H–CO– K]$^+$ calcd for $C_{57}H_{80}O_{10}P_2Rh$, 1089.4276, found, 1089.4264. Attempts to isolate this complex in analytically pure form failed.

Direct formation of [Rh(H)(CO)$_2$(κ^2P,P'–KBArF•(*R*,*S*)-L2)]

A 0.02 M solution of (*R*,*S*)-**L2** (11.6 mg, 9.47 μmol), [Rh(κ^2O,O'–acac)(CO)$_2$] (2.47 mg, 9.47 μmol), and KBArF (10.6 mg, 12.3 μmol) in C_7D_8/C_4D_8O (97:3 v/v) were transferred to a 25 mL autoclave reactor, which was pressurized to 10 bar of syngas (1:1 H_2/CO) and warmed to 40 °C. The mixture was allowed to stir for 2 h. The reactor was cooled to room temperature and depressurized in a well-ventilated fume hood, and the reaction mixture was transferred to 5 mm HP-NMR sapphire tube. The tube was pressurized with syngas (1:1 H_2/CO, 10 bar) and the HP-NMR spectra were collected at 25 °C (see section 3.6.2). MS samples were immediately recorded under N_2 after depressurizing the autoclave. Spectroscopic data obtained from this solution was in agreement with the quantitative formation of the [Rh(H)(CO)$_2$(κ^2P,P´–KBArF•(*R*,*S*)-**L2**)] complex: ^{1}H NMR (C_7D_8/C_4D_8O (97:3 v/v), 500 MHz): δ 7.79 (s, 1H), 7.77 (s, 1H), 7.66 (s, 4H), 7.25 (s, 1H), 7.23 (s, 3H), 7.20–7.17 (m, 2H), 7.15 (s, 2H), 7.00 (s, 2H), 3.94-3.92 (m, 2H), 3.51–3.48 (m, 2H), 3.26–3.22 (m, 2H), 3.07–2.97 (m, 4H), 2.75– 2.72 (m, 2H), 2.37–2.35 (m, 2H), 2.24–2.22 (m, 2H), 2.11 (s, 6H), 2.00 (s, 6H), 1.64 (s, 6H), 1.63 (s, 6H), 1.51 (s, 18H), 1.43 (s, 18H), –10.38 (br s, 1H). ^{13}C{^{1}H} NMR (C_7D_8/C_4D_8O (97:3 v/v), 125 MHz): δ 191.1, 154.0, 146.9, 144.3, 136.1, 136.1, 134.4, 133.8, 133.6, 131.5, 131.4, 131.0, 130.0, 130.0, 129.8, 126.4, 126.1, 125.8, 124.2, 123.3, 122.0, 119.6, 71.1, 70.4, 69.7, 66.6, 35.6, 34.8, 32.9, 31.1, 20.1, 20.0, 16.4, 16.3. ^{31}P NMR (C_7D_8/C_4D_8O (97:3 v/v), 202 MHz): δ 143.8 (dd, $J_{Rh\text{-}P}$ = 234.4 Hz; $J_{P\text{-}H}$ = 22.8 Hz). HMRS–MALDI–TOF (*m/z*): [M–H–CO–K]$^+$ calcd for $C_{77}H_{92}O_{11}P_2Rh$, 1357.5164, found, 1357.5135. Attempts to isolate this complex in analytically pure form failed.

3.6. Supporting information

3.6.1. NMR spectra of ligands (*S*)-L1, (*R*,*S*)-L2 and (*S*,*S*)-L3 and synthetic intermediates in their preparation

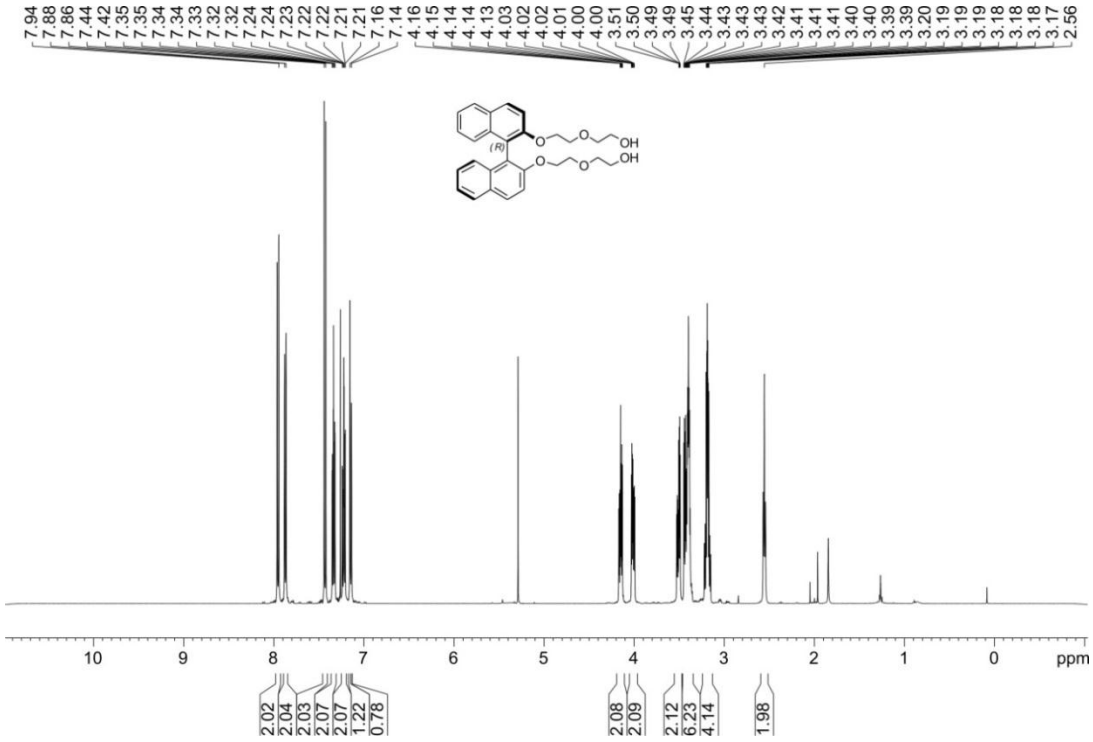

Figure S1. ^{1}H NMR spectrum of diol (*R*)-**D1**.

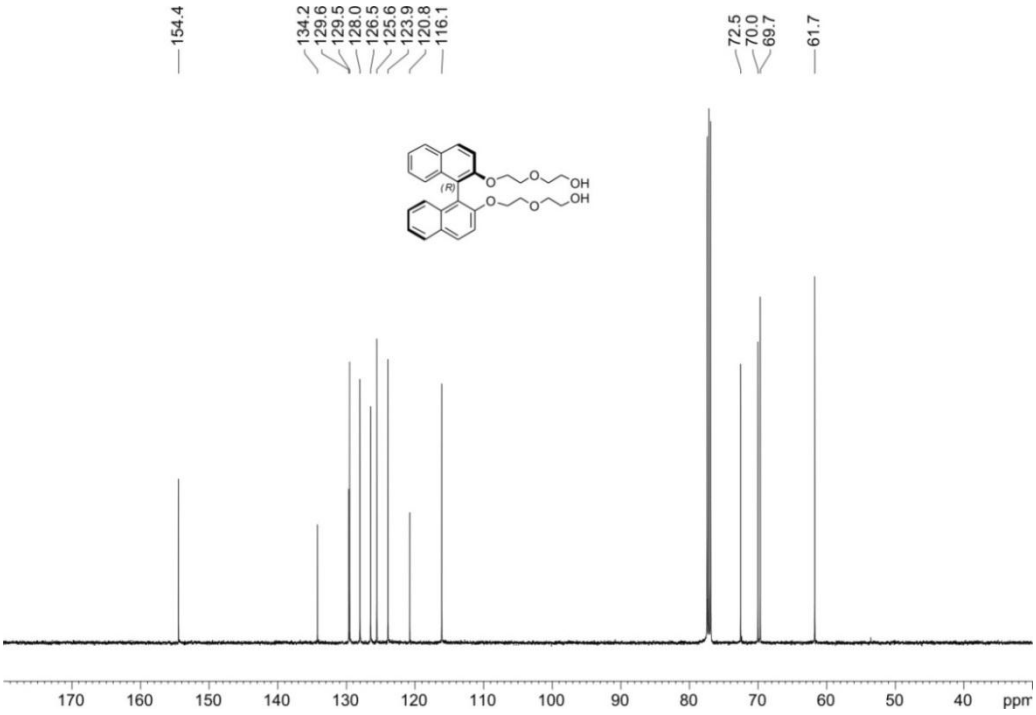

Figure S2. ^{13}C{^{1}H} NMR spectrum of diol (*R*)-**D1**.

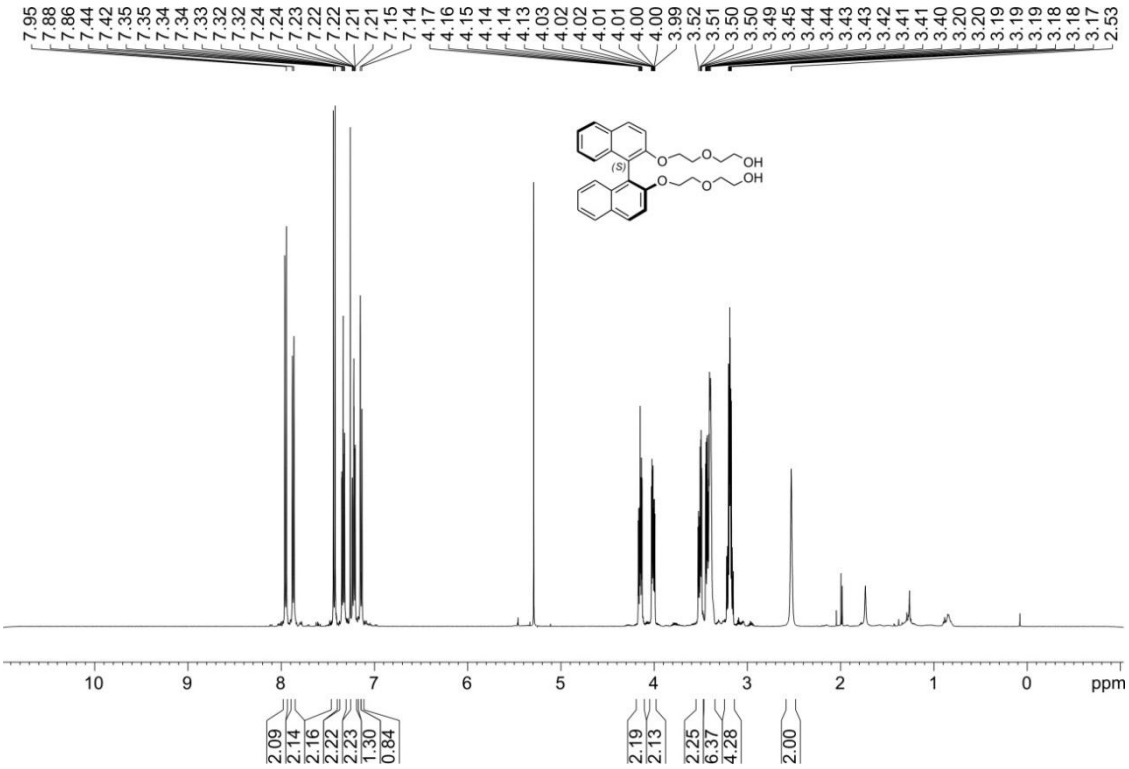

Figure S3. ^{1}H NMR spectrum of diol (*S*)-**D1**.

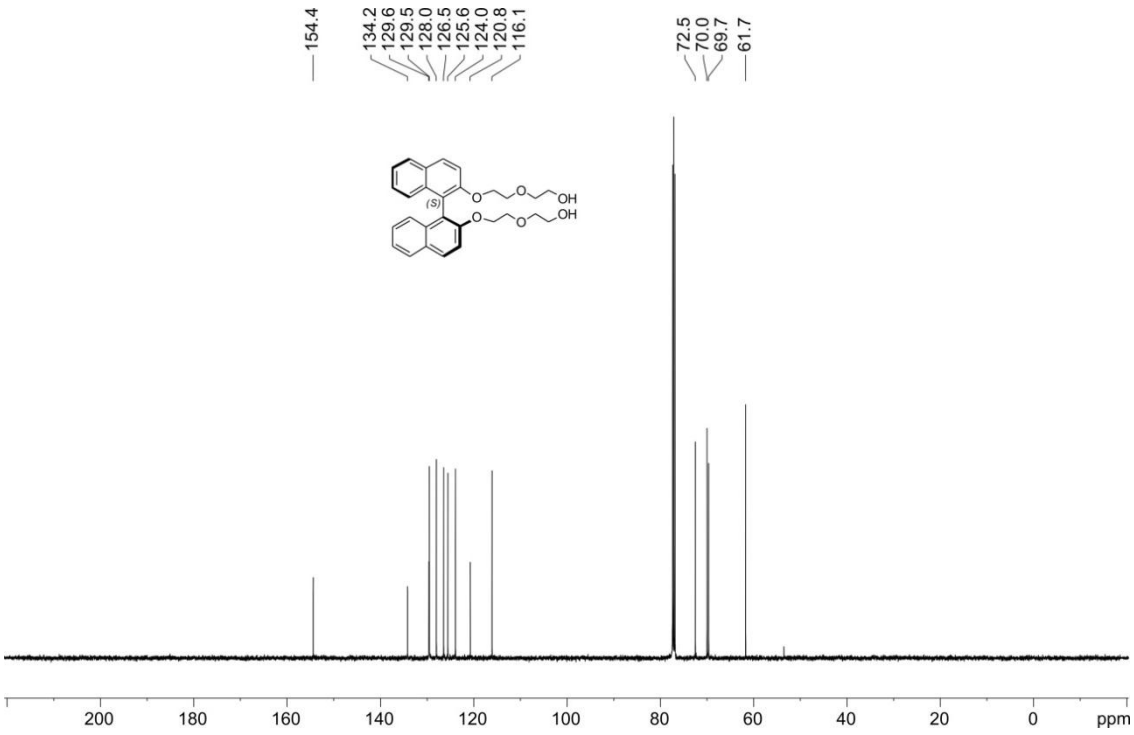

Figure S4. ^{13}C{^{1}H} NMR spectrum of diol (*S*)-**D1**.

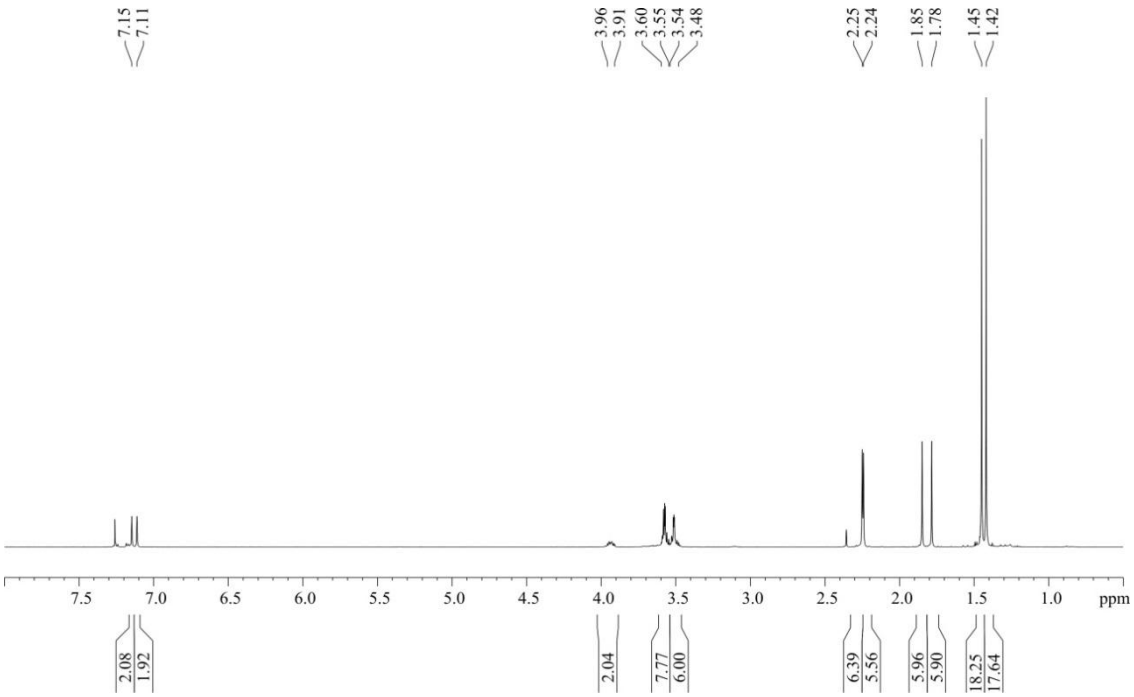

Figure S5. ^{1}H NMR spectrum of ligand (*S*)-**L1**.

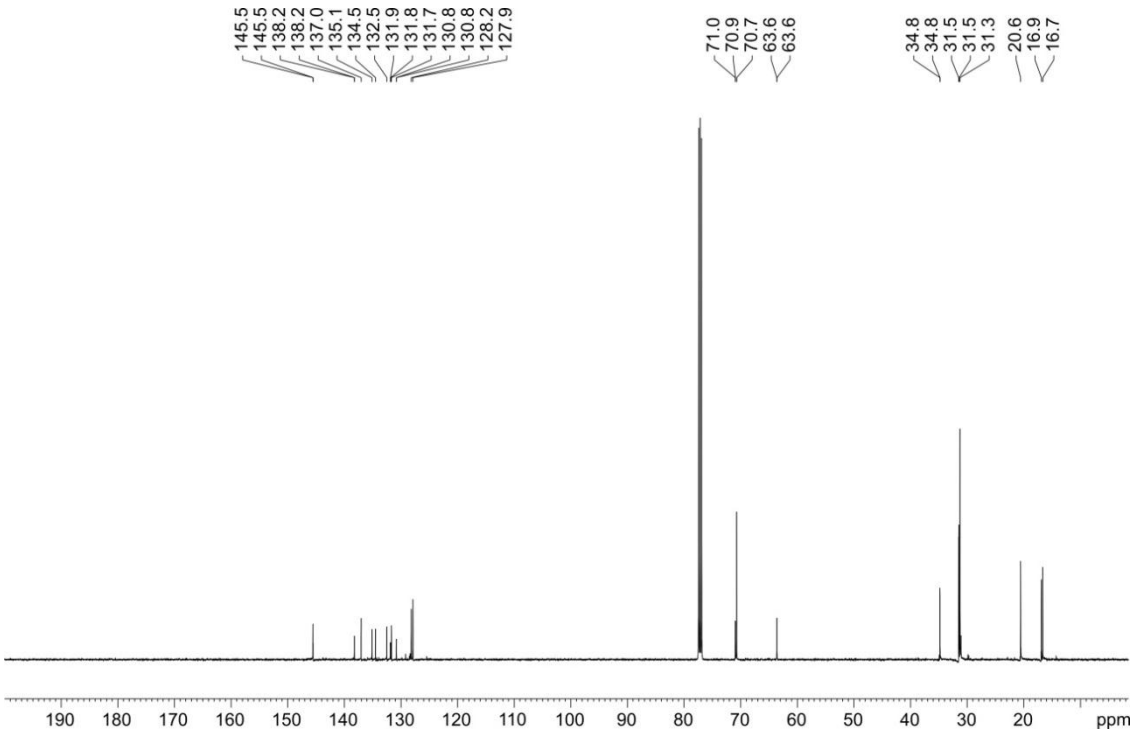

Figure S6. ^{13}C{^{1}H,^{31}P} NMR spectrum of ligand (*S*)-**L1**.

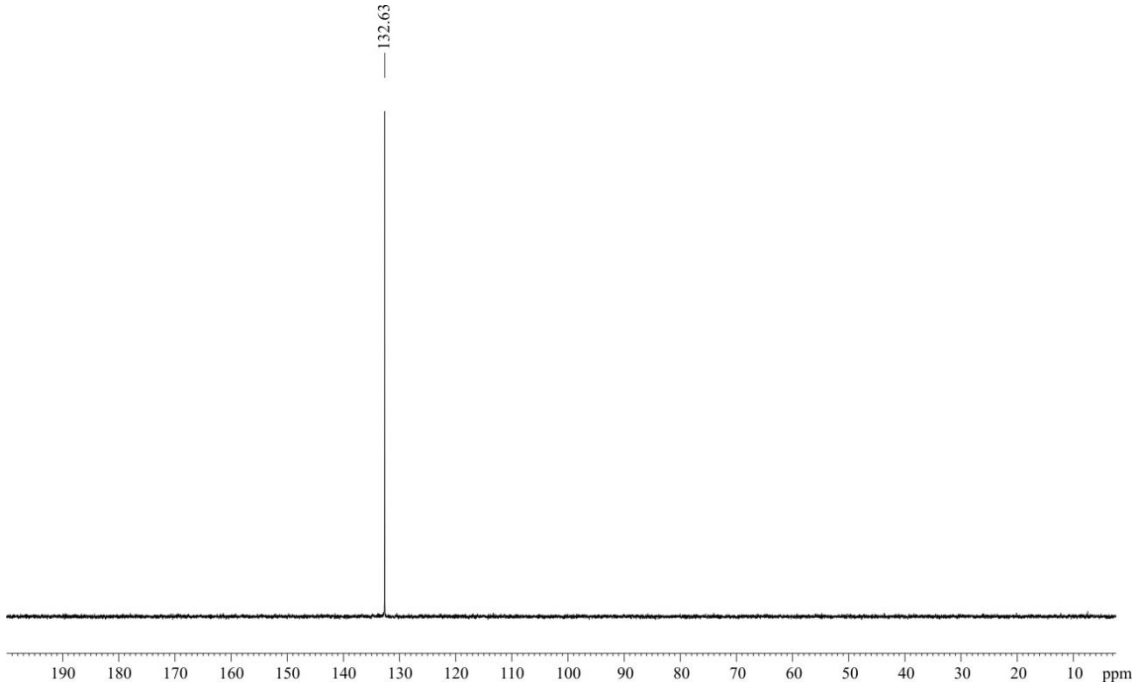

Figure S7. $^{31}P\{^{1}H\}$ NMR spectrum of ligand (*S*)-**L1**.

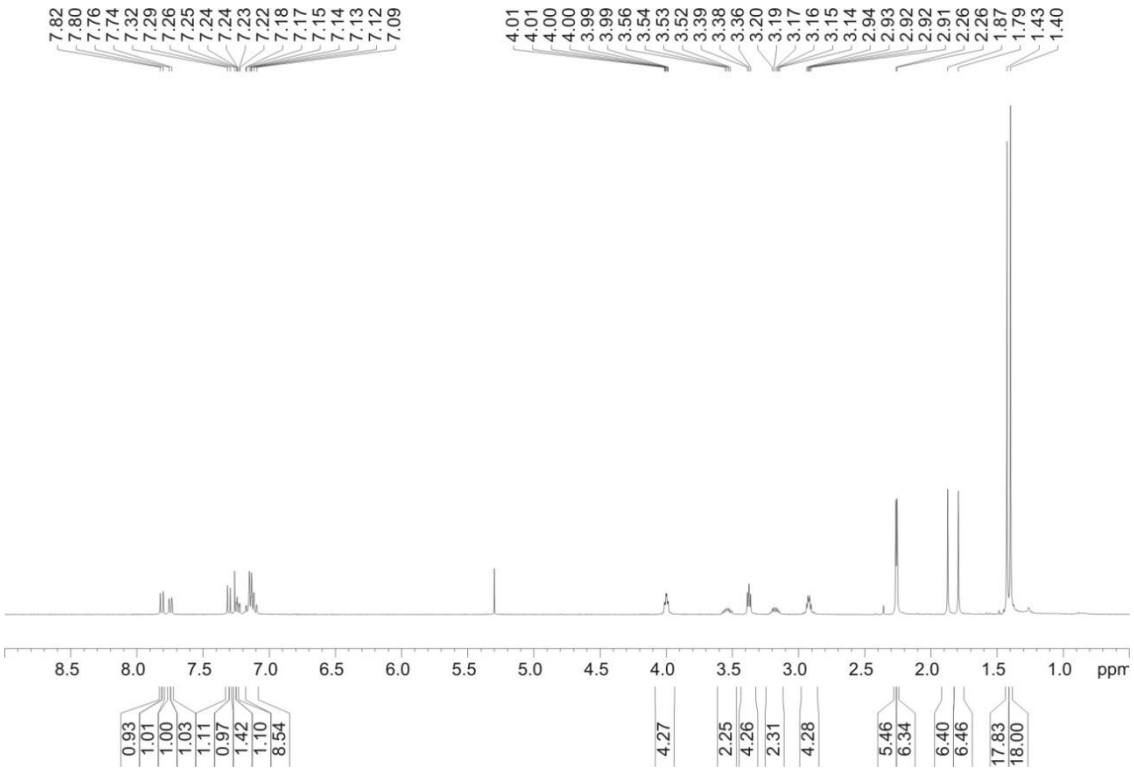

Figure S8. ^{1}H NMR spectrum of ligand (*R*,*S*)-**L2**.

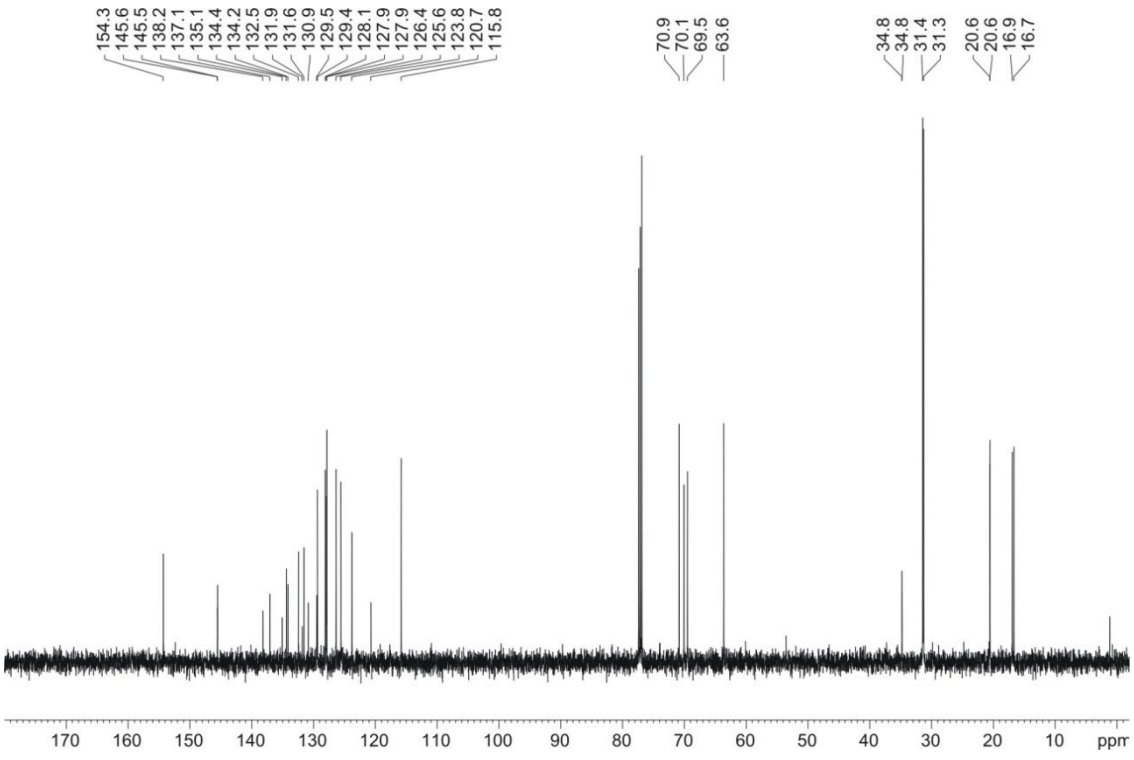

Figure S9. $^{13}C\{^{1}H,^{31}P\}$ NMR spectrum of ligand (*R*,*S*)-**L2**.

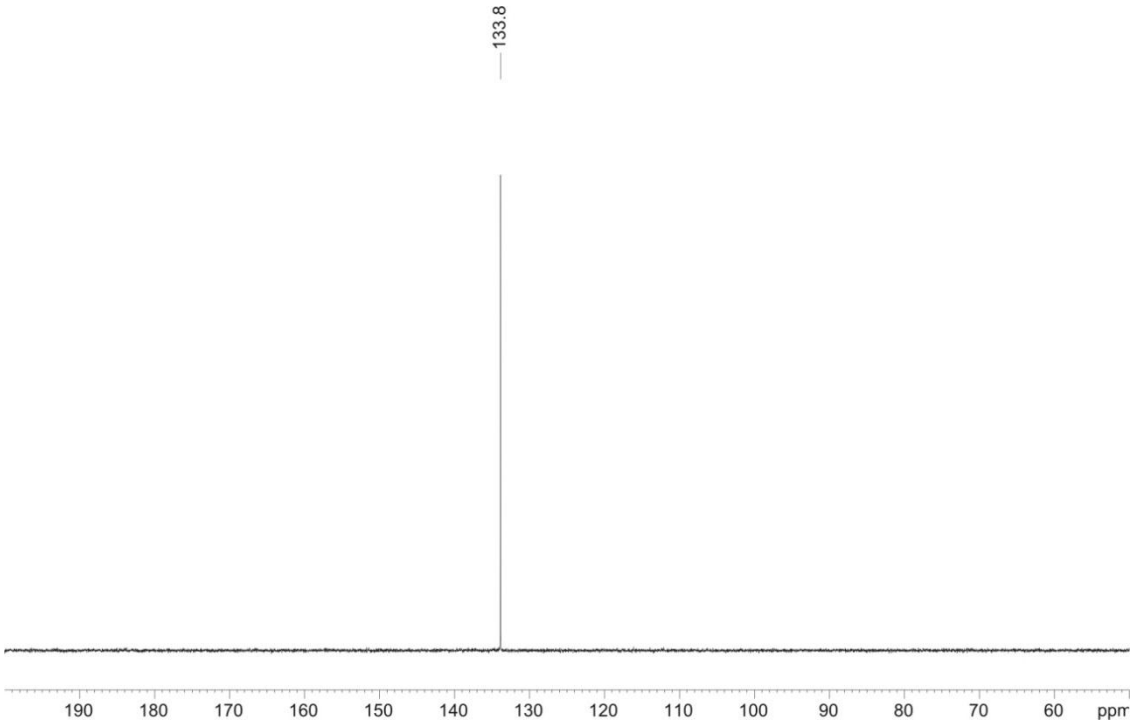

Figure S10. $^{31}P\{^{1}H\}$ NMR spectrum of ligand (*R*,*S*)-**L2**.

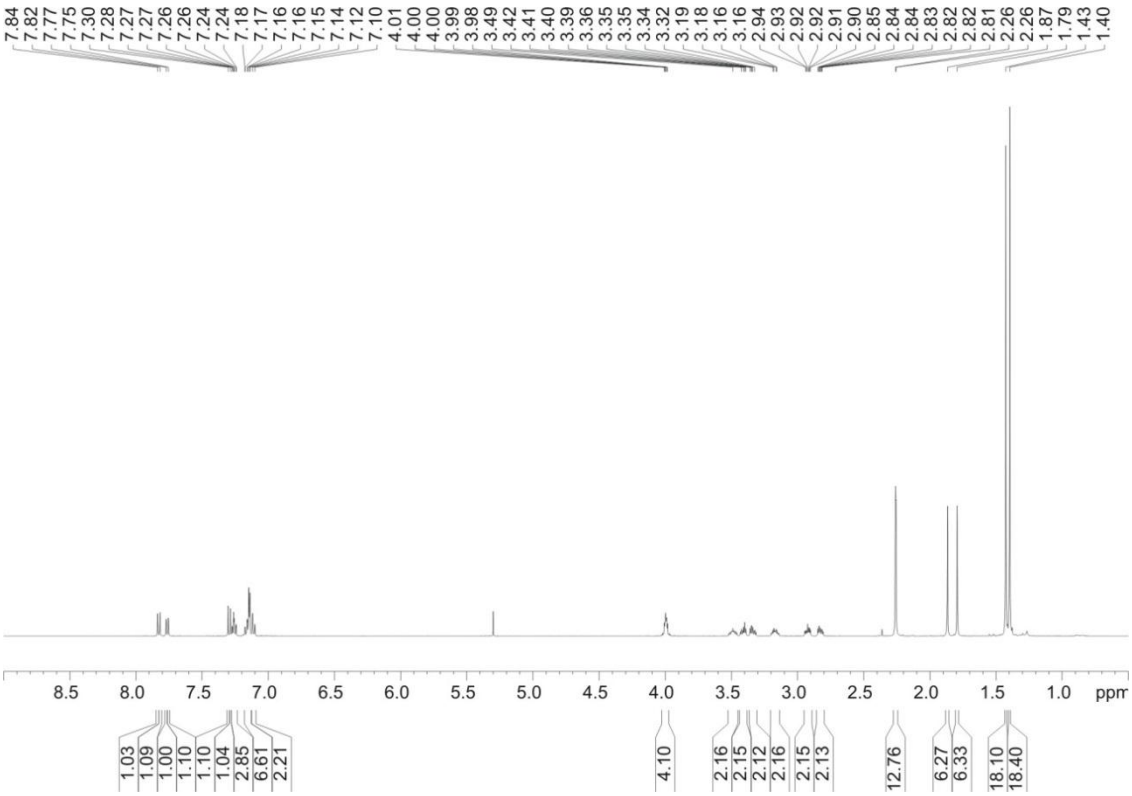

Figure S11. ^{1}H NMR spectrum of ligand (*S*,*S*)-**L3**.

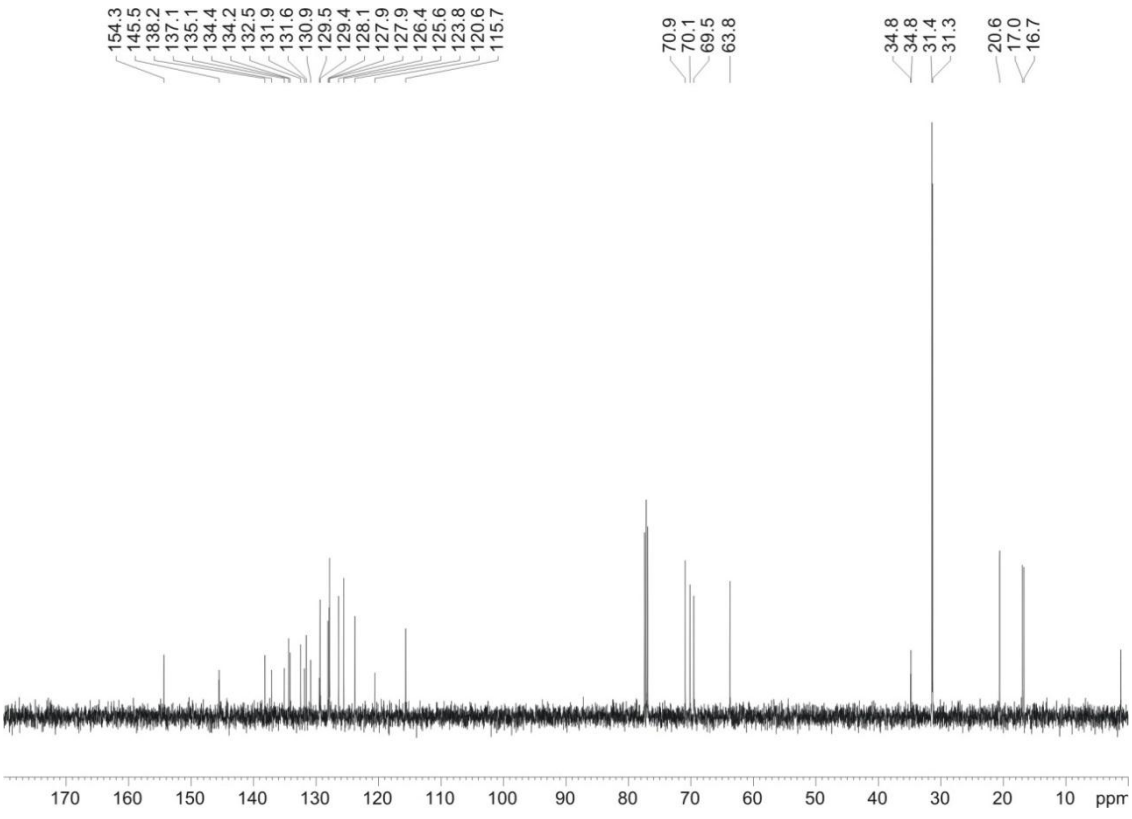

Figure S12. $^{13}C\{^{1}H,^{31}P\}$ NMR spectrum of ligand (*S*,*S*)-**L3**.

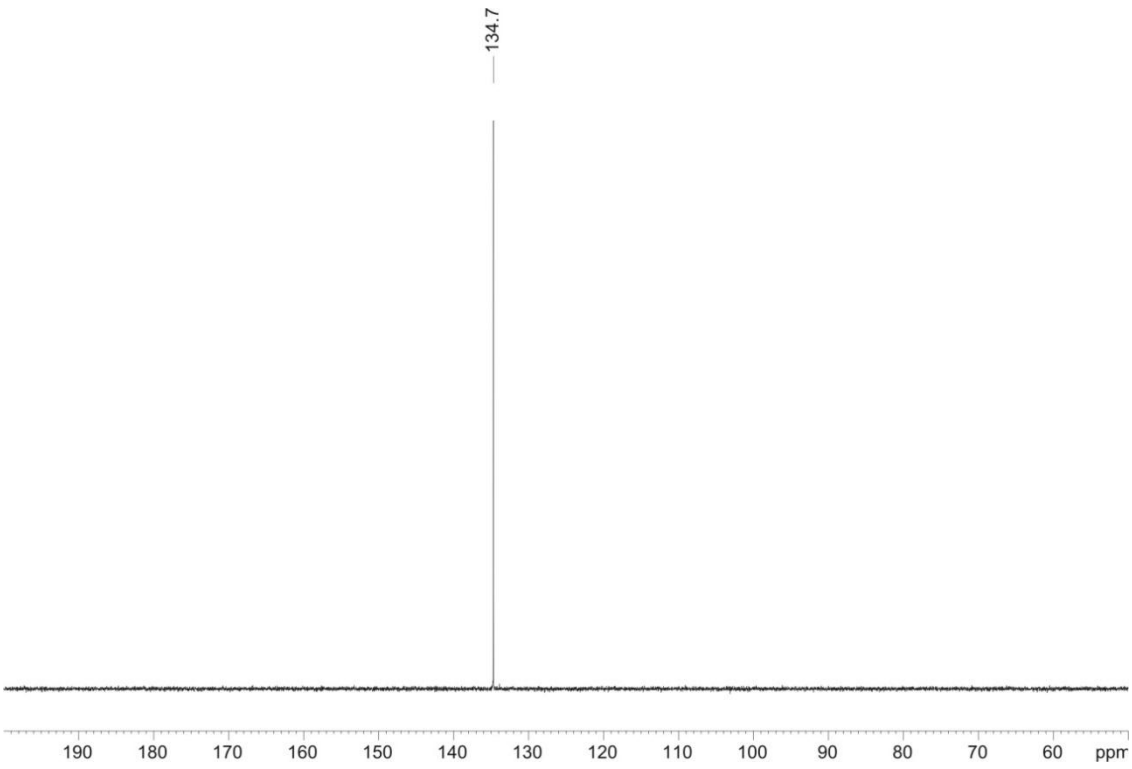

Figure S13. $^{31}P\{^{1}H\}$ NMR spectrum of ligand (*S*,*S*)-**L3**.

3.6.2. Characterization of [Rh(H)(CO)$_2$(κ^2P,P'–KBArF•(*S*)-L1)] and [Rh(H)(CO)$_2$ (κ^2P,P'–KBArF•(*R,S*)-L2)]

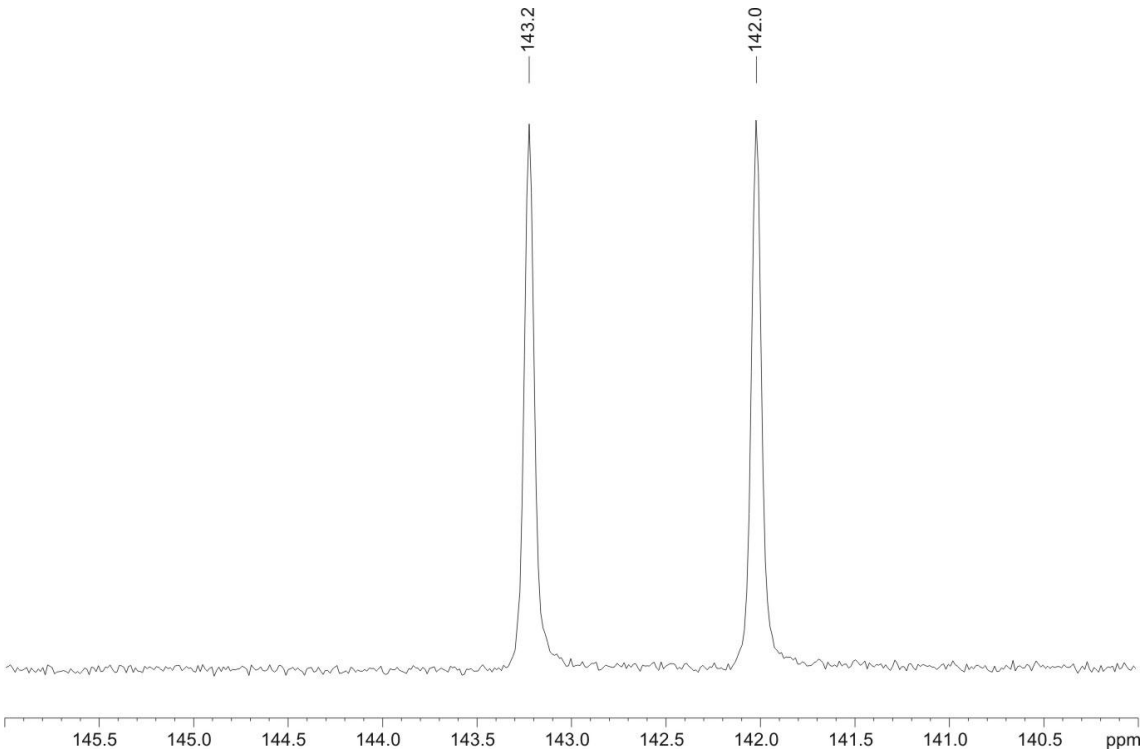

Figure S14. ^{31}P NMR spectrum of [Rh(H)(CO)$_2$(κ^2P,P´–KBArF•(*S*)-**L1**)].

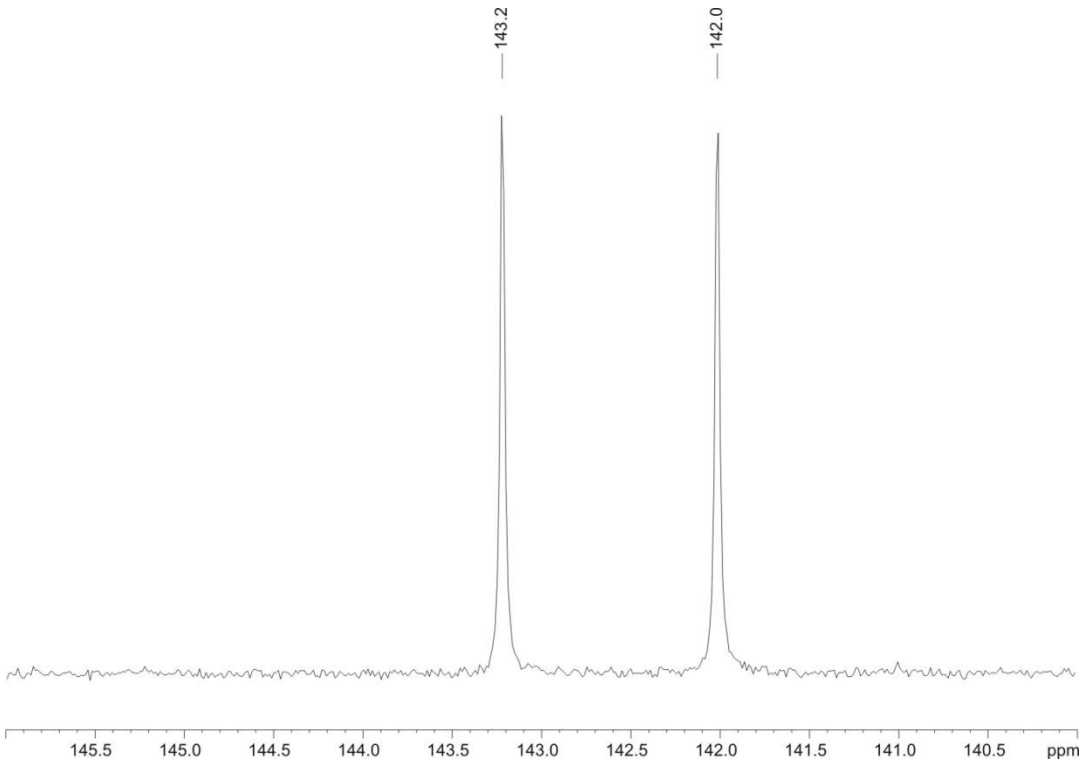

Figure S15. ^{31}P{^{1}H} NMR spectrum of [Rh(H)(CO)$_2$(κ^2P,P´–KBArF•(*S*)-**L1**)].

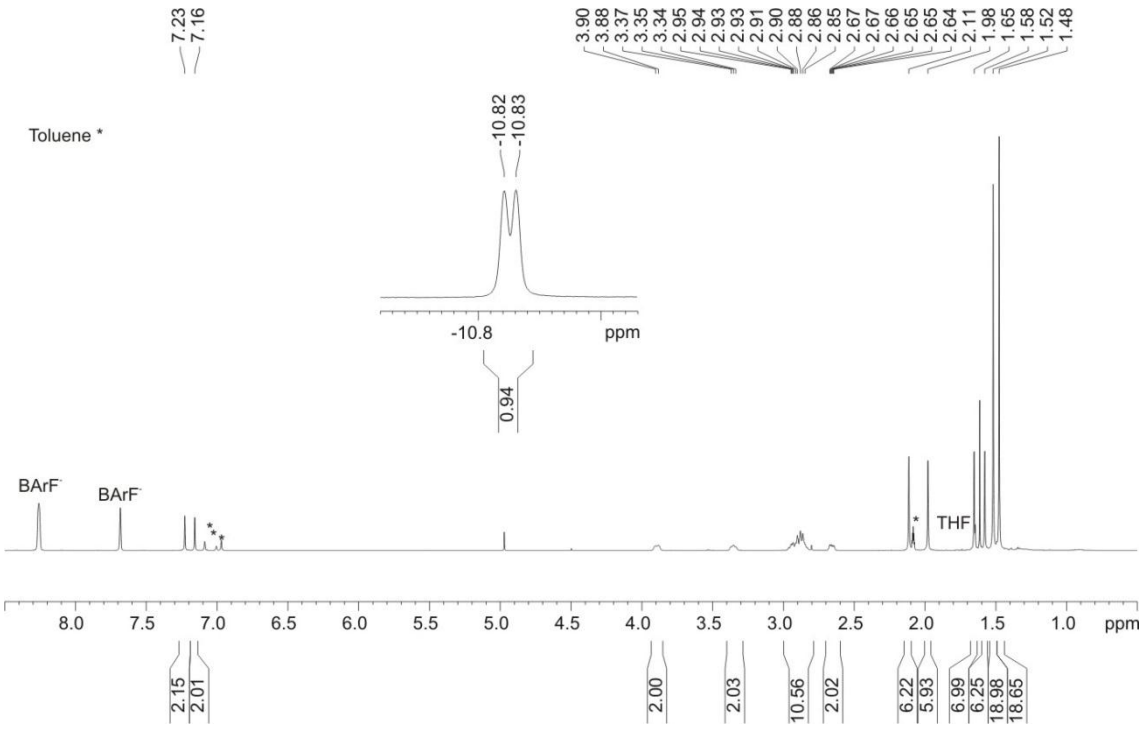

Figure S16. ^{1}H NMR spectrum of [Rh(H)(CO)$_2$(κ^2P,P´–KBArF•(*S*)-**L1**)].

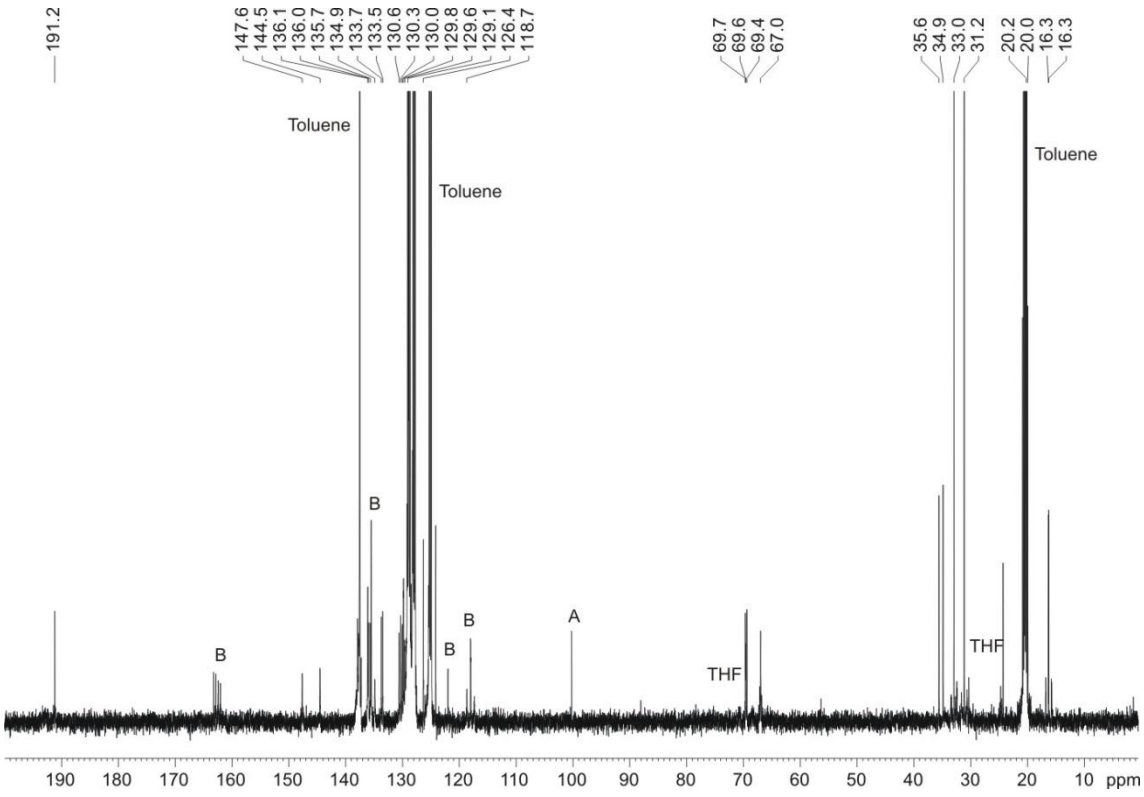

Figure S17. ^{13}C{^{1}H} NMR spectrum of [Rh(H)(CO)$_2$(κ^2P,P´–KBArF•(*S*)-**L1**)] (A= signals corresponding to free acac, B= BArF signals).

Characterization of [Rh(H)(CO)$_2$(κ^2P,P'–KBArF•(*R*,*S*)-L2)]

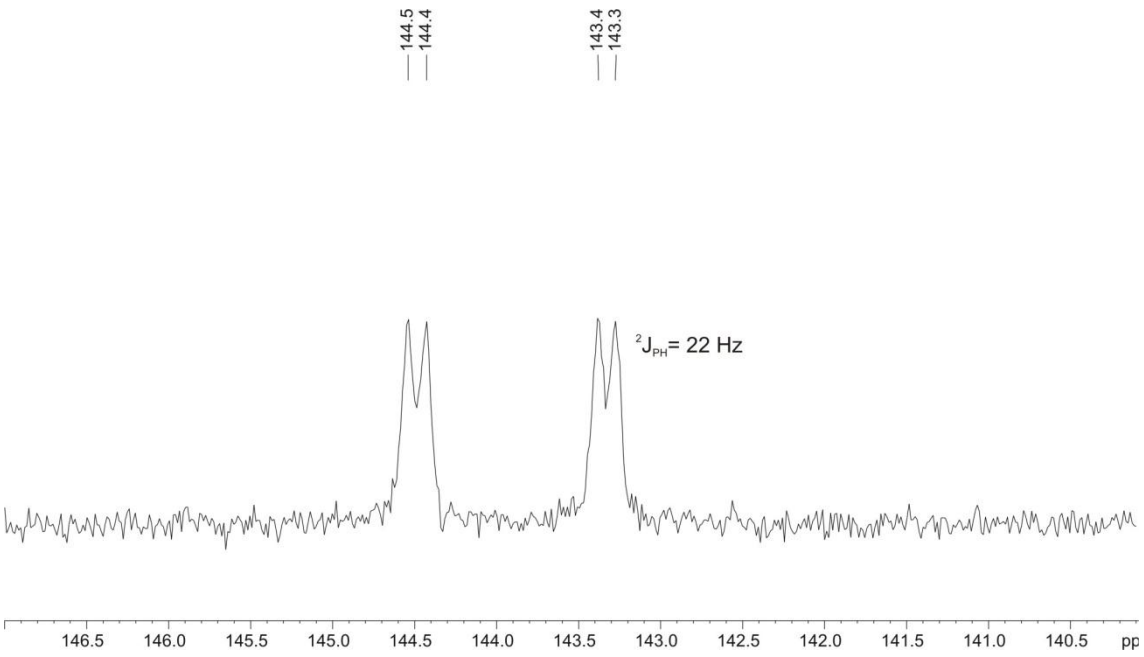

Figure S18. ^{31}P NMR spectrum of [Rh(H)(CO)$_2$(κ^2P,P´–KBArF•(*R*,*S*)-**L2**)].

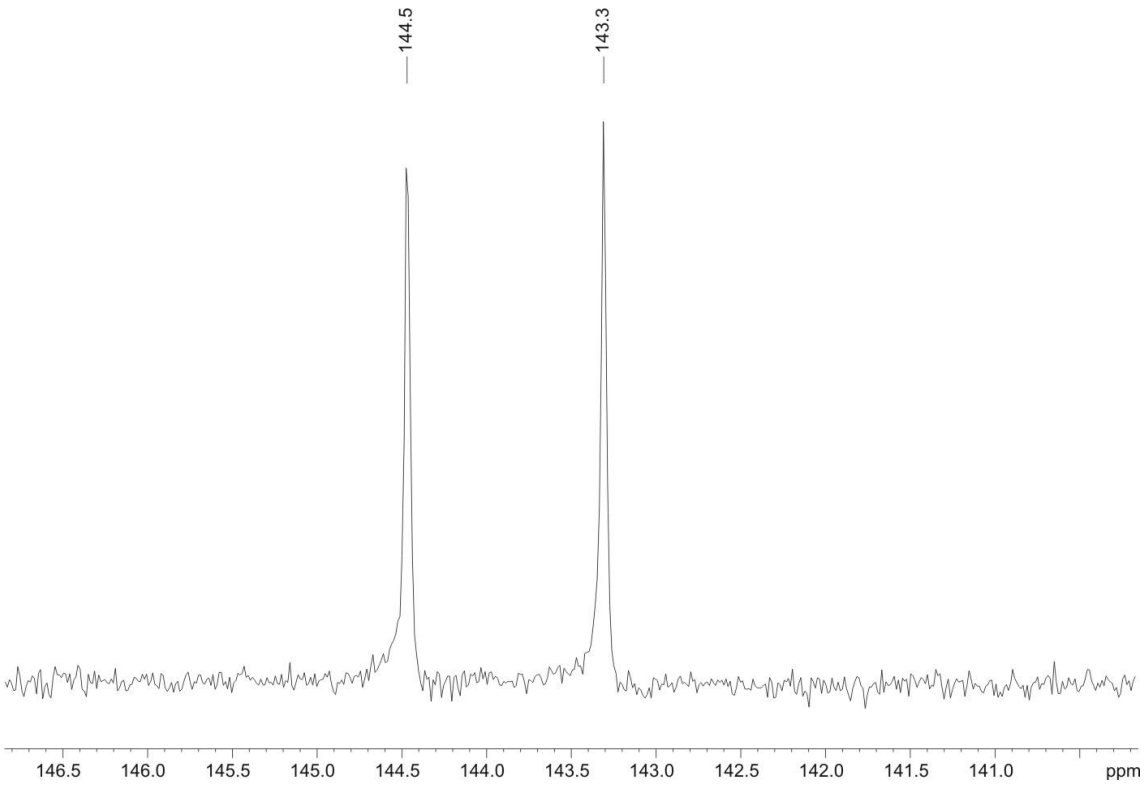

Figure S19. ^{31}P{^{1}H} NMR spectrum of [Rh(H)(CO)$_2$(κ^2P,P´–KBArF•(*R*,*S*)-**L2**)].

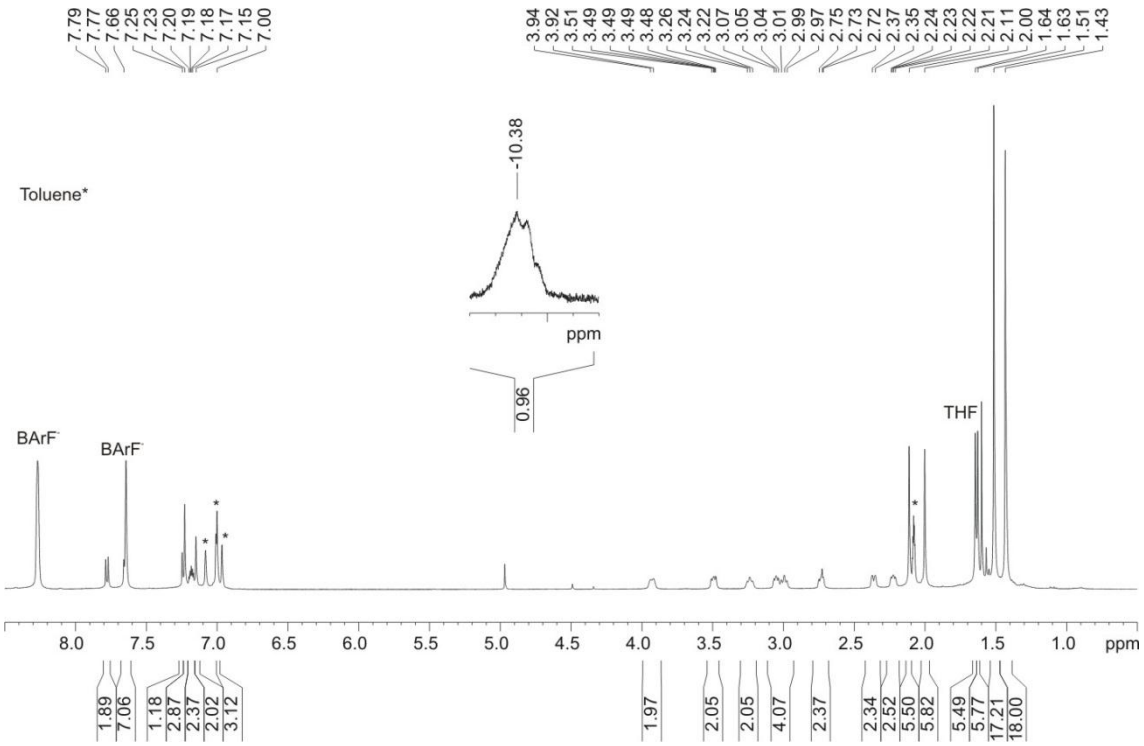

Figure S20. ^{1}H NMR spectrum of [Rh(H)(CO)$_2$(κ^2P,P´–KBArF•(*R*,*S*)-**L2**)].

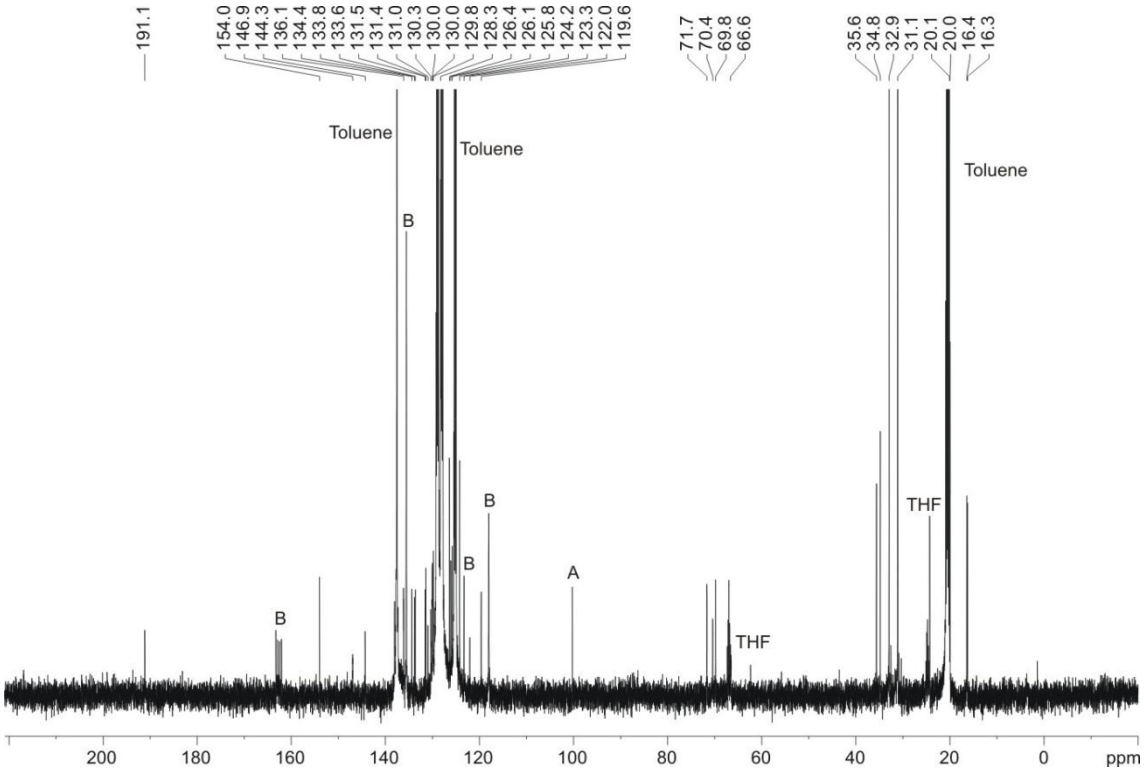

Figure S21. ^{13}C{^{1}H} NMR spectrum of [Rh(H)(CO)$_2$(κ^2P,P´–KBArF•(*R*,*S*)-**L2**)] (A= signals corresponding to free acac, B= BArF signals).

3.6.3. Extended tables of hydroformylation

Table S1. AHF of vinyl acetate (**1a**) with ligands **L1**–**L3** and a set of RAs.[a]

Entry	Ligand	RA	Conv. (%)	b:l ratio	ee (%) config.
1		-	91	98:2	32 (*R*)
2		NaBArF	78	97:3	41 (*R*)
3	(*S*)-**L1**	KBArF	>99	86:14	86 (*R*)
4		RbBArF	>99	97:3	90 (*R*)
5		CsBArF	>99	>99:1	88 (*R*)
6		-	92	>99:1	23 (*R*)
7		NaBArF	40	>99:1	81 (*R*)
8	(*R*,*S*)-**L2**	KBArF	63	>99:1	93 (*R*)
9		RbBArF	>99	>99:1	92 (*R*)
10		CsBArF	>99	>99:1	89 (*R*)
11		-	87	>99:1	22 (*R*)
12		NaBArF	32	>99:1	41 (*R*)
13	(*S*,*S*)-**L3**	KBArF	8	>99:1	66 (*R*)
14		RbBArF	29	>99:1	79 (*R*)
15		CsBArF	96	>99:1	79 (*R*)

[a] AHF reactions were performed in a HEL parallel reactor. The values shown are the average values of at least two independent runs. The reaction conditions are shown in the Scheme 2 (S/C ratio= 100; [**1a**–**e**] = 0.26 M; T = 40 ºC, *t* = 18 h). Conversion was determined by chiral GC chromatography using *n*-dodecane (*β*-Dex™ 225) as internal standard, unless otherwise stated. Regioselectivity and ee´s were determined by GC analysis on a chiral stationary phases *β*-Dex™ 225, unless otherwise stated. Absolute configuration was assigned by comparison of the elution order in GC analysis with the reported data (for details, see section 3.5).

Table S2. AHF of vinyl propionate (**1b**) with ligands **L1**–**L3** and a set of RAs.[a]

Entry	Ligand	RA	Conv. (%)	b:l ratio	ee (%) config.
1		-	81	>99:1	23 (*R*)
2		NaBArF	78	>99:1	52 (*R*)
3	(*S*)-**L1**	KBArF	>99	>99:1	87 (*R*)
4		RbBArF	>99	>99:1	84 (*R*)
5		CsBArF	>99	>99:1	84 (*R*)
6		-	94	>99:1	15 (*R*)
7		NaBArF	38	>99:1	80 (*R*)
8	(*R*,*S*)-**L2**	KBArF	>99	>99:1	92 (*R*)
9		RbBArF	>99	>99:1	90 (*R*)
10		CsBArF	>99	>99:1	83 (*R*)
11		-	94	>99:1	19 (*R*)
12		NaBArF	39	>99:1	43 (*R*)
13	(*S*,*S*)-**L3**	KBArF	67	>99:1	59 (*R*)
14		RbBArF	86	>99:1	73 (*R*)
15		CsBArF	91	>99:1	58 (*R*)

[a] See Table S1 for details.

Table S3. AHF of vinyl benzoate (**1c**) with ligands **L1**–**L3** and a set of RAs.[a]

Entry	Ligand	RA	Conv. (%)	b:l ratio	ee (%) config.
1		-	90	>99:1	7 (*S*)
2		NaBArF	78	98:2	76 (*R*)
3	(*S*)-**L1**	KBArF	64	65:35	44 (*R*)
4		RbBArF	40	95:5	44 (*R*)
5		CsBArF	56	97:3	29 (*R*)
6		-	94	>99:1	7 (*R*)
7		NaBArF	38	>99:1	37 (*R*)
8	(*R*,*S*)-**L2**	KBArF	33	>99:1	66 (*R*)
9		RbBArF	38	>99:1	60 (*R*)
10		CsBArF	31	>99:1	57 (*R*)
11		-	88	>99:1	8 (*S*)
12		NaBArF	43	>99:1	10 (*R*)
13	(*S*,*S*)-**L3**	KBArF	86	>99:1	50 (*S*)
14		RbBArF	87	>99:1	*rac*
15		CsBArF	42	>99:1	27 (*R*)

[a] See Table S1 for details.

Table S4. AHF of styrene (**1d**) with ligands **L1**–**L3** and a set of RAs.[a]

Entry	Ligand	RA	Conv. (%)	b:l ratio	ee (%) config.
1		-	>99	96:4	41 (*R*)
2		NaBArF	>99	85:15	2 (*R*)
3	(*S*)-**L1**	KBArF	>99	74:26	9 (*R*)
4		RbBArF	>99	80:20	12 (*R*)
5		CsBArF	>99	89:11	41 (*R*)
6		-	>99	95:5	41 (*R*)
7		NaBArF	>99	93:7	36 (*R*)
8	(*R*,*S*)-**L2**	KBArF	>99	83:17	4 (*R*)
9		RbBArF	>99	82:18	3 (*R*)
10		CsBArF	>99	78:22	15 (*R*)
11		-	>99	95:5	42 (*R*)
12		NaBArF	>99	96:4	54 (*R*)
13	(*S*,*S*)-**L3**	KBArF	>99	80:20	19 (*R*)
14		RbBArF	>99	81:19	16 (*R*)
15		CsBArF	>99	86:14	32 (*R*)

[a] See Table S1 for details.

Table S5. AHF of allyloxy-*tert*-butyldimethylsilane (**1e**) with ligands **L1**–**L3** and a set of RAs.[a]

Entry	Ligand	RA	Conv. (%)[b]	b:l ratio[b]	ee (%) config.
1		-	>99	61:39	19 (*R*)
2		NaBArF	>99	37:63	9 (*R*)
3	(*S*)-**L1**	KBArF	>99	6:94	*rac*
4		RbBArF	>99	9:90	18 (*R*)
5		CsBArF	>99	22:78	17 (*R*)
6		-	92	61:39	17 (*R*)
7		NaBArF	>99	60:40	8 (*R*)
8	(*R*,*S*)-**L2**	KBArF	>99	11:89	3 (*R*)
9		RbBArF	>99	7:93	6 (*R*)
10		CsBArF	>99	8:92	11 (*R*)
11		-	>99	61:39	17 (*R*)
12		NaBArF	>99	58:42	17 (*R*)
13	(*S*,*S*)-**L3**	KBArF	>99	30:70	16 (*R*)
14		RbBArF	>99	19:81	21 (*R*)
15		CsBArF	>99	18:82	23 (*R*)

[a] See Table S1 for details. [b] Conversion and regioselectivity were determined by ^{1}H NMR.

Table S6. Pressure studies of AHF of 2,5-dihydrofuran (**4**) with KBArF.[a]

Entry	Total pressure	H_2/CO ratio	Regio (**5**:**6**) (%)	(**7**) (%)	ee of **5** (%) config.	ee of **6** (%) config.
1	5 bar	1:4	26:34	40	84 (*R*)	62 (*S*)
2		1:2	33:37	30	82 (*R*)	54 (*S*)
3		1:1	46:36	18	80 (*R*)	44 (*S*)
4		2:1	69:28	3	74 (*R*)	24 (*S*)
5		4:1	71:29	0	69 (*R*)	10 (*S*)
6	10 bar	1:2	25:40	35	84 (*R*)	57 (*S*)
7		1:1	35:39	26	82 (*R*)	56 (*S*)
8		2:1	49:34	17	77 (*R*)	50 (*S*)
9	20 bar	1:2	9:42	49	81 (*R*)	64 (*S*)
10		1:1	12:51	37	83 (*R*)	60 (*S*)
11		2:1	27:41	32	82 (*R*)	56 (*S*)
12		4:1	34:39	27	83 (*R*)	50 (*S*)

[a] AHF reactions were performed in a HEL parallel reactor. The values shown are the average values of at least two independent runs. Complete conversion was observed in all reactions. The reaction conditions are shown in the Scheme 3 (S/C ratio= 100; [**4**] = 0.26 M; T = 40 ºC, *t* = 18 h). Conversion and isomerization were determined by ^{1}H NMR. Regioselectivity and ee´s were determined by GC analysis on a chiral stationary phases *β*-Dex™ 225. Absolute configuration was assigned by comparison of the elution order in GC analysis with the reported data (for details, see section 3.5).

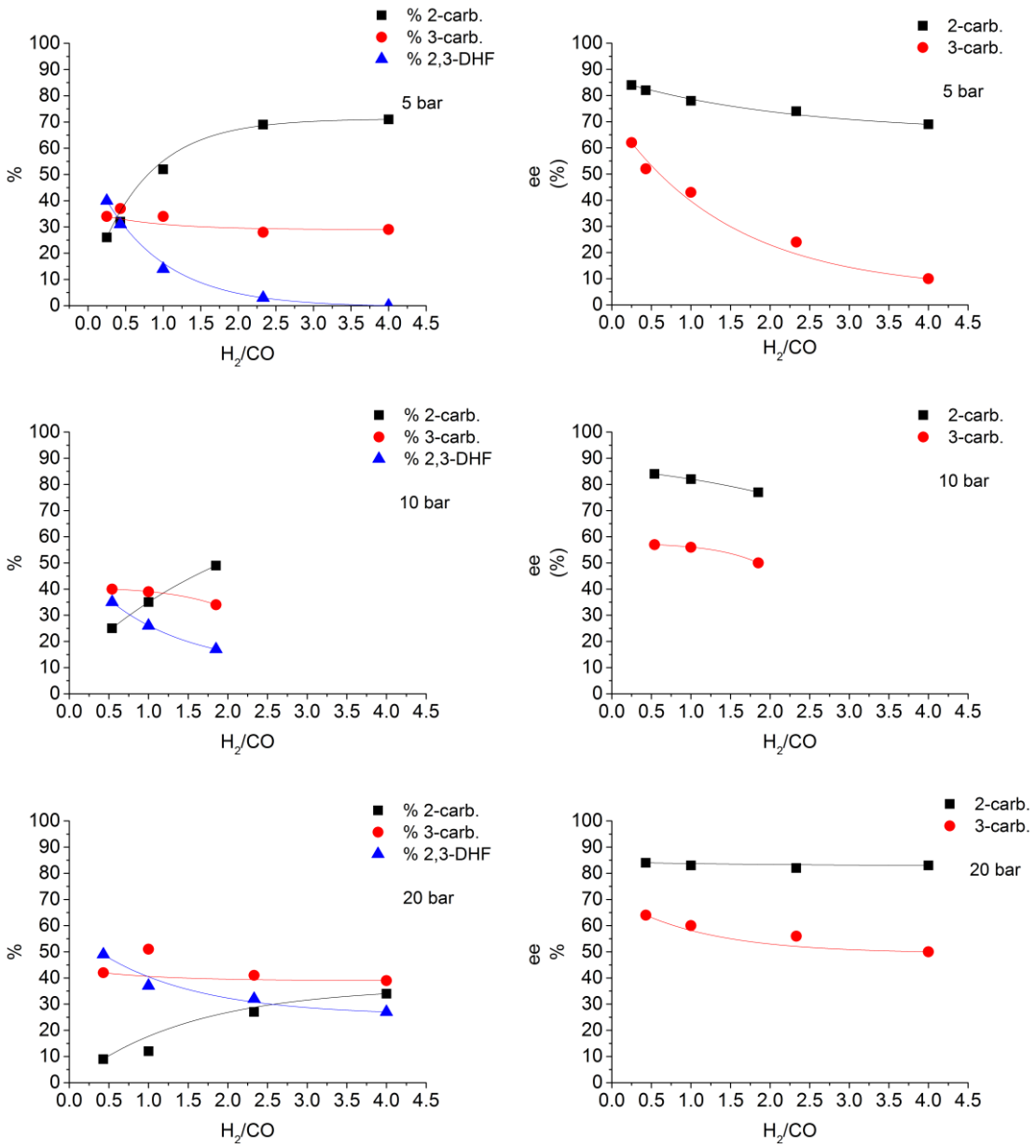

Figure S22. Selectivity in the AHF of 2,5-dihydrofuran (**4**) *versus* ratio H_2/CO (left), and enantiomeric excess (%) of aldehydes *versus* pressure ratio H_2/CO (right).

Table S7. AHF of six-membered heterocyclic olefins (**10**–**12**) using Rh-complexes of ligands **L1**–**L3** and a set of RAs.[a]

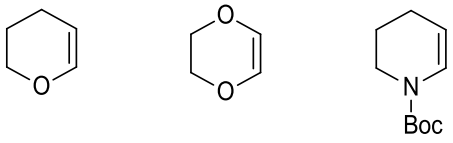

10 **11** **12**

Entry	Ligand	Substrate	RA	Conv. (%)
1	(*S*)-**L1**	**10**	-	<1
2			NaBArF	<1
3			RbBArF	<1
4		**11**	-	<1
5			NaBArF	<1
6			RbBArF	<1
7		**12**	-	<1
8			NaBArF	<1
9			RbBArF	<1
10	(*R*,*S*)-**L2**	**10**	-	<1
11			NaBArF	<1
12			RbBArF	<1
13		**11**	-	<1
14			NaBArF	<1
15			RbBArF	<1
16		**12**	-	<1
17			NaBArF	<1
18			RbBArF	<1
19	(*S*,*S*)-**L3**	**10**	-	<1
20			NaBArF	<1
21			RbBArF	<1
22		**11**	-	<1
23			NaBArF	<1
24			RbBArF	<1
25		**12**	-	<1
26			NaBArF	<1
27			RbBArF	<1

[a] AHF reactions were performed in a HEL parallel reactor. Reaction conditions: S/C ratio= 100; [**10**–**12**] = 0.26 M; T = 40 ºC, *t* = 18 h. Conversion was determined by ^{1}H NMR.

Table S8. AHF of *cis*-4,7-dihydro-1,3-dioxepin (**8**) using Rh-complexes of ligands **L1**–**L3**.[a]

Entry	Ligand	RA	Conv. (%)	ee (%)[b]
1	(*S*)-**L1**	-	28	6 (+)
2		NaBArF	>99	85 (+)
3		KBArF	>99	74 (+)
4		RbBArF	>99	75 (+)
5		CsBArF	>99	69 (+)
6		NaBArF[c]	95	92 (+)
7	(*R*,*S*)-**L2**	-	23	10 (-)
8		NaBArF	>99	36 (+)
9		KBArF	>99	83 (+)
10		RbBArF	>99	80 (+)
11		CsBArF	>99	71 (+)
12		KBArF[c]	>99	93 (+)
13	(*S*,*S*)-**L3**	-	17	*rac*
14		NaBArF	>99	*rac*
15		KBArF	>99	66 (+)
16		RbBArF	>99	74 (+)
17		CsBArF	>99	49 (+)
18		RbBArF[c]	>99	89 (+)

[a] AHF reactions were performed in a HEL parallel reactor. Reaction conditions: (S/C ratio= 100; [**8**] = 0.26 M; T = 40 ºC , *t* = 18 h). Conversion was determined by ^{1}H NMR and ee´s were determined by GC analysis on a chiral stationary phase (*β*-Dex™ 225, for details, see section 3.5). [b] Optical rotation was determined of the crude mixture of reaction of entry 12 (93% ee). [c] Reaction at 25ºC.

3.6.4. Selected GC chromatograms

GC chromatogram of the hydroformylation products of **1a** (entry 2, Table 1)

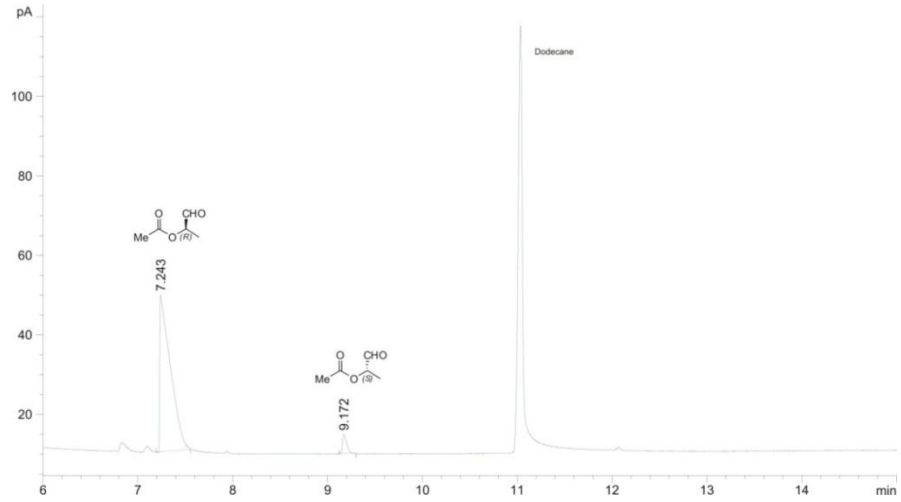

Peak #	RetTime [min]	Type	Width [min]	Area [pA*s]	Height [pA]	Area %
1	7.243	MM	0.1292	306.12534	39.49296	95.56899
2	9.172	MM	0.0495	14.19335	4.78162	4.43101

GC chromatogram of the hydroformylation products of **1b** (entry 4, Table 1)

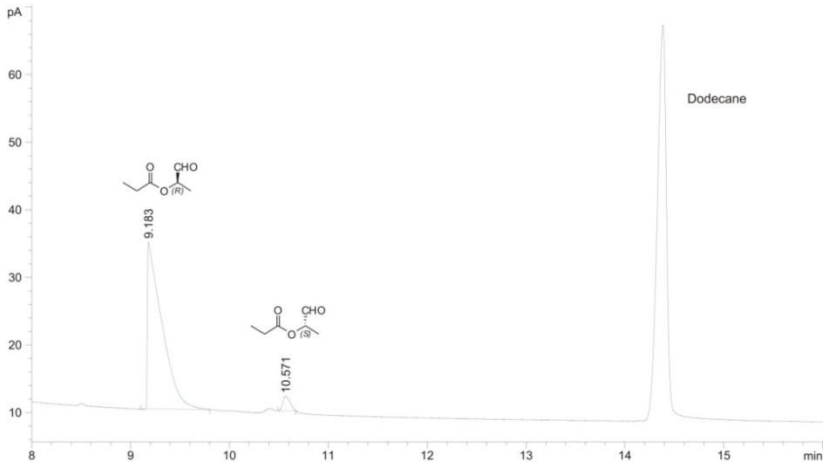

Peak #	RetTime [min]	Type	Width [min]	Area [pA*s]	Height [pA]	Area %
1	9.183	MM	0.1694	250.88936	24.68830	95.80476
2	10.571	MM	0.0849	10.98631	2.15688	4.19524

GC chromatogram of the hydroformylation products of **1c** (entry 13, Table S3)

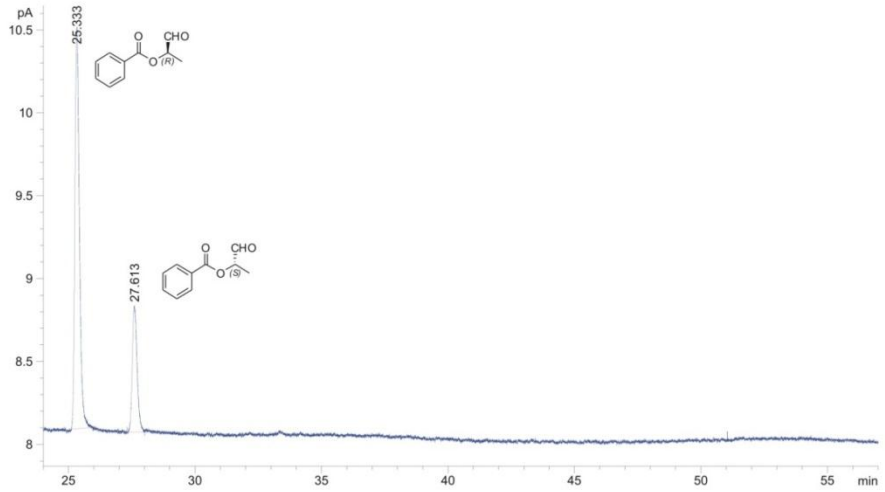

Peak #	RetTime [min]	Type	Width [min]	Area [pA*s]	Height [pA]	Area %
1	25.333	MM	0.2066	30.06023	2.42488	74.90263
2	27.613	MM	0.2194	10.07218	7.65131e-1	25.09737

GC chromatogram of the hydroformylation products of **1d** (entry 8, Table 1)

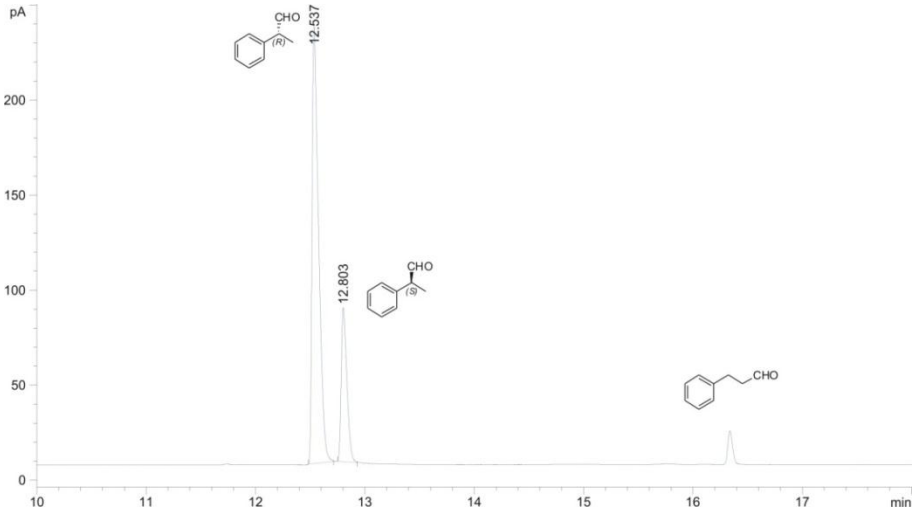

Peak #	RetTime [min]	Type	Width [min]	Area [pA*s]	Height [pA]	Area %
1	12.537	PB	0.0603	951.95575	230.01012	76.65126
2	12.803	BB	0.0558	289.97522	80.98436	23.34874

GC chromatogram of the hydroformylation products of **1e** (entry 10, Table 1)

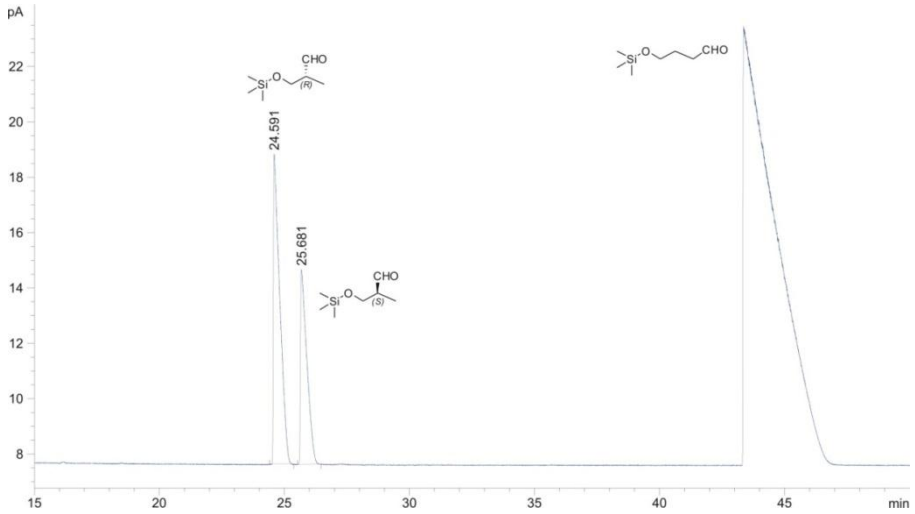

Peak #	RetTime [min]	Type	Width [min]	Area [pA*s]	Height [pA]	Area %
1	24.591	MM	0.2957	198.75360	11.20195	61.37665
2	25.681	MM	0.2959	125.07246	7.04548	38.62335

GC chromatogram of the hydroformylation products of **4** (entry 8, Table 2)

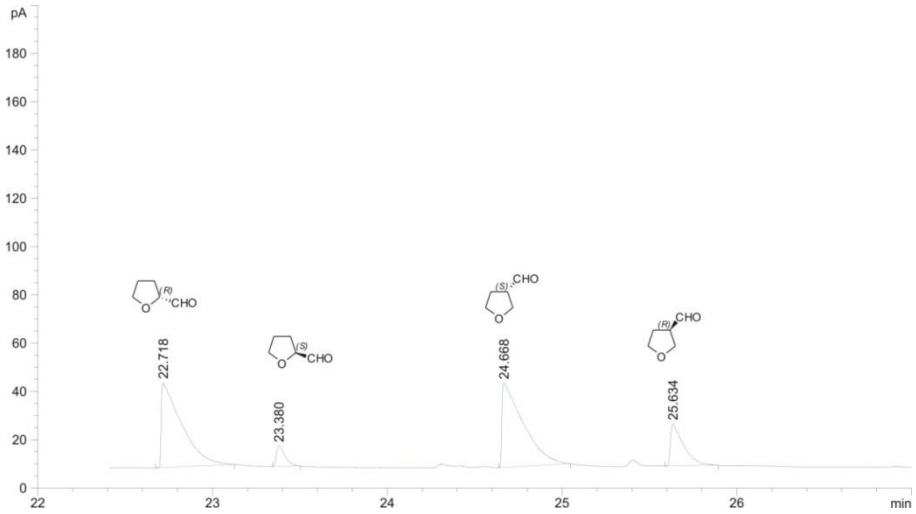

Peak #	RetTime [min]	Type	Width [min]	Area [pA*s]	Height [pA]	Area %
1	22.718	MM	0.1340	282.52631	35.14518	40.68495
2	23.380	MM	0.0556	28.65801	8.58994	4.12687
3	24.668	MM	0.1402	294.64420	35.02204	42.42998
4	25.634	MM	0.0855	88.59611	17.27253	12.75820

GC chromatogram of the hydroformylation products of **8** (entry 6, Table 4)

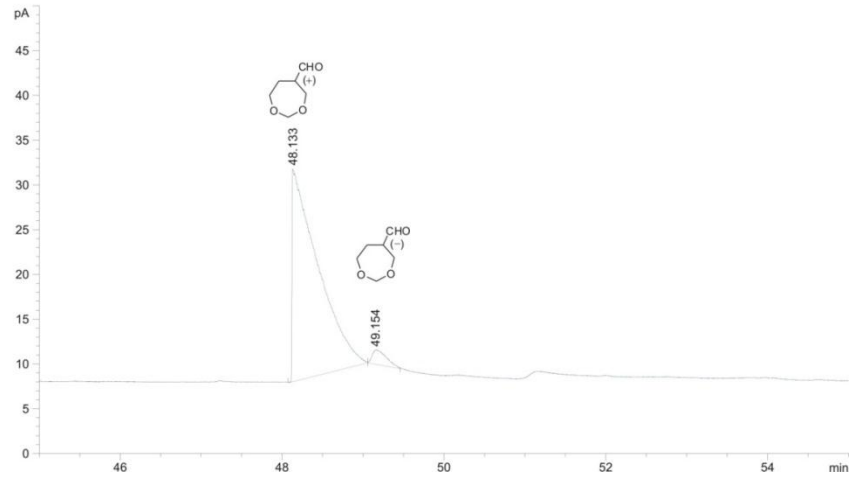

Peak #	RetTime [min]	Type	Width [min]	Area [pA*s]	Height [pA]	Area %
1	48.133	MM	0.3686	526.08917	23.78606	96.32818
2	49.154	MM	0.2086	20.05338	1.60190	3.67182

3.6.5. Characterization the hydroformylation products of 8

GC chromatogram of the racemic mixture of **9**

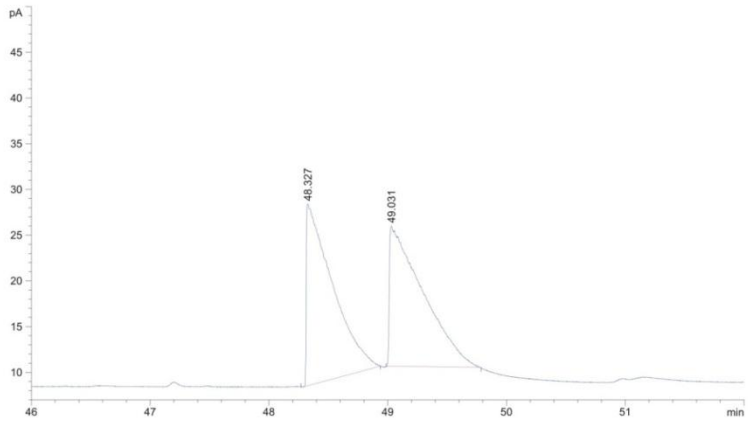

Peak #	RetTime [min]	Type	Width [min]	Area [pA*s]	Height [pA]	Area %
1	48.327	MM	0.2529	301.59155	19.87812	50.33478
2	49.031	MM	0.3230	297.57971	15.35663	49.66522

GC-MS chromatogram of the racemic mixture of **9**

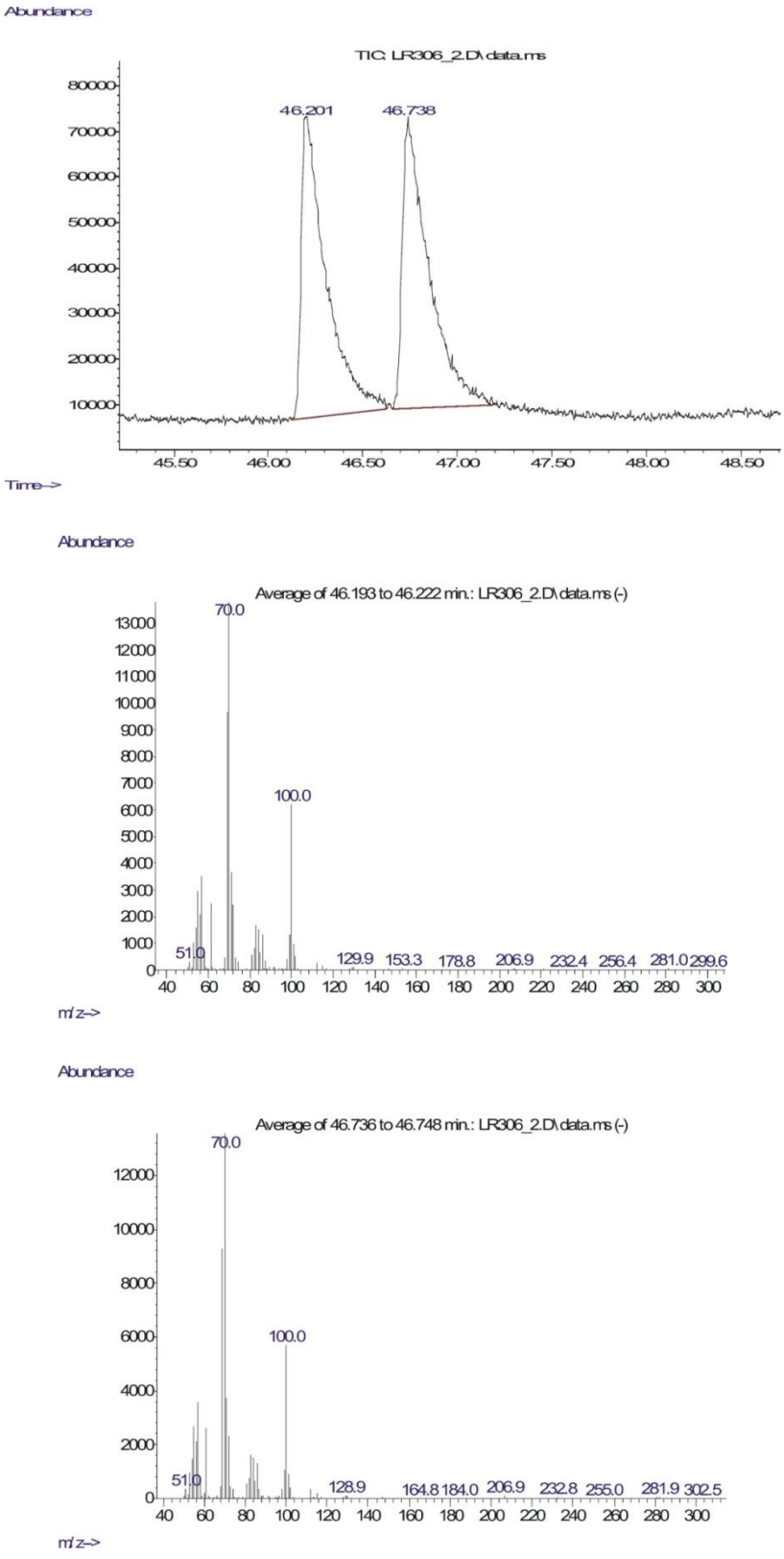

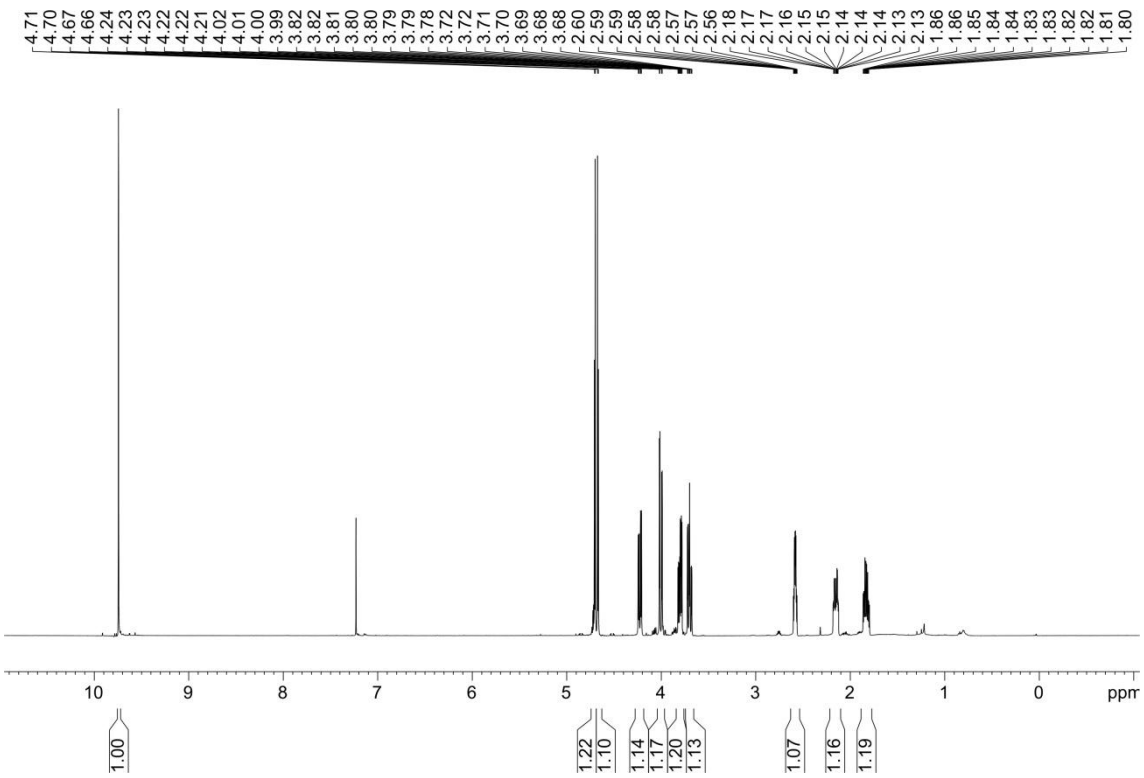

Figure S23. ^{1}H NMR spectrum of isolated aldehyde **9**.

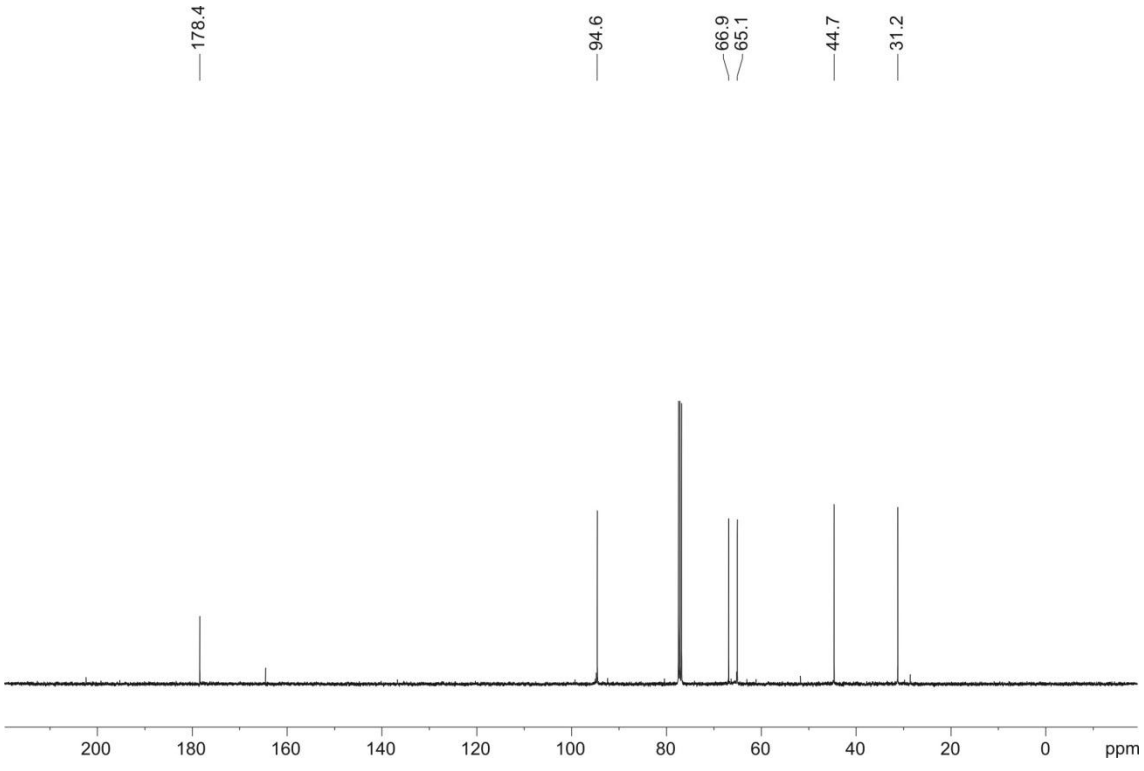

Figure S24. $^{13}C\{^{1}H\}$ NMR spectrum of isolated aldehyde **9**.

GC chromatogram of isolated aldehyde **9**

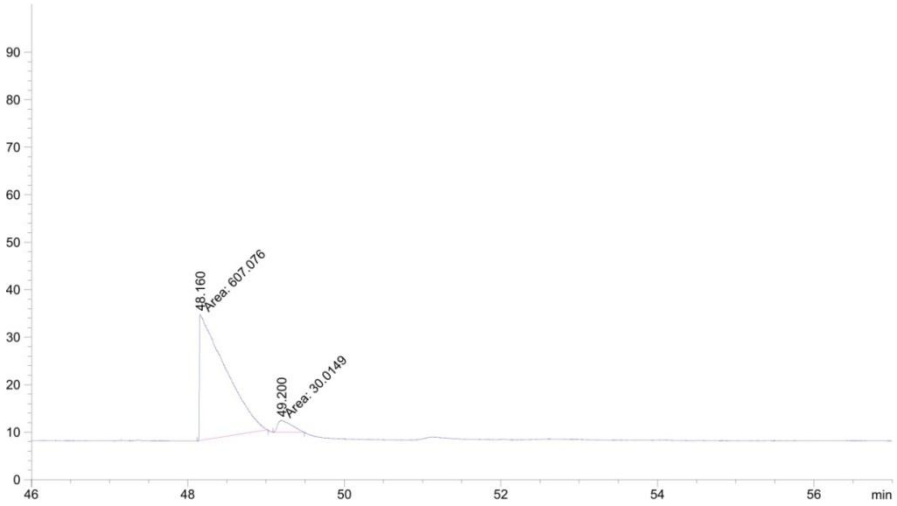

Peak #	RetTime [min]	Type	Width [min]	Area [pA*s]	Height [pA]	Area %
1	48.160	MM	0.3810	607.07568	26.55940	95.28876
2	49.200	MM	0.2028	30.01486	2.46724	4.71124

3.7. Additional studies on the hydroformylation of heterocyclic olefins and on the structure of catalytically relevant rhodium complexes

3.7.1. Preparation of new ligands with a smaller regulation site and application in the hydroformylation of heterocyclic olefins

3.7.1.1. Discussion

Previous studies on supramolecularly regulated bisphosphite ligands for hydroformylation dealt with ligands incorporating larger regulation sites than those in **L2** or **L3** (*i.e.* up to 8 ethyleneoxy units with a conformationally labile [1,1'-biphenyl]-2,2'-diol) in the regulation site).[2c] These ligands turned out to be inefficient in hydroformylation reactions probably due to their high flexibility. For this reason, we became interested in studying the catalytic properties of ligands as **L4** and **L5**, which may be considered more rigid analogues of **L2** and **L3**, respectively, as they contain two ethyleneoxy units bonded to the BINOL´s hydroxyl groups in the regulation site. These new ligands were straightforwardly prepared following an analogous synthetic strategy than that for **L2** and **L3** (See section 3.7.1.2).

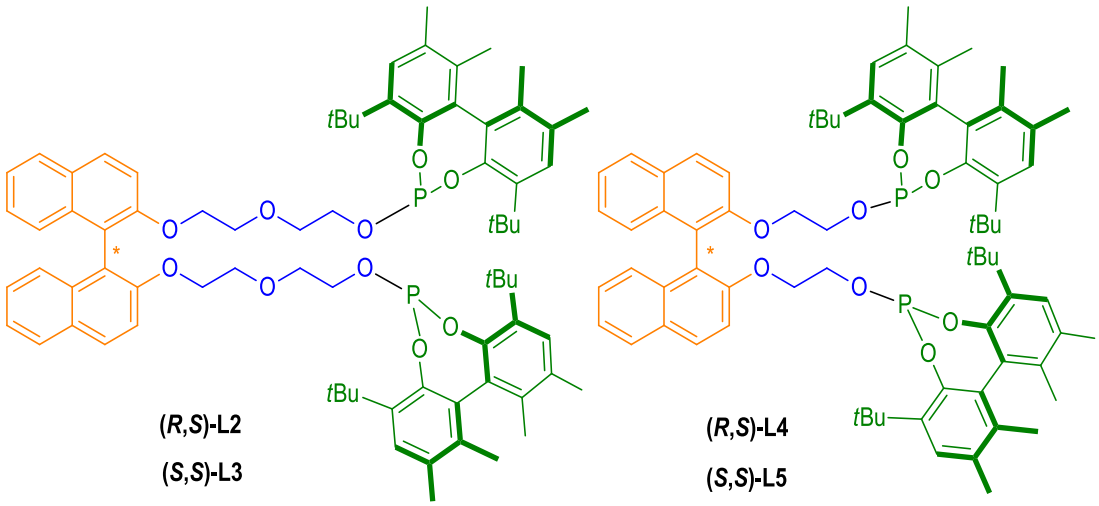

Figure A1. Enantiomerically pure bisphosphite ligands with a distal regulation site.

With the new ligands in hand, we tested them in the AHF of the previously studied heterocyclic olefins (*i.e.* 2,5-dihydrofuran (**4**), 2,3-dihydrofuran (**7**) and *cis*-4,7-dihydro-1,3-dioxepin (**8**)). The hydroformylation studies were performed under standard hydroformylation screening conditions that involved catalytic amounts of [Rh(κ^2O,O´–acac)(CO)$_2$] (1 mol%) as the rhodium precursor, the corresponding ligands and the regulation agents at 40 °C under 10 bar of a 1:1 H_2/CO mixture in toluene, with the minimum amount of THF to solubilize the RA (97:3 v/v).

Initially 2,5-dihydrofuran (**4**) was chosen to evaluate the regio- and enantio-selectivity of the reaction (Table A1). In the absence of alkali metal BArF salts, low conversions were observed for the hydroformylation of **4** mediated by ligands (*R*,*S*)-**L4** and (*S*,*S*)-**L5**. For all the combinations of ligand and

RA tested, 2-carbaldehyde (**5**) and the isomerization product **7** were not detected, which indicates that the chemo- and regio-selectivity in the hydroformylation of **4** is higher with the rigid ligands **L4** and **L5** than with the ligands **L2** and **L3** having a longer polyether chain. Unfortunately, enantioselectivities were lower with these rigid ligands (compare the results summarized in Table 2 for **L2** and **L3** and in Table A1 for **L4** and **L5**). The highest value of enantiomeric excess obtained for 3-carbaldehyde **6** was 36% ee when (*S*,*S*)-**L5** was employed in combination with CsBArF as RA (see entry 12 in Table A1).

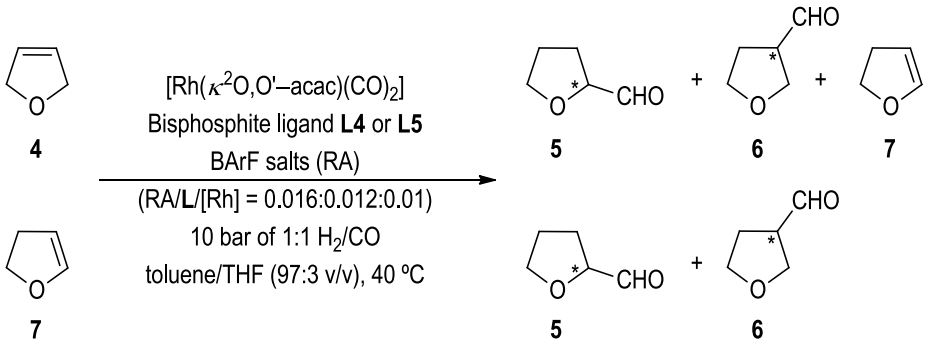

Scheme A1. AHF of **4** and **7** mediated by supramolecularly regulated ligands **L4** or **L5**.

Table A1. AHF of **4** using Rh-complexes of ligands **L4** or **L5** and a set of BArF salts as RAs.[a]

Entry	Ligand	RA	Conv. (%)	ratio **5**:**6**:**7**	ee of **5** (%) config.	ee of **6** (%) config.
1	(*R*,*S*)-**L4**	-	54	<1:44:56	n.d	6 (*R*)
2		LiBArF	>99	<1:90:10	n.d	16 (*R*)
3		NaBArF	>99	<1:99:1	n.d	17 (*R*)
4		KBArF	>99	<1:99:1	n.d	18 (*R*)
5		RbBArF	>99	<1:99:1	n.d	16 (*S*)
6		CsBArF	>99	<1:99:1	n.d	22 (*R*)
7	(*S*,*S*)-**L5**	-	13	<1:>99:<1	n.d	29 (*R*)
8		LiBArF	>99	<1:>99:<1	n.d	30 (*R*)
9		NaBArF	>99	<1:>99:<1	n.d	32 (*R*)
10		KBArF	>99	<1:>99:<1	n.d	33 (*R*)
11		RbBArF	>99	<1:>99:<1	n.d	32 (*S*)
12		CsBArF	>99	<1:>99:<1	n.d	36 (*R*)

[a] See footnote a in Table 1 for details, with the following remarks: Reaction conditions are shown in Scheme A1 and the amount of **7** was determined by ^{1}H NMR.

In the case of 2,3-dihydrofuran (**7**), the substrate reacted more slowly than 2,5-dihydrofuran (**4**), with both ligands: the substrate was not fully converted into hydroformylation products, even in the presence of the RAs. The best result in terms of conversion was provided by the combination of (*S*,*S*)-**L5** and KBArF as RA (up to 76%, entry 10 in Table A2). The ee values were lower compared with those obtained with

ligands **L2** and **L3**. For instance, the ligand (*R*,*S*)-**L4** provided the highest ee's in combination with LiBArF or RbBArF as RAs (up to 31% for aldehyde **5** and 28-29% for aldehyde **6**; see entries 2 and 5 in Table A2), whilst the analogous ligand with four ethyleneoxy groups bonded to the BINOL´s hydroxyl groups provided the highest ee in combination with KBArF (81% ee for aldehyde **5** and 20% ee for aldehyde **6**, see entry 8 in Table 3).

Table A2. AHF of **7** using Rh-complexes of ligands **L4** or **L5** and a set of BArF salts as RAs.[a]

Entry	Ligand	RA	Conv. (%)	ratio **5**:**6**:**7**	ee of **5** (%) config.	ee of **6** (%) config.
1	(*R*,*S*)-**L4**	-	0	n.d	n.d	n.d
2		LiBArF	50	10:40:50	31 (*R*)	29 (*R*)
3		NaBArF	56	10:46:44	27 (*R*)	30 (*R*)
4		KBArF	60	13:47:40	23 (*R*)	29 (*R*)
5		RbBArF	53	11:42:47	31 (*R*)	28 (*R*)
6		CsBArF	64	15:49:36	21 (*S*)	25 (*R*)
7	(*S*,*S*)-**L5**	-	0	n.d	n.d	n.d
8		LiBArF	69	17:52:31	5 (*R*)	15 (*S*)
9		NaBArF	67	15:52:33	3 (*S*)	14 (*S*)
10		KBArF	76	20:56:24	3 (*R*)	17 (*S*)
11		RbBArF	51	12:39:49	6 (*S*)	12 (*S*)
12		CsBArF	57	17:40:43	3 (*S*)	14 (*S*)

[a] See footnote a in Table 1 for details, with the following remarks: Reaction conditions are shown in Scheme A1 and the amount of **7** was determined by ^{1}H NMR.

As regards the hydroformylation of *cis*-4,7-dihydro-1,3-dioxepin (**8**), ligands (*R*,*S*)-**L4** and (*S*,*S*)-**L5** were very active in this transformation displaying full conversion under all reaction conditions tested. The ee values were lower compared to those obtained with **L2** and **L3**. The highest enantioselectivity was obtained employing ligand (*R*,*S*)-**L4** in combination with LiBArF or KBArF (76% ee, entry 2 and 4 in Table A3), whilst the analogous ligand with four ethyleneoxy groups bonded to the hydroxyl groups in the BINOL fragment provided the highest ee in combination with KBArF (83% ee, see entry 5 in Table 4).

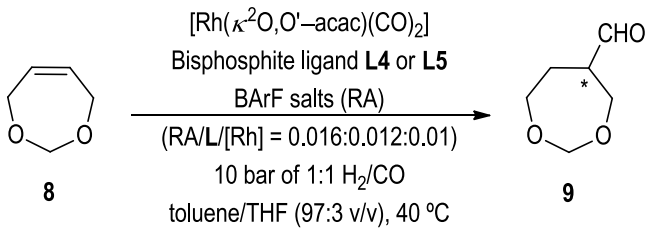

8 **9**

Scheme A2. AHF of **8** mediated by supramolecularly regulated ligands **L4** or **L5**.

Table A3. AHF of **8** using Rh-complexes of ligands **L4** or **L5** and a set of BArF salts as RAs.[a]

Entry	Ligand	RA	Conv. (%)	ee of **9** (%) config.[b]
1	(*R*,*S*)-**L4**	-	68	67 (+)
2		LiBArF	>99	76 (+)
3		NaBArF	39	3 (+)
4		KBArF	>99	76 (+)
5		RbBArF	>99	52 (+)
6		CsBArF	>99	55 (+)
7	(*S*,*S*)-**L5**	-	23	17 (+)
8		LiBArF	>99	10 (+)
9		NaBArF	>99	7 (+)
10		KBArF	>99	22 (+)
11		RbBArF	>99	11 (–)
12		CsBArF	>99	20 (+)

[a] See footnote a in Table 1 for details, with the following remarks: Reaction conditions are shown in Scheme A2. [b] Absolute configuration is unknown, and the sign of the optical rotation is provided.

In short, the increased rigidity of the ligands associated with the reduction in the number of ethyleneoxy units from four to two in the regulation site turned out to be detrimental for the catalytic activity and the regulation ability of these supramolecular ligands in the asymmetric hydroformylation of heterocyclic olefins.

3.7.1.2. Experimental section and NMR spectra of ligands (*R*,*S*)-**L4** and (*S*,*S*)-**L5**

Synthesis of ligand (*R*,*S*)-L4: Ligand (*R*,*S*)-**L4** was synthesized from (*S*)-5,5'-6,6´-Tetramethyl-3,3´-di-*tert*-butyl-1,1'-biphenyl-2,2'-diol (347 mg, 0.98 mmol), which was azeotropically dried with toluene (3 × 2 mL) under argon atmosphere. The remaining solid was dissolved in anhydrous toluene (*ca*. 16 mL) and slowly added to a stirred solution of PCl_3 (108 μL, 1.23 mmol) and NEt_3 (389 μL, 2.80 mmol) in dry toluene (*ca*. 16 mL) at 0 °C. The solution was allowed to reach room temperature and was stirred overnight. The turbid reaction mixture was filtered, and the solvent was evaporated under reduced pressure. The resulting residue was dissolved in *ca*. 16 mL of dry toluene and NEt_3 (389 μL, 2.80 mmol). A solution of (*R*)- 2,2'-([1,1'-binaphthalene]-2,2'-diylbis(oxy))diethanol[19] (169 mg, 0.45 mmol in *ca*. 16 mL of toluene) was slowly added to the previous solution, and the mixture was allowed to react overnight at room temperature. The reaction mixture was filtered, and the solvent was evaporated under reduced pressure. The resulting crude mixture was purified by column chromatography on silica gel using cyclohexane/EtOAc 90:10, as the elution solvent, to obtain the expected bisphosphite ligand (*R*,*S*)-**L4** as a white solid. Isolated 221 mg, 43% yield, quantitatively pure by ^{31}P NMR. ^{1}H NMR ($CDCl_3$, 400 MHz): δ 7.85 (s, 1H), 7.82 (bs, 2H), 7.80 (s, 1H), 7.34–7.28 (m, 4H), 7.19–7.14 (m, 4H), 7.02 (bs, 2H), 6.99 (s, 1H), 6.97 (s, 1H), 3.95–3.84 (m, 4H), 3.75–3.67 (m, 2H), 3.23–3.16 (m, 2H), 2.25 (s, 6H), 2.11 (s, 6H), 1.76 (d, *J* = 7.2 Hz, 12H), 1.41 (s, 18H), 1.28 (s, 18H). $^{13}C\{^{1}H,^{31}P\}$ NMR ($CDCl_3$, 126 MHz,): δ154.3, 145.4, 145.4, 138.2, 137.0, 135.1, 134.4, 134.1, 132.5, 131.8, 131.7, 131.74 , 130.7, 129.7, 129.5, 128.1, 128.0, 127.9, 127.88, 126.3, 125.5, 123.9, 120.8, 116.7, 69.5, 62.5, 34.8, 34.7, 31.5, 31.1, 20.6, 20.4, 16.8, 16.6. $^{31}P\{^{1}H\}$ NMR ($CDCl_3$, 202 MHz): δ130.7 (s). HRMS–ESI–TOF (*m/z*): $[M + H]^+$ calcd for $C_{72}H_{85}O_8P_2$, 1139.5714; found, 1139.5712. $[\alpha]_D^{25}$= +422.2 (*c* 0.1, DCM). IR (neat, cm^{-1}) $\bar{\upsilon}$ 2956, 2868, 1226, 1024, 870. mp 128.6–130.4 °C.

Synthesis of ligand (*S*,*S*)-L5: Ligand (*S*,*S*)-**L5** was synthesized from (*S*)-5,5'-6,6´-Tetramethyl-3,3´-di-*tert*-butyl-1,1'-biphenyl-2,2'-diol (384 mg, 1.08 mmol), which was azeotropically dried with toluene (3 × 2 mL) under argon atmosphere. The remaining solid was dissolved in anhydrous toluene (*ca.* 18 mL) and slowly added to a stirred solution of PCl_3 (119 μL, 1.36 mmol) and NEt_3 (431 μL, 3.10 mmol) in dry toluene (*ca.* 18 mL) at 0 °C. The solution was allowed to reach room temperature and was stirred overnight. The turbid reaction mixture was filtered, and the solvent was evaporated under reduced pressure. The resulting residue was dissolved in *ca*. 18 mL of dry toluene and NEt_3 (431 μL, 3.10 mmol). A solution of (*S*)- 2,2'-([1,1'-binaphthalene]-2,2'-diylbis(oxy))diethanol[19] (187 mg, 0.49 mmol in *ca.* 18 mL of toluene) was slowly added to the previous solution, and the mixture was allowed to react overnight at room temperature. The reaction mixture was filtered, and the solvent was evaporated under reduced pressure. The resulting crude mixture was purified by column chromatography on silica gel using cyclohexane/EtOAc 90:10 as the elution solvent to obtain the expected bisphosphite ligand (*S*,*S*)-**L5** as a white solid. Isolated 210 mg, 37%

yield, quantitatively pure by ^{31}P NMR. ^{1}H NMR ($CDCl_3$, 400 MHz,): δ 7.89 (s, 1H), 7.87 (s, 1H), 7.85 (s, 1H), 7.83 (s, 1H), 7.34–7.29 (m, 4H), 7.19–7.13 (m, 4H), 7.05 (s, 1H), 7.03 (s, 1H), 7.01 (bs, 2H), 3.90–3.87 (m, 4H), 3.77–3.69 (m, 2H), 3.21–3.15 (m, 2H), 2.24 (s, 6H), 2.15 (s, 6H), 1.77 (d, *J* = 17.5 Hz, 12H), 1.38 (s, 18H), 1.29 (s, 18H). $^{13}C\{^{1}H,^{31}P\}$ NMR ($CDCl_3$, 100 MHz,): δ 154.3, 145.5, 145.46, 138.2, 136.9, 135.1, 134.4, 134.1, 132.5, 131.8, 131.6, 130.7, 129.8, 129.5, 128.1, 128.0, 127.9, 126.4, 125.7, 124.0, 121.0, 116.9, 69.7, 62.8, 34.7, 34.66, 31.4, 31.1, 20.5, 20.47, 16.8, 16.6. $^{31}P\{^{1}H\}$ NMR ($CDCl_3$, 162 MHz): δ 131.3 (s). HRMS–ESI–TOF (*m/z*): [M + H]+ calcd for $C_{72}H_{85}O_8P_2$, 1139.5714; found, 1139.5690. $[\alpha]_D^{25}$ = +389.6 (*c* 0.1, DCM). IR (neat, cm^{-1}) $\tilde{\upsilon}$ 2956, 2868, 1225, 1024, 870. mp 127.3–140.5 °C.

The spectra of the new ligands synthesized are shown in the following figures:

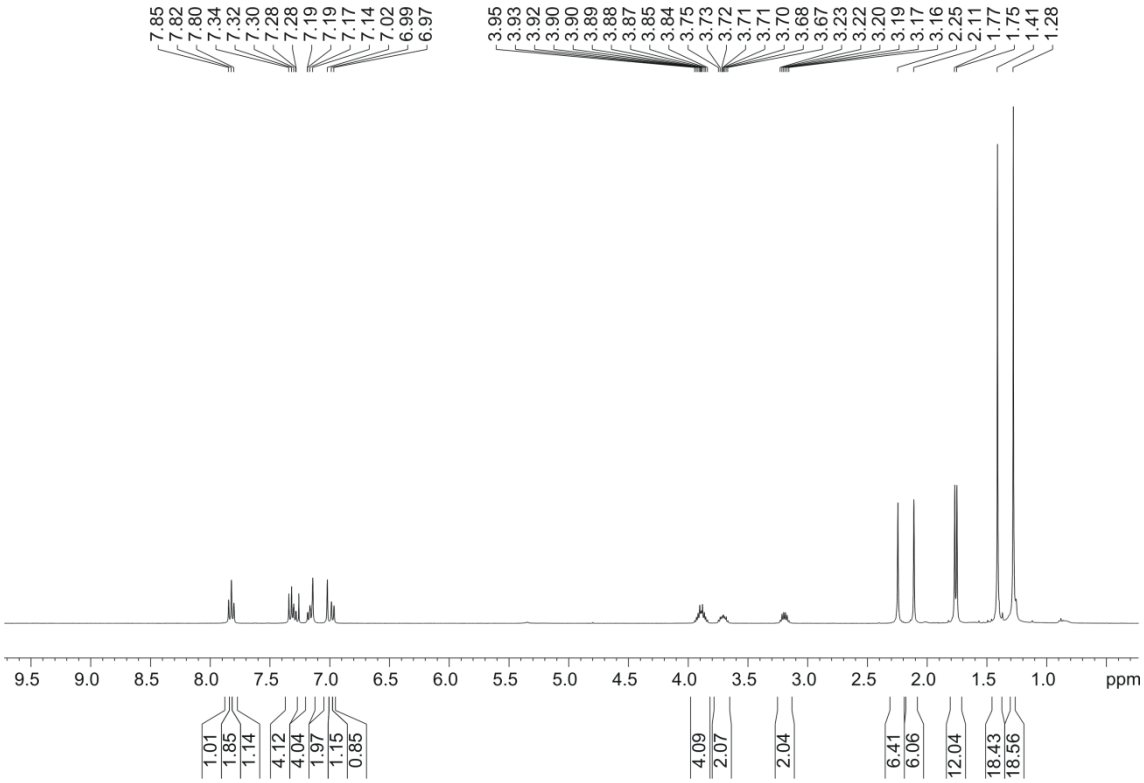

Figure A2. ^{1}H NMR spectrum of (*R*,*S*)-**L4**.

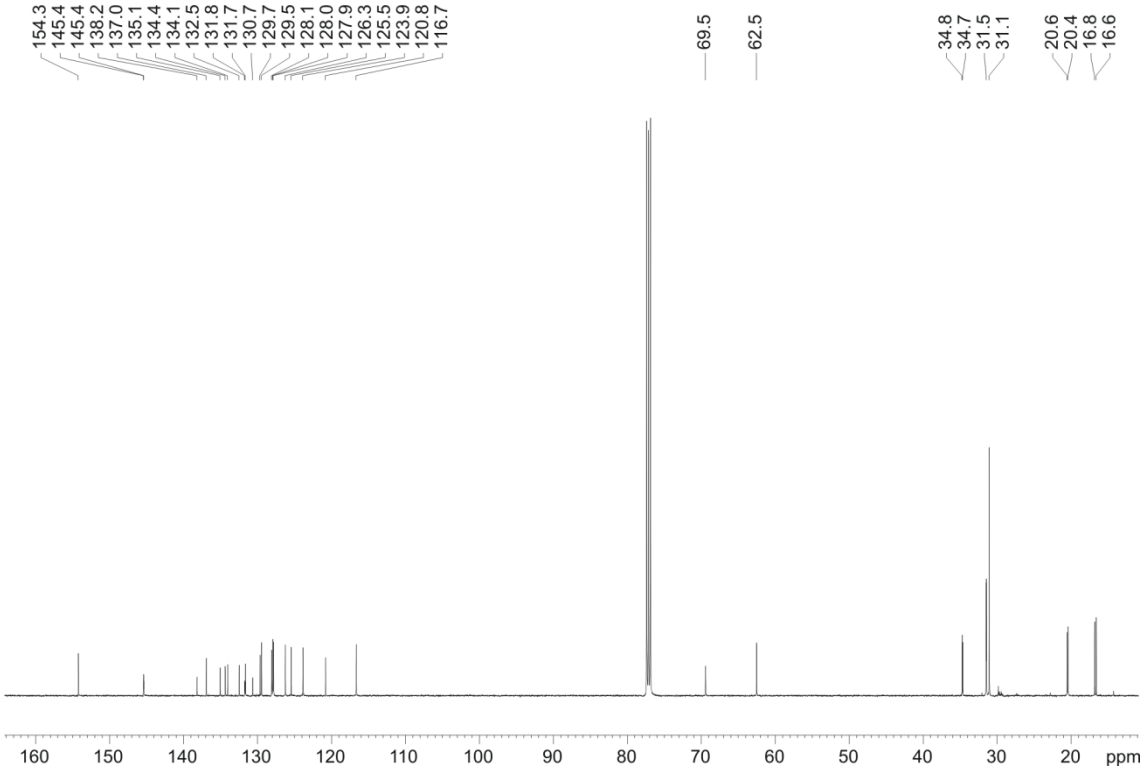

Figure A3. $^{13}C\{^{1}H,^{31}P\}$ NMR spectrum of (*R*,*S*)-**L4**.

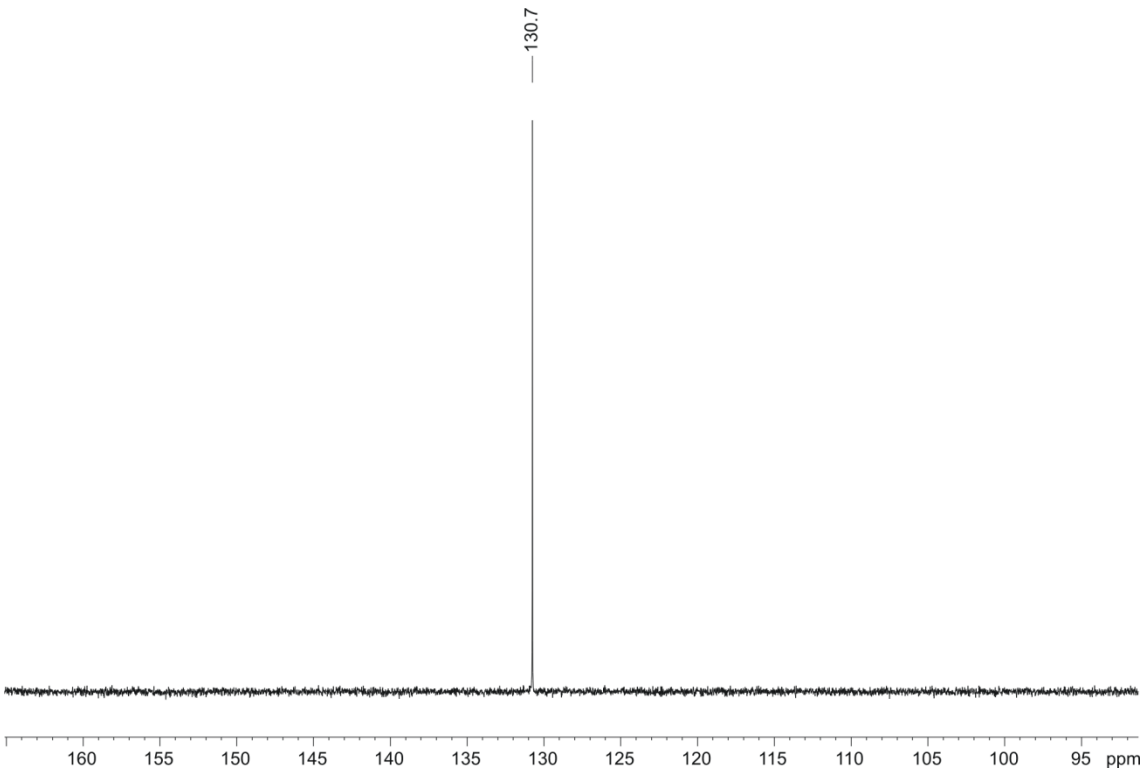

Figure A4. $^{31}P\{^{1}H\}$ NMR spectrum of (*R*,*S*)-**L4**.

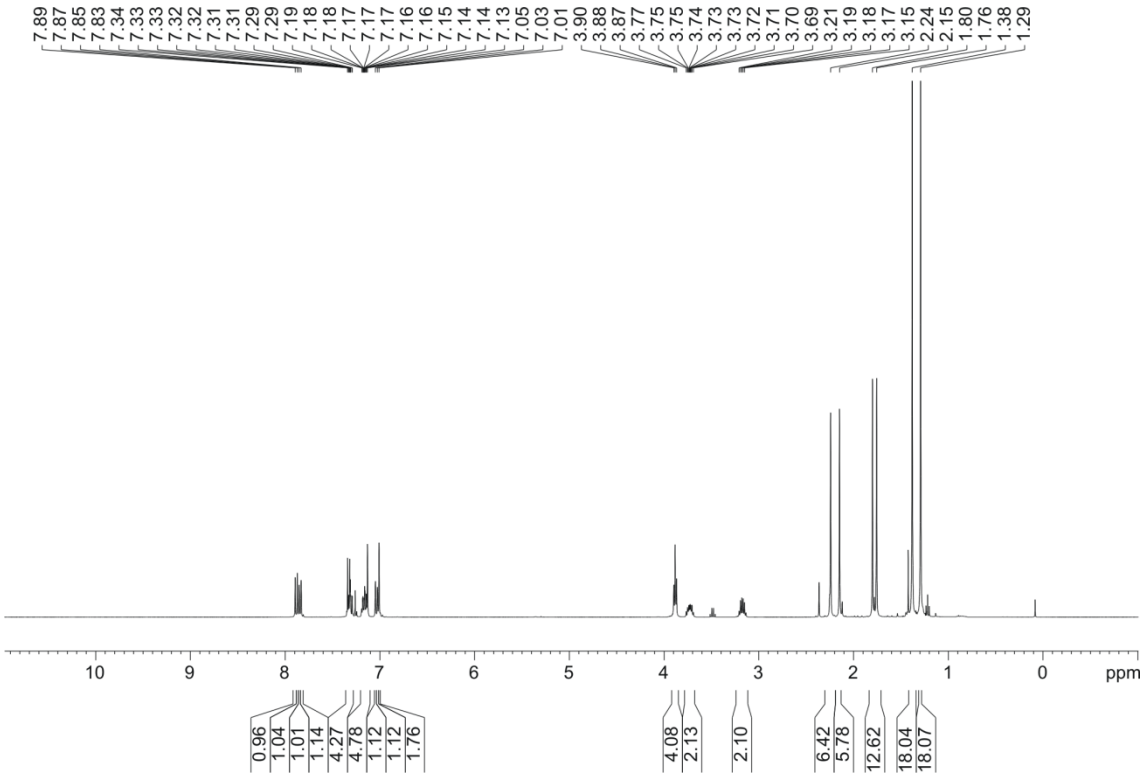

Figure A5. ^{1}H NMR spectrum of (*S*,*S*)-**L5**.

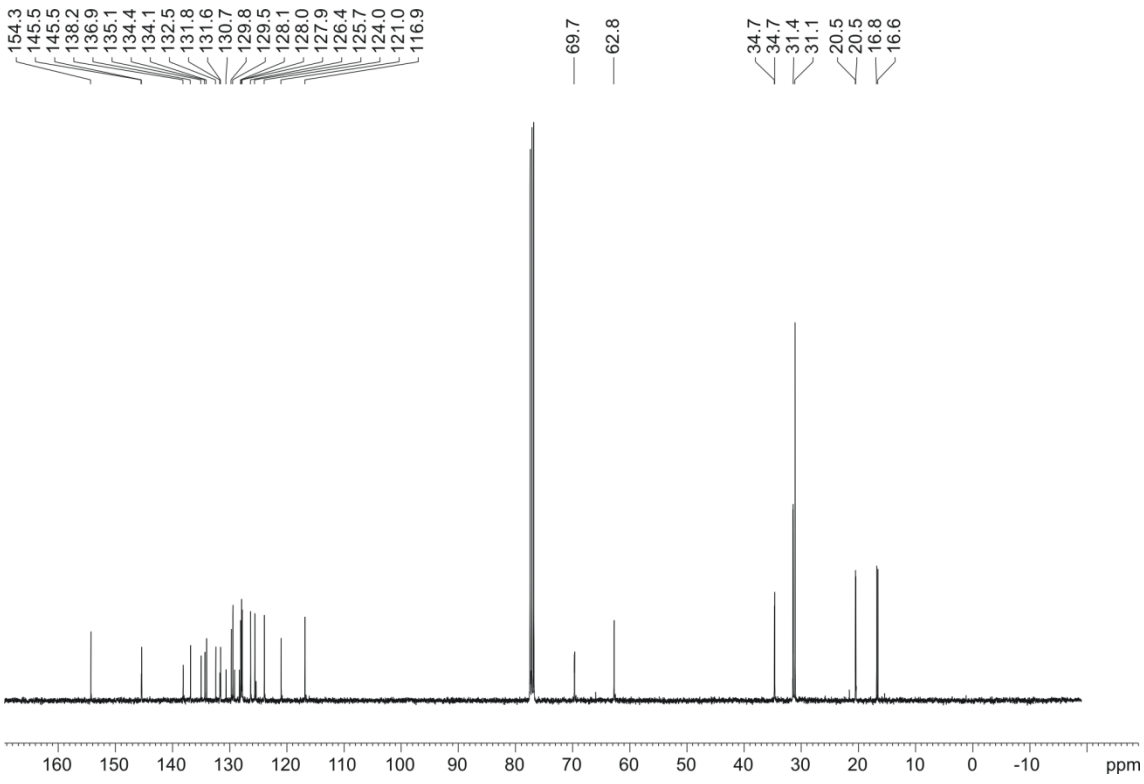

Figure A6. $^{13}C\{^{1}H,^{31}P\}$ NMR spectrum of (*S*,*S*)-**L5**.

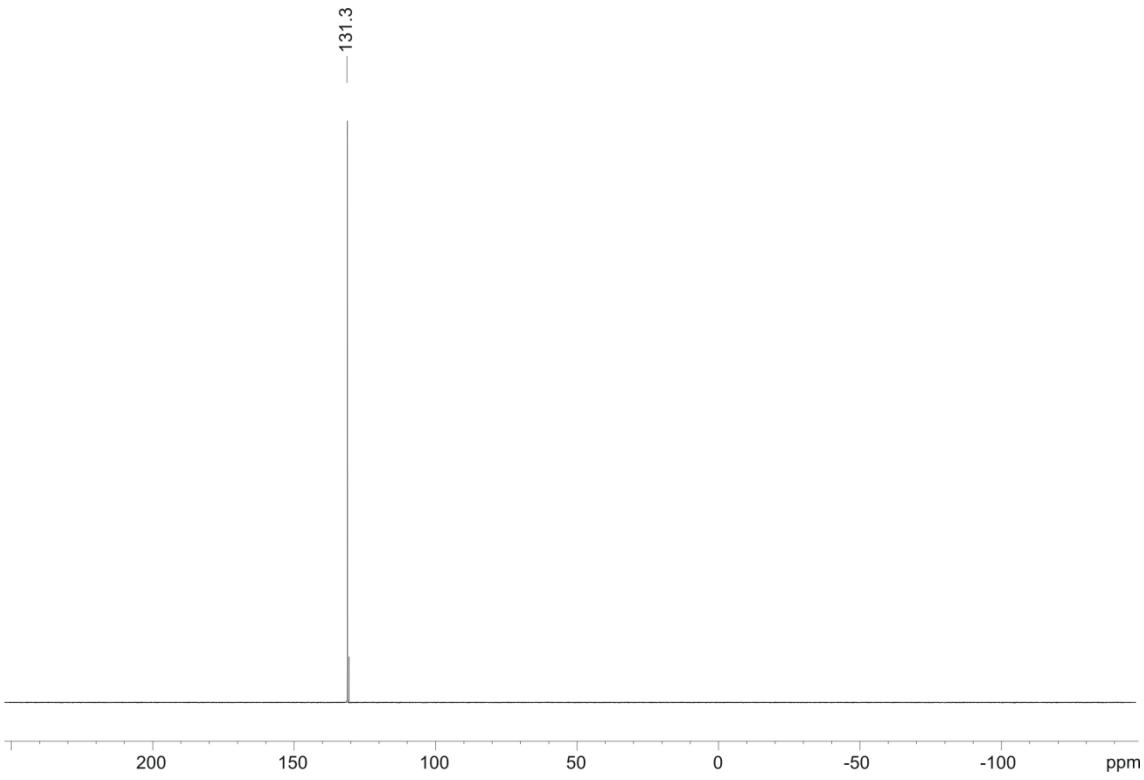

Figure A7. $^{31}P\{^{1}H\}$ NMR spectrum of (*S*,*S*)-**L5**.

3.7.2. Studies on the structure of catalytically relevant species in hydroformylation derived from ligand (*R*)-L6

3.7.2.1. Discussion

Taking into account the notable regulation properties of the supramolecular bisphosphite ligand (*R*)-**L6** in Rh-mediated asymmetric hydroformylations of several functionalized alkenes,[2c] and in order to elucidate the structure of catalytically relevant species, complexation experiments between (*R*)-**L6** and [Rh(κ^2O,O'–acac)(CO)$_2$] (in the presence and absence of the appropriate regulation agent) were performed within this PhD Thesis. The results of these complexation experiments have been summarized in the discussion that follows.

[Rh(κ^2O,O'–acac)(CO)$_2$] and (*R*)-**L6** were reacted at 40 ºC in a typical solvent mixture for hydroformylations toluene/THF (97:3 v/v) under 10 bar of 1:1 H_2/CO. Interestingly, the addition of equimolar amounts of [Rh(κ^2O,O'–acac)(CO)$_2$] to a solution of (*R*)-**L6**, followed by reaction for 2 h, did not lead to the expected hydrido-dicarbonyl chelate [Rh(H)(CO)$_2$(κ^2P,P'–(*R*)-**L6**)], but rather to the complex [Rh(κ^2O,O'–acac)(CO)(κ^1P–(*R*)-**L6**)] (see Scheme A3 and Figure A9), which was formed upon displacement of a CO ligand by a phosphite group. The complex [Rh(κ^2O,O'–acac)(CO)(κ^1P–(*R*)-**L6**)] evolved to the expected chelate [Rh(H)(CO)$_2$(κ^2P,P'–(*R*)-**L6**)] with time (16 h total), even in the absence of a polyether chain binder.

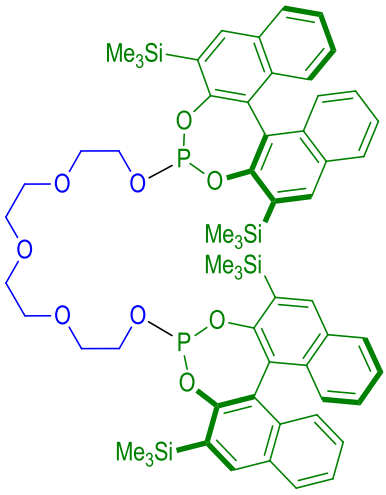

(*R*)-L6

Figure A8. Supramolecularly regulated bisphosphite ligand **(*R*)-L6**.

Binding between RbBArF and the ligand (*R*)-**L6** is strong ((1.2 x 10^4 ± 2 x 10^3) M^{-1}; measured by NMR spectroscopy at 25 ºC in C_7D_8/C_4D_8O (99.8:0.2, v/v)).[2c] This high affinity translates into the efficient formation under hydroformylation reaction conditions of the chelate [Rh(H)(CO)$_2$(κ^2P,P'–RbBArF•(*R*)-**L6**)] after only 2 h (instead of the 16 h required for the reaction without RA; see Scheme A3 and Figure A9).

This behavior clearly demonstrated that binding of the RA to (*R*)-**L6**, serves to bring the two terminal phosphorus groups closer together, thereby favoring the formation of chelate species.

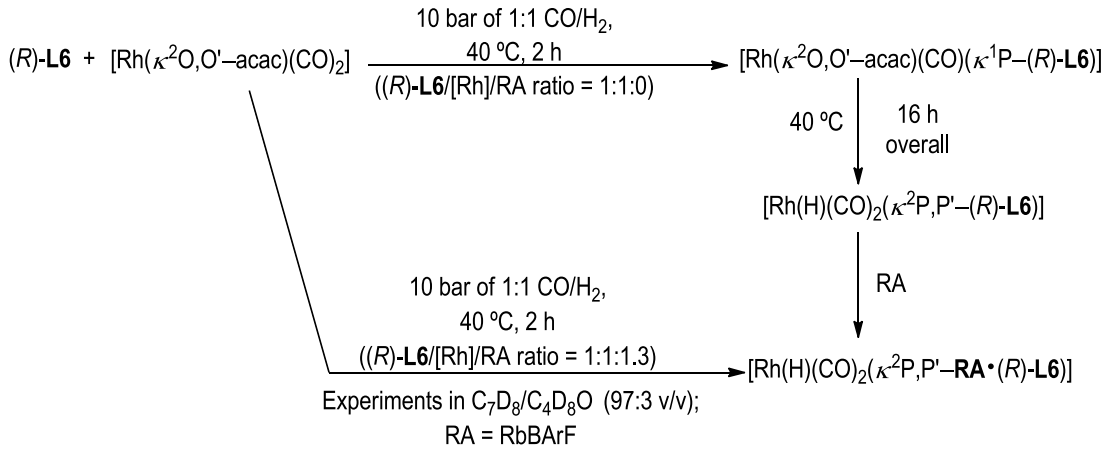

Scheme A3. Complexation of [Rh(κ^2O,O'–acac)(CO)$_2$] and (*R*)-**L6** in the presence or absence of RbBArF.

Formation of the rhodium chelate ([Rh(H)(CO)$_2$(κ^2P,P'–RbBArF•(*R*)-**L6**)] was unequivocally proven with standard spectroscopic techniques,[20] from which ^{31}P and ^{1}H high-pressure (HP) NMR analysis proved to be invaluable. For instance, the ^{31}P NMR spectrum of [Rh(H)(CO)$_2$(κ^2P,P'–RbBArF•(*R*)-**L6**)] showed a doublet at δ 146.3 ppm ($^1J_{Rh-P}$ = 249 Hz), which clearly indicated a bidentate coordination mode for RbBArF•(*R*)-**L6** towards the rhodium center (see Figure A18). Only one hydrido signal was observed in the ^{1}H NMR spectrum, which exhibited a broad, poorly resolved doublet centered at δ –10.62 ppm. The Rh–H coupling constant value ($^1J_{Rh-H}$) was calculated to be 3.4 Hz, but the P–H coupling (through two bonds) was too small to be directly measurable, and only led to signal broadening rather than to proper signal splitting (width of the hydride signal at half height: ≈ 9 Hz; see Figure A18). This P–H coupling was demonstrated by ^{1}H–^{31}P HMBC spectroscopy, which showed a cross-peak signal between the signals of the hydrido group and the phosphite moieties (Figure A19 in section 3.7.2.2). This combination of small P–H coupling and large Rh–P coupling indicated that the hydrido ligand has a strong preference for a *cis*-orientation relative to the P-ligating groups, which are coordinated in an equatorial–equatorial fashion to a trigonal-bipyramidal rhodium center.[8a,21] Many other rhodium complexes with this type of spatial orientation between the bisphosphite ligand and the hydride have been reported as excellent catalysts for hydroformylations.[8a] Similar conclusions were drawn from the studies on complexation of the rhodium precursor [Rh(κ^2O,O'–acac)(CO)$_2$] and the ligand (*R*)-**L6**: also in this case, a trigonal–bipyramidal hydrido–dicarbonyl rhodium complex with two equatorial sites occupied by the phosphorus ligating groups was formed (Figure A9).

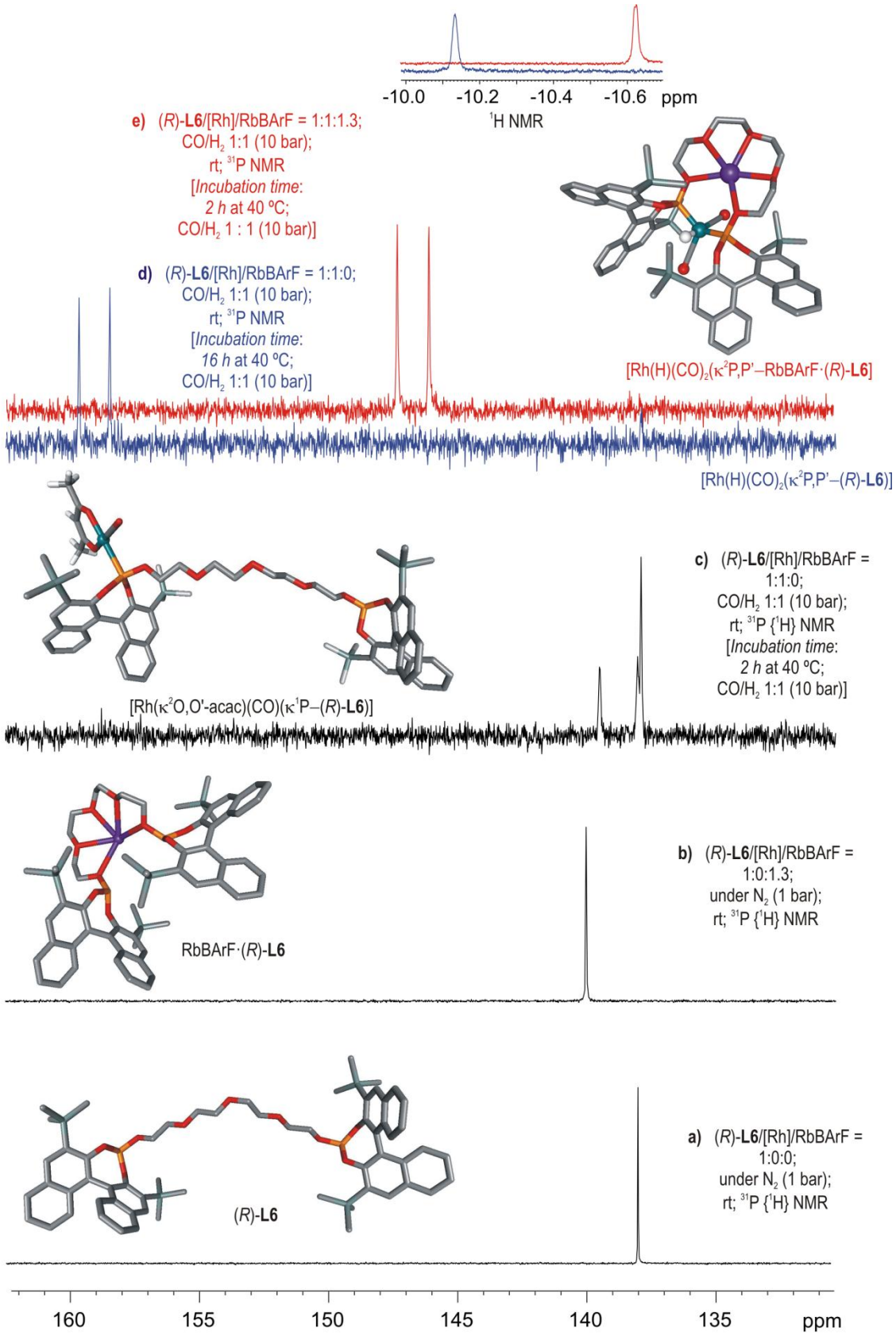

Figure A9. Comparison of $^{31}P\{^{1}H\}$ NMR spectra of : a) (*R*)-**L6** under N_2, b) (*R*)-**L6** and RbBArF under N_2, c) [Rh(κ^2O,O'–acac)(CO)(κ^1P–(*R*)-**L6**)] under H_2/CO (1:1), d) ^{31}P NMR [Rh(H)(CO)$_2$(κ^2P,P´–(*R*)-**L6**)] complex and ^{1}H NMR hydride-region, e) ^{31}P NMR [Rh(H)(CO)$_2$(κ^2P,P'–RbBArF•(*R*)-**L6**)] complex and ^{1}H NMR hydride-region.

3.7.2.2. Coordination studies of ligand (*R*)-**L6** and [Rh(κ^2O,O'–acac)(CO)$_2$] and NMR spectra

Formation of [Rh(κ^2O,O'–acac)(CO)(κ^1P–(*R*)-**L6**)]

An equimolar solution of (*R*)-**L6** and [Rh(κ^2O,O'–acac)(CO)$_2$] in C_7D_8/C_4D_8O (97:3 v/v) (*ca.* 5 mM) was stirred at rt for 2 h under N_2. Spectroscopic data obtained from this solution were in agreement with the quantitative formation of the [Rh(κ^2O,O'–acac)(CO)(κ^1P–(*R*)-**L6**)] complex: ^{1}H NMR (C_7D_8/C_4D_8O (97:3 v/v), 500 MHz): δ 8.13 (s, 1H), 8.09–8.08 (m, 2H), 8.06 (s, 1H), 7.69–7.63 (m, 4H), 7.27 (d, *J* = 8.5 Hz, 1H), 7.19–7.15 (m, 3H), 7.12–7.09 (m, 4H), 6.88–6.81 (m, 4H), 5.20 (s, 1H), 4.27–4.21 (m, 1H), 4.02–3.97 (m, 1H), 3.82–3.77 (m, 1H), 3.36–3.21 (m, 11H), 3.16 (t, *J* = 5.0 Hz, 2H), 1.79 (s, 3H), 1.42 (s, 3H), 0.69 (s, 9H), 0.59 (s, 9H), 0.52 (s, 18H). ^{31}P{^{1}H} NMR (C_7D_8/C_4D_8O (97:3 v/v), 202 MHz): δ 137.5 (s), 138.3 (d, *J* = 283 Hz); MALDI–TOF (*m*/*z*): [M – CO]$^+$ calcd for $C_{65}H_{79}O_{11}P_2Si_4Rh$ 1312.3230, found 1312.3153. IR (ATR under N_2 cm^{-1}) $\bar{\upsilon}$ 2005. Attempts to isolate this rhodium complex in analytically pure form failed.

Stepwise formation of [Rh(H)(CO)$_2$(κ^2P,P'–RbBArF•(*R*)-**L6**)] *via* [Rh(κ^2O,O'–acac)(CO)(κ^1P–(*R*)-**L6**)]

An equimolar solution of (*R*)-**L6** and [Rh(κ^2O,O'–acac)(CO)$_2$] in C_7D_8/C_4D_8O (97:3 v/v) (*ca.* 5 mM) was stirred at 40 ºC for 2 h at 10 bar of syngas (1:1 H_2/CO) in an autoclave. Spectroscopic data at this point were in agreement with the formation of the [Rh(κ^2O,O'–acac)(CO)(κ^1P–(*R*)-**L6**)] complex (see spectroscopic data indicated above and Figure A11), together with minor amounts of [Rh(H)(CO)$_2$(κ^2P,P'–(*R*)-**L6**)]. Further stirring of the previous reaction mixture at 40 ºC for an overall reaction time of 16 h under 10 bar of syngas (1:1 H_2/CO) in an autoclave led to the formation of the [Rh(H)(CO)$_2$(κ^2P,P'–(*R*)-**L6**)] complex. The autoclave was cooled to room temperature, depressurized in a well-ventilated fume hood and the reaction mixture was transferred to 5 mm HP-NMR sapphire tube. The tube was pressurized with syngas (1:1 H_2/CO, 10 bar) and the HP-NMR spectra were collected at 25 ºC (see Figure A12 to Figure A15). MS samples were immediately recorded under N_2 after depressurizing the autoclave.

Spectroscopic data obtained from this solution were in agreement with the quantitative formation of the [Rh(H)(CO)$_2$(κ^2P,P'–(*R*)-**L6**)] complex: ^{1}H NMR (C_7D_8/C_4D_8O (97:3 v/v), 500 MHz): δ 8.11 (s, 2H), 8.03 (s, 2H), 7.64 (d, *J* = 8.0 Hz, 2H), 7.58 (d, *J* = 7.9 Hz, 2H), 7.14–6.95 (m, 8H), 6.80–6.77 (m, 2H), 6.75–6.72 (m, 2H), 4.46–4.36 (m, 2H), 3.90–3.85 (m, 2H), 3.57–3.53 (m, 3H), 3.51–3.45 (m, 3H), 3.41–3.37 (m, 6H), 0.69 (s, 18H), 0.48 (s, 18H), –10.13 (s, 1H). ^{13}C{^{1}H} NMR (C_7D_8/C_4D_8O (97:3 v/v), 125 MHz): δ 191.3, 154.0, 151.4, 137.8, 137.7, 137.25, 137.18, 134.8, 134.7, 134.3, 133.2, 132.9, 132.0, 131.6, 131.4, 131.25, 131.15, 129.2, 128.6, 128.5, 128.3, 127.2, 127.1, 127.0, 126.9, 126.8, 126.7, 126.5, 123.6, 122.5, 70.8, 70.7, 70.1, 66.4, 1.8, 0.0. ^{31}P{^{1}H} NMR (C_7D_8/C_4D_8O (97:3 v/v), 202 MHz): δ 158.7 (d, J_{Rh-P} = 242 Hz). MALDI–TOF (*m*/*z*): [M–2CO–H]$^+$ calcd for $C_{60}H_{72}O_9P_2Si_4Rh$ 1213.2784, found 1213.2803. IR (recorded at 10 bar of 1:1 H_2/CO in a HP cell, cm^{-1}) $\bar{\upsilon}$ 2024, 2046. Attempts to isolate this rhodium complex in analytically pure form failed.

Further addition of 1.3 equiv. of RbBArF, followed by repressurization at 10 bar of syngas (1:1 H_2/CO) and stirring for 2 h under these conditions, led to the formation of the [Rh(H)(CO)$_2$(κ^2P,P'–RbBArF•(*R*)-**L6**)] complex. Spectroscopic data were in agreement with those observed when this complex was directly prepared by mixing [Rh(κ^2O,O'–acac)(CO)$_2$], ligand (*R*)-**L6** and RbBArF in a 1:1:1.3 ratio (see below).

Direct formation of [Rh(H)(CO)$_2$(κ^2P,P'–RbBArF•(*R*)-**L6**)]

A 5 mM solution of (*R*)-**L6** (1 equiv.), [Rh(κ^2O,O'–acac)(CO)$_2$] (1 equiv.) and RbBArF (1.3 equiv.) in C_7D_8/C_4D_8O (97:3 v/v) was transferred to a 25 mL autoclave reactor, which was pressurized to 10 bar of syngas (1:1 H_2/CO) and warmed to 40 ºC. The mixture was allowed to stir for 2 hours. The reactor was cooled to room temperature, depressurized in a well-ventilated fume hood and the reaction mixture was transferred to 5 mm HP-NMR sapphire tube. The tube was pressurized with syngas (1:1 H_2/CO, 10 bar) and the HP-NMR spectra were collected at 25 ºC (see Figure A16 to Figure A19). MS samples were immediately recorded under N_2 after depressurizing the autoclave. Spectroscopic data obtained from this solution were in agreement with the quantitative formation of the [Rh(H)(CO)$_2$(κ^2P,P'–RbBArF•(*R*)-**L6**)] complex: ^{1}H NMR (C_7D_8/C_4D_8O (97:3 v/v), 500 MHz): δ 8.13 (s, 3H), 7.97 (s, 2H), 7.70–7.66 (m, 8H), 7.54 (d, *J* = 8.0 Hz, 2H), 6.79–6.76 (m, 5H), 3.74–3.72 (m, 2H), 3.47–3.39 (m, 2H), 2.98–2.87 (m, 10H), 2.68–2.56 (m, 2H), 0.54 (s, 18H), 0.41 (s, 18H), –10.62 (d, *J* = 3.1 Hz, 1H). ^{13}C{^{1}H} NMR (C_7D_8/C_4D_8O (97:3 v/v), 125 MHz): δ 191.3, 162.6 (q, *J* = 49.7 Hz), 154.0, 150.3, 138.5, 138.4, 135.5, 134.5, 134.3, 131.9, 131.6, 131.1, 130.3, 130.1, 129.8, 129.5, 129.2, 128.5, 128.3, 127.9, 127.5, 127.0, 126.9, 126.4, 126.0, 125.9, 125.4, 124.2, 123.0, 122.0, 118.0, 70.1, 69.5, 69.4, 67.3, 1.6, 0.3. ^{31}P{^{1}H} NMR (C_7D_8/C_4D_8O (97:3 v/v), 202 MHz): δ 146.3 (d, *J* = 249 Hz). MALDI–TOF (*m*/*z*): [M–RbBArF–2CO–H]$^+$ calcd for $C_{60}H_{72}O_9P_2Si_4Rh$ 1213.2784, found 1213.2790. IR (recorded at 10 bar of 1:1 H_2/CO in a HP cell, cm^{-1}) $\bar{\upsilon}$ 2040, 2077. Attempts to isolate this rhodium complex in analytically pure form failed.

The spectra of complexes derived from (*R*)-**L6** and [Rh(κ^2O,O'–acac)(CO)$_2$] are shown in the following figures:

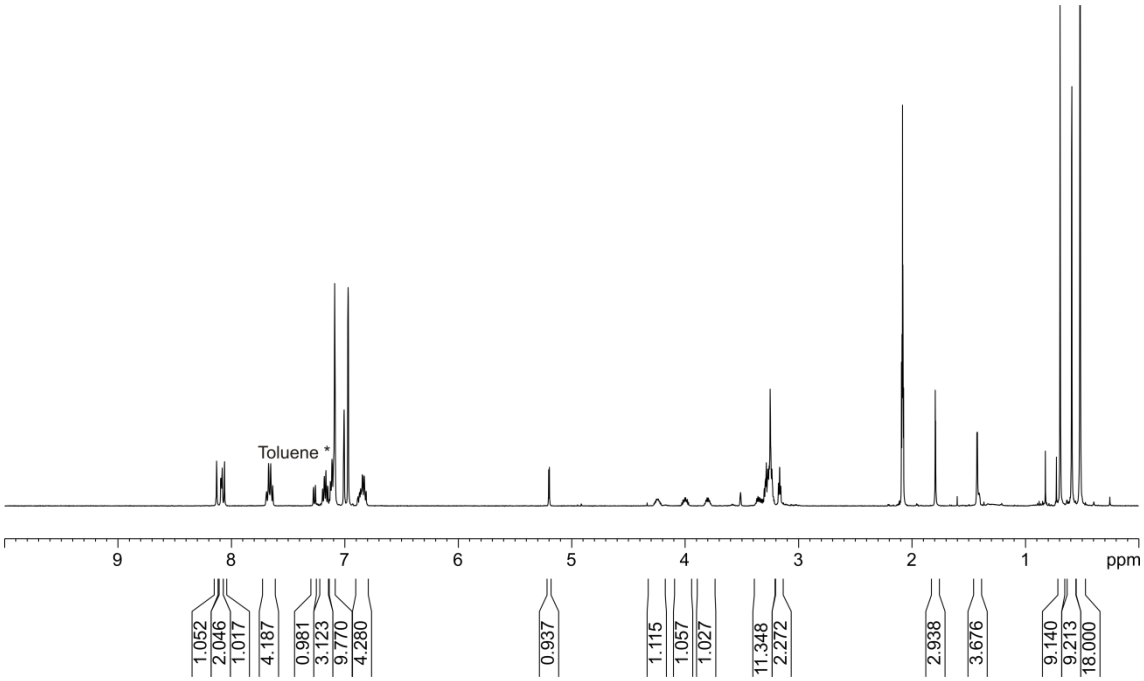

Figure A10. ^{1}H NMR spectrum of [Rh(κ^2O,O'–acac)(CO)(κ^1P–(*R*)-**L6**)] (25 ºC, C_7D_8/C_4D_8O (97:3 v/v)).

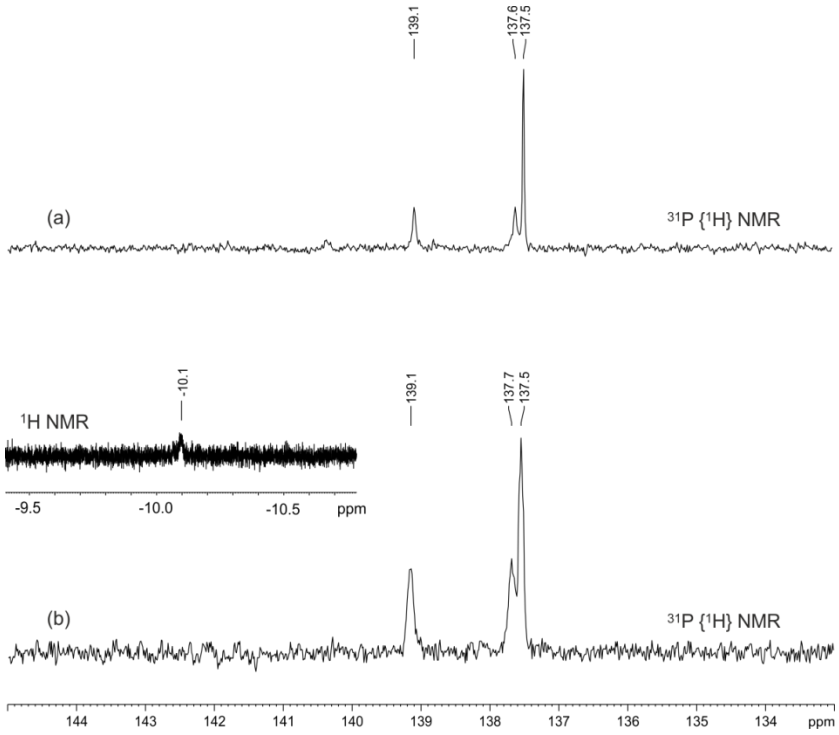

Figure A11. Comparison of ^{31}P{^{1}H} NMR spectra of [Rh(κ^2O,O'–acac)(CO)(κ^1P–(*R*)-**L6**)] under (a) N_2 and (b) H_2/CO (1:1).

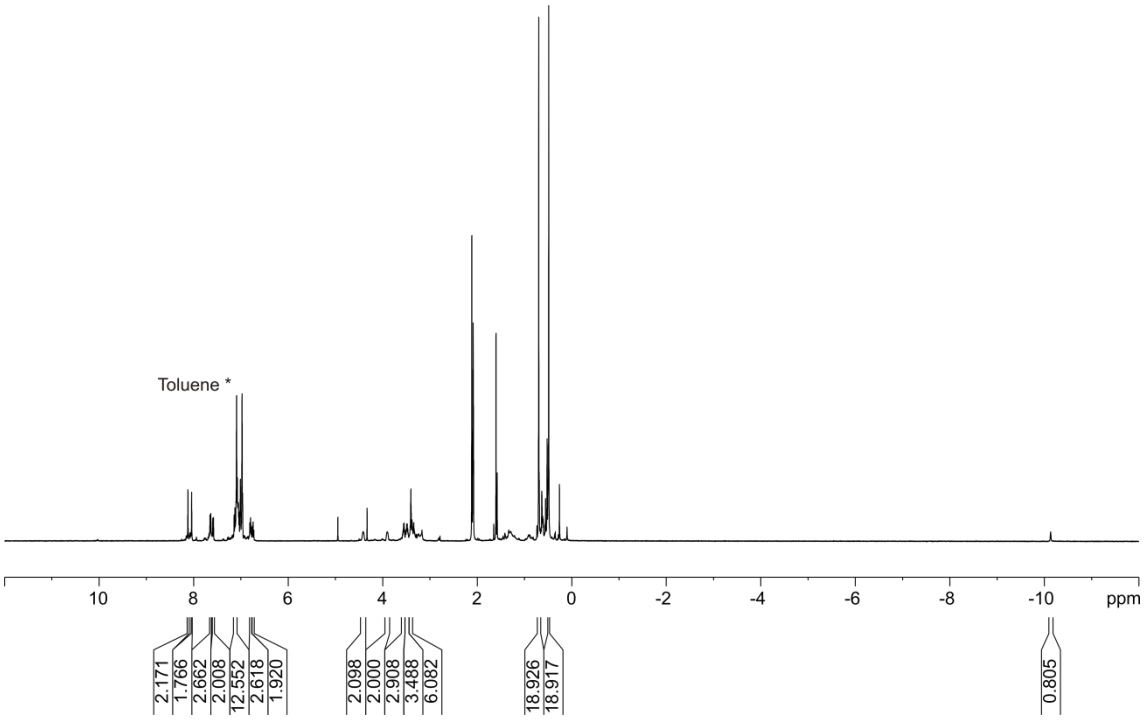

Figure A12. High pressure ^{1}H NMR spectrum of [Rh(H)(CO)$_2$(κ^2P,P´–(*R*)-**L6**)] complex (25 ºC, C_7D_8/C_4D_8O (97:3 v/v)).

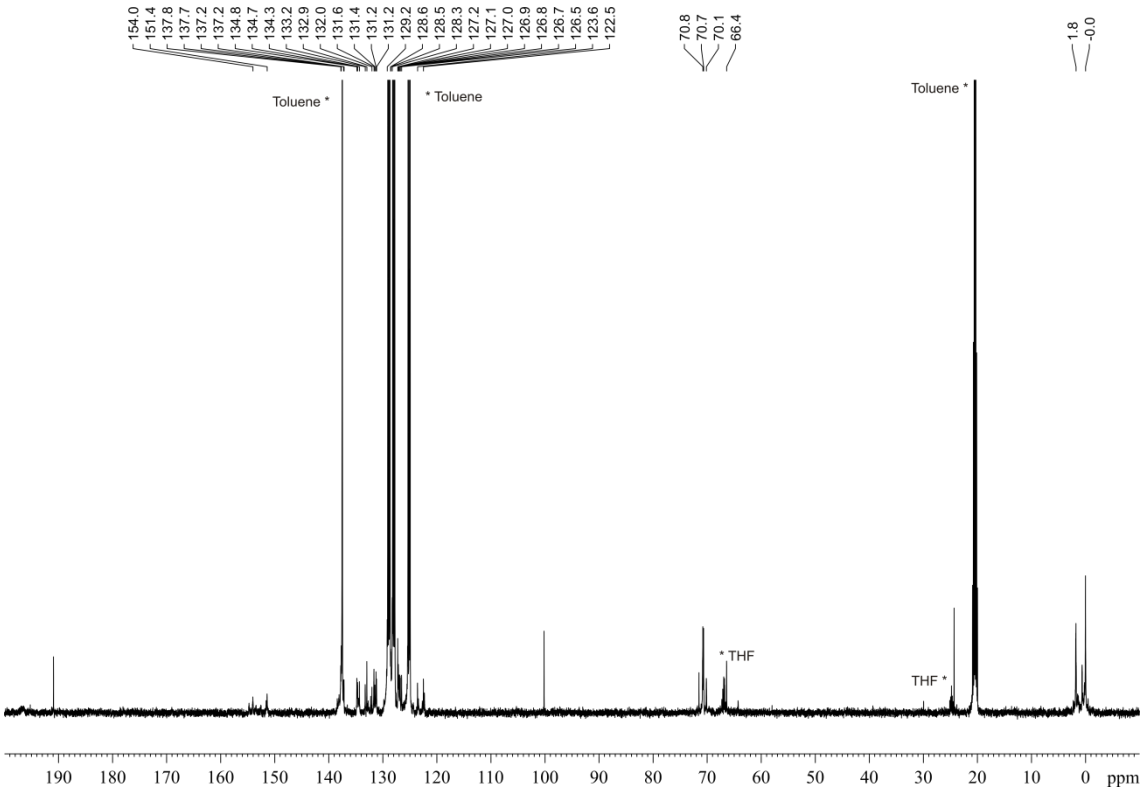

Figure A13. High pressure $^{13}C\{^{1}H\}$ NMR spectrum of [Rh(H)(CO)$_2$(κ^2P,P´–(*R*)-**L6**)] complex (25 ºC, C_7D_8/C_4D_8O (97:3 v/v)).

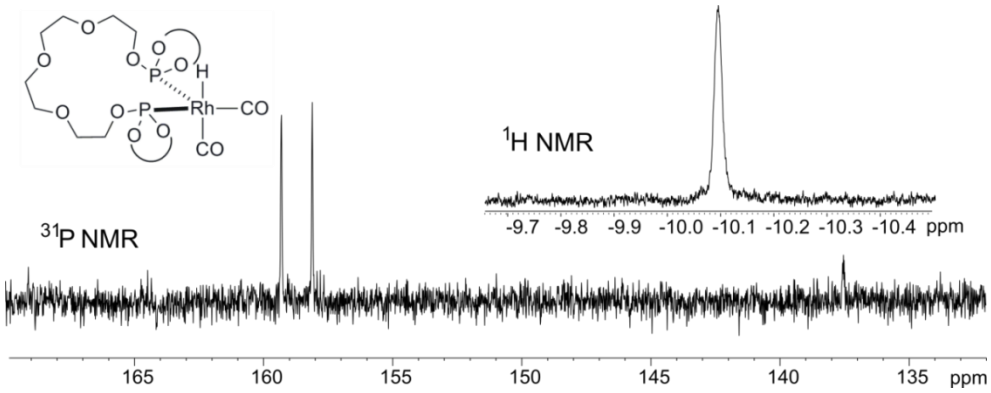

Figure A14. High pressure ^{31}P NMR spectrum and ^{1}H NMR hydride-region (25 ºC, C_7D_8/C_4D_8O (97:3 v/v)) of the [Rh(H)$(CO)_2(\kappa^2$P,P´–(*R*)-**L6**)] complex.

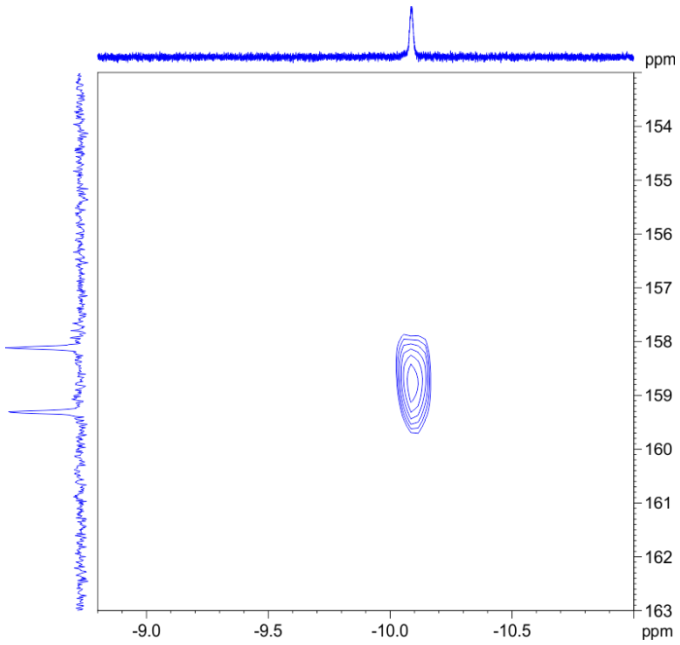

Figure A15. High pressure ^{1}H–^{31}P HMBC spectrum (25 ºC, C_7D_8/C_4D_8O (97:3 v/v)) of the [Rh(H)$(CO)_2(\kappa^2$P,P´–(*R*)-**L6**)] complex.

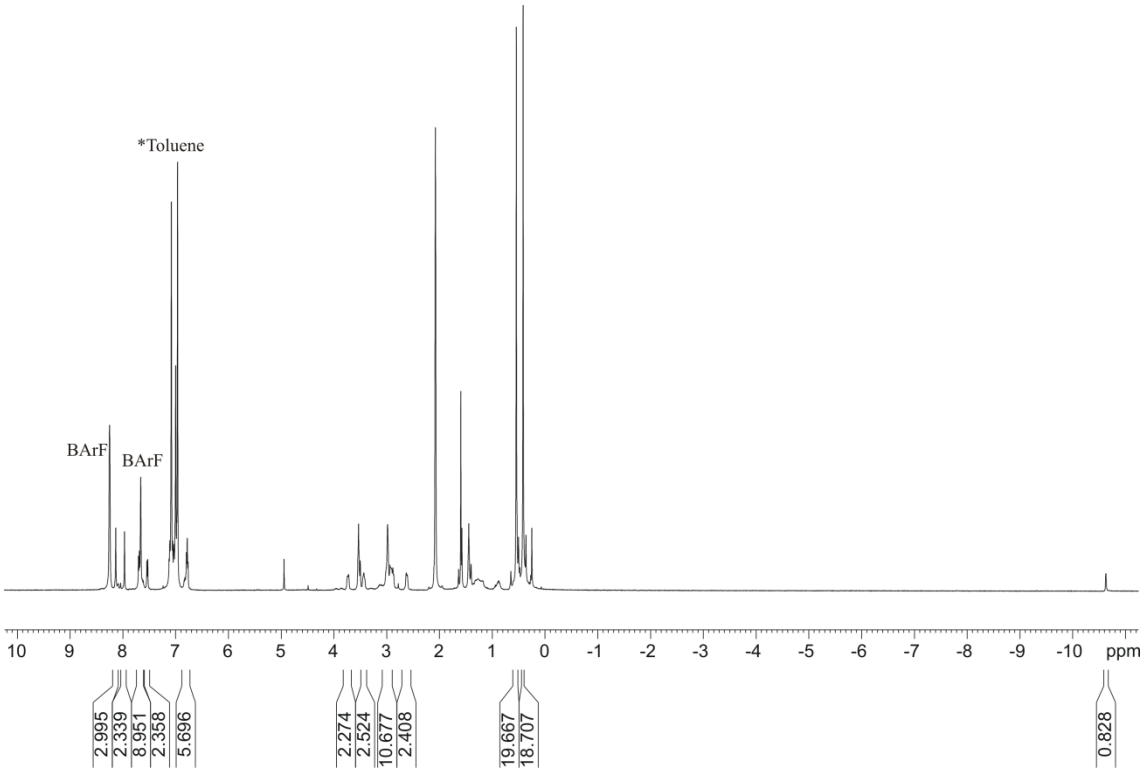

Figure A16. High pressure ^{1}H NMR spectrum of the [Rh(H)(CO)$_2$(κ^2P,P'–RbBArF•(*R*)-**L6**)] complex (25 ºC, C_7D_8/C_4D_8O (97:3 v/v)).

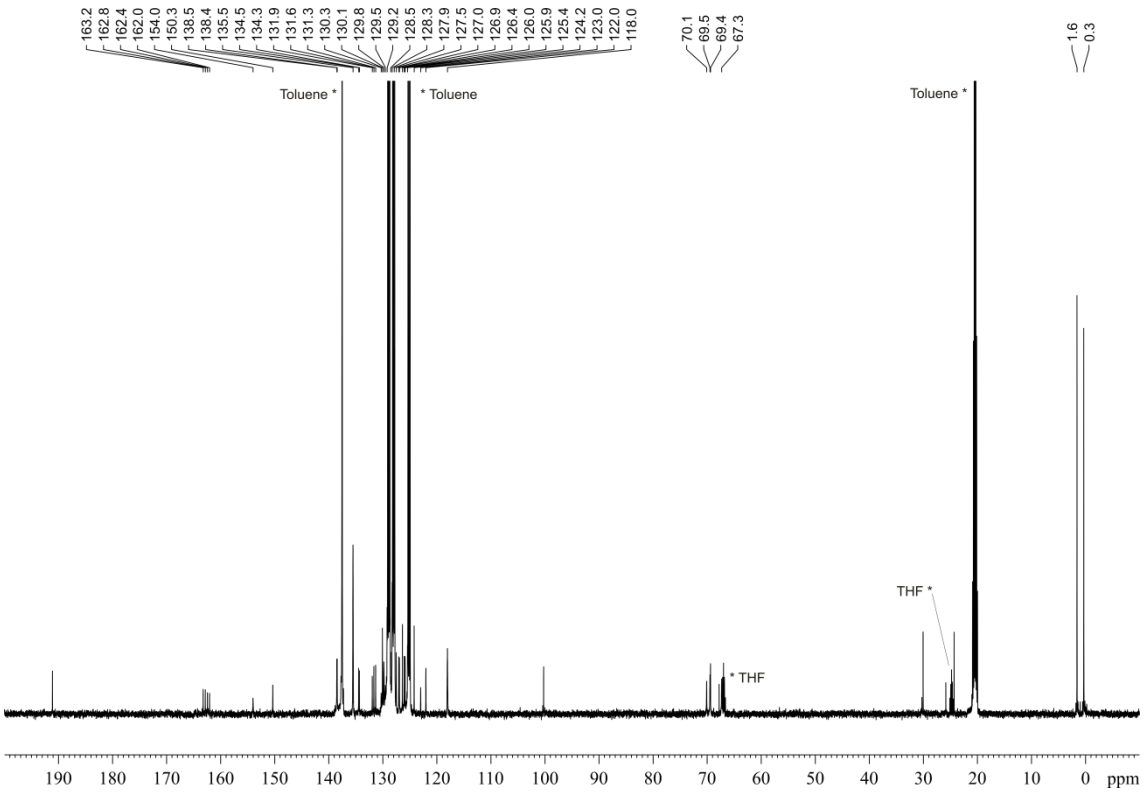

Figure A17. High pressure ^{13}C{^{1}H} NMR spectrum of the [Rh(H)(CO)$_2$(κ^2P,P'–RbBArF•(*R*)-**L6**)] complex (25 ºC, C_7D_8/C_4D_8O (97:3 v/v)).

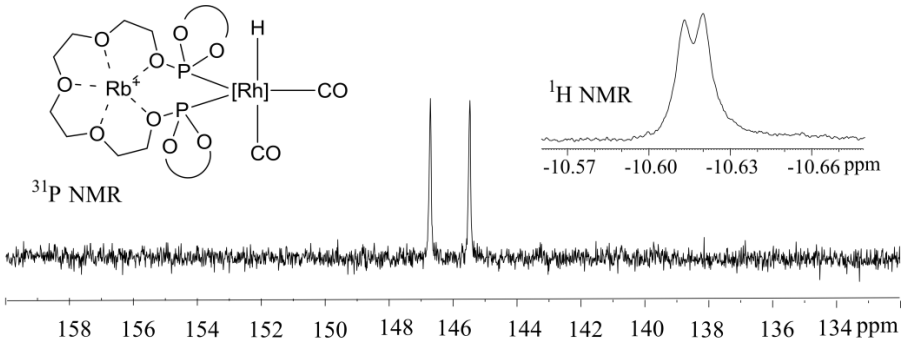

Figure A18. High pressure ^{31}P NMR spectrum and ^{1}H NMR hydride-region (25 ºC, C_7D_8/C_4D_8O (97:3 v/v)) of the [Rh(H)(CO)$_2$(κ^2P,P'–RbBArF•(*R*)-**L6**)] complex.

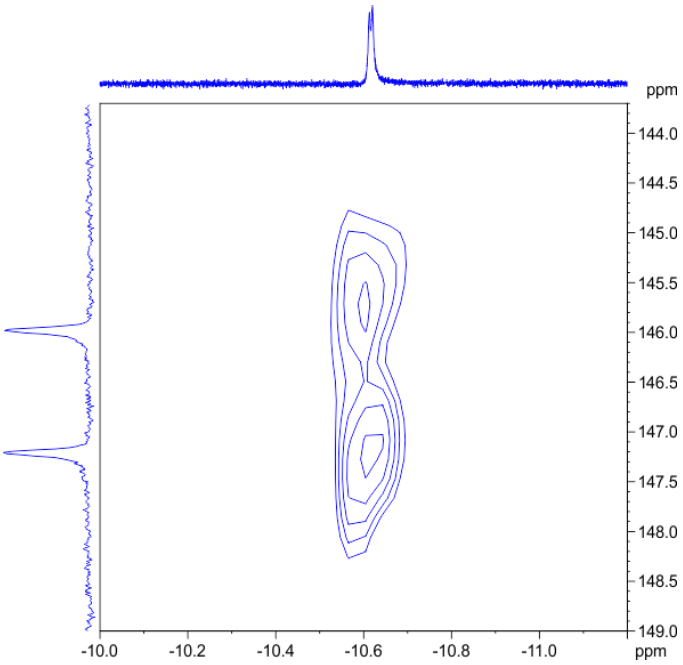

Figure A19. High pressure ^{1}H–^{31}P HMBC spectrum (25 ºC, C_7D_8/C_4D_8O (97:3 v/v)) of the [Rh(H)(CO)$_2$(κ^2P,P'–RbBArF•(*R*)-**L6**)] complex.

3.8. References

1) For selected reviews, see: (a) Breit, B. *Angew. Chem., Int. Ed.* **2005**, *44*, 6816−6825. (b) Breit, B.; Seiche, W. *Pure Appl. Chem*. **2006**, *78*, 249−256. (c) Takacs, J. M.; Chaiseeda, K.; Moteki, S. A.; Reddy, D. S.; Wu, D.; Chandra, K. *Pure Appl. Chem.* **2006**, *78*, 501−509. (d) Breit, B. *Pure Appl. Chem*. **2008**, *80*, 855−860. (e) Meeuwissen, J.; Reek, J. N. H. *Nat. Chem.* **2010**, *2*, 615−621. (f) Dydio, P.; Reek, J. N. H. *Chem. Sci.* **2014**, *5*, 2135−2145. (g) Raynal, M.; Ballester, P.; Vidal-Ferran, A.; van Leeuwen, P. W. N. M. *Chem. Soc. Rev.* **2014**, *43*, 1660−1733. (h) Raynal, M.; Ballester, P.; Vidal-Ferran, A.; van Leeuwen, P. W. N. M. *Chem. Soc. Rev.* **2014**, *43*, 1734−1787.

2) (a) Mon, I.; Jose, D. A.; Vidal-Ferran, A. *Chem. –Eur. J.* **2013**, *19*, 2720–2725. (b) Fernández-Pérez, H.; Mon, I.; Frontera, A.; Vidal-Ferran, A. *Tetrahedron* **2015**, *71*, 4490–4494. (c) Vidal-Ferran, A.; Mon, I.; Bauza, A.; Frontera, A.; Rovira, L. *Chem. –Eur. J.* **2015**, *21*, 11417–11426.

3) (a) Clarke, M. L.; Fuentes, J. A. *Angew. Chem., Int. Ed.* **2007**, *46*, 930–933. (b) Li, Y.; Ma, B.; He, Y.; Zhang, F.; Fan, Q.-H. *Chem. Asian J.* **2010**, *5*, 2454–2458. (c) van Leeuwen, P. W. N. M.; Rivillo, D.; Raynal, M.; Freixa, Z. *J. Am. Chem. Soc.* **2011**, *133*, 18562–18565. (d) Song, F.-T.; Ouyang, G.-H.; Li, Y.; He, Y.-M.; Fan, Q.-H. *Eur. J. Org. Chem.* **2014**, 6713–6719. (e) Ouyang, G.-H.; He, Y.-M.; Fan, Q.-H. *Chem. –Eur. J.* **2014**, *20*, 16454–16457.

4) (a) Thomas, P. J.; Axtell, A. T.; Klosin, J.; Peng, W.; Rand, C. L.; Clark, T. P.; Landis, C. R.; Abboud, K. A. *Org. Lett.* **2007**, *9*, 2665–2668. (b) Franke, R.; Selent, D.; Boerner, A. *Chem. Rev.* **2012**, *112*, 5675–5732.

5) (a) Diéguez, M.; Pàmies, O.; Claver, C. *Chem. Commun.* **2005**, 1221–1223. (b) Mazuela, J.; Coll, M.; Pàmies, O.; Diéguez, M. *J. Org. Chem.* **2009**, *74*, 5440–5445.

6) Pereira, M. M.; Calvete, M. J. F.; Carrilho, R. M. B.; Abreu, A. R. *Chem. Soc. Rev.* **2013**, *42*, 6990–7027.

7) For the full set of results, the reader is referred to the Tables S1–S5 in the section 3.6.3.

8) See, for example: (a) Chikkali, S. H.; Bellini, R.; de Bruin, B.; van der Vlugt, J. I.; Reek, J. N. H. *J. Am. Chem. Soc.* **2012**, *134*, 6607–6616. (b) Li, S.; Wu, W.; Ji, W.; Liang, Y.; Ou, L.; Zeng, G.; Wu, W. *Biol. Med.* **2014**, *6*, 1000203/1000201-1000203/1000206

9) Fernández-Pérez, H.; Benet-Buchholz, J.; Vidal-Ferran, A. *Org. Lett.* **2013**, *15*, 3634–3637.

10) (a) Horiuchi, T.; Ohta, T.; Shirakawa, E.; Nozaki, K.; Takaya, H. *J. Org. Chem.* **1997**, *62*, 4285–4292. (b) Del Rio, I.; Van Leeuwen, P. W. N. M.; Claver, C. *Can. J. Chem.* **2001**, *79*, 560–565. (c) Mazuela, J.; Pàmies, O.; Diéguez, M.; Palais, L.; Rosset, S.; Alexakis, A. *Tetrahedron: Asymmetry* **2010**, *21*, 2153–2157. (d) McDonald, R. I.; Wong, G. W.; Neupane, R. P.; Stahl, S. S.; Landis, C. R. *J. Am. Chem. Soc.*

2010, *132*, 14027–14029. (e) Chikkali, S. H.; Bellini, R.; Berthon-Gelloz, G.; van der Vlugt, J. I.; de Bruin, B.; Reek, J. N. H. *Chem. Commun.* **2010**, *46*, 1244–1246. (f) Adint, T. T.; Wong, G. W.; Landis, C. R. *J. Org. Chem.* **2013**, *78*, 4231–4238. (g) Zheng, X.; Xu, K.; Zhang, X. *Tetrahedron Lett.* **2015**, *56*, 1149–1152.

11) Polo, A.; Claver, C.; Castillón, S.; Ruiz, A.; Bayon, J. C.; Real, J.; Mealli, C.; Masi, D. *Organometallics* **1992**, *11*, 3525–3533.

12) See Figure S22 and Table S6 in section 3.6.3 for the full set of results employing syngas mixtures with different H_2/CO ratios.

13) Hydrido-dicarbonyl rhodium complexes are considered the catalyst resting-states in hydroformylation reactions. See, for example: Del Rio, I.; Pàmies, O.; Van Leeuwen, P. W. N. M.; Claver, C. *J. Organomet. Chem.* **2000**, *608*, 115–121.

14) Small P–H couplings indicate that the hydrido ligand has a strong preference for a *cis*-orientation relative to the P-ligating groups, which are coordinated in an equatorial–equatorial fashion to a trigonal–bipyramidal rhodium center. See, for example: (a) Nozaki, K.; Sakai, N.; Nanno, T.; Higashijima, T.; Mano, S.; Horiuchi, T.; Takaya, H. *J. Am. Chem. Soc.* **1997**, *119*, 4413–4423. (b) Buisman, G. J. H.; Vos, E. J.; Kamer, P. C. J.; van, L. P. W. N. M. *J. Chem. Soc., Dalton Trans.* **1995**, 409–417.

15) Rubinshtein, M.; James, C. R.; Young, J. L.; Ma, Y. J.; Kobayashi, Y.; Gianneschi, N. C.; Yang, J. *Org. Lett.* **2010**, *12*, 3560–3563.

16) Spectroscopic data of hydroformylated products: For **2a**–**b**, see: (a) Zhang, X.; Cao, B.; Yan, Y.; Yu, S.; Ji, B.; Zhang, X. *Chem. –Eur. J.* **2010**, *16*, 871–877. For **2c**, see: (b) Kano, T.; Mii, H.; Maruoka, K. *J. Am. Chem. Soc.* **2009**, *131*, 3450–3451. For **2d**, see: (c) Friest, J. A.; Maezato, Y.; Broussy, S.; Blum, P.; Berkowitz, D. B. *J. Am. Chem. Soc.* **2010**, *132*, 5930–5931. For **2e**, see: (d) Ref 10f. For **5**, see: (e) Carley, S.; Brimble, M. A. *Org. Lett.* **2009**, *11*, 563–566. For **6** and **9**, see: (f) ref 10a.

17) (a) Cobley, C. J.; Klosin, J.; Qin, C.; Whiteker, G. T. *Org. Lett.* **2004**, *6*, 3277–3280. (b) Cobley, C. J.; Klosin, J.; Qin, C.; Whiteker, G. T. *Org. Lett.* **2005**, *7*, 1197

18) The racemic mixture of the hydroformylated product derived from **8** was prepared using the Xantphos ligand (see section 3.6.5 for details).

19) Stock, H. T.; Kellogg, R. M. *J. Org. Chem.* **1996**, *61*, 3093–3105.

20) See section 3.7.2.2.

21) Damoense, L.; Datt, M.; Green, M.; Steenkamp, C. *Coord. Chem. Rev.* **2004**, *248*, 2393–2407.

Chapter 4

Solid State Structure of Alkali Metal BArF Salts

Chapter 4.

Solid State Structure of Alkali Metal BArF Salts

Laura Rovira†, Jordi Benet-Buchholz† and Anton Vidal-Ferran†‡*

†Institute of Chemical Research of Catalonia (ICIQ) & The Barcelona Institute of Science and Technology, Avgda. Països Catalans 16, 43007 Tarragona, Spain.

‡Catalan Institution for Research and Advanced Studies (ICREA), Passeig Lluís Companys 23, 08010 Barcelona, Spain.

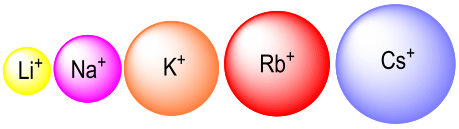

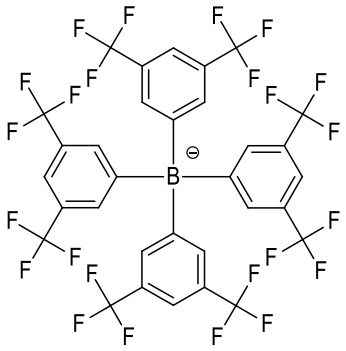

4.1. Abstract

The solid state structure of the alkali metal salts derived from the weakly coordinating BArF anion (BArF = $[B(3,5\text{-}(CF_3)_2C_6H_3)_4]^-$) has been determined by single crystal X-ray diffraction analysis. An efficient synthetic method for the lithium BArF salt has been developed. Alkali metal BArF salts crystallized as water solvates with the exception of the cesium BArF salt, which crystallized as a dichloromethane solvate. The boron atom in the BArF moiety displays in all cases a tetrahedral geometry, with disordered CF_3 groups. Lithium and sodium BArF salts are isostructural and display two geometries (a trigonal bipyramidal and an octahedral metal geometries). Potassium and rubidium BArF salts are also isostructural with nine atoms (one oxygen and eight fluorine atoms) coordinated to the alkali metal. The cesium salt shows a similar arrangement of the atoms in the crystal structure than the potassium and rubidium salts. The distance between the alkali metal and the boron atom shows an increasing tendency with the size of the cation. The observed distances demonstrate that the boron atom is in all cases isolated from the alkali metal cation.

4.2. Introduction

The term *weakly coordinating anion* (WCA) appeared in the literature in the 90´s and was used to describe anions that interacted weakly with cations.[1] This qualifying term was used in the past for counterions such as $[ClO_4]^-$, $[PF_6]^-$, $[SbF_6]^-$, $[AsF_6]^-$, $[BF_4]^-$, $[CF_3SO_3]^-$ and $[AlCl_4]^-$, as it was believed that they had a weakly coordinating character. Although the accuracy of this statement was proven for aqueous solutions of these salts, researchers demonstrated that this class of anions lost their non-coordinating character when water was eliminated.[2] The ideal property of weakly coordinating anions should be the delocalization of the negative charge over the non-nucleophilic region. They were built around a chemically robust core and showed overall low nucleophilicity and basicity and allowed the stabilization of very reactive cations.[3]

A wide variety of WCA species are known[3] and, amongst them, borate-based anions (*i.e.* $[BPh_4]^-$ and its derivatives)[4] deserve special mention. For instance, the tetraphenylborate anion $[BPh_4]^-$, which results from the exchange of fluorine atoms by phenyl groups in the tetrafluoroborate ($[BF_4]^-$) anion, was used as a phase-transfer catalyst in a number of transformations and as counterion in Fe-based Ziegler-Natta olefin polymerization catalysts.[5c] The tetraphenylborate group is prone to hydrolysis, sensitive to photochemical decomposition and to cleavage of its phenyl groups.[3] All these drawbacks were solved by attaching fluorine-containing substituents to the phenyl groups.

Several fluorine-containing derivatives of $[BPh_4]^-$ have been developed (*i.e.* $[B(C_6F_5)_4]^-$, $[B(3,5\text{-}(CF_3)_2C_6H_3)_4]^-$ and $[B(CF_3)_4]^-$; see references 4a, 4f and 4h, respectively). The tetrakis[3,5-bis(trifluoromethyl)phenyl]borate anion ($[B(3,5\text{-}(CF_3)_2C_6H_3)_4]^-$ or BArF anion; Figure 1) has gained relevance within this group of fluorine-containing anions given its weak interaction with cations. Bis(trifluoromethyl)phenyl groups are lipophilic and, as they are situated at the surface of the molecule, the BArF anion forms hydrophobic ion pairs with various monovalent cations, such as potassium,[6] silver,[6] and thallium.[7] It is interesting to note that the negatively charged boron atom is coordinately saturated and cannot be covalently bonded to the corresponding cation. Furthermore, the BArF anion is resistant to a variety of oxidants as well as very lipophilic with a high chemical stability and solubility in organic solvents.

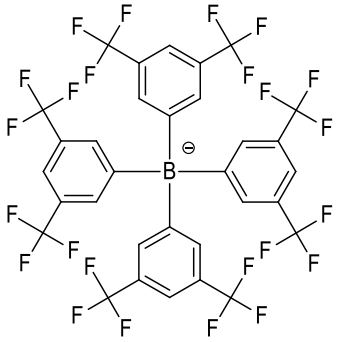

Figure 1. BArF anion $[B(3,5\text{-}(CF_3)_2C_6H_3)_4]^-$.

BArF salts were used as the first effective catalysts in anionic phase transfer catalysis reactions.[4b,5a-b] New and important applications for the BArF anion have been reported in the last years, replacing classical anions.[8-16] BArF salts have been used in organic transformations as a Lewis acid catalysts in Diels-Alder reactions[8] and cycloaddition reactions.[9] Applications of BArF salts in electrochemistry,[10] in lithium batteries,[11] as components of ionic liquids[12] and as an extractant of lanthanide ions[13] have also been described. As regards asymmetric catalysis, the BArF anion has been widely used as a counterion in Ir-mediated asymmetric hydrogenation of unfunctionalized alkenes (iridium precatalysts that contain the BArF anion are less prone to form inactive hydrido-bridged trimeric iridium species).[14] More recently, our group[15] and others[16] have used alkali metal BArF salts in combination with supramolecular ligands to fine-regulate the geometry of the catalytic site in asymmetric transformations of interest, such as asymmetric hydrogenation and hydroformylation reactions.

The synthesis of sodium BArF was first reported by the Kobayashi´s group (Scheme 1a)[4b,c] following a three step procedure: (i) formation of [3,5-bis(trifluoromethyl)phenyl] magnesium iodide (**2**), (ii) reaction of boron trifluoride with arylmagnesium species, and (iii) aqueous cation exchange. Due to the hazards associated with this synthetic method (*i.e.* explosive decomposition of (trifluoromethyl)-aryl Grignard reagents in the presence of an excess of magnesium metal), Bergman and co-workers[17] described a safer and more efficient preparation method for sodium BArF excluding the use of magnesium metal as reagent and using $NaBF_4$ instead of BF_3 as the boron source (see Scheme 1b).

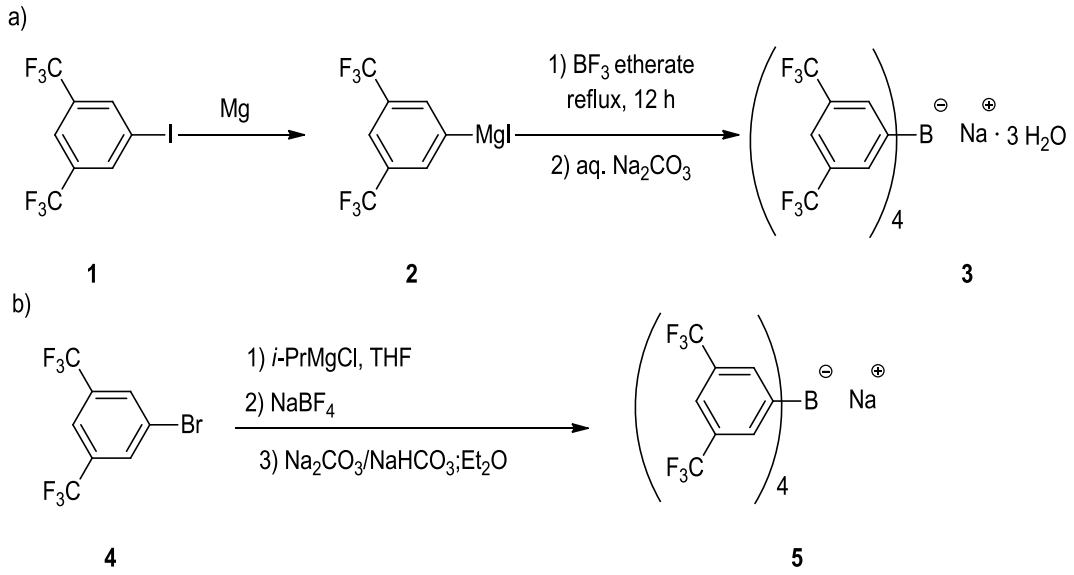

Scheme 1. Synthesis of sodium tetrakis[3,5-bis(trifluoromethyl)phenyl]borate.

As regards the preparation of other alkali metal BArF salts, an analogous synthetic protocol for potassium BArF involving Grignard reagents had also been reported.[6] The preparation of the heavier alkali metal BArF salts had also been reported by displacement of the sodium cation in NaBArF by rubidium[15b]

or cesium.[15a] Given the lower solubility of RbBArF or CsBArF than NaBArF in water, a mixture of rubidium or cesium nitrate with NaBArF at 90 ºC allowed the isolation of the heavier alkali metal BArF salts in good yields just by a simple filtration operation. Unfortunately, this method was not applicable to the preparation of LiBArF. We wish to report herein an efficient method for the preparation of this compound. Furthermore, though alkali metal BArF salts were known in the literature, no characterization data had been previously reported and their structures in the solid state had not been previously determined and studied. Thus, we wish to report herein our efforts in the characterization in solution and in the solid state of the alkali metal BArF salts.

4.3. Results and discussion

As regards to the preparation of LiBArF, we envisaged that this compound could be prepared *via* an acid-base reaction (see Scheme 2) between the acid corresponding to the protonated BArF anion[18] and lithium bis(trimethylsilyl)amide (*i.e.* $LiN(SiMe_3)_2$) in a low boiling point organic solvent. We considered that this method would be suitable for the preparation of LiBArF, as acid-base reactions are irreversible and LiBArF and free $HN(SiMe_3)_2$ would hence be quantitatively formed. We also considered that elimination of the liquid components of the mixture (*i.e.* solvent and $HN(SiMe_3)_2$) *in vacuo* would finally render the desired compound. This synthetic procedure was followed and, as expected, LiBArF was isolated as an analytically pure white solid in 89% yield.

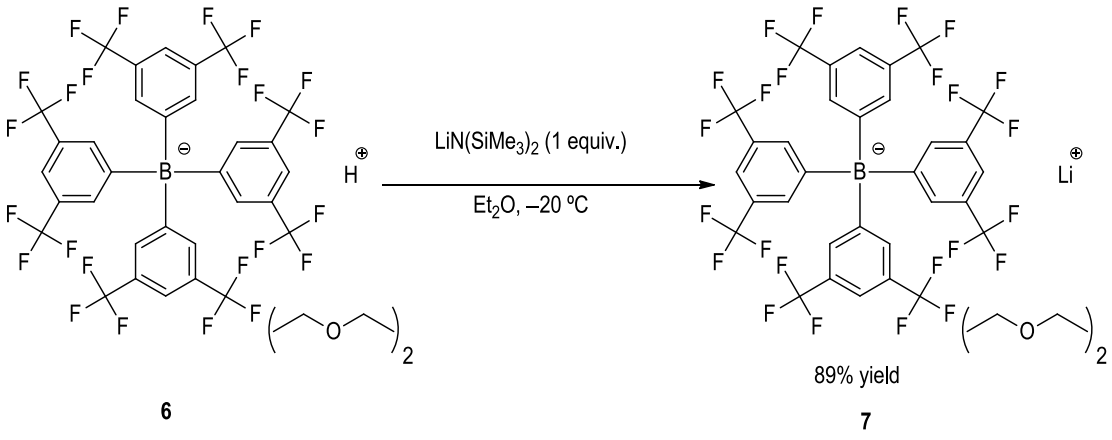

6 **7**

Scheme 2. Synthesis of lithium BArF.

The whole array of alkali metal BArF salts was characterized by standard spectroscopic techniques (IR and ^{1}H, ^{13}C, ^{11}B and ^{19}F NMR spectroscopy). $^{19}F\{^{1}H\}$ and $^{11}B\{^{1}H\}$ NMR spectra showed just a singlet for the signals of the BArF anion with very small differences in the chemical shifts (see Table 1). ^{1}H was in

agreement with the proposed structures and ^{13}C NMR showed the expected set of signals for the four equivalent 3,5-bis(trifluoromethyl)phenyl groups. IR spectroscopy also confirmed the structure of the BArF salts with intense bands in the C=C stretching (*ca.* 1600–1650 cm^{-1}) and C–F stretching (*ca.* 1100–1350 cm^{-1}) vibration regions.

Table 1. $^{19}F\{^1H\}$ and $^{11}B\{^1H\}$ chemical shift (ppm) for the alkali metal BArF salts in C_4D_8O.

Entry	Compound	$^{11}B\{^1H\}$	$^{19}F\{^1H\}$
1	LiBArF	–8.572	–63.184
2	NaBArF	–8.562	–63.129
3	KBArF	–8.598	–63.165
4	RbBArF	–8.553	–63.309
5	CsBArF	–8.589	–63.146

^{11}B chemical shifts are quoted in ppm relative to trimethyl borate (TMB) in C_4D_8O.
^{19}F shifts are quoted in ppm relative to trifluoroacetic acid (TFA) in C_4D_8O.

Interestingly, we could obtain single crystals suitable for X-Ray analysis for the whole series of alkali metal BArF salts. A detailed single crystal X-ray diffraction study not only confirmed the structure of the compounds, but also provided additional information about the interactions between some atoms of the $[B(3,5\text{-}(CF_3)_2C_6H_3)_4]^-$ moiety and the alkali metal atoms. These interactions are generated by short contacts between neighboring atoms, which are not considered strong enough to be real chemical bonds. The main values for these short contacts are summarized in the discussion that follows and in Table 2.

The asymmetric unit in the structure of LiBArF contains a quarter of one BArF molecule (corresponding to a *S*4 symmetry), a quarter of one lithium atom and 0.68 highly disordered molecules of water. The water molecules crystallize disordered in two ways forming two types of structures. In Figure 2A, three oxygen atoms (O1, O2 and O2A) from the water molecules are coordinated to the lithium atom. Therefore, the geometry of the compound in this case is trigonal bipyramidal, with the fluorine atoms (F4 and F4A) coordinated in the axial positions of the bypiramid. In Figure 2B, there are two oxygens (O1 and O2´) from the water molecules, and four fluorine atoms from a neighboring CF_3 group (F4, F4A, F4B and F4C), forming an octahedral geometry. The octahedral coordination is minor (28%), while the trigonal bipyramidal geometry is major (72%). The oxygen and fluorine atoms interact with the lithium atom as indicated by the short contacts between them. The shortest distance in the crystal structure between boron and lithium is 7.51 Å. The aromatic rings of the BArF anion are disordered over two orientations (ratio 62:38). One of the CF_3 groups is disordered over three positions with a ratio 55:38:7. The angle between the boron and the carbon atoms of the phenyl groups of the BArF moiety is 108.9 (5) º, which classifies its geometry as tetrahedral.

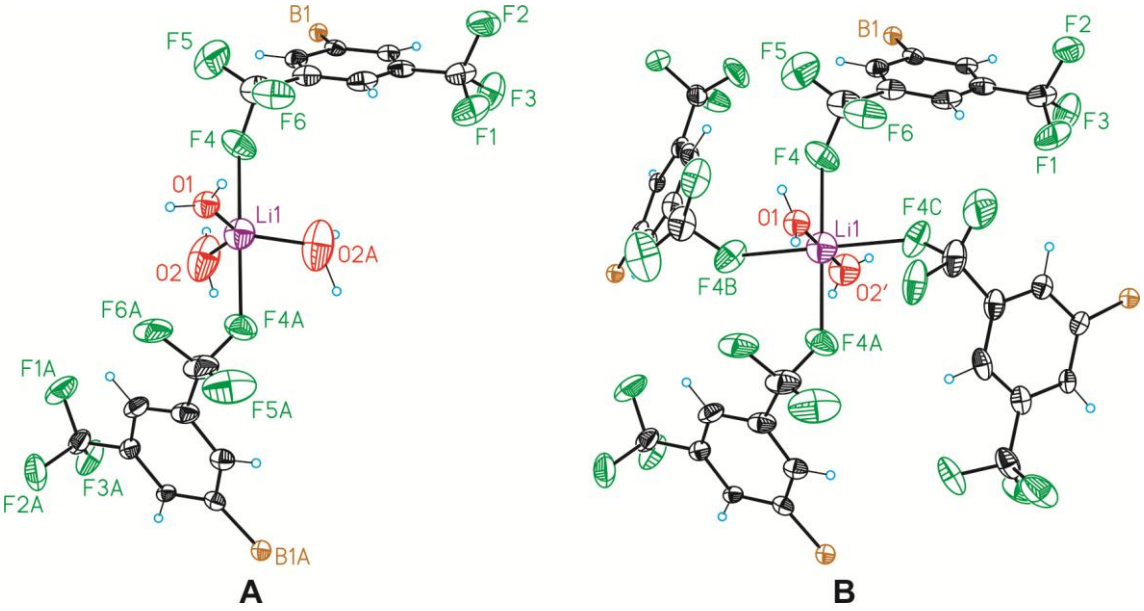

Figure 2. Crystal structure of the LiBArF salt: trigonal bipyramidal (A) and octahedral (B) geometries. Some phenyl rings from the BArF unit have been omitted for the sake of clarity. Color scheme: C: black, H: blue, B: orange, F: green, Li: violet, O: red. Atomic displacement ellipsoids are drawn at 50% probability. Fluorine atoms F4 (A–C) are symmetry equivalent to F4 and show identical distances.

The asymmetric unit of NaBArF contains a quarter of one BArF molecule (corresponding to a *S*4 symmetry), a quarter of one sodium atom and 0.59 highly disordered molecules of water. On account of the disorder on the water molecules, NaBArF structure shows two different geometries as those observed in LiBArF. In Figure 3, we illustrate the different geometries that NaBArF molecule can adopt: a trigonal bipyramidal geometry (Figure 3A), where the sodium atom interacts with two fluorine atoms (F4 and F4A) and with the three oxygens from the water molecules (O1, O2 and O2A), and an octahedral geometry (Figure 3B), where the two oxygens from the water molecules (O1 and O2´) and the four fluorine atoms (F4–F4C) are coordinated to the sodium atom. In contrast to LiBArF, the octahedral coordination is major (62%) in this case, while the trigonal bipyramidal geometry is minor (38%). The shortest distance between boron and sodium atoms in the crystal structure is 7.55 Å. The angle between boron and carbon atoms from phenyl moieties is 110.3(3) º showing a tetrahedral geometry for the BArF unit. The aromatic groups of the BArF anion are disordered over two orientations with a ratio of 70:30. In short, the single crystal structure obtained for NaBArF is isostructural to that obtained for LiBArF.

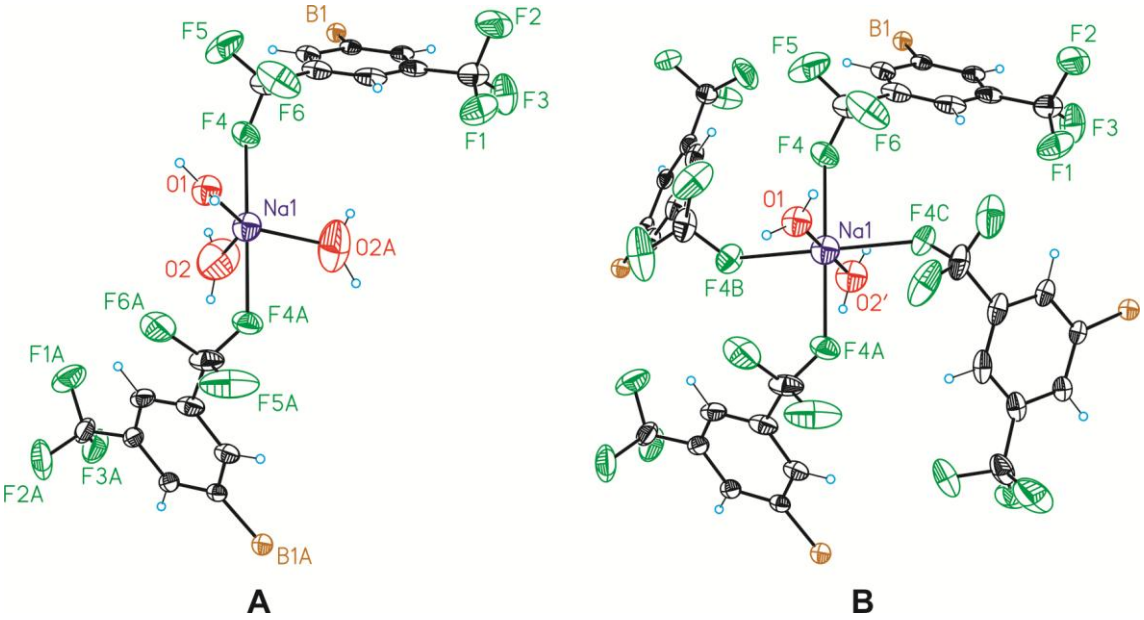

Figure 3. Crystal structure of the NaBArF salt: trigonal bipyramidal (A) and octahedral (B) geometries. Some phenyl rings from the BArF unit have been omitted for the sake of clarity. Fluorine atoms F4 (A–C) are symmetry equivalent to F4 and show identical distances. See the legend in Figure 2 for other details.

The crystal structure obtained for KBArF corresponds to the space group *P*4/n and is not isostructural to the structure of lithium and sodium BArF salts. In the asymmetric unit we identified a quarter of one BArF molecule (corresponding to *S*4 symmetry), a quarter of a potassium atom and 1/8 of a water molecule. The asymmetric unit of KBArF displaying a tetrahedral geometry (C1–B–C1´=110.27(3) º) is depicted in Figure 4. The CF_3 groups in the phenyl rings are rotationally disordered in a 75:25 ratio.

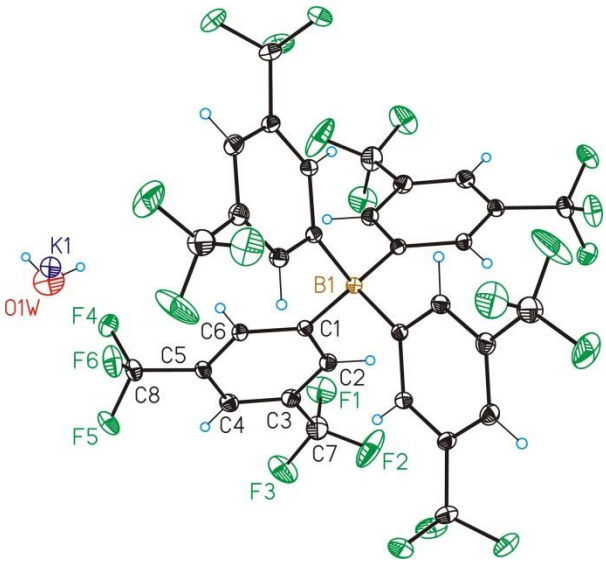

Figure 4. Crystal structure of the KBArF salt. See the legend in Figure 2 for other details.

The shortest distance between potassium and boron atoms in the crystal structure is 7.89 Å. The potassium coordinative sphere is formed by eight fluorine atoms (F3, F4 and their symmetry equivalents) and one oxygen atom (O1w) from a water molecule (see Figure 5). The K–F coordination length in the potassium BArF is 2.79 Å (F4) and 2.87 (F3) and the coordination length to the oxygen atom is 2.81 Å (O1W; for a summary of all distances, see Table 2).

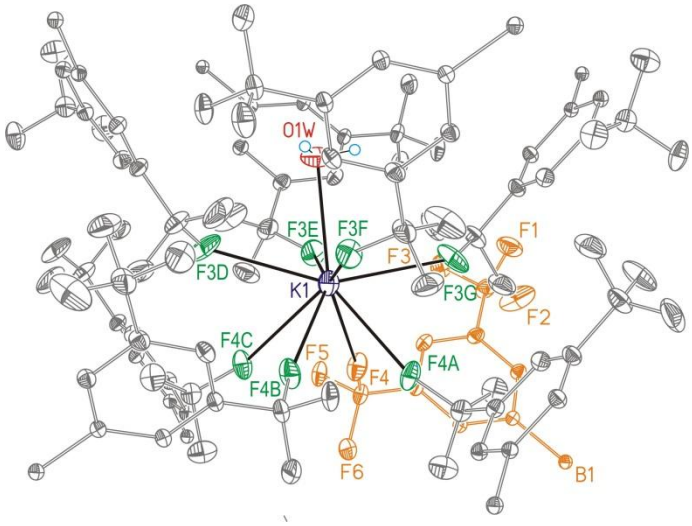

Figure 5. Crystal structure of KBArF showing the coordinative sphere of the potassium atom. Interactions between potassium, fluorine and oxygen atoms are indicated with dark solid lines. The original fragment of the BArF moiety in the asymmetric unit has been represented in orange. The symmetry equivalent aromatic rings have been represented in grey color for the sake of clarity. Fluorine atoms F3 (D–G) and F4 (A–C) are symmetry equivalent to F3 and F4 and show identical distances.

The colorless crystals obtained from the RbBArF solution are isostructural to those obtained for KBArF. The asymmetric unit contains a quarter of one BArF molecule, a quarter of one rubidium atom and a quarter of one water molecule. The BArF anion is located on a rotation-reflexion axis, presents *S*4 symmetry and displays a tetrahedral geometry (C1–B–C1´=110.19(8) º) with the CF_3 groups disordered over two orientations (see Figure 6). The disorder ratio in this case is 90:10. The shortest distance between the rubidium and boron atoms in the crystal structure is 7.99 Å. Since this structure is isostructural to KBArF, the coordination sphere of the rubidium atom is identical to that for potassium (compare Figure 5 with Figure 7). The Rb–F coordination length in the rubidium BArF is 2.92 Å (F4) and 2.99 Å (F3), and the coordination length to the oxygen is 2.94 Å (O1W; for a summary of all distances see Table 2).

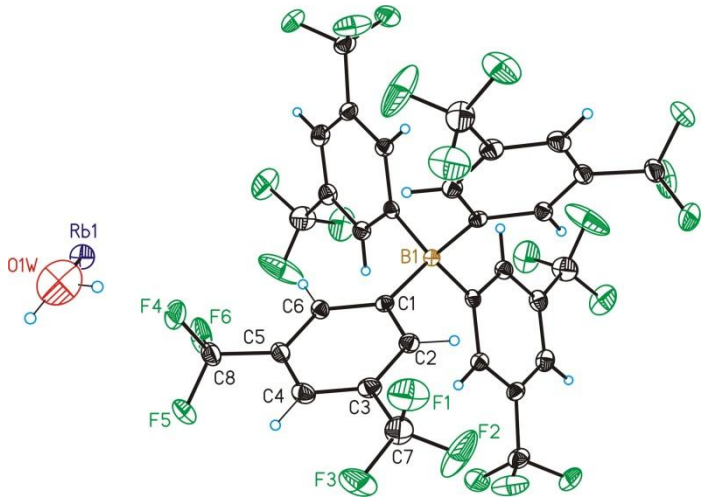

Figure 6. Crystal structure of the RbBArF salt. See the legend in Figure 2 for other details.

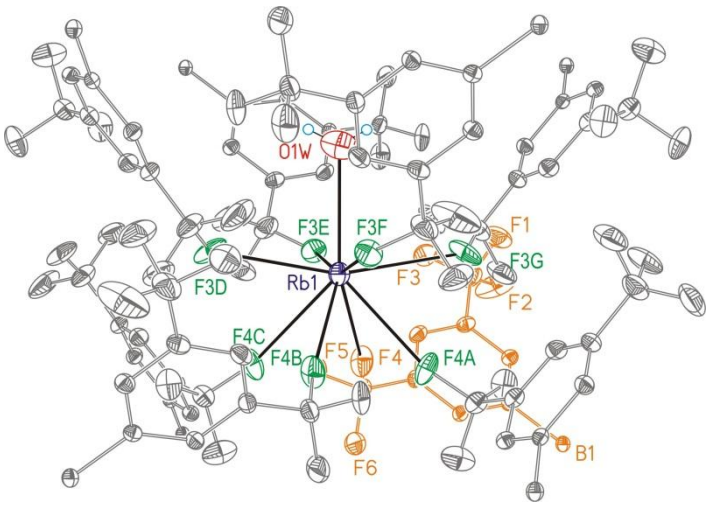

Figure 7. Crystal structure of RbBArF showing the coordinative sphere of the rubidium atom. Interactions between rubidium, fluorine and oxygen atoms are indicated with dark solid lines. The original fragment of the BArF moiety in the asymmetric unit has been represented in orange. The symmetry equivalent aromatic rings have been represented in grey color for the sake of clarity. Fluorine atoms F3 (D–G) and F4 (A–C) are symmetry equivalent to F3 and F4 and show identical distances.

Finally, the CsBArF crystal structure was studied. The asymmetric unit of this salt contains a quarter of one BArF molecule with a *S*4 symmetry, a quarter of one cesium atom located on a four-fold rotation axis and a quarter of one solvent molecule (DCM). In the BArF unit, the aromatic rings and the corresponding trifluoromethyl groups are disordered over two orientations in a 55:45 ratio. One of the trifluoromethyl groups is additionally rotationally disordered. The dichloromethane molecule, which is

located on a four-fold rotation axis, is also disordered over two orientations in a 50:50 ratio. The CsBArF crystal asymmetric unit is depicted in Figure 8. The boron atom presents a tetrahedral geometry (C1–B–C1´=109.7(3) º). The shortest distance observed between the cesium and boron atoms in the crystal structure is 8.02 Å. In this case, the crystal symmetry changes from the *P*4/n space group observed in the other BArF salts to the *P*4/ncc space group. Nevertheless, if the crystal structure is analyzed, the BArF unit shows a similar arrangement around the cesium atom than those in the structures of KBArF and RbBArF (compare Figures 5, 7 and 9). Since the cesium atom has a larger coordinative sphere than those in potassium and rubidium, a higher number of interactions with the surrounding atoms were observed. The interactions with the fluorine atoms F3, F4 and F5 (and their symmetry equivalents) and with the chlorine atoms from the crystallization solvent, formed a coordination sphere with fourteen interactions with distances between these atoms and the cesium being 3.07, 3.67, 3.29 and 3.8 Å, respectively (see Figure 9 and Table 2).

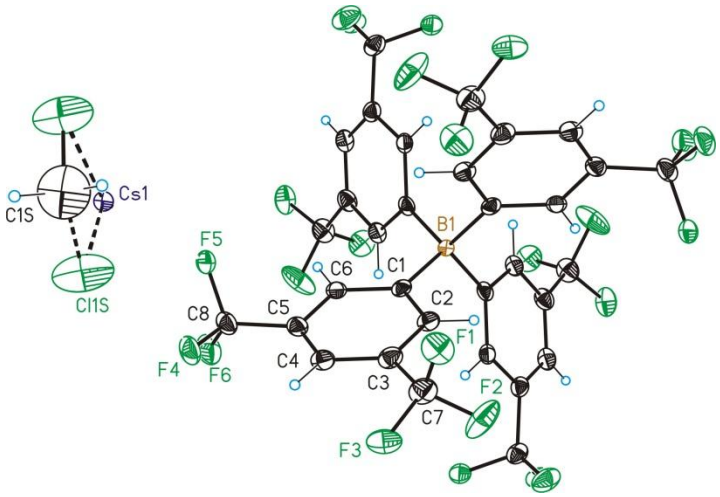

Figure 8. Crystal structure of the CsBArF salt. See the legend in Figure 2 for other details.

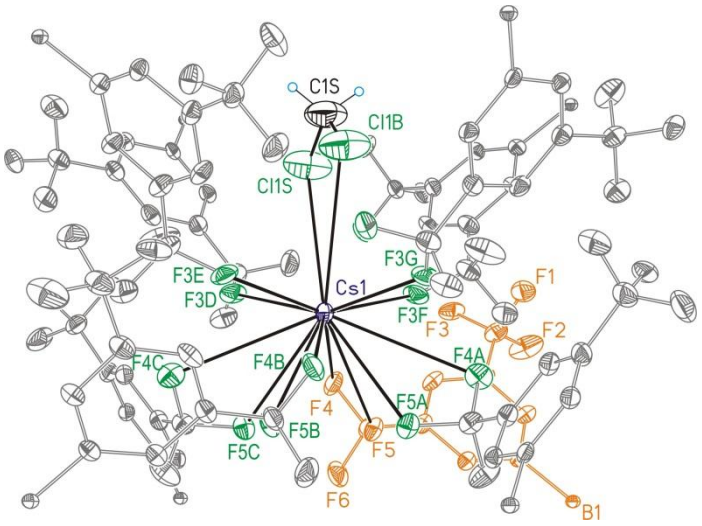

Figure 9. Crystal structure of CsBArF showing the coordinative sphere of the cesium atom. Interactions between cesium, fluorine and chlorine atoms are indicated by solid dark lines. The original fragment of the BArF moiety in the asymmetric unit has been represented in orange. The symmetry equivalent aromatic rings have been represented in grey color for the sake of clarity. Fluorine atoms F3 (D–G), F4 (A–C) and F5 (A–C) are symmetry equivalent to F3, F4 and F5 and show identical distances.

Table 2. Selected distances (Å) and angle (º) for alkali metal BArF salts.

Entry	Distance	LiBArF	NaBArF	KBArF	RbBArF	CsBArF
1	**M–B**	7.509(4)	7.546(1)	7.891(4)	7.994(9)	8.025(3)
2	**M–X**	O2´– 1.856(15)	O1 – 2.193(5)	O1 – 2.813(8)	O1 – 2.939(8)	Cl1S – 3.810(3)
3		O1 – 1.874(9)	O2´ – 2.258(7)			
4		O2 – 1.930(8)	O2 – 2.274(17)			
5	**M–F**	F4 – 2.287(3)	F4 – 2.395(2)	F4 – 2.792(2)	F4 – 2.925(18)	F3 – 3.069(11)
6		F4´´– 2.520(2)	F4´– 2.995(11)	F3– 2.873(18)	F3– 2.997(2)	F5 – 3.290(8)
7		F4´– 3.490(4)		F4´– 2.728(6)	F3´– 3.055(2)	F4 – 3.667(7)
8				F3´– 2.615(4)	F1´– 3.154(3)	F2´– 3.056(19)
9						F6´– 3.042(10)
	Angle					
10	**C1–B–C1´**	108.9(5)	110.3(3)	110.27(3)	110.19(8)	109.7(3)

(´) The prime code corresponds to disordered atoms.

Table 3. Selected crystallographic data for studied alkali metal salts.

Compound	LiBArF	NaBArF	KBArF	RbBArF	CsBArF
Formula	$C_{32}H_{17.44}BF_{24}LiO_{2.72}$	$C_{32}H_{18.76}BF_{24}NaO_{2.38}$	$C_{32}H_{13}BF_{24}KO_{0.5}$	$C_{32}H_{14}BF_{24}RbO$	$C_{33}H_{14}BF_{24}Cl_2Cs$
Solvent	DCM	DCM	DCM	DCM	DCM
Formula weight	919.17	931.11	911.33	966.71	1081.06
Crystal size (mm^3)	0.20 x 0.10 x 0.07	0.30 x 0.18 x 0.10	0.30 x 0.30 x 0.20	0.20 x 0.20 x 0.20	0.30 x 0.20 x 0.05
Crystal color	colourless	colourless	colourless	colourless	colourless
Temp (K)	100	100	100	100	100
Crystal system	Tetragonal	Tetragonal	Tetragonal	Tetragonal	Tetragonal
Space group	*P*4/n	*P*4/n	*P*4/n	*P*4/n	*P*4/ncc
A (Å)	13.546(8)	13.554(7)	13.509(5)	13.596(17)	13.756(4)
B (Å)	13.546(8)	13.554(7)	13.509(5)	13.596(17)	13.756(4)
C (Å)	9.529(5)	9.785(7)	9.287(4)	9.298(18)	19.030(7)
α (deg)	90	90	90	90	90
β (deg)	90	90	90	90	90
γ (deg)	90	90	90	90	90
V ($Å^3$)	1748(2)	1798(2)	1695(15)	1719(5)	3601(2)
Z	2	2	2	2	4
ρ (g/cm^3)	1.746	1.720	1.786	1.868	1.994
μ (mm^{-1})	0.196	0.202	0.317	1.600	1.329
θ_{max} (°)	28.003	28.503	36.405	32.723	30.176
Reflec. measured	20179	9218	21387	6734	9316
Unique reflections	2113[R_{int} = 0.039]	2249[R_{int} = 0.031]	4145[R_{int} = 0.027]	3049[R_{int} = 0.035]	2386[R_{int} = 0.025]
Absorpt. correct.	Empirical	Empirical	Empirical	Empirical	Empirical
Parameters/ Restrains	264/527	277/283	195/180	157/85	296/362
R1/wR2 [I > 2σ(I)]	0.051/0.129	0.062/0.1726	0.054/0.164	0.056/0.144	0.042/0.126
R1/wR2 [all data]	0.069/0.141	0.089/0.1984	0.061/0.169	0.077/0.153	0.056/0.135
Goodness-of-fit (F^2)	1.069	1.042	1.112	1.051	1.134
Peak/hole ($e/Å^3$)	0.432/–0.440	0.467/–0.406	1.162 /–0.657	0.863 /–0.534	0.957/–1.188

4.4. Conclusions

Lithium BArF etherate has been efficiently prepared by reaction between the acid corresponding to the protonated BArF anion and lithium bis(trimethylsilyl)amide (*i.e.* $LiN(SiMe_3)_2$). This compound, as well as the rest of metal alkali BArF salts, has been characterized by standard spectroscopic techniques.

Single crystals suitable for X-ray analysis were obtained by slow evaporation of solutions of the salts in dichloromethane. All the compounds crystallized as water solvates with the exception of the cesium BArF salt, which crystallized as a dichloromethane solvate. All the structures crystallized in a tetragonal crystal system, with the BArF unit maintaining a *S*4 symmetry in the solid state. In accordance with this symmetry, boron atoms in the BArF unit show a tetrahedral geometry. Single crystal X-ray analysis of these molecules provided a framework of the spatial distribution and the distances and geometries of the alkali metal salts in the solid state.

The lithium, sodium, potassium and rubidium salts crystallized in the space group *P*4/n, whilst the cesium salt did it in the space group *P*4/ncc. The lithium and the sodium structures are isostructural and both correspond to a disordered mixture of trigonal bipyramidal and octahedral metal geometries. The potassium and rubidium structures are also isostructural, with the alkali metal atom being coordinated to nine surrounding atoms. The structure of the cesium salt, which differs in the solvent contained and in the space group, shows also a similar arrangement in the crystal structure, with the cesium center being coordinated in this case to 14 surrounding atoms.

The increasing number of interactions of the alkali metal with the surrounding atoms can be rationalized in terms of the size of the alkali metal center. In the case of lithium and sodium salts, the metal atom interacts with five or six surrounding atoms (three oxygen and two fluorine atoms or two oxygen and four fluorine atoms) depending on the geometry of the metal atom (*i.e.* trigonal bipyramidal or octahedral). In the case of the potassium and rubidium salts, the metal atom interacts with eight fluorine and one oxygen atoms. Finally, the cesium atom interacts with twelve fluorine and two chlorine atoms.

The shortest distances between the metal and boron centers show an increasing tendency with the size of the metal center, though the distances in the heavier metal centers *(i.e.* K^+, Rb^+, Cs^+) are very similar (see Table 2). The observed distances clearly demonstrate that the boron atom is in all cases isolated from the alkali metal atoms.

4.5. Experimental section

General information: All syntheses were carried out using chemicals as purchased from commercial sources unless otherwise stated. All manipulations and reactions were performed under an inert atmosphere. Glassware was dried *in vacuo* before use with a hot air gun. All solvents were dried and deoxygenated by using a solvent purification system (SPS). NMR spectra were recorded in CD_2Cl_2 or C_4D_8O unless otherwise cited. ^1H and ^{13}C NMR chemical shifts are quoted in ppm relative to residual solvent peaks. ^{11}B chemical shifts are quoted in ppm relative to trimethyl borate (TMB) in C_4D_8O. ^{19}F shifts are quoted in ppm relative to trifluoroacetic acid (TFA) in C_4D_8O. The content of lithium was determined by ICP-AES (Inductively Coupled Plasma Atomic Emission Spectroscopy). HBArF was synthesized as described in the bibliography.[18]

Synthesis of lithium tetrakis[3,5-bis(trifluoromethyl)phenyl]borate, LiBArF etherate (7). Lithium bis(trimethylsilyl)amide (0.212 g, 1.23 mmol) was dissolved in 30 mL of diethyl ether. This solution was added dropwise over a solution of HBArF (compound **6**, 1.24 g, 1.23 mmol) in 40 mL diethyl ether at −20 ºC. After stirring overnight at −10 ºC, the organic solvent was concentrated under reduced pressure to dryness. The solid was dissolved in 6 mL of diethyl ether and the solution was cooled at −78 ºC. Hexane (20 mL) was slowly added over this solution to precipitate the desired product, which was filtered off *via* cannula and dried under reduced pressure to afford the product $[Li(OEt_2)_2]^+[BArF]^-$ (**7**) as a white solid. Isolated 1.11g, 89% yield. ^1H NMR (CD_2Cl_2, 400 MHz): δ 7.72 (br s, 8H). 7.57 (br s, 4H), 3.69 (q, J = 7.1 Hz, 8H), 1.25 (t, J = 7.1 Hz, 12H). $^{13}C\{^1H\}$ NMR (C_4D_8O, 125 MHz): δ 162.8 (q, $J_{C\text{-}B}$ = 50 Hz), 135.6, 130.2−129.9 (m), 125.5 (q, $J_{C\text{-}F}$ = 272 Hz), 118.2, 66.3, 15.7. $^{19}F\{^1H\}$ NMR (C_4D_8O, 376 MHz): δ −63.184 (24F). $^{11}B\{^1H\}$ NMR (C_4D_8O, 128 MHz): δ −8.572. IR (neat, cm^{-1}) $\tilde{\upsilon}$ 1624, 1611, 1354, 1274, 1111, 1101. Content in Li by ICP-AES: calcd 0.68%, found 0.67%.

NaBArF was purchased and dried *in vacuo* (120 ºC) before performing characterization studies. KBArF[6], RbBArF[15b] and CsBArF[15a] were prepared following reported synthetic methods and were subsequently characterized.

NaBArF: ^1H NMR (C_4D_8O, 400 MHz): δ 7.78 (br s, 8H). 7.57 (br s, 4H). $^{13}C\{^1H\}$ NMR (C_4D_8O, 125 MHz): δ 162.8 (q, $J_{C\text{-}B}$ = 50 Hz), 135.6, 130.2−129.9 (m), 122.6 (q, $J_{C\text{-}F}$ = 270 Hz), 118.2. $^{19}F\{^1H\}$ NMR (C_4D_8O, 376 MHz): δ −63.129 (24F). $^{11}B\{^1H\}$ NMR (C_4D_8O, 128 MHz): δ −8.562. IR (neat, cm^{-1}) $\tilde{\upsilon}$ 1629, 1611, 1357, 1280, 1116, 1102.

KBArF: ^1H NMR (C_4D_8O, 400 MHz): δ 7.78 (br s, 8H). 7.57 (br s, 4H). $^{13}C\{^1H\}$ NMR (C_4D_8O, 125 MHz): δ 162.8 (q, $J_{C\text{-}B}$ = 50 Hz), 135.6, 130.4−129.7 (m), 125.5 (q, $J_{C\text{-}F}$ = 270 Hz), 118.2. $^{19}F\{^1H\}$ NMR (C_4D_8O, 376

MHz): δ –63.165 (24F). $^{11}B\{^1H\}$ NMR (C_4D_8O, 128 MHz): δ –8.598. IR (neat, cm^{-1}) $\tilde{\upsilon}$ 1612, 1357, 1281, 1187, 1124.

RbBArF: ^1H NMR (C_4D_8O, 400 MHz): δ 7.78 (br s, 8H). 7.57 (br s, 4H). $^{13}C\{^1H\}$ NMR (C_4D_8O, 125 MHz): δ 162.8 (q, $J_{C\text{-}B}$ = 50 Hz), 135.6, 130.5–129.8 (m), 125.5 (q, $J_{C\text{-}F}$ = 270 Hz), 118.2. $^{19}F\{^1H\}$ NMR (C_4D_8O, 376 MHz): δ –63.309 (24F). $^{11}B\{^1H\}$ NMR (C_4D_8O, 128 MHz): δ –8.553. IR (neat, cm^{-1}) $\tilde{\upsilon}$ 1612, 1357, 1281, 1122, 1084.

CsBArF: ^1H NMR (C_4D_8O, 400 MHz): δ 7.78 (br s, 8H). 7.57 (br s, 4H). $^{13}C\{^1H\}$ NMR (C_4D_8O, 125 MHz): δ 162.8 (q, $J_{C\text{-}B}$ = 50 Hz), 135.6, 130.2–129.6 (m), 125.6 (q, $J_{C\text{-}F}$ = 270 Hz), 118.2. $^{19}F\{^1H\}$ NMR (C_4D_8O, 376 MHz): δ –63.146 (24F). $^{11}B\{^1H\}$ NMR (C_4D_8O, 128 MHz): δ –8.589. IR (neat, cm^{-1}) $\tilde{\upsilon}$ 1612, 1357, 1281, 1184, 1117, 1087.

Single crystal X-ray diffraction structure determination. Crystals of the alkali metal BArF salts were obtained by slow evaporation in DCM at room temperature under inert atmosphere. The measured crystals were prepared under inert conditions immersed in perfluoropolyether as protecting oil for manipulation.

Data collection: Crystal structure determinations for LiBArF, KBArF and NaBArF were carried out using an Apex DUO diffractometer equipped with a Kappa 4-axis goniometer, an APEX II 4K CCD area detector, a Microfocus Source E025 IuS using MoK_α radiation, Quazar MX multilayer Optics as monochromator and an Oxford Cryosystems low temperature device Cryostream 700 plus (T = –173 ˚C). Crystal structure determinations for RbBArF and CsBArF were carried out using a Bruker-Nonius diffractometer equipped with an APEX II 4K CCD area detector, a FR591 rotating anode with MoK_α radiation, Montel mirrors as monochromator, a Kappa 4-axis goniometer and an Oxford Cryosystems low temperature device Cryostream 700 plus (T = –173 ˚C). Full-sphere data collection was used with ω and φ scans. *Programs used:* Data collection APEX-2,[19] data reduction Bruker Saint[20] V/.60A and absorption correction SADABS.[21]

Structure solution and refinement: Crystal structure solution was achieved using direct methods as implemented in SHELXTL[22] and visualized using the program SHELXIe.[23] Missing atoms were subsequently located from difference Fourier synthesis and added to the atom list. Least-squares refinement on F^2 using all measured intensities was carried out using the program SHELXL 2015.[24] All non-hydrogen atoms were refined including anisotropic displacement parameters.

4.6. Supporting information

4.6.1. NMR spectrum of alkali metal BArF salts

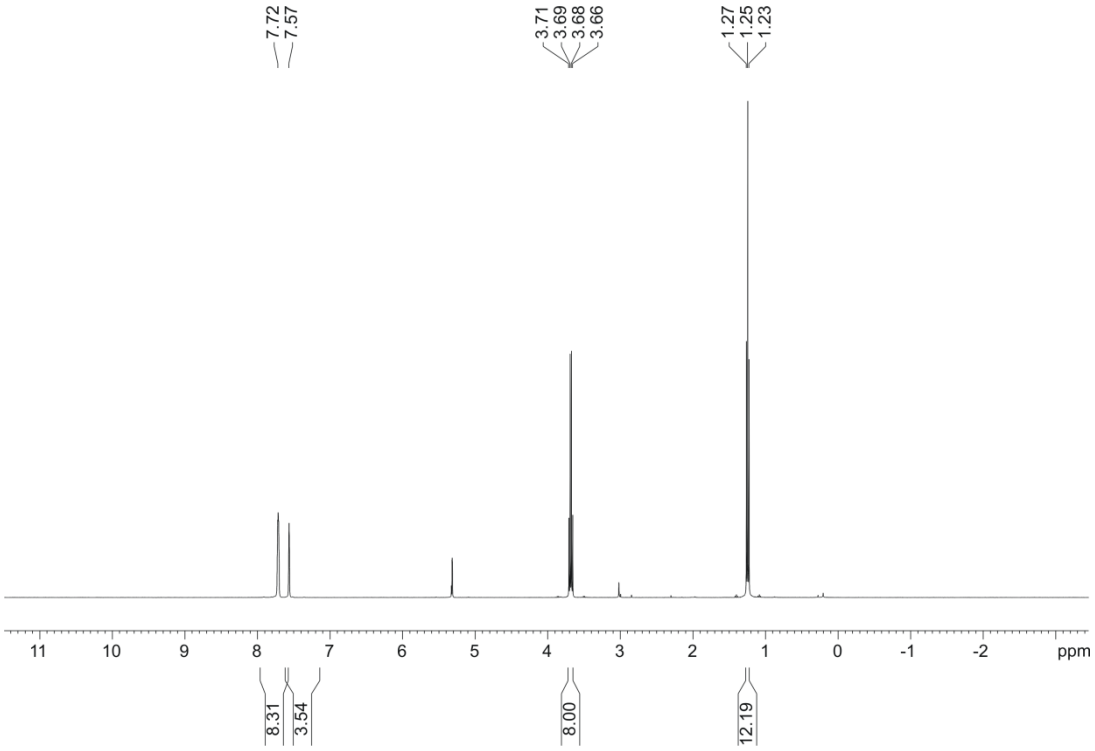

Figure S1. ^{1}H NMR spectrum of LiBArF etherate.

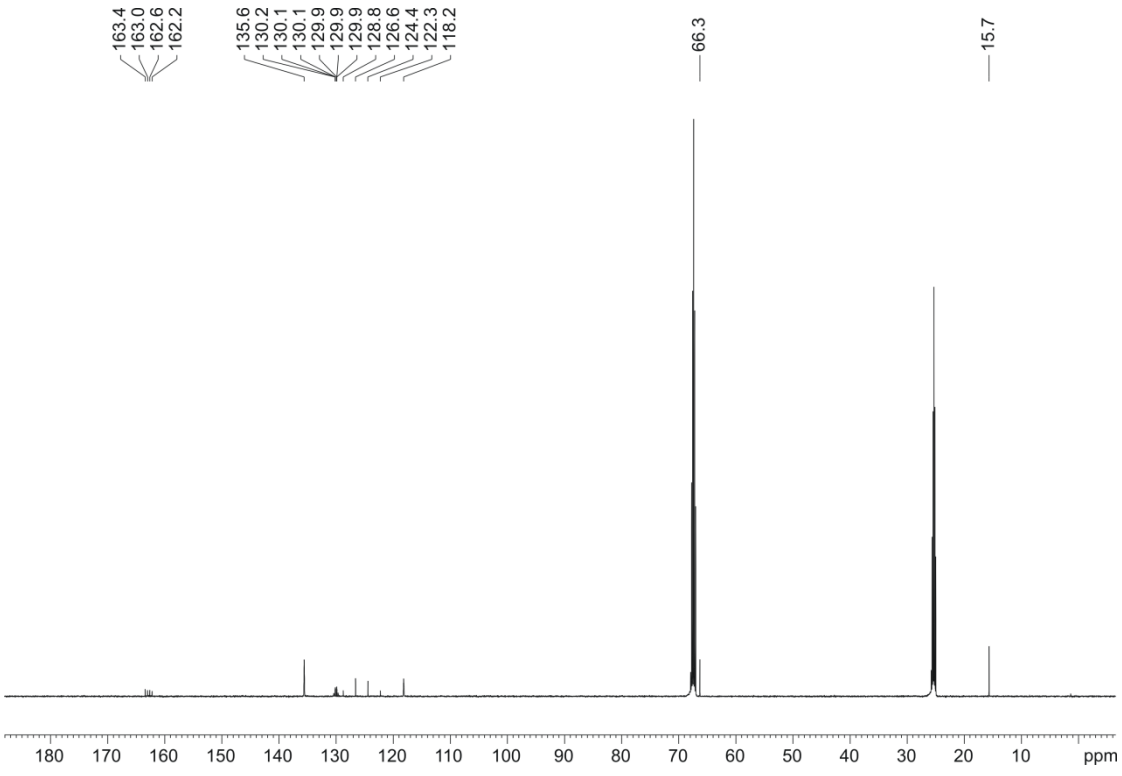

Figure S2. $^{31}C\{^{1}H\}$ NMR spectrum of LiBArF etherate.

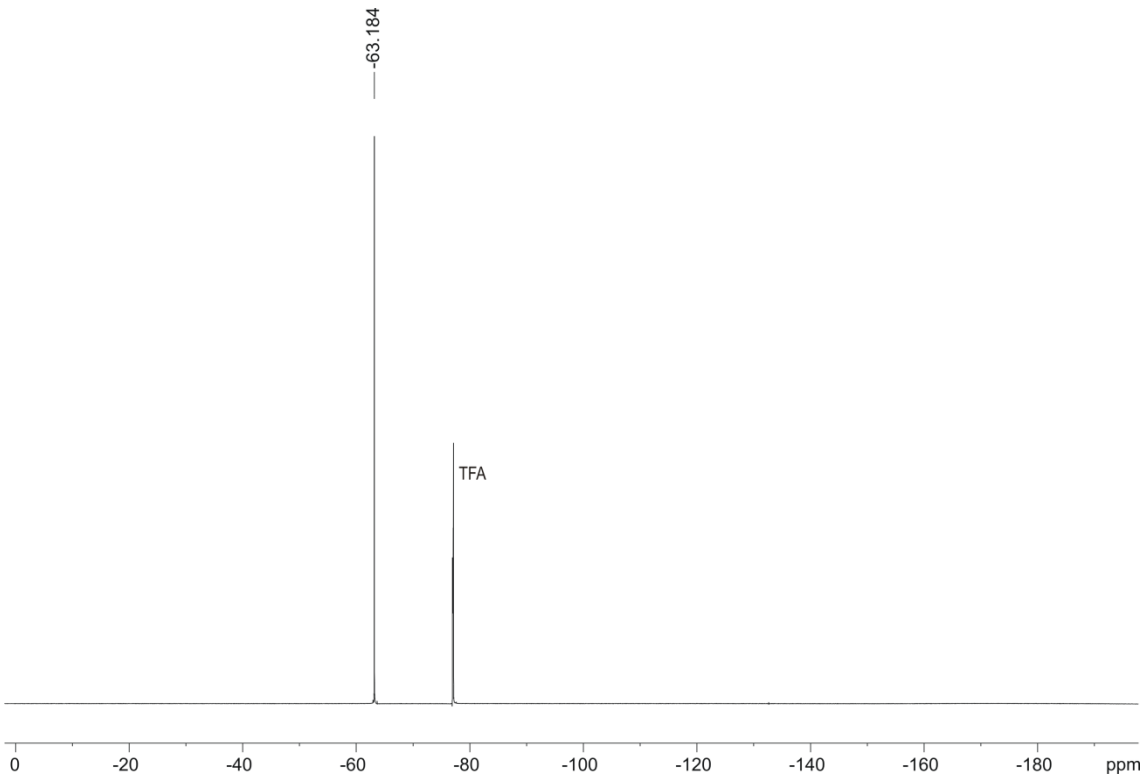

Figure S3. $^{19}F\{^{1}H\}$ NMR spectrum of LiBArF etherate (TFA = Trifluoroacetic acid).

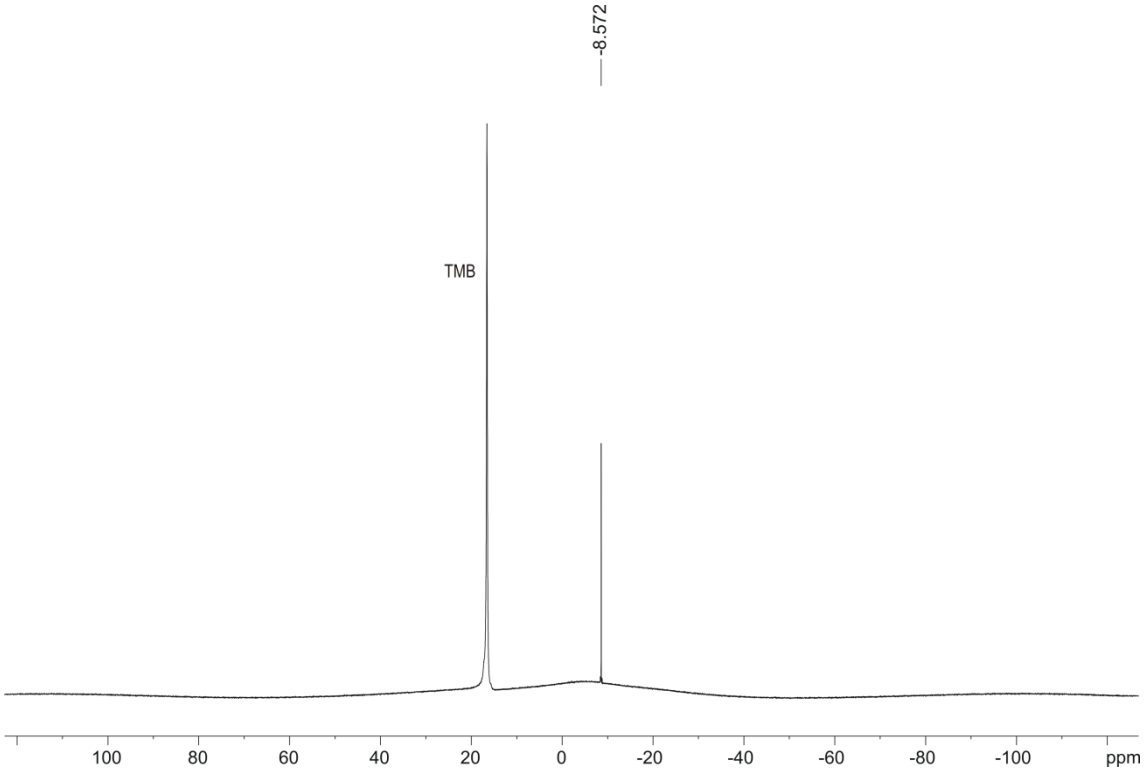

Figure S4. $^{11}B\{^{1}H\}$ NMR spectrum of LiBArF etherate (TMB = Trimethyl borate).

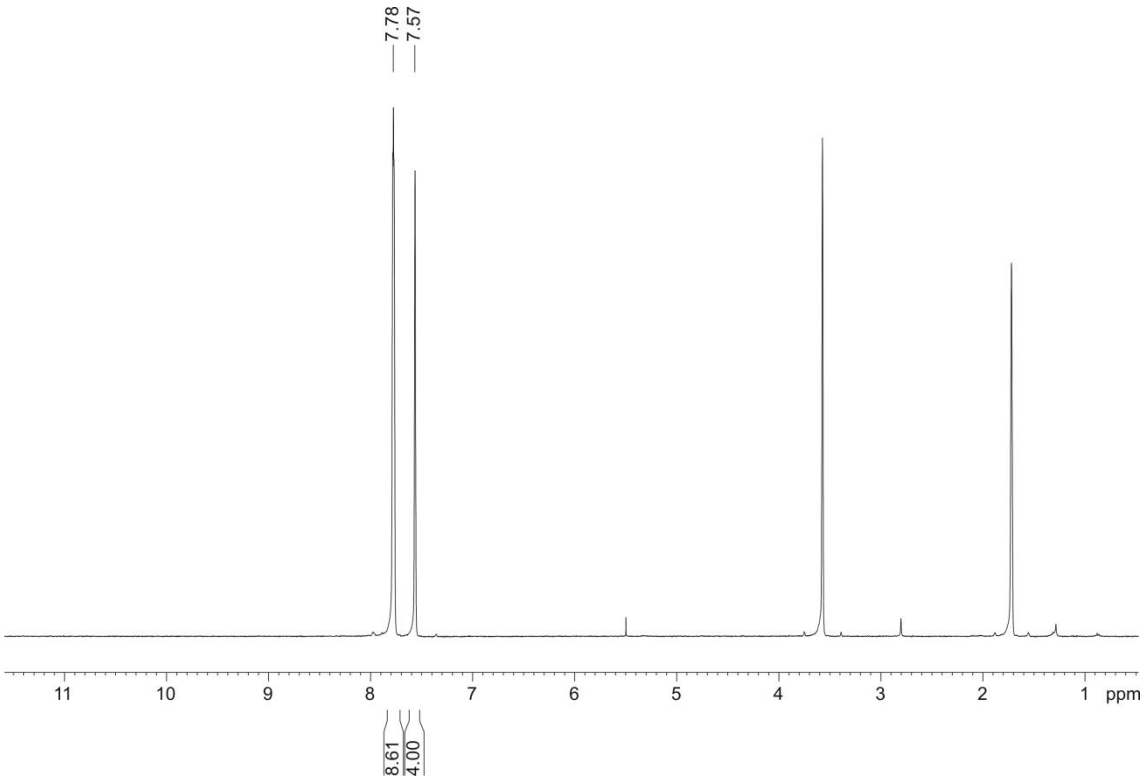

Figure S5. ^{1}H NMR spectrum of NaBArF salt.

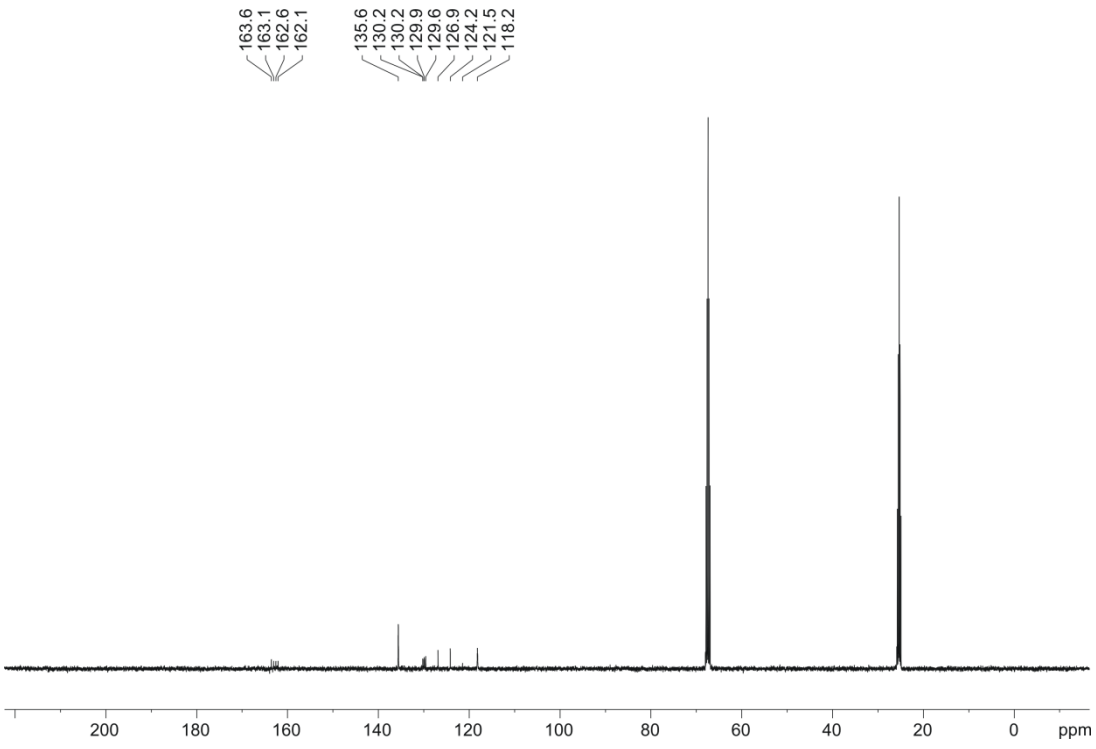

Figure S6. $^{31}C\{^{1}H\}$ NMR spectrum of NaBArF salt.

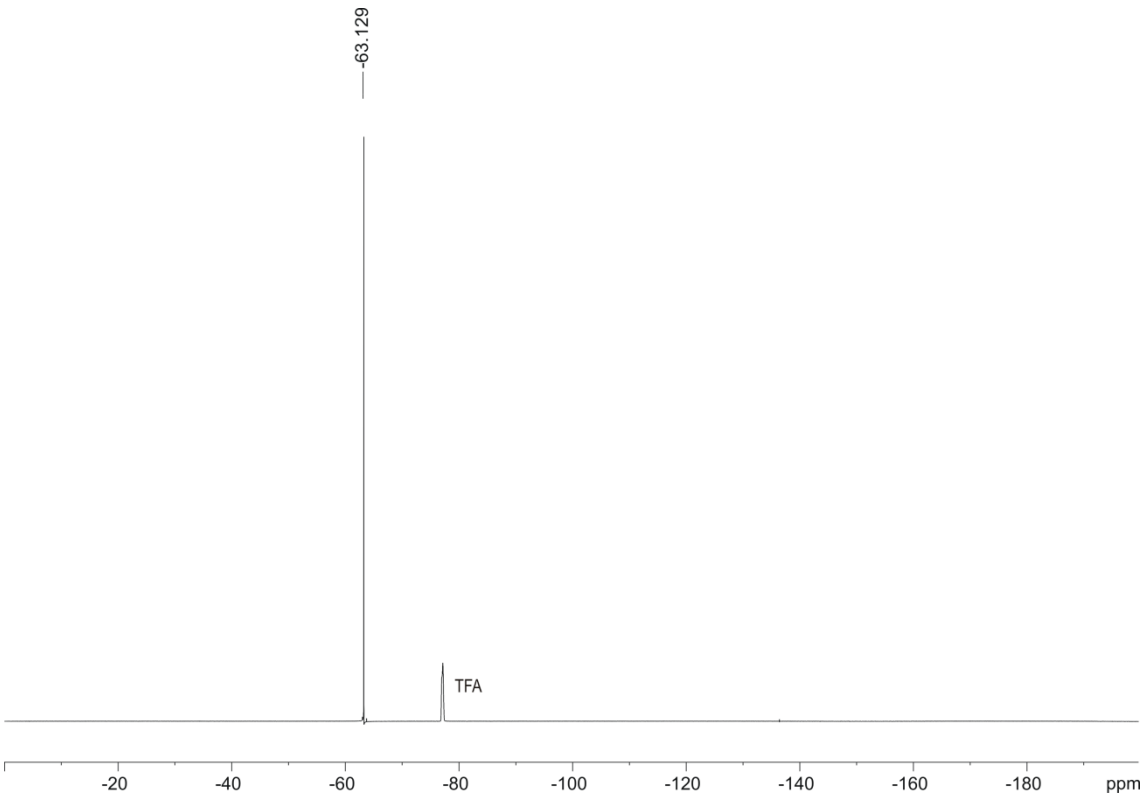

Figure S7. $^{19}F\{^{1}H\}$ NMR spectrum of NaBArF salt (TFA = Trifluoroacetic acid).

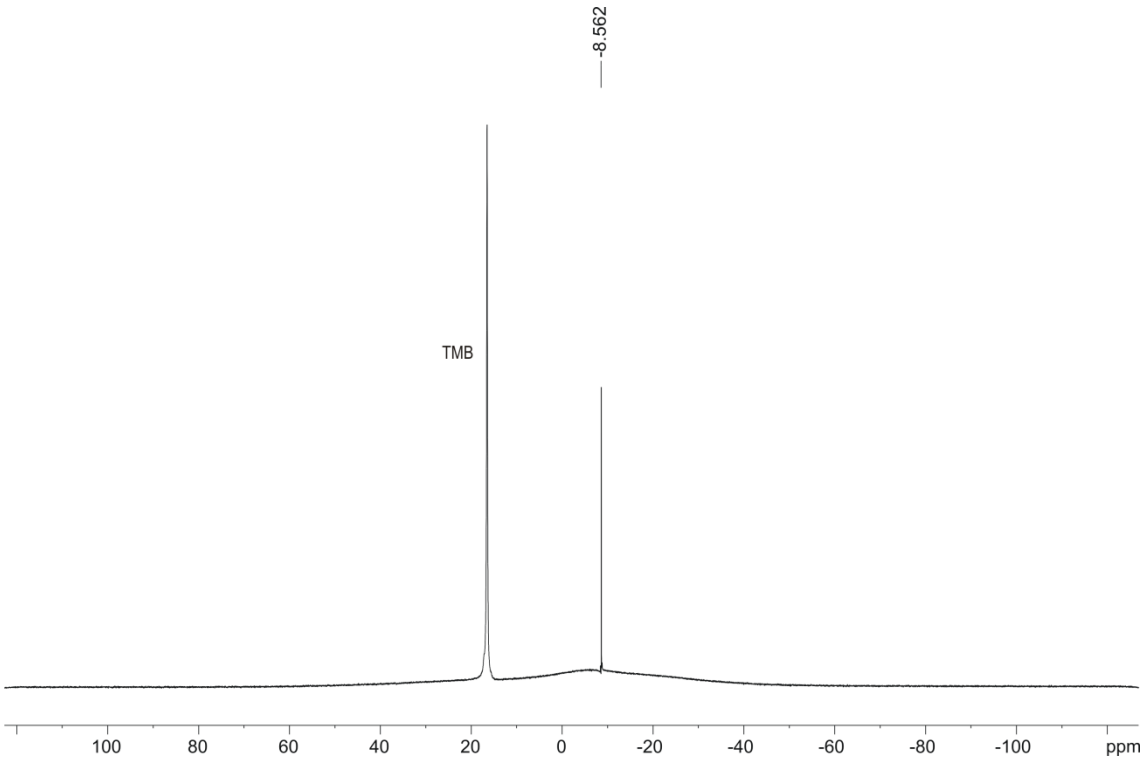

Figure S8. $^{11}B\{^{1}H\}$ NMR spectrum of NaBArF salt (TMB = Trimethyl borate).

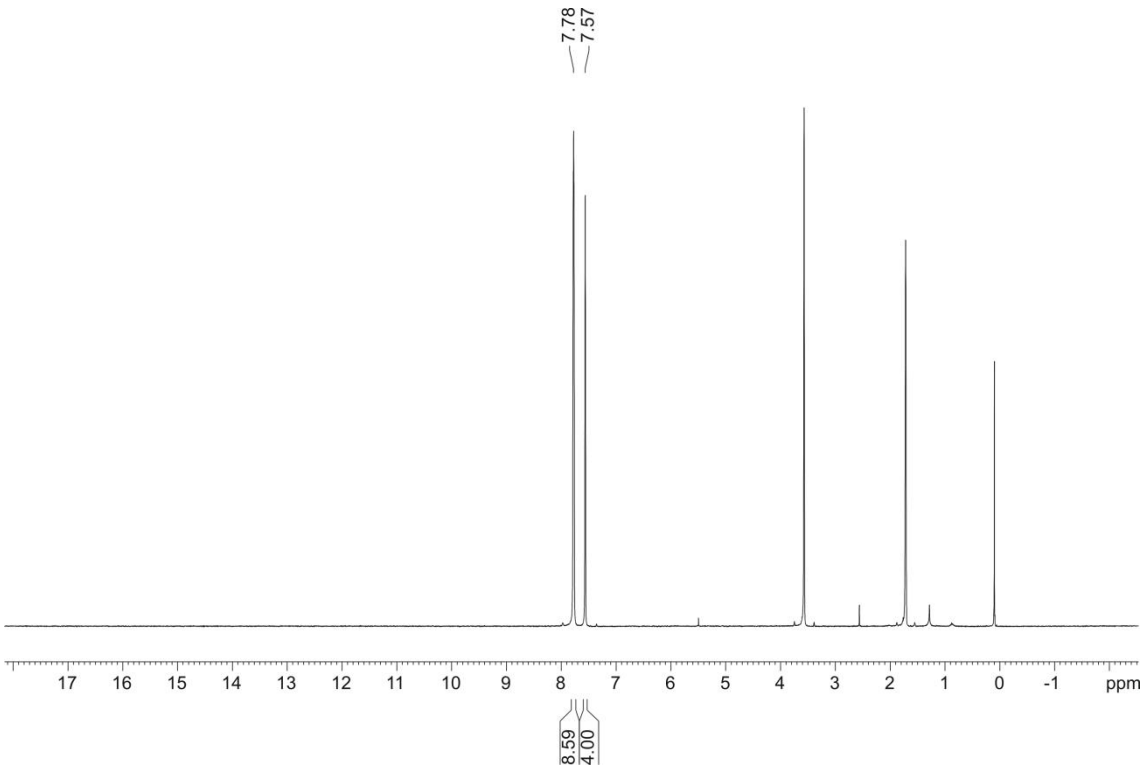

Figure S9. ^{1}H NMR spectrum of KBArF salt.

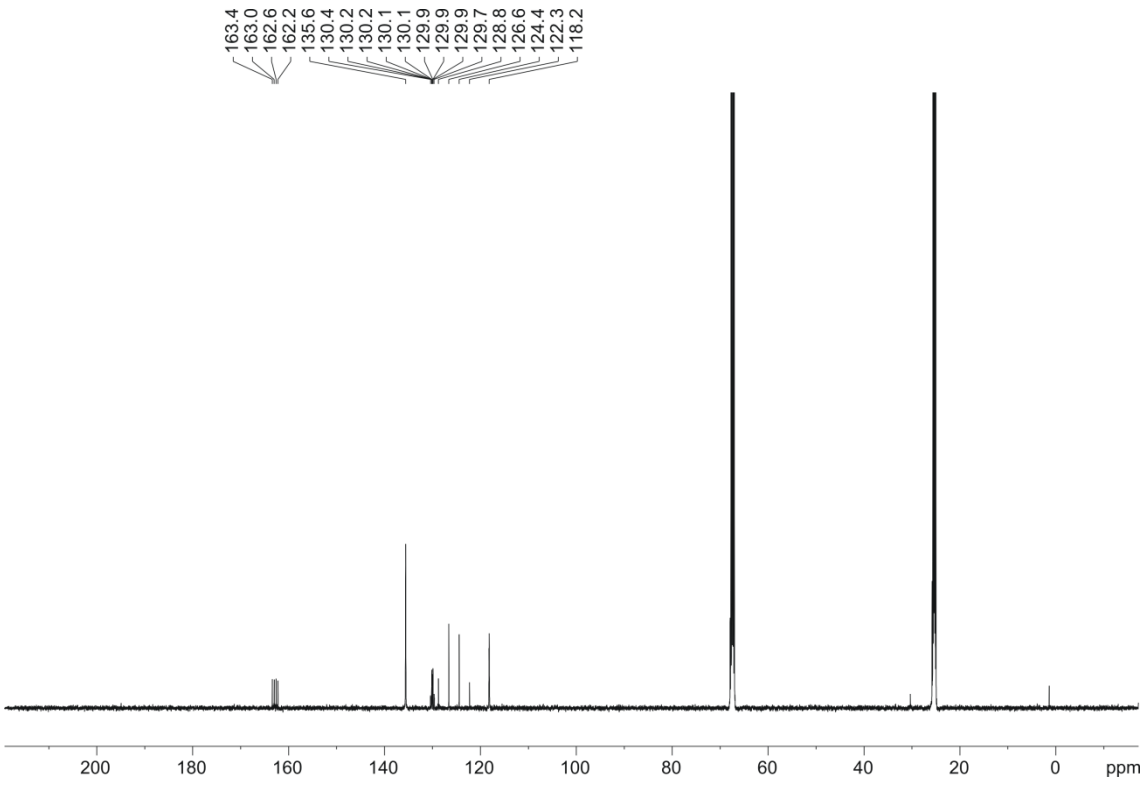

Figure S10. $^{31}C\{^{1}H\}$ NMR spectrum of KBArF salt.

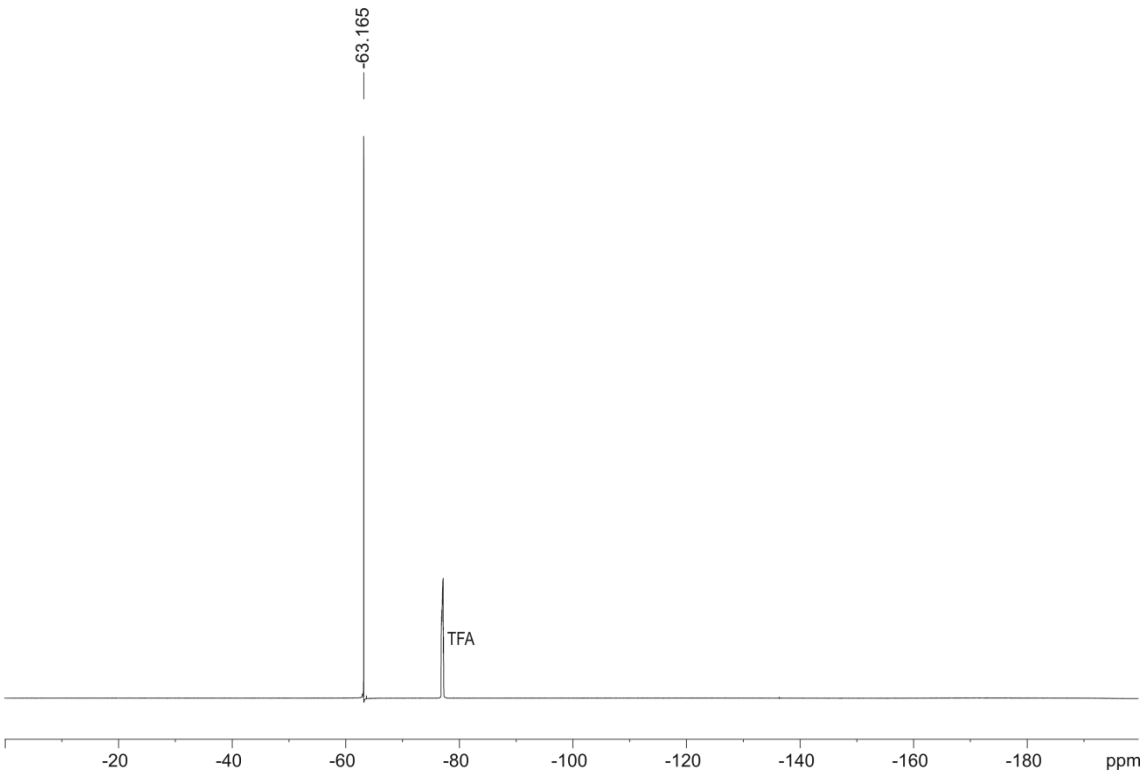

Figure S11. $^{19}F\{^{1}H\}$ NMR spectrum of KBArF salt (TFA = Trifluoroacetic acid).

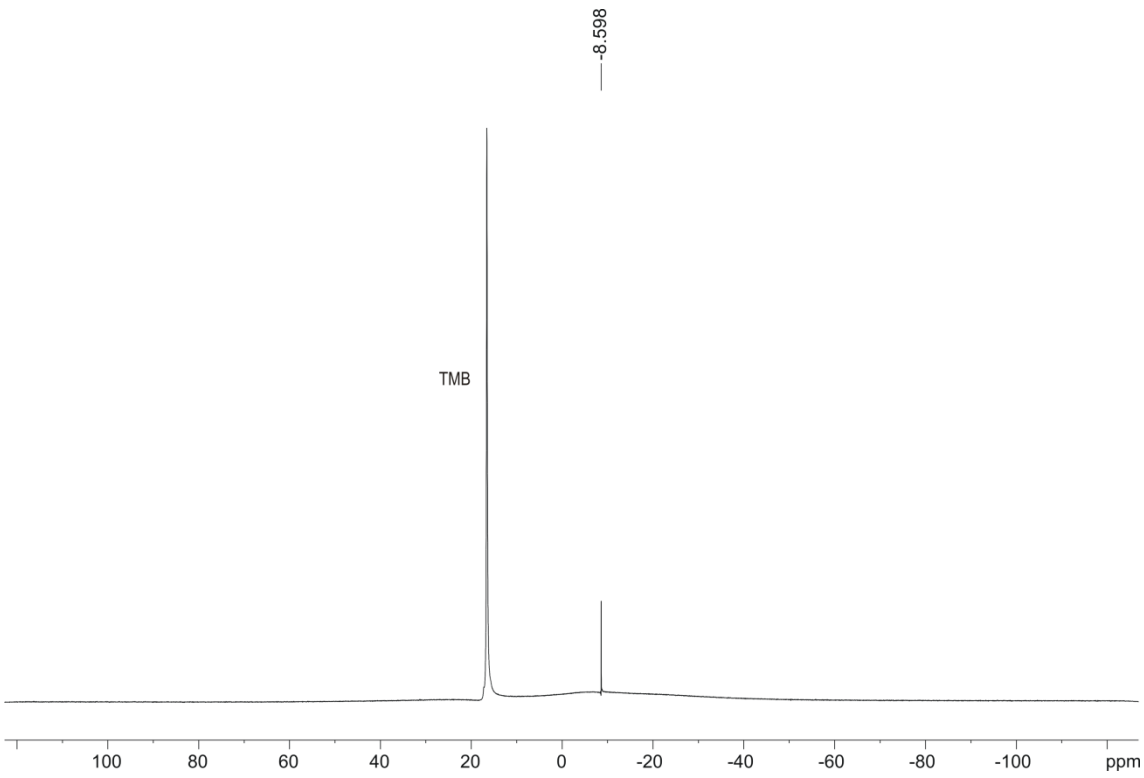

Figure S12. $^{11}B\{^{1}H\}$ NMR spectrum of KBArF salt (TMB = Trimethyl borate).

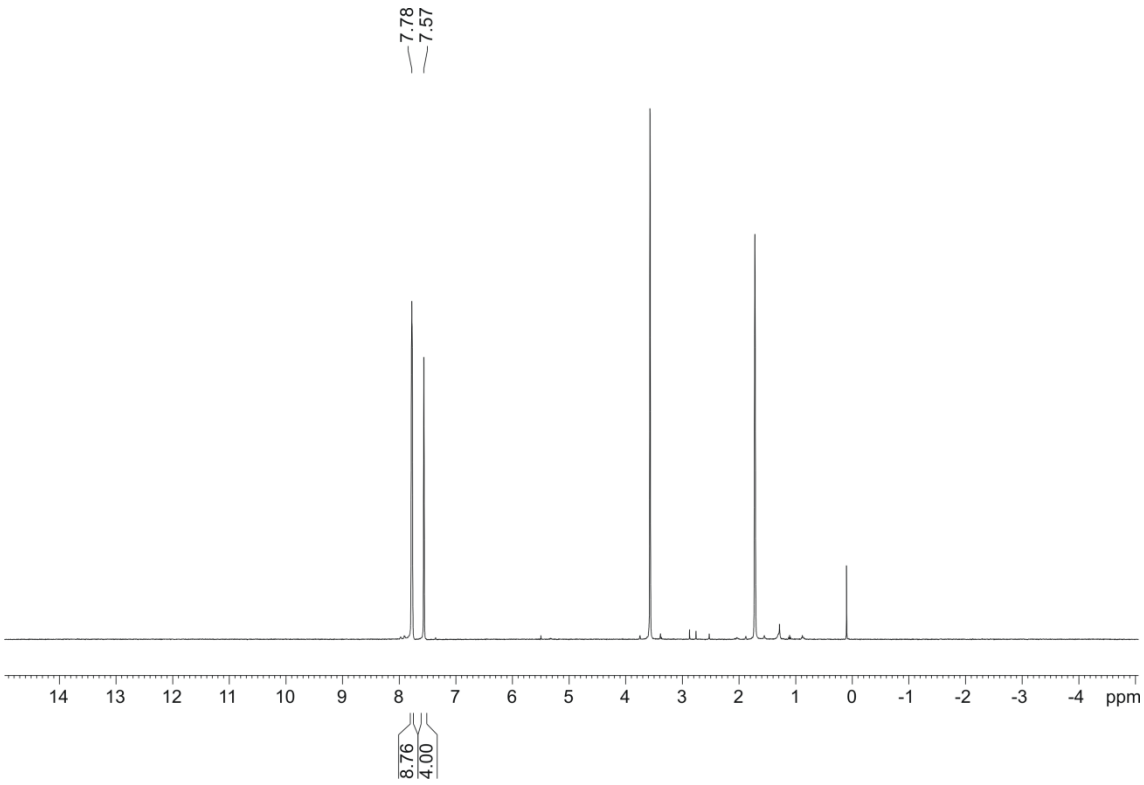

Figure S13. ^{1}H NMR spectrum of RbBArF salt.

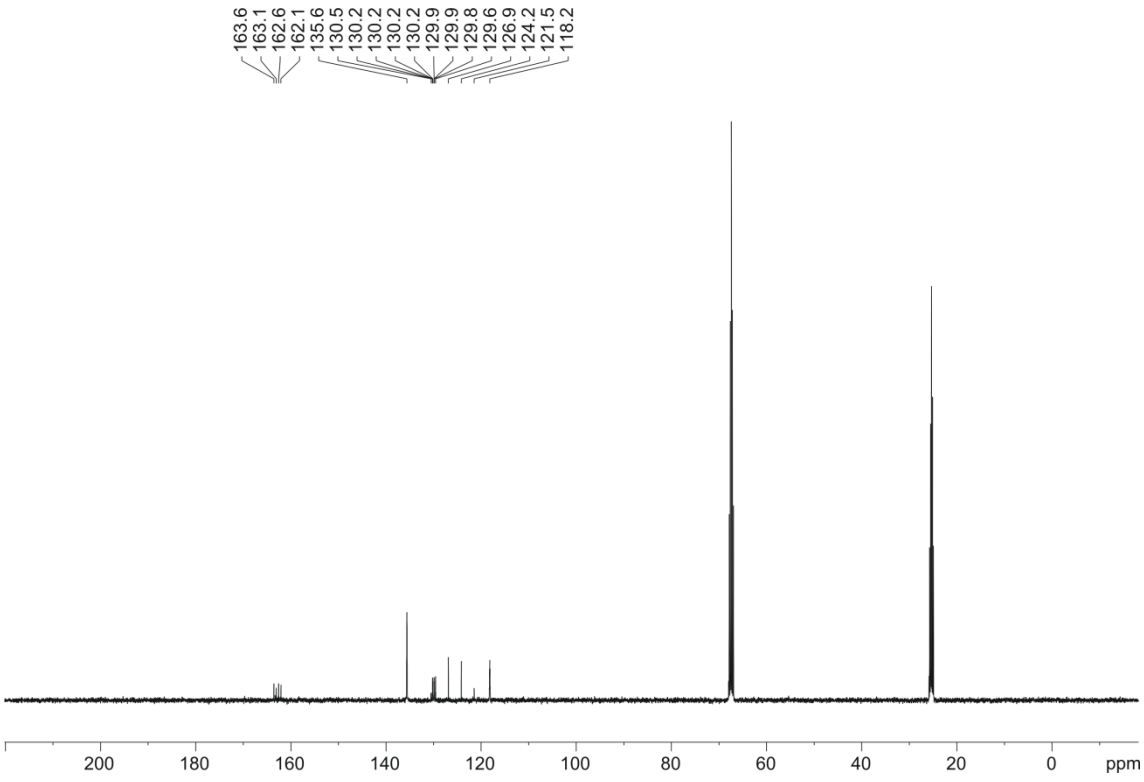

Figure S14. $^{31}C\{^{1}H\}$ NMR spectrum of RbBArF salt.

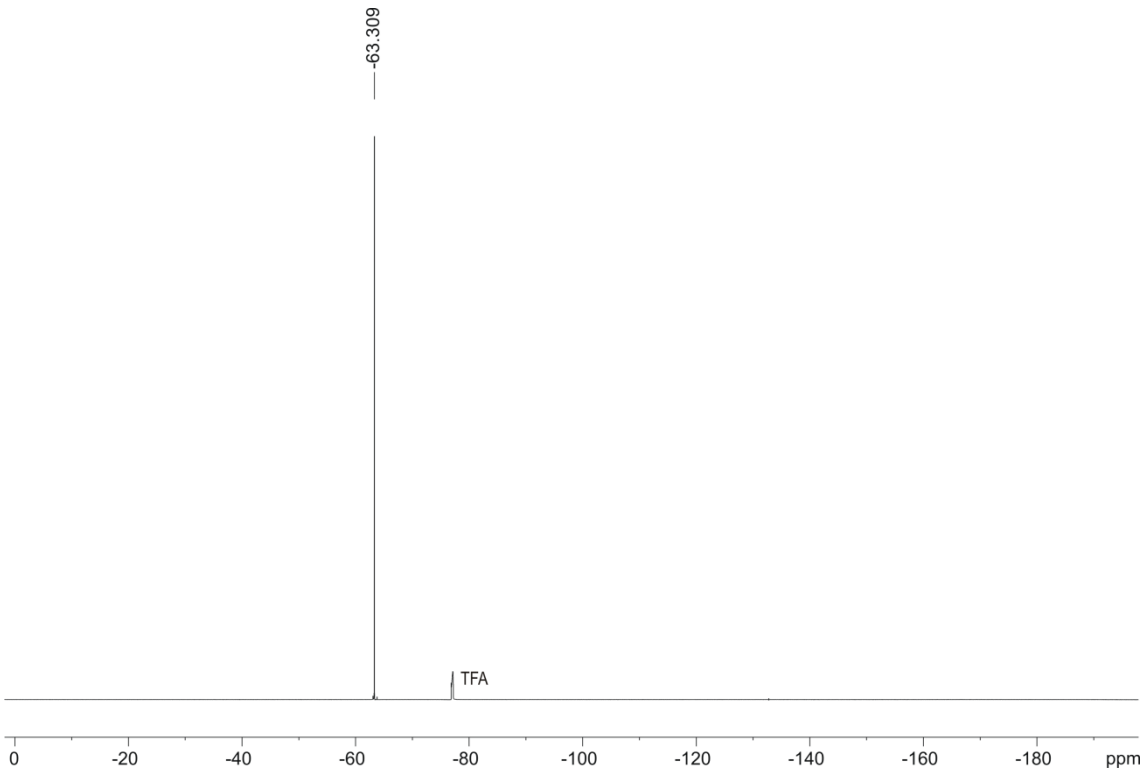

Figure S15. $^{19}F\{^{1}H\}$ NMR spectrum of RbBArF salt (TFA = Trifluoroacetic acid).

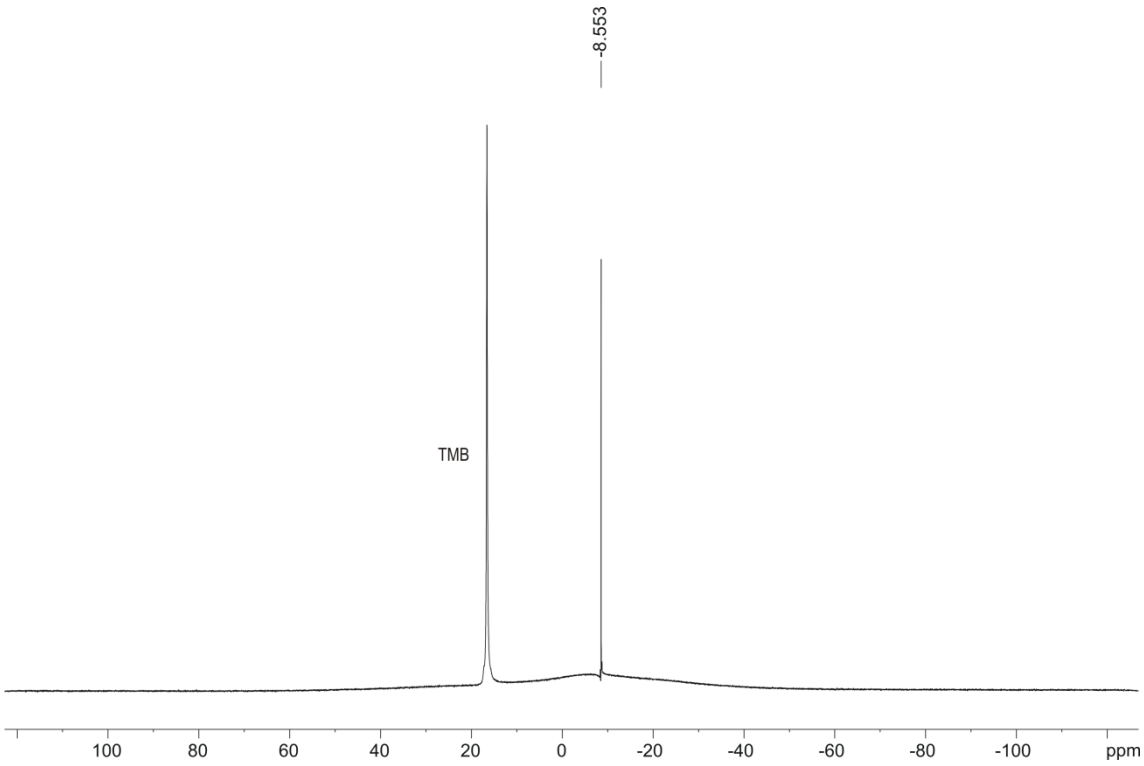

Figure S16. $^{11}B\{^{1}H\}$ NMR spectrum of RBArF salt (TMB = Trimethyl borate).

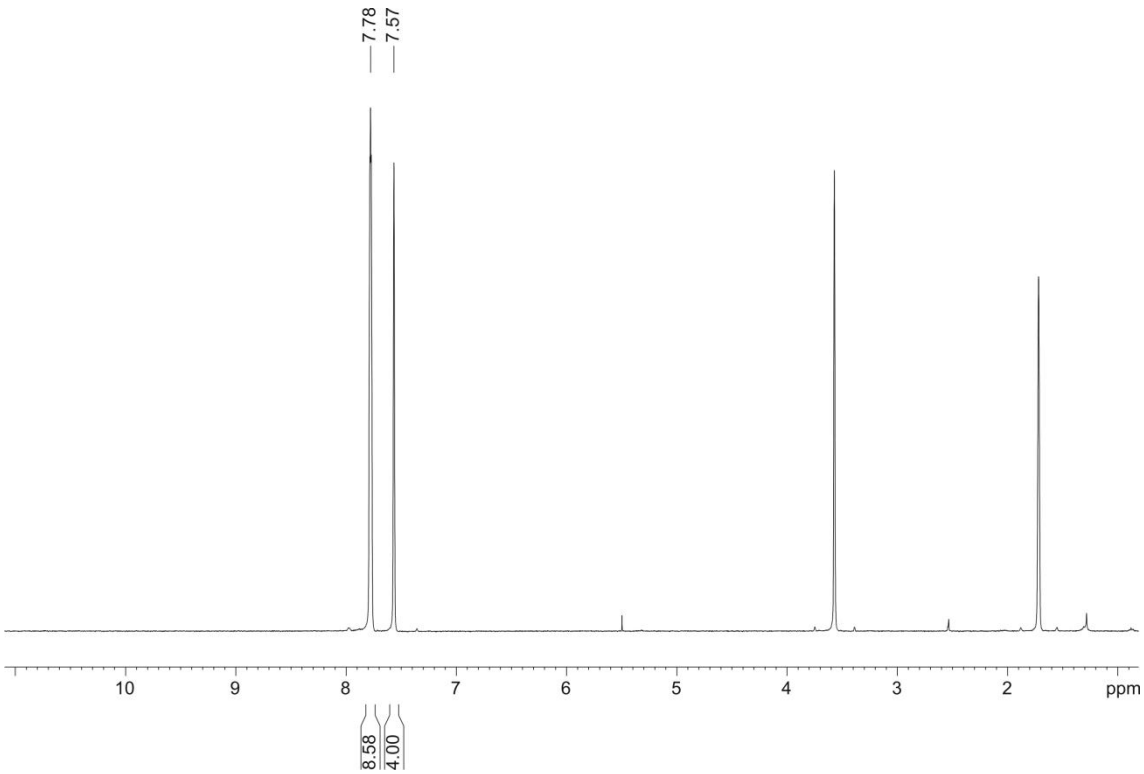

Figure S17. ^{1}H NMR spectrum of CsBArF salt.

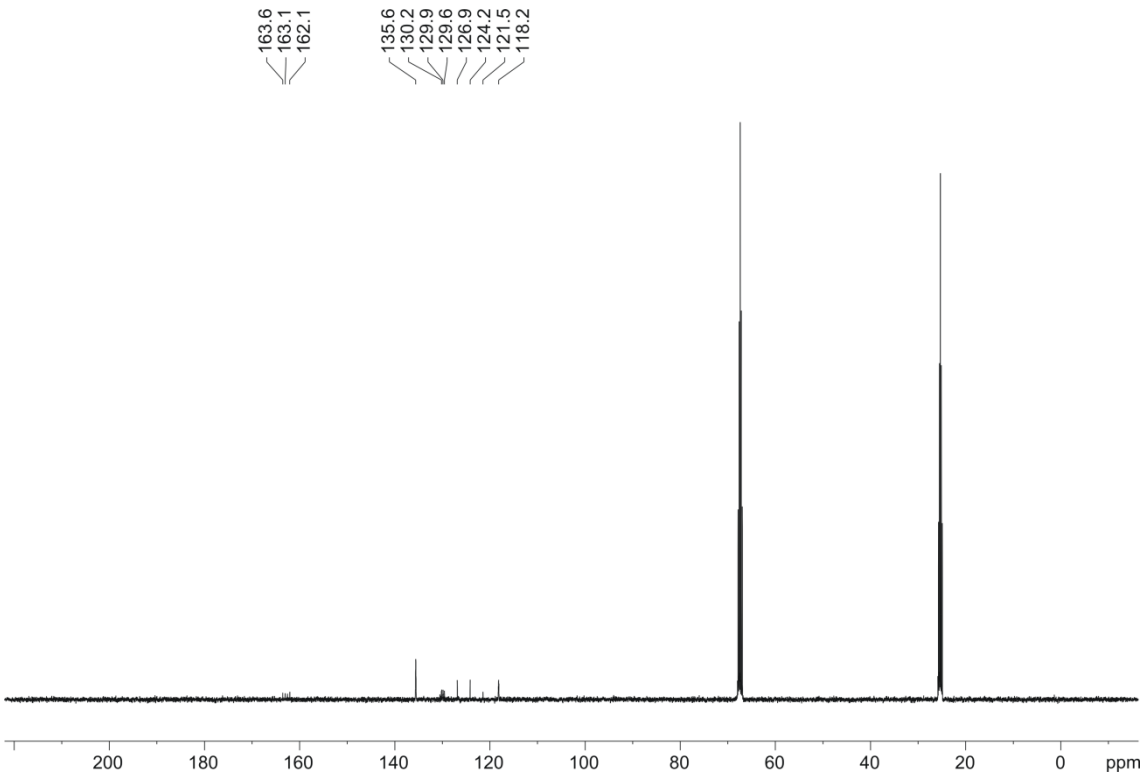

Figure S18. $^{31}C\{^{1}H\}$ NMR spectrum of CsBArF salt.

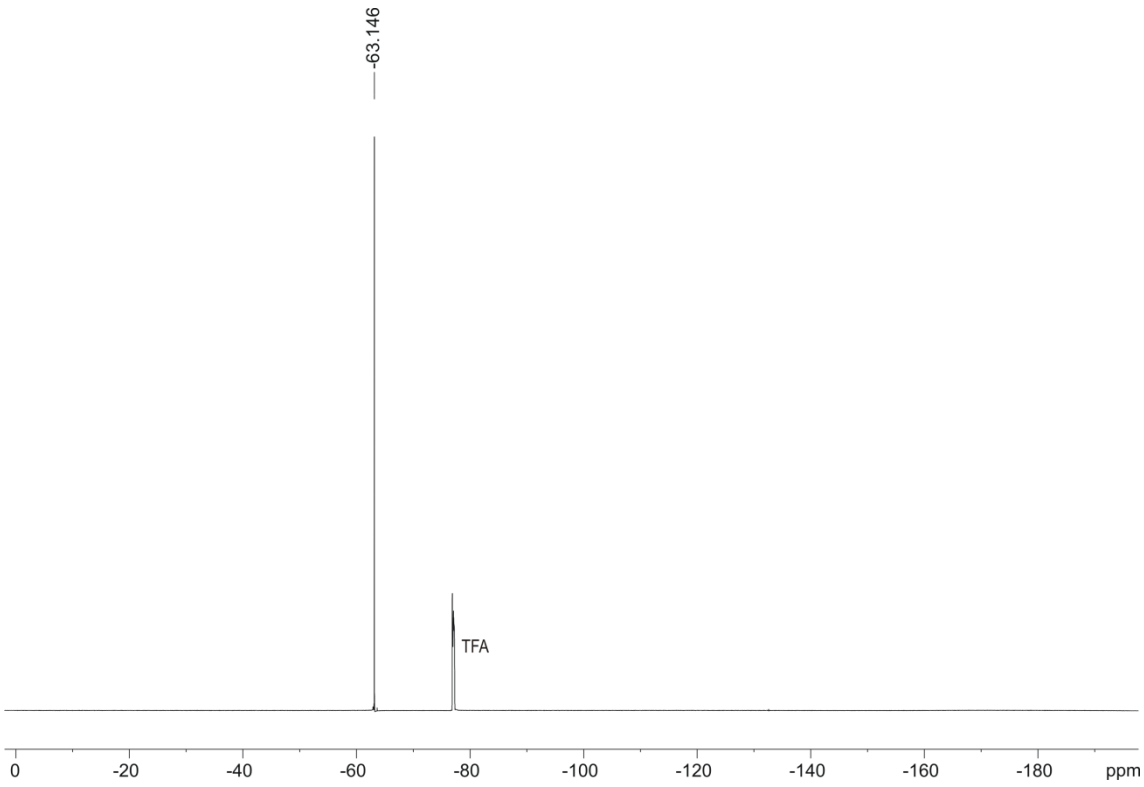

Figure S19. $^{19}F\{^{1}H\}$ NMR spectrum of CsBArF salt (TFA = Trifluoroacetic acid).

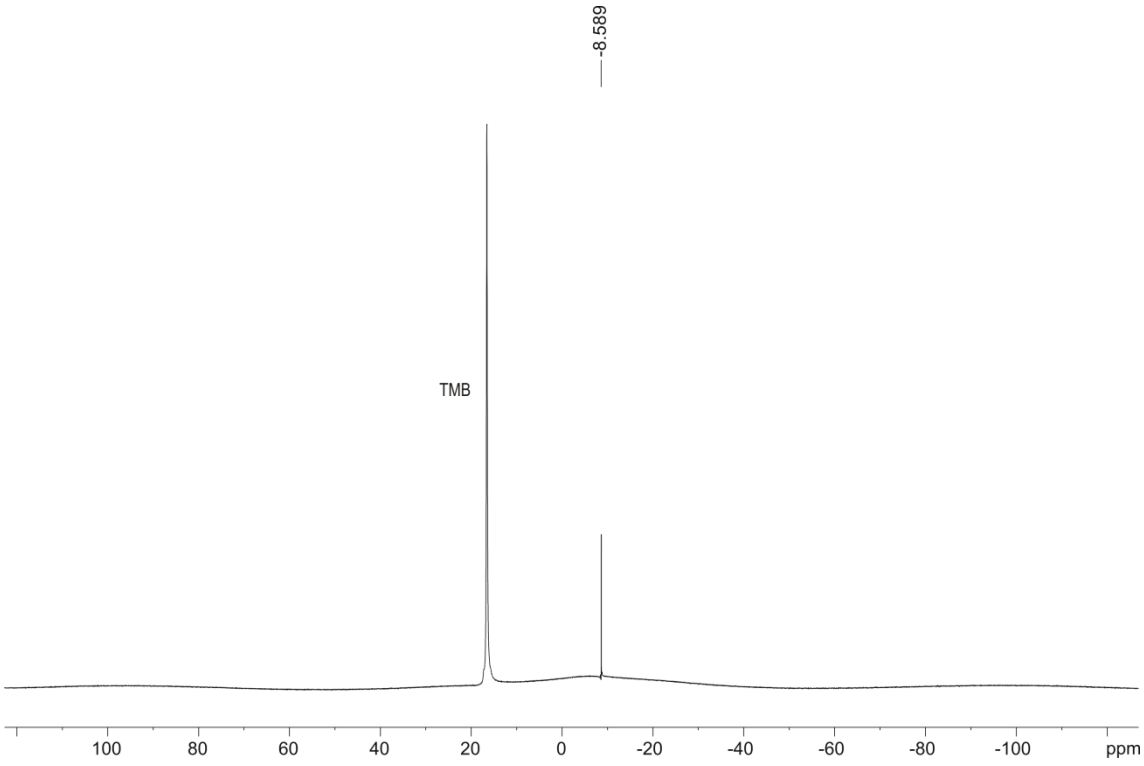

Figure S20. $^{11}B\{^{1}H\}$ NMR spectrum of CsBArF salt (TMB = Trimethyl borate).

4.6.2. Tables with crystallographic data for alkali metal BArF salts

Table S1. Crystal data and structure refinement for LiBArF.

Identification code	LiBArF	
Empirical formula	C32 H17.44 B F24 Li O2.72	
Formula weight	919.17	
Temperature	100(2) K	
Wavelength	0.71073 Å	
Crystal system	Tetragonal	
Space group	P4/n	
Unit cell dimensions	a = 13.5464(8) Å	α= 90°.
	b = 13.5464(8) Å	β= 90°.
	c = 9.5297(5) Å	γ = 90°.
Volume	1748.7(2) $Å^3$	
Z	2	
Density (calculated)	1.746 Mg/m^3	
Absorption coefficient	0.196 mm^{-1}	
F(000)	910	
Crystal size	0.200 x 0.100 x 0.070 mm^3	
Theta range for data collection	2.126 to 28.003°.	
Index ranges	-17<=h<=17, -17<=k<=17, -12<=l<=8	
Reflections collected	20179	
Independent reflections	2113 [R(int) = 0.0392]	
Completeness to theta =	25.242° 100.0 %	
Absorption correction	Empirical	
Refinement method	Full-matrix least-squares on F^2	
Data / restraints / parameters	2113 / 527 / 264	
Goodness-of-fit on F^2	1.069	
Final R indices [I>2sigma(I)]	R1 = 0.0510, wR2 = 0.1289	
R indices (all data)	R1 = 0.0688, wR2 = 0.1410	
Extinction coefficient	n/a	
Largest diff. peak and hole	0.432 and -0.440 $e.Å^{-3}$	

Table S2. Bond lengths [Å] and angles [°] for LiBArF.

B(1)-C(1)#1	1.616(14)	C(7)-F(1)	1.334(3)
B(1)-C(1)#2	1.616(14)	C(7)-F(3)	1.344(3)
B(1)-C(1)#3	1.616(14)	C(7)-C(3)	1.483(6)
B(1)-C(1)	1.616(14)	C(8)-F(5)	1.303(8)
B(1)-C(1')	1.68(2)	C(8)-F(6)	1.366(9)
B(1)-C(1')#2	1.68(2)	C(8)-F(4)	1.386(6)
B(1)-C(1')#1	1.68(2)	C(8)-C(5)	1.500(6)
B(1)-C(1')#3	1.68(2)	F(4)-O(2)#4	1.478(7)
Li(1)-O(2')	1.856(15)	C(1)-C(2)	1.397(6)
Li(1)-O(1)	1.874(9)	C(1)-C(6)	1.409(7)
Li(1)-O(2)	1.930(8)	C(2)-C(3)	1.391(6)
Li(1)-O(2)#4	1.930(8)	C(3)-C(4)	1.387(7)
Li(1)-O(2)#5	1.930(8)	C(4)-C(5)	1.389(6)
Li(1)-O(2)#6	1.930(8)	C(5)-C(6)	1.384(6)
Li(1)-F(4)#6	2.287(3)	C(8')-F(4')	1.241(16)
Li(1)-F(4)#4	2.287(3)	C(8')-F(6')	1.302(11)
Li(1)-F(4)#5	2.287(3)	C(8')-F(5')	1.343(13)
Li(1)-F(4)	2.287(3)	C(8')-C(5')	1.499(8)
Li(1)-F(4")	2.53(2)	C(1')-C(6')	1.392(9)
Li(1)-F(4")#4	2.53(2)	C(1')-C(2')	1.393(9)
O(2')-O(2)#5	1.593(8)	C(2')-C(3')	1.391(9)
O(2')-O(2)#6	1.593(8)	C(3')-C(4')	1.387(9)
O(2')-O(2)#4	1.593(8)	C(4')-C(5')	1.371(9)
O(2)-F(4)#5	1.478(7)	C(5')-C(6')	1.381(9)
F(4")-C(8)	1.320(10)		
F(5")-F(4)	1.13(3)		
F(5")-C(8)	1.319(10)		
F(6")-C(8)	1.334(10)		
C(7)-F(2)	1.332(3)		

C(1)#1-B(1)-C(1)#2	110.6(10)	O(2)#5-Li(1)-F(4)#6	39.9(2)
C(1)#1-B(1)-C(1)#3	108.9(5)	O(2)#6-Li(1)-F(4)#6	87.4(3)
C(1)#2-B(1)-C(1)#3	108.9(5)	O(2')-Li(1)-F(4)#4	89.6(2)
C(1)#1-B(1)-C(1)	108.9(5)	O(1)-Li(1)-F(4)#4	90.4(2)
C(1)#2-B(1)-C(1)	108.9(5)	O(2)-Li(1)-F(4)#4	139.2(4)
C(1)#3-B(1)-C(1)	110.6(10)	O(2)#4-Li(1)-F(4)#4	87.4(3)
C(1')-B(1)-C(1')#2	113.2(9)	O(2)#5-Li(1)-F(4)#4	92.0(3)
C(1')-B(1)-C(1')#1	113.2(9)	O(2)#6-Li(1)-F(4)#4	39.9(2)
C(1')#2-B(1)-C(1')#1	102.2(16)	F(4)#6-Li(1)-F(4)#4	89.996(4)
C(1')-B(1)-C(1')#3	102.2(16)	O(2')-Li(1)-F(4)#5	89.6(2)
C(1')#2-B(1)-C(1')#3	113.2(9)	O(1)-Li(1)-F(4)#5	90.4(2)
C(1')#1-B(1)-C(1')#3	113.2(9)	O(2)-Li(1)-F(4)#5	39.9(2)
O(2')-Li(1)-O(1)	180.0	O(2)#4-Li(1)-F(4)#5	92.0(3)
O(2')-Li(1)-O(2)	49.7(3)	O(2)#5-Li(1)-F(4)#5	87.4(3)
O(1)-Li(1)-O(2)	130.3(3)	O(2)#6-Li(1)-F(4)#5	139.2(4)
O(2')-Li(1)-O(2)#4	49.7(3)	F(4)#6-Li(1)-F(4)#5	89.997(4)
O(1)-Li(1)-O(2)#4	130.3(3)	F(4)#4-Li(1)-F(4)#5	179.1(4)
O(2)-Li(1)-O(2)#4	65.3(3)	O(2')-Li(1)-F(4)	89.5(2)
O(2')-Li(1)-O(2)#5	49.7(3)	O(1)-Li(1)-F(4)	90.5(2)
O(1)-Li(1)-O(2)#5	130.3(3)	O(2)-Li(1)-F(4)	87.4(3)
O(2)-Li(1)-O(2)#5	65.3(3)	O(2)#4-Li(1)-F(4)	39.9(2)
O(2)#4-Li(1)-O(2)#5	99.4(5)	O(2)#5-Li(1)-F(4)	139.2(4)
O(2')-Li(1)-O(2)#6	49.7(3)	O(2)#6-Li(1)-F(4)	92.0(3)
O(1)-Li(1)-O(2)#6	130.3(3)	F(4)#6-Li(1)-F(4)	179.1(4)
O(2)-Li(1)-O(2)#6	99.4(5)	F(4)#4-Li(1)-F(4)	89.997(4)
O(2)#4-Li(1)-O(2)#6	65.3(3)	F(4)#5-Li(1)-F(4)	89.996(4)
O(2)#5-Li(1)-O(2)#6	65.3(3)	O(2')-Li(1)-F(4")	109.8(6)
O(2')-Li(1)-F(4)#6	89.6(2)	O(1)-Li(1)-F(4")	70.2(6)
O(1)-Li(1)-F(4)#6	90.4(2)	O(2)-Li(1)-F(4")	122.0(5)
O(2)-Li(1)-F(4)#6	92.0(3)	O(2)#4-Li(1)-F(4")	64.6(6)
O(2)#4-Li(1)-F(4)#6	139.2(4)	O(2)#5-Li(1)-F(4")	150.0(7)

O(2)#6-Li(1)-F(4")	84.7(7)	F(5)-C(8)-F(5")	55.6(12)
F(4)#6-Li(1)-F(4")	146.0(5)	F(5)-C(8)-F(4")	130.2(13)
F(4)#4-Li(1)-F(4")	63.4(5)	F(5")-C(8)-F(4")	107.5(13)
F(4)#5-Li(1)-F(4")	117.0(5)	F(5)-C(8)-F(6")	52.3(12)
F(4)-Li(1)-F(4")	34.6(4)	F(5")-C(8)-F(6")	106.6(13)
O(2')-Li(1)-F(4")#4	109.8(6)	F(4")-C(8)-F(6")	107.7(13)
O(1)-Li(1)-F(4")#4	70.2(6)	F(5)-C(8)-F(6)	113.6(6)
O(2)-Li(1)-F(4")#4	150.0(7)	F(5")-C(8)-F(6)	131.4(14)
O(2)#4-Li(1)-F(4")#4	122.0(5)	F(4")-C(8)-F(6)	38.0(13)
O(2)#5-Li(1)-F(4")#4	84.7(7)	F(6")-C(8)-F(6)	72.2(13)
O(2)#6-Li(1)-F(4")#4	64.6(6)	F(5)-C(8)-F(4)	102.5(5)
F(4)#6-Li(1)-F(4")#4	63.4(5)	F(5")-C(8)-F(4)	49.5(12)
F(4)#4-Li(1)-F(4")#4	34.6(4)	F(4")-C(8)-F(4)	64.8(12)
F(4)#5-Li(1)-F(4")#4	146.0(5)	F(6")-C(8)-F(4)	142.5(12)
F(4)-Li(1)-F(4")#4	117.0(5)	F(6)-C(8)-F(4)	101.3(5)
F(4")-Li(1)-F(4")#4	83.4(4)	F(5)-C(8)-C(5)	115.7(5)
O(2)#5-O(2')-O(2)#6	81.6(3)	F(5")-C(8)-C(5)	115.4(14)
O(2)#5-O(2')-O(2)#4	135.2(9)	F(4")-C(8)-C(5)	113.6(13)
O(2)#6-O(2')-O(2)#4	81.6(3)	F(6")-C(8)-C(5)	105.5(12)
O(2)#5-O(2')-Li(1)	67.6(5)	F(6)-C(8)-C(5)	111.2(6)
O(2)#6-O(2')-Li(1)	67.6(5)	F(4)-C(8)-C(5)	111.1(4)
O(2)#4-O(2')-Li(1)	67.6(5)	F(5")-F(4)-C(8)	62.2(7)
F(4)#5-O(2)-Li(1)	83.1(3)	F(5")-F(4)-O(2)#4	133.9(13)
C(8)-F(4")-Li(1)	123.2(16)	C(8)-F(4)-O(2)#4	136.5(4)
F(4)-F(5")-C(8)	68.3(9)	F(5")-F(4)-Li(1)	147.0(13)
F(2)-C(7)-F(1)	106.01(18)	C(8)-F(4)-Li(1)	137.4(3)
F(2)-C(7)-F(3)	106.6(2)	O(2)#4-F(4)-Li(1)	56.9(3)
F(1)-C(7)-F(3)	105.22(19)	C(2)-C(1)-C(6)	113.8(11)
F(2)-C(7)-C(3)	112.5(7)	C(2)-C(1)-B(1)	125.1(7)
F(1)-C(7)-C(3)	115.3(5)	C(6)-C(1)-B(1)	121.1(9)
F(3)-C(7)-C(3)	110.6(5)	C(3)-C(2)-C(1)	120.5(10)

C(4)-C(3)-C(2)	125.1(7)
C(4)-C(3)-C(7)	113.6(7)
C(2)-C(3)-C(7)	121.3(8)
C(3)-C(4)-C(5)	115.1(6)
C(6)-C(5)-C(4)	120.2(6)
C(6)-C(5)-C(8)	118.8(6)
C(4)-C(5)-C(8)	121.0(5)
C(5)-C(6)-C(1)	125.3(9)
F(4')-C(8')-F(6')	98.7(9)
F(4')-C(8')-F(5')	108.1(11)
F(6')-C(8')-F(5')	107.5(9)
F(4')-C(8')-C(5')	117.4(11)
F(6')-C(8')-C(5')	113.9(7)
F(5')-C(8')-C(5')	110.2(8)
C(6')-C(1')-C(2')	117.6(18)
C(6')-C(1')-B(1)	118.0(14)
C(2')-C(1')-B(1)	124.4(12)
C(3')-C(2')-C(1')	125.6(18)
C(4')-C(3')-C(2')	113.5(12)
C(5')-C(4')-C(3')	123.5(11)
C(4')-C(5')-C(6')	121.0(10)
C(4')-C(5')-C(8')	118.4(9)
C(6')-C(5')-C(8')	120.3(10)
C(5')-C(6')-C(1')	118.7(14)

Symmetry transformations used to generate equivalent atoms:

#1 -y+1,x+1/2,-z #2 y-1/2,-x+1,-z #3 -x+1/2,-y+3/2,z #4 y,-x+3/2,z #5 -y+3/2,x,z #6 -x+3/2,-y+3/2,z

Table S3. Torsion angles [°] for LiBArF.

O(2)-Li(1)-O(2')-O(2)#5	-90.001(2)
O(2)#4-Li(1)-O(2')-O(2)#5	180.000(1)
O(2)#6-Li(1)-O(2')-O(2)#5	90.000(2)
F(4)#6-Li(1)-O(2')-O(2)#5	3.0(4)
F(4)#4-Li(1)-O(2')-O(2)#5	93.0(4)
F(4)#5-Li(1)-O(2')-O(2)#5	-87.0(4)
F(4)-Li(1)-O(2')-O(2)#5	-177.0(4)
F(4")-Li(1)-O(2')-O(2)#5	154.4(6)
F(4")#4-Li(1)-O(2')-O(2)#5	64.4(6)
O(2)-Li(1)-O(2')-O(2)#6	179.999(2)
O(2)#4-Li(1)-O(2')-O(2)#6	90.000(2)
O(2)#5-Li(1)-O(2')-O(2)#6	-90.000(2)
F(4)#6-Li(1)-O(2')-O(2)#6	-87.0(4)
F(4)#4-Li(1)-O(2')-O(2)#6	3.0(4)
F(4)#5-Li(1)-O(2')-O(2)#6	-177.0(4)
F(4)-Li(1)-O(2')-O(2)#6	93.0(4)
F(4")-Li(1)-O(2')-O(2)#6	64.4(6)
F(4")#4-Li(1)-O(2')-O(2)#6	-25.6(6)
O(2)-Li(1)-O(2')-O(2)#4	89.999(2)
O(2)#5-Li(1)-O(2')-O(2)#4	180.000(1)
O(2)#6-Li(1)-O(2')-O(2)#4	-90.000(2)
F(4)#6-Li(1)-O(2')-O(2)#4	-177.0(4)
F(4)#4-Li(1)-O(2')-O(2)#4	-87.0(4)
F(4)#5-Li(1)-O(2')-O(2)#4	93.0(4)
F(4)-Li(1)-O(2')-O(2)#4	3.0(4)
F(4")-Li(1)-O(2')-O(2)#4	-25.6(6)
F(4")#4-Li(1)-O(2')-O(2)#4	-115.6(6)
F(4)-F(5")-C(8)-F(5)	-158(2)
F(4)-F(5")-C(8)-F(4")	-31(2)
F(4)-F(5")-C(8)-F(6")	-146.4(15)

F(4)-F(5")-C(8)-F(6)	-66(2)	C(1)#2-B(1)-C(1)-C(6)	-69.3(7)
F(4)-F(5")-C(8)-C(5)	96.7(13)	C(1)#3-B(1)-C(1)-C(6)	50.3(9)
Li(1)-F(4")-C(8)-F(5)	84(2)	C(6)-C(1)-C(2)-C(3)	0.6(9)
Li(1)-F(4")-C(8)-F(5")	25(2)	B(1)-C(1)-C(2)-C(3)	-178.6(14)
Li(1)-F(4")-C(8)-F(6")	139.5(18)	C(1)-C(2)-C(3)-C(4)	0.4(11)
Li(1)-F(4")-C(8)-F(6)	161(3)	C(1)-C(2)-C(3)-C(7)	-178.4(14)
Li(1)-F(4")-C(8)-F(4)	-0.9(10)	F(2)-C(7)-C(3)-C(4)	-94.9(11)
Li(1)-F(4")-C(8)-C(5)	-104.1(16)	F(1)-C(7)-C(3)-C(4)	26.9(14)
C(8)-F(5")-F(4)-O(2)#4	-129.1(8)	F(3)-C(7)-C(3)-C(4)	146.1(9)
C(8)-F(5")-F(4)-Li(1)	135.6(13)	F(2)-C(7)-C(3)-C(2)	84.0(11)
F(5)-C(8)-F(4)-F(5")	18.2(18)	F(1)-C(7)-C(3)-C(2)	-154.3(8)
F(4")-C(8)-F(4)-F(5")	147(2)	F(3)-C(7)-C(3)-C(2)	-35.0(12)
F(6")-C(8)-F(4)-F(5")	60(3)	C(2)-C(3)-C(4)-C(5)	-0.5(15)
F(6)-C(8)-F(4)-F(5")	135.8(18)	C(7)-C(3)-C(4)-C(5)	178.4(9)
C(5)-C(8)-F(4)-F(5")	-106.0(18)	C(3)-C(4)-C(5)-C(6)	-0.5(11)
F(5)-C(8)-F(4)-O(2)#4	143.8(6)	C(3)-C(4)-C(5)-C(8)	177.5(9)
F(5")-C(8)-F(4)-O(2)#4	125.7(19)	F(5)-C(8)-C(5)-C(6)	-34.5(8)
F(4")-C(8)-F(4)-O(2)#4	-87.4(15)	F(5")-C(8)-C(5)-C(6)	27.8(15)
F(6")-C(8)-F(4)-O(2)#4	-174(2)	F(4")-C(8)-C(5)-C(6)	152.6(14)
F(6)-C(8)-F(4)-O(2)#4	-98.6(7)	F(6")-C(8)-C(5)-C(6)	-89.7(14)
C(5)-C(8)-F(4)-O(2)#4	19.6(7)	F(6)-C(8)-C(5)-C(6)	-166.2(6)
F(5)-C(8)-F(4)-Li(1)	-127.6(5)	F(4)-C(8)-C(5)-C(6)	81.8(6)
F(5")-C(8)-F(4)-Li(1)	-145.8(18)	F(5)-C(8)-C(5)-C(4)	147.4(7)
F(4")-C(8)-F(4)-Li(1)	1.2(14)	F(5")-C(8)-C(5)-C(4)	-150.3(15)
F(6")-C(8)-F(4)-Li(1)	-85(2)	F(4")-C(8)-C(5)-C(4)	-25.5(15)
F(6)-C(8)-F(4)-Li(1)	-10.0(7)	F(6")-C(8)-C(5)-C(4)	92.2(14)
C(5)-C(8)-F(4)-Li(1)	108.2(5)	F(6)-C(8)-C(5)-C(4)	15.7(8)
C(1)#1-B(1)-C(1)-C(2)	-10.8(12)	F(4)-C(8)-C(5)-C(4)	-96.2(6)
C(1)#2-B(1)-C(1)-C(2)	109.9(16)	C(4)-C(5)-C(6)-C(1)	1.7(12)
C(1)#3-B(1)-C(1)-C(2)	-130.5(14)	C(8)-C(5)-C(6)-C(1)	-176.3(10)
C(1)#1-B(1)-C(1)-C(6)	170.0(12)	C(2)-C(1)-C(6)-C(5)	-1.7(14)

B(1)-C(1)-C(6)-C(5)	177.6(9)
C(1')#2-B(1)-C(1')-C(6')	-77.8(10)
C(1')#1-B(1)-C(1')-C(6')	166.5(18)
C(1')#3-B(1)-C(1')-C(6')	44.4(14)
C(1')#2-B(1)-C(1')-C(2')	102(3)
C(1')#1-B(1)-C(1')-C(2')	-14(2)
C(1')#3-B(1)-C(1')-C(2')	-136(2)
C(6')-C(1')-C(2')-C(3')	0.4(17)
B(1)-C(1')-C(2')-C(3')	-179(2)
C(1')-C(2')-C(3')-C(4')	-0.4(16)
C(2')-C(3')-C(4')-C(5')	0(2)
C(3')-C(4')-C(5')-C(6')	0(2)
C(3')-C(4')-C(5')-C(8')	-173.9(17)
F(4')-C(8')-C(5')-C(4')	-22.8(17)
F(6')-C(8')-C(5')-C(4')	91.9(11)
F(5')-C(8')-C(5')-C(4')	-147.1(11)
F(4')-C(8')-C(5')-C(6')	163.1(13)
F(6')-C(8')-C(5')-C(6')	-82.2(12)
F(5')-C(8')-C(5')-C(6')	38.8(14)
C(4')-C(5')-C(6')-C(1')	0(2)
C(8')-C(5')-C(6')-C(1')	173.7(16)
C(2')-C(1')-C(6')-C(5')	0(2)
B(1)-C(1')-C(6')-C(5')	179.5(15)

Symmetry transformations used to generate equivalent atoms:

#1 -y+1,x+1/2,-z #2 y-1/2,-x+1,-z #3 -x+1/2,-y+3/2,z #4 y,-x+3/2,z #5 -y+3/2,x,z #6 -x+3/2,-y+3/2,z

Table S4. Crystal data and structure refinement for NaBArF.

Identification code	NaBArF	
Empirical formula	C32 H18.76 B F24 Na O2.38	
Formula weight	931.11	
Temperature	100(2) K	
Wavelength	0.71073 Å	
Crystal system	Tetragonal	
Space group	P4/n	
Unit cell dimensions	a = 13.5537(7) Å	α= 90°.
	b = 13.5537(7) Å	β= 90°.
	c = 9.7850(7) Å	γ = 90°.
Volume	1797.5(2) $Å^3$	
Z	2	
Density (calculated)	1.720 Mg/m^3	
Absorption coefficient	0.202 mm^{-1}	
F(000)	924	
Crystal size	0.300 x 0.180 x 0.100 mm^3	
Theta range for data collection	2.081 to 28.503°.	
Index ranges	-18<=h<=17, -16<=k<=15, -12<=l<=11	
Reflections collected	9218	
Independent reflections	2249 [R(int) = 0.0307]	
Completeness to theta =	25.242° 98.9 %	
Absorption correction	Empirical	
Refinement method	Full-matrix least-squares on F^2	
Data / restraints / parameters	2249 / 283 / 277	
Goodness-of-fit on F^2	1.042	
Final R indices [I>2sigma(I)]	R1 = 0.0624, wR2 = 0.1726	
R indices (all data)	R1 = 0.0895, wR2 = 0.1984	
Extinction coefficient	n/a	
Largest diff. peak and hole	0.467 and -0.406 $e.Å^{-3}$	

Table S5. Bond lengths [Å] and angles [°] for NaBArF.

Na(1)-O(1)	2.193(5)	C(1')-C(6')	1.402(5)
Na(1)-O(2')	2.258(7)	C(6')-C(5')	1.392(5)
Na(1)-O(2)	2.274(17)	C(5')-C(4')	1.380(6)
Na(1)-O(2)#1	2.274(17)	C(5')-C(8')	1.509(7)
Na(1)-O(2)#2	2.274(17)	C(4')-C(3')	1.386(6)
Na(1)-O(2)#3	2.274(17)	C(3')-C(2')	1.396(5)
Na(1)-F(4)	2.395(2)	C(3')-C(7')	1.497(5)
Na(1)-F(4)#3	2.395(2)	C(8')-F(6')	1.344(9)
Na(1)-F(4)#2	2.395(2)	C(8')-F(4')	1.345(9)
Na(1)-F(4)#1	2.395(2)	C(8')-F(5')	1.371(9)
Na(1)-F(4')	2.995(10)	C(7')-F(1')	1.347(9)
Na(1)-F(4')#2	2.995(10)	C(7')-F(2')	1.376(9)
B(1)-C(1')#4	1.601(12)	C(7')-F(3')	1.377(9)
B(1)-C(1')#5	1.601(12)		
B(1)-C(1')#6	1.601(12)	O(1)-Na(1)-O(2')	180.0
B(1)-C(1')	1.601(12)	O(1)-Na(1)-O(2)	138.0(5)
B(1)-C(1)#4	1.650(4)	O(1)-Na(1)-O(2)#1	138.0(5)
B(1)-C(1)#5	1.650(4)	O(2)-Na(1)-O(2)#1	83.9(11)
B(1)-C(1)#6	1.650(4)	O(1)-Na(1)-O(2)#2	138.0(5)
B(1)-C(1)	1.650(4)	O(2)-Na(1)-O(2)#2	56.4(6)
C(1)-C(2)	1.397(4)	O(2)#1-Na(1)-O(2)#2	56.4(6)
C(1)-C(6)	1.404(4)	O(1)-Na(1)-O(2)#3	138.0(5)
C(6)-C(5)	1.390(4)	O(2)-Na(1)-O(2)#3	56.4(6)
C(5)-C(4)	1.378(5)	O(2)#1-Na(1)-O(2)#3	56.4(6)
C(5)-C(8)	1.502(5)	O(2)#2-Na(1)-O(2)#3	83.9(10)
C(4)-C(3)	1.385(4)	O(1)-Na(1)-F(4)	89.71(8)
C(3)-C(2)	1.393(4)	O(2)-Na(1)-F(4)	92.7(6)
C(3)-C(7)	1.493(4)	O(2)#1-Na(1)-F(4)	87.7(6)
C(8)-F(6)	1.327(5)	O(2)#2-Na(1)-F(4)	132.1(5)
C(8)-F(4)	1.342(4)	O(2)#3-Na(1)-F(4)	48.4(5)
C(8)-F(5)	1.363(5)	O(1)-Na(1)-F(4)#3	89.71(8)
C(7)-F(3)	1.320(5)	O(2)-Na(1)-F(4)#3	132.1(5)
C(7)-F(2)	1.325(6)	O(2)#1-Na(1)-F(4)#3	48.4(5)
C(7)-F(1)	1.329(5)	O(2)#2-Na(1)-F(4)#3	87.7(6)
C(1')-C(2')	1.396(5)	O(2)#3-Na(1)-F(4)#3	92.7(6)

F(4)-Na(1)-F(4)#3	89.998(2)	C(5)-C(6)-C(1)	121.8(3)
O(1)-Na(1)-F(4)#2	89.71(8)	C(4)-C(5)-C(6)	121.7(3)
O(2)-Na(1)-F(4)#2	48.4(5)	C(4)-C(5)-C(8)	119.5(3)
O(2)#1-Na(1)-F(4)#2	132.1(5)	C(6)-C(5)-C(8)	118.6(4)
O(2)#2-Na(1)-F(4)#2	92.7(6)	C(5)-C(4)-C(3)	117.7(3)
O(2)#3-Na(1)-F(4)#2	87.7(6)	C(4)-C(3)-C(2)	120.7(3)
F(4)-Na(1)-F(4)#2	89.999(2)	C(4)-C(3)-C(7)	119.6(3)
F(4)#3-Na(1)-F(4)#2	179.43(16)	C(2)-C(3)-C(7)	119.6(3)
O(1)-Na(1)-F(4)#1	89.71(8)	C(3)-C(2)-C(1)	122.6(3)
O(2)-Na(1)-F(4)#1	87.7(6)	F(6)-C(8)-F(4)	106.2(4)
O(2)#1-Na(1)-F(4)#1	92.7(6)	F(6)-C(8)-F(5)	106.6(4)
O(2)#2-Na(1)-F(4)#1	48.4(5)	F(4)-C(8)-F(5)	107.0(3)
O(2)#3-Na(1)-F(4)#1	132.1(5)	F(6)-C(8)-C(5)	112.3(4)
F(4)-Na(1)-F(4)#1	179.43(16)	F(4)-C(8)-C(5)	113.0(4)
F(4)#3-Na(1)-F(4)#1	89.999(1)	F(5)-C(8)-C(5)	111.4(4)
F(4)#2-Na(1)-F(4)#1	89.999(1)	F(3)-C(7)-F(2)	108.8(5)
O(1)-Na(1)-F(4')	65.3(2)	F(3)-C(7)-F(1)	106.8(4)
O(2')-Na(1)-F(4')	114.7(2)	F(2)-C(7)-F(1)	107.0(5)
O(1)-Na(1)-F(4')#2	65.3(2)	F(3)-C(7)-C(3)	109.0(8)
O(2')-Na(1)-F(4')#2	114.7(2)	F(2)-C(7)-C(3)	113.4(6)
F(4')-Na(1)-F(4')#2	79.90(18)	F(1)-C(7)-C(3)	111.6(6)
C(1')#4-B(1)-C(1')#5	112.1(13)	C(8)-F(4)-Na(1)	135.8(2)
C(1')#4-B(1)-C(1')#6	104(2)	C(2')-C(1')-C(6')	115.5(5)
C(1')#5-B(1)-C(1')#6	112.1(13)	C(2')-C(1')-B(1)	122.3(8)
C(1')#4-B(1)-C(1')	112.1(13)	C(6')-C(1')-B(1)	122.1(9)
C(1')#5-B(1)-C(1')	104(2)	C(5')-C(6')-C(1')	122.3(6)
C(1')#6-B(1)-C(1')	112.1(13)	C(4')-C(5')-C(6')	120.8(5)
C(1)#4-B(1)-C(1)#5	110.3(3)	C(4')-C(5')-C(8')	120.6(7)
C(1)#4-B(1)-C(1)#6	107.8(7)	C(6')-C(5')-C(8')	117.6(7)
C(1)#5-B(1)-C(1)#6	110.3(3)	C(5')-C(4')-C(3')	118.5(5)
C(1)#4-B(1)-C(1)	110.3(3)	C(4')-C(3')-C(2')	120.3(6)
C(1)#5-B(1)-C(1)	107.8(7)	C(4')-C(3')-C(7')	121.2(6)
C(1)#6-B(1)-C(1)	110.3(3)	C(2')-C(3')-C(7')	118.2(6)
C(2)-C(1)-C(6)	115.4(3)	C(3')-C(2')-C(1')	122.5(5)
C(2)-C(1)-B(1)	125.8(3)	F(6')-C(8')-F(4')	108.2(8)
C(6)-C(1)-B(1)	118.8(3)	F(6')-C(8')-F(5')	100.7(8)

F(4')-C(8')-F(5')	102.1(8)	B(1)-C(1)-C(2)-C(3)	178.9(11)
F(6')-C(8')-C(5')	114.7(10)	C(4)-C(5)-C(8)-F(6)	-143.1(7)
F(4')-C(8')-C(5')	111.0(11)	C(6)-C(5)-C(8)-F(6)	40.5(9)
F(5')-C(8')-C(5')	118.9(14)	C(4)-C(5)-C(8)-F(4)	96.8(7)
F(1')-C(7')-F(2')	103.1(9)	C(6)-C(5)-C(8)-F(4)	-79.6(8)
F(1')-C(7')-F(3')	103.4(8)	C(4)-C(5)-C(8)-F(5)	-23.7(9)
F(2')-C(7')-F(3')	99.7(7)	C(6)-C(5)-C(8)-F(5)	159.9(7)
F(1')-C(7')-C(3')	117.8(11)	C(4)-C(3)-C(7)-F(3)	92.6(12)
F(2')-C(7')-C(3')	112.3(17)	C(2)-C(3)-C(7)-F(3)	-86.8(13)
F(3')-C(7')-C(3')	118.2(19)	C(4)-C(3)-C(7)-F(2)	-146.0(10)
C(8')-F(4')-Na(1)	126.6(7)	C(2)-C(3)-C(7)-F(2)	34.6(14)
		C(4)-C(3)-C(7)-F(1)	-25.1(14)
		C(2)-C(3)-C(7)-F(1)	155.5(11)
		F(6)-C(8)-F(4)-Na(1)	132.5(3)
		F(5)-C(8)-F(4)-Na(1)	19.0(6)
		C(5)-C(8)-F(4)-Na(1)	-103.9(4)
		C(1')#4-B(1)-C(1')-C(2')	-111(5)
		C(1')#5-B(1)-C(1')-C(2')	127(4)
		C(1')#6-B(1)-C(1')-C(2')	6(4)
		C(1')#4-B(1)-C(1')-C(6')	72(2)
		C(1')#5-B(1)-C(1')-C(6')	-50(3)
		C(1')#6-B(1)-C(1')-C(6')	-171(4)
		C(2')-C(1')-C(6')-C(5')	1(6)
		B(1)-C(1')-C(6')-C(5')	178(3)
		C(1')-C(6')-C(5')-C(4')	0(5)
		C(1')-C(6')-C(5')-C(8')	-169(3)
		C(6')-C(5')-C(4')-C(3')	0(5)
		C(8')-C(5')-C(4')-C(3')	169(3)
		C(5')-C(4')-C(3')-C(2')	-2(6)
		C(5')-C(4')-C(3')-C(7')	-176(3)
		C(4')-C(3')-C(2')-C(1')	4(7)
		C(7')-C(3')-C(2')-C(1')	178(4)
		C(6')-C(1')-C(2')-C(3')	-3(6)
		B(1)-C(1')-C(2')-C(3')	180(4)
		C(4')-C(5')-C(8')-F(6')	163(2)
		C(6')-C(5')-C(8')-F(6')	-28(3)

Symmetry transformations used to generate equivalent atoms:

#1 -x+1/2,-y+5/2,z #2 y-1,-x+3/2,z

#3 -y+3/2,x+1,z #4 y-1/2,-x+1,-z+1

#5 -x+1/2,-y+3/2,z #6 -y+1,x+1/2,-z+1

Table S6. Torsion angles [°] for NaBArF.

C(1)#4-B(1)-C(1)-C(2)	-108.6(15)
C(1)#5-B(1)-C(1)-C(2)	130.9(14)
C(1)#6-B(1)-C(1)-C(2)	10.4(12)
C(1)#4-B(1)-C(1)-C(6)	70.8(7)
C(1)#5-B(1)-C(1)-C(6)	-49.7(8)
C(1)#6-B(1)-C(1)-C(6)	-170.2(10)
C(2)-C(1)-C(6)-C(5)	1.5(17)
B(1)-C(1)-C(6)-C(5)	-178.0(9)
C(1)-C(6)-C(5)-C(4)	-1.5(15)
C(1)-C(6)-C(5)-C(8)	174.8(9)
C(6)-C(5)-C(4)-C(3)	0.5(14)
C(8)-C(5)-C(4)-C(3)	-175.8(9)
C(5)-C(4)-C(3)-C(2)	0.4(18)
C(5)-C(4)-C(3)-C(7)	-179.0(9)
C(4)-C(3)-C(2)-C(1)	0(2)
C(7)-C(3)-C(2)-C(1)	179.0(12)
C(6)-C(1)-C(2)-C(3)	-0.5(19)

C(4')-C(5')-C(8')-F(4')	40(3)
C(6')-C(5')-C(8')-F(4')	-151(2)
C(4')-C(5')-C(8')-F(5')	-78(3)
C(6')-C(5')-C(8')-F(5')	91(3)
C(4')-C(3')-C(7')-F(1')	-11(4)
C(2')-C(3')-C(7')-F(1')	175(3)
C(4')-C(3')-C(7')-F(2')	-130(3)
C(2')-C(3')-C(7')-F(2')	56(4)
C(4')-C(3')-C(7')-F(3')	114(3)
C(2')-C(3')-C(7')-F(3')	-59(4)
F(6')-C(8')-F(4')-Na(1)	-51.7(13)
F(5')-C(8')-F(4')-Na(1)	-157.4(7)
C(5')-C(8')-F(4')-Na(1)	74.9(14)

Symmetry transformations used to generate equivalent atoms:

#1 -x+1/2,-y+5/2,z #2 y-1,-x+3/2,z

#3 -y+3/2,x+1,z

#4 y-1/2,-x+1,-z+1 #5 -x+1/2,-y+3/2,

#6 -y+1,x+1/2,-z+1

Table S7. Crystal data and structure refinement for KBArF.

Identification code	KBArF	
Empirical formula	C32 H13 B F24 K O0.50	
Formula weight	911.33	
Temperature	100(2) K	
Wavelength	0.71073 Å	
Crystal system	Tetragonal	
Space group	P 4/n	
Unit cell dimensions	a = 13.5095(5) Å	α= 90°.
	b = 13.5095(5) Å	β= 90°.
	c = 9.2868(4) Å	γ = 90°.
Volume	1694.90(15) Å^3	
Z	2	
Density (calculated)	1.786 Mg/m^3	
Absorption coefficient	0.317 mm^{-1}	
F(000)	898	
Crystal size	0.300 x 0.300 x 0.200 mm^3	
Theta range for data collection	2.132 to 36.405°.	
Index ranges	-22<=h<=22, -21<=k<=22, -15<=l<=15	
Reflections collected	21387	
Independent reflections	4145 [R(int) = 0.0265]	
Completeness to theta =	25.242° 99.7 %	
Absorption correction	Empirical	
Refinement method	Full-matrix least-squares on F^2	
Data / restraints / parameters	4145 / 180 / 195	
Goodness-of-fit on F^2	1.112	
Final R indices [I>2sigma(I)]	R1 = 0.0541, wR2 = 0.1635	
R indices (all data)	R1 = 0.0607, wR2 = 0.1687	
Extinction coefficient	n/a	
Largest diff. peak and hole	1.162 and -0.657 e.Å^{-3}	

Table S8. Bond lengths [Å] and angles [°] for KBArF.

B(1)-C(1)#1	1.6382(10)	K(1)-F(3')#6	2.615(4)
B(1)-C(1)#2	1.6382(10)	K(1)-F(3')#7	2.615(4)
B(1)-C(1)#3	1.6382(10)	K(1)-F(6')#8	2.728(6)
B(1)-C(1)	1.6382(10)	K(1)-F(6')#9	2.728(6)
C(1)-C(6)	1.4002(14)	K(1)-F(6')#10	2.728(6)
C(1)-C(2)	1.4049(14)	K(1)-F(6)#8	2.792(2)
C(2)-C(3)	1.3920(15)	K(1)-F(6)#9	2.792(2)
C(3)-C(4)	1.3921(17)	K(1)-F(6)#10	2.792(2)
C(3)-C(7)	1.4926(17)		
C(4)-C(5)	1.3883(16)	C(1)#1-B(1)-C(1)#2	107.87(7)
C(5)-C(6)	1.3956(14)	C(1)#1-B(1)-C(1)#3	110.28(3)
C(5)-C(8)	1.4949(16)	C(1)#2-B(1)-C(1)#3	110.28(3)
C(7)-F(1')	1.260(5)	C(1)#1-B(1)-C(1)	110.27(3)
C(7)-F(2)	1.306(2)	C(1)#2-B(1)-C(1)	110.28(3)
C(7)-F(3)	1.3401(19)	C(1)#3-B(1)-C(1)	107.87(7)
C(7)-F(2')	1.348(5)	C(6)-C(1)-C(2)	115.97(9)
C(7)-F(1)	1.377(2)	C(6)-C(1)-B(1)	124.36(8)
C(7)-F(3')	1.398(4)	C(2)-C(1)-B(1)	119.67(8)
C(8)-F(5')	1.317(6)	C(3)-C(2)-C(1)	122.09(10)
C(8)-F(4')	1.329(5)	C(2)-C(3)-C(4)	121.04(10)
C(8)-F(5)	1.340(2)	C(2)-C(3)-C(7)	119.25(11)
C(8)-F(4)	1.346(2)	C(4)-C(3)-C(7)	119.63(10)
C(8)-F(6)	1.348(2)	C(5)-C(4)-C(3)	117.71(10)
C(8)-F(6')	1.388(6)	C(4)-C(5)-C(6)	121.20(10)
F(3)-K(1)#4	2.8733(18)	C(4)-C(5)-C(8)	118.94(10)
F(3')-K(1)#4	2.615(4)	C(6)-C(5)-C(8)	119.75(10)
F(6)-K(1)	2.792(2)	C(5)-C(6)-C(1)	121.97(9)
F(6')-K(1)	2.728(6)	F(2)-C(7)-F(3)	110.17(19)
K(1)-F(3')#4	2.615(4)	F(1')-C(7)-F(2')	109.1(5)
K(1)-F(3')#5	2.615(4)	F(2)-C(7)-F(1)	105.0(2)

F(3)-C(7)-F(1)	102.05(15)	F(3')#4-K(1)-F(6')	72.0(2)
F(1')-C(7)-F(3')	105.1(4)	F(3')#5-K(1)-F(6')	83.4(2)
F(2')-C(7)-F(3')	100.6(4)	F(3')#6-K(1)-F(6')	150.1(2)
F(1')-C(7)-C(3)	118.1(3)	F(3')#7-K(1)-F(6')	132.3(3)
F(2)-C(7)-C(3)	114.28(17)	F(3')#4-K(1)-F(6')#8	150.1(2)
F(3)-C(7)-C(3)	113.26(13)	F(3')#5-K(1)-F(6')#8	132.3(3)
F(2')-C(7)-C(3)	112.9(3)	F(3')#6-K(1)-F(6')#8	72.0(2)
F(1)-C(7)-C(3)	111.08(13)	F(3')#7-K(1)-F(6')#8	83.4(2)
F(3')-C(7)-C(3)	109.4(2)	F(6')-K(1)-F(6')#8	106.0(3)
F(5')-C(8)-F(4')	109.5(5)	F(3')#4-K(1)-F(6')#9	132.3(3)
F(5)-C(8)-F(4)	106.55(19)	F(3')#5-K(1)-F(6')#9	72.0(2)
F(5)-C(8)-F(6)	105.89(19)	F(3')#6-K(1)-F(6')#9	83.4(2)
F(4)-C(8)-F(6)	106.39(18)	F(3')#7-K(1)-F(6')#9	150.1(2)
F(5')-C(8)-F(6')	105.2(5)	F(6')-K(1)-F(6')#9	68.78(17)
F(4')-C(8)-F(6')	104.5(4)	F(6')#8-K(1)-F(6')#9	68.78(17)
F(5')-C(8)-C(5)	114.5(5)	F(3')#4-K(1)-F(6')#10	83.4(2)
F(4')-C(8)-C(5)	113.9(4)	F(3')#5-K(1)-F(6')#10	150.1(2)
F(5)-C(8)-C(5)	112.76(19)	F(3')#6-K(1)-F(6')#10	132.3(3)
F(4)-C(8)-C(5)	112.85(16)	F(3')#7-K(1)-F(6')#10	72.0(2)
F(6)-C(8)-C(5)	111.88(16)	F(6')-K(1)-F(6')#10	68.78(17)
F(6')-C(8)-C(5)	108.4(4)	F(6')#8-K(1)-F(6')#10	68.78(17)
C(7)-F(3)-K(1)#4	126.57(14)	F(6')#9-K(1)-F(6')#10	106.0(3)
C(7)-F(3')-K(1)#4	143.2(3)	F(6)-K(1)-F(6)#8	92.28(11)
C(8)-F(6)-K(1)	163.04(17)	F(6)-K(1)-F(6)#9	61.31(6)
C(8)-F(6')-K(1)	169.3(6)	F(6)#8-K(1)-F(6)#9	61.31(6)
F(3')#4-K(1)-F(3')#5	77.60(13)	F(6)-K(1)-F(6)#10	61.31(6)
F(3')#4-K(1)-F(3')#6	124.8(3)	F(6)#8-K(1)-F(6)#10	61.31(6)
F(3')#5-K(1)-F(3')#6	77.60(13)	F(6)#9-K(1)-F(6)#10	92.28(11)
F(3')#4-K(1)-F(3')#7	77.60(13)		
F(3')#5-K(1)-F(3')#7	124.8(3)		
F(3')#6-K(1)-F(3')#7	77.60(13)		

Symmetry transformations used to generate equivalent atoms:

#1 y-1/2,-x+1,-z+1 #2 -y+1,x+1/2,-z+1 #3 -x+1/2,-y+3/2,z #4 -x,-y+2,-z #5 y-1/2,-x+1,-z #6 x+1/2,y+1/2,-z #7 -y+1,x+3/2,-z #8 -x+1/2,-y+5/2,z #9 -y+3/2,x+1,z #10 y-1,-x+3/2,z

Table S9. Torsion angles [°] for KBArF.

C(1)#1-B(1)-C(1)-C(6)	-12.62(9)
C(1)#2-B(1)-C(1)-C(6)	106.41(11)
C(1)#3-B(1)-C(1)-C(6)	-133.10(10)
C(1)#1-B(1)-C(1)-C(2)	168.05(9)
C(1)#2-B(1)-C(1)-C(2)	-72.92(6)
C(1)#3-B(1)-C(1)-C(2)	47.57(7)
C(6)-C(1)-C(2)-C(3)	-1.49(15)
B(1)-C(1)-C(2)-C(3)	177.90(9)
C(1)-C(2)-C(3)-C(4)	0.40(17)
C(1)-C(2)-C(3)-C(7)	177.13(11)
C(2)-C(3)-C(4)-C(5)	0.69(17)
C(7)-C(3)-C(4)-C(5)	-176.03(12)
C(3)-C(4)-C(5)-C(6)	-0.64(17)
C(3)-C(4)-C(5)-C(8)	175.66(11)
C(4)-C(5)-C(6)-C(1)	-0.51(16)
C(8)-C(5)-C(6)-C(1)	-176.78(10)
C(2)-C(1)-C(6)-C(5)	1.54(15)
B(1)-C(1)-C(6)-C(5)	-177.82(8)
C(2)-C(3)-C(7)-F(1')	-111.2(4)
C(4)-C(3)-C(7)-F(1')	65.6(5)
C(2)-C(3)-C(7)-F(2)	37.7(2)
C(4)-C(3)-C(7)-F(2)	-145.6(2)
C(2)-C(3)-C(7)-F(3)	164.93(15)
C(4)-C(3)-C(7)-F(3)	-18.3(2)
C(2)-C(3)-C(7)-F(2')	17.7(4)
C(4)-C(3)-C(7)-F(2')	-165.5(4)
C(2)-C(3)-C(7)-F(1)	-80.91(17)
C(4)-C(3)-C(7)-F(1)	95.87(16)
C(2)-C(3)-C(7)-F(3')	128.7(3)
C(4)-C(3)-C(7)-F(3')	-54.5(4)
C(4)-C(5)-C(8)-F(5')	44.1(5)
C(6)-C(5)-C(8)-F(5')	-139.6(5)
C(4)-C(5)-C(8)-F(4')	171.2(4)
C(6)-C(5)-C(8)-F(4')	-12.5(4)
C(4)-C(5)-C(8)-F(5)	30.7(2)
C(6)-C(5)-C(8)-F(5)	-152.99(18)
C(4)-C(5)-C(8)-F(4)	151.47(15)
C(6)-C(5)-C(8)-F(4)	-32.18(18)
C(4)-C(5)-C(8)-F(6)	-88.58(17)
C(6)-C(5)-C(8)-F(6)	87.77(17)
C(4)-C(5)-C(8)-F(6')	-73.0(4)
C(6)-C(5)-C(8)-F(6')	103.3(4)
F(1')-C(7)-F(3)-K(1)#4	113.3(3)
F(2)-C(7)-F(3)-K(1)#4	-3.0(3)
F(2')-C(7)-F(3)-K(1)#4	10.6(5)
F(1)-C(7)-F(3)-K(1)#4	108.12(16)
F(3')-C(7)-F(3)-K(1)#4	-41.9(4)
C(3)-C(7)-F(3)-K(1)#4	-132.40(12)
F(1')-C(7)-F(3')-K(1)#4	55.3(8)
F(2)-C(7)-F(3')-K(1)#4	-63.6(7)
F(3)-C(7)-F(3')-K(1)#4	79.9(7)
F(2')-C(7)-F(3')-K(1)#4	-58.0(8)
F(1)-C(7)-F(3')-K(1)#4	40.2(9)
C(3)-C(7)-F(3')-K(1)#4	-177.0(6)
F(5')-C(8)-F(6)-K(1)	-25.8(9)

F(4')-C(8)-F(6)-K(1)	-137.4(7)
F(5)-C(8)-F(6)-K(1)	-16.4(7)
F(4)-C(8)-F(6)-K(1)	-129.5(6)
F(6')-C(8)-F(6)-K(1)	27.5(15)
C(5)-C(8)-F(6)-K(1)	106.8(6)
F(5')-C(8)-F(6')-K(1)	83(3)
F(4')-C(8)-F(6')-K(1)	-32(3)
F(5)-C(8)-F(6')-K(1)	90(3)
F(4)-C(8)-F(6')-K(1)	-22(3)
F(6)-C(8)-F(6')-K(1)	-47.7(19)
C(5)-C(8)-F(6')-K(1)	-154(3)

Symmetry transformations used to generate equivalent atoms:

#1 y-1/2,-x+1,-z+1 #2 -y+1,x+1/2,-z+1

#3 -x+1/2,-y+3/2,z #4 -x,-y+2,-z #5 y-1/2,-x+1,-z

#6 x+1/2,y+1/2,-z #7 -y+1,x+3/2,-z #8 -x+1/2,-y+5/2,z #9 -y+3/2,x+1,z #10 y-1,-x+3/2,z

Table S10. Crystal data and structure refinement for RbBArF.

Identification code	RbBArF	
Empirical formula	C32 H14 B F24 O Rb	
Formula weight	966.71	
Temperature	100(2) K	
Wavelength	0.71073 Å	
Crystal system	Tetragonal	
Space group	P 4/n	
Unit cell dimensions	a = 13.5956(17) Å	α= 90°.
	b = 13.5956(17) Å	β= 90°.
	c = 9.2978(18) Å	γ = 90°.
Volume	1718.6(5) Å^3	
Z	2	
Density (calculated)	1.868 Mg/m^3	
Absorption coefficient	1.600 mm^{-1}	
F(000)	944	
Crystal size	0.200 x 0.200 x 0.200 mm^3	
Theta range for data collection	2.190 to 32.723°.	
Index ranges	-20<=h<=12, -19<=k<=12, -13<=l<=12	
Reflections collected	6734	
Independent reflections	3049 [R(int) = 0.0348]	
Completeness to theta =	25.000° 97.8 %	
Absorption correction	Empirical	
Max. and min. transmission	0.740 and 0.560	
Refinement method	Full-matrix least-squares on F^2	
Data / restraints / parameters	3049 / 85 / 157	
Goodness-of-fit on F^2	1.051	
Final R indices [I>2sigma(I)]	R1 = 0.0560, wR2 = 0.1438	
R indices (all data)	R1 = 0.0776, wR2 = 0.1533	
Extinction coefficient	n/a	
Largest diff. peak and hole	0.864 and -0.534 e.Å^{-3}	

Table S11. Bond lengths [Å] and angles [°] for RbBArF.

Rb(1)-F(6)	2.9295(18)	C(8)-F(5)	1.332(3)
Rb(1)-F(6)#1	2.9295(18)	C(8)-F(4)	1.343(3)
Rb(1)-F(6)#2	2.9295(18)	C(8)-F(6)	1.347(3)
Rb(1)-F(6)#3	2.9295(18)	F(2)-Rb(1)#5	2.996(2)
Rb(1)-O(1W)	2.939(2)	F(3)-Rb(1)#5	3.577(4)
Rb(1)-O(1W')	2.946(2)	F(1')-Rb(1)#5	3.16(3)
Rb(1)-F(2)#4	2.996(2)	F(2')-Rb(1)#5	3.05(2)
Rb(1)-F(2)#5	2.996(2)		
Rb(1)-F(2)#6	2.996(2)	F(6)-Rb(1)-F(6)#1	59.25(5)
Rb(1)-F(2)#7	2.996(2)	F(6)-Rb(1)-F(6)#2	59.25(5)
Rb(1)-F(2')#6	3.05(3)	F(6)#1-Rb(1)-F(6)#2	88.71(9)
Rb(1)-F(2')#4	3.05(3)	F(6)-Rb(1)-F(6)#3	88.71(9)
B(1)-C(1)	1.642(2)	F(6)#1-Rb(1)-F(6)#3	59.25(5)
B(1)-C(1)#8	1.642(2)	F(6)#2-Rb(1)-F(6)#3	59.25(5)
B(1)-C(1)#9	1.642(2)	F(6)-Rb(1)-O(1W)	130.84(7)
B(1)-C(1)#10	1.642(2)	F(6)#1-Rb(1)-O(1W)	133.70(6)
C(1)-C(2)	1.402(3)	F(6)#2-Rb(1)-O(1W)	137.19(5)
C(1)-C(6)	1.403(3)	F(6)#3-Rb(1)-O(1W)	140.40(3)
C(2)-C(3)	1.392(3)	F(6)-Rb(1)-O(1W')	152.98(8)
C(3)-C(4)	1.385(4)	F(6)#1-Rb(1)-O(1W')	136.05(6)
C(3)-C(7)	1.494(4)	F(6)#2-Rb(1)-O(1W')	129.92(6)
C(4)-C(5)	1.384(3)	F(6)#3-Rb(1)-O(1W')	118.09(2)
C(5)-C(6)	1.396(3)	F(6)-Rb(1)-F(2)#4	136.85(7)
C(5)-C(8)	1.498(3)	F(6)#1-Rb(1)-F(2)#4	116.08(6)
C(7)-F(3)	1.305(4)	F(6)#2-Rb(1)-F(2)#4	78.40(6)
C(7)-F(2)	1.339(4)	F(6)#3-Rb(1)-F(2)#4	60.59(7)
C(7)-F(1)	1.361(4)	O(1W)-Rb(1)-F(2)#4	85.45(7)
C(7)-F(3')	1.366(10)	F(6)-Rb(1)-F(2)#5	60.59(7)
C(7)-F(1')	1.377(9)	F(6)#1-Rb(1)-F(2)#5	78.40(6)
C(7)-F(2')	1.432(9)	F(6)#2-Rb(1)-F(2)#5	116.08(6)

F(6)#3-Rb(1)-F(2)#5	136.85(7)	C(1)#8-B(1)-C(1)#9	108.05(15)
O(1W)-Rb(1)-F(2)#5	75.35(6)	C(1)-B(1)-C(1)#10	108.05(15)
F(2)#4-Rb(1)-F(2)#5	160.80(11)	C(1)#8-B(1)-C(1)#10	110.19(8)
F(6)-Rb(1)-F(2)#6	116.08(6)	C(1)#9-B(1)-C(1)#10	110.19(8)
F(6)#1-Rb(1)-F(2)#6	60.59(7)	C(2)-C(1)-C(6)	115.9(2)
F(6)#2-Rb(1)-F(2)#6	136.85(7)	C(2)-C(1)-B(1)	119.93(17)
F(6)#3-Rb(1)-F(2)#6	78.40(6)	C(6)-C(1)-B(1)	124.17(17)
O(1W)-Rb(1)-F(2)#6	81.10(7)	C(3)-C(2)-C(1)	122.1(2)
F(2)#4-Rb(1)-F(2)#6	88.406(18)	C(4)-C(3)-C(2)	121.2(2)
F(2)#5-Rb(1)-F(2)#6	88.406(18)	C(4)-C(3)-C(7)	119.6(2)
F(6)-Rb(1)-F(2)#7	78.40(6)	C(2)-C(3)-C(7)	119.2(2)
F(6)#1-Rb(1)-F(2)#7	136.85(7)	C(5)-C(4)-C(3)	117.9(2)
F(6)#2-Rb(1)-F(2)#7	60.59(7)	C(4)-C(5)-C(6)	121.2(2)
F(6)#3-Rb(1)-F(2)#7	116.08(6)	C(4)-C(5)-C(8)	119.2(2)
O(1W)-Rb(1)-F(2)#7	79.77(6)	C(6)-C(5)-C(8)	119.6(2)
F(2)#4-Rb(1)-F(2)#7	88.406(18)	C(5)-C(6)-C(1)	121.8(2)
F(2)#5-Rb(1)-F(2)#7	88.406(18)	F(3)-C(7)-F(2)	109.7(3)
F(2)#6-Rb(1)-F(2)#7	160.80(11)	F(3)-C(7)-F(1)	104.1(3)
F(6)-Rb(1)-F(2')#6	149.6(4)	F(2)-C(7)-F(1)	102.8(3)
F(6)#1-Rb(1)-F(2')#6	92.9(3)	F(3')-C(7)-F(1')	101.0(12)
F(6)#2-Rb(1)-F(2')#6	138.7(5)	F(3')-C(7)-F(2')	99.7(12)
F(6)#3-Rb(1)-F(2')#6	86.6(4)	F(1')-C(7)-F(2')	96.0(11)
O(1W')-Rb(1)-F(2')#6	45.2(3)	F(3)-C(7)-C(3)	112.9(3)
F(6)-Rb(1)-F(2')#4	138.7(5)	F(1)-C(7)-C(3)	112.1(3)
F(6)#1-Rb(1)-F(2')#4	149.6(4)	F(3')-C(7)-C(3)	120.7(12)
F(6)#2-Rb(1)-F(2')#4	86.6(4)	F(1')-C(7)-C(3)	132.6(13)
F(6)#3-Rb(1)-F(2')#4	92.9(3)	F(2')-C(7)-C(3)	97.9(11)
O(1W')-Rb(1)-F(2')#4	43.8(4)	F(5)-C(8)-F(4)	106.4(2)
F(2')#6-Rb(1)-F(2')#4	71.7(3)	F(5)-C(8)-F(6)	105.6(2)
C(1)-B(1)-C(1)#8	110.19(8)	F(4)-C(8)-F(6)	106.3(2)
C(1)-B(1)-C(1)#9	110.19(8)	F(5)-C(8)-C(5)	113.3(2)

F(4)-C(8)-C(5)	113.4(2)
F(6)-C(8)-C(5)	111.2(2)
C(7)-F(2)-Rb(1)#5	120.8(2)
C(7)-F(3)-Rb(1)#5	92.3(2)
C(7)-F(1')-Rb(1)#5	110.2(13)
C(7)-F(2')-Rb(1)#5	113.7(13)
C(8)-F(6)-Rb(1)	164.44(17)

Symmetry transformations used to generate equivalent atoms:

#1 -y+1/2,x+1,z #2 y-1,-x+1/2,z #3 -x-1/2,-y+3/2,z #4 x-1/2,y-1/2,-z+1 #5 -x,-y+2,-z+1 #6 y-3/2,-x+1,-z+1 #7 -y+1,x+1/2,-z+1 #8 y-1/2,-x+1,-z+2 #9 -y+1,x+1/2,-z+2 #10 -x+1/2,-y+3/2,z

Table S12. Torsion angles [°] for RbBArF

C(1)#8-B(1)-C(1)-C(2)	73.69(13)
C(1)#9-B(1)-C(1)-C(2)	-167.18(19)
C(1)#10-B(1)-C(1)-C(2)	-46.74(16)
C(1)#8-B(1)-C(1)-C(6)	-104.5(3)
C(1)#9-B(1)-C(1)-C(6)	14.7(2)
C(1)#10-B(1)-C(1)-C(6)	135.1(2)
C(6)-C(1)-C(2)-C(3)	0.8(3)
B(1)-C(1)-C(2)-C(3)	-177.46(19)
C(1)-C(2)-C(3)-C(4)	0.2(4)
C(1)-C(2)-C(3)-C(7)	-177.0(3)
C(2)-C(3)-C(4)-C(5)	-1.0(4)
C(7)-C(3)-C(4)-C(5)	176.1(3)
C(3)-C(4)-C(5)-C(6)	0.9(4)
C(3)-C(4)-C(5)-C(8)	-175.8(2)
C(4)-C(5)-C(6)-C(1)	0.2(4)
C(8)-C(5)-C(6)-C(1)	176.8(2)
C(2)-C(1)-C(6)-C(5)	-1.0(3)
B(1)-C(1)-C(6)-C(5)	177.22(18)
C(4)-C(3)-C(7)-F(3)	140.6(3)
C(2)-C(3)-C(7)-F(3)	-42.2(4)
C(4)-C(3)-C(7)-F(2)	14.3(4)
C(2)-C(3)-C(7)-F(2)	-168.5(3)
C(4)-C(3)-C(7)-F(1)	-101.2(3)
C(2)-C(3)-C(7)-F(1)	76.0(3)
C(4)-C(3)-C(7)-F(3')	-158.9(15)
C(2)-C(3)-C(7)-F(3')	18.3(15)
C(4)-C(3)-C(7)-F(1')	-10.8(16)
C(2)-C(3)-C(7)-F(1')	166.4(15)
C(4)-C(3)-C(7)-F(2')	94.6(12)
C(2)-C(3)-C(7)-F(2')	-88.2(12)
C(4)-C(5)-C(8)-F(5)	-33.0(3)
C(6)-C(5)-C(8)-F(5)	150.3(2)
C(4)-C(5)-C(8)-F(4)	-154.6(2)
C(6)-C(5)-C(8)-F(4)	28.8(3)
C(4)-C(5)-C(8)-F(6)	85.7(3)
C(6)-C(5)-C(8)-F(6)	-91.0(3)
F(3)-C(7)-F(2)-Rb(1)#5	-0.3(4)
F(1)-C(7)-F(2)-Rb(1)#5	-110.7(2)
F(3')-C(7)-F(2)-Rb(1)#5	-58.9(16)
F(1')-C(7)-F(2)-Rb(1)#5	-93(3)
F(2')-C(7)-F(2)-Rb(1)#5	34.9(13)
C(3)-C(7)-F(2)-Rb(1)#5	128.3(2)
F(2)-C(7)-F(3)-Rb(1)#5	0.2(3)
F(1)-C(7)-F(3)-Rb(1)#5	109.7(2)
F(3')-C(7)-F(3)-Rb(1)#5	120.8(15)

F(1')-C(7)-F(3)-Rb(1)#5	30.3(12)
F(2')-C(7)-F(3)-Rb(1)#5	-50.4(17)
C(3)-C(7)-F(3)-Rb(1)#5	-127.7(2)
F(3)-C(7)-F(1')-Rb(1)#5	-37.4(14)
F(2)-C(7)-F(1')-Rb(1)#5	59.9(19)
F(1)-C(7)-F(1')-Rb(1)#5	-137.9(13)
F(3')-C(7)-F(1')-Rb(1)#5	-92.5(16)
F(2')-C(7)-F(1')-Rb(1)#5	9.0(17)
C(3)-C(7)-F(1')-Rb(1)#5	115.1(12)
F(3)-C(7)-F(2')-Rb(1)#5	100.2(19)
F(2)-C(7)-F(2')-Rb(1)#5	-31.8(10)
F(1)-C(7)-F(2')-Rb(1)#5	64(3)
F(3')-C(7)-F(2')-Rb(1)#5	93.0(16)
F(1')-C(7)-F(2')-Rb(1)#5	-9.6(18)
C(3)-C(7)-F(2')-Rb(1)#5	-143.7(11)
F(5)-C(8)-F(6)-Rb(1)	23.7(7)
F(4)-C(8)-F(6)-Rb(1)	136.5(6)
C(5)-C(8)-F(6)-Rb(1)	-99.6(6)
F(6)#1-Rb(1)-F(6)-C(8)	-81.1(7)
F(6)#2-Rb(1)-F(6)-C(8)	170.0(6)
F(6)#3-Rb(1)-F(6)-C(8)	-135.6(6)
O(1W)-Rb(1)-F(6)-C(8)	42.1(7)
O(1W)#3-Rb(1)-F(6)-C(8)	47.2(6)
O(1W)#2-Rb(1)-F(6)-C(8)	51.1(7)
O(1W)#1-Rb(1)-F(6)-C(8)	37.4(6)
O(1W')#2-Rb(1)-F(6)-C(8)	18.8(7)
O(1W')#1-Rb(1)-F(6)-C(8)	67.5(6)
O(1W')#3-Rb(1)-F(6)-C(8)	40.8(6)
O(1W')-Rb(1)-F(6)-C(8)	51.5(7)

Symmetry transformations used to generate equivalent atoms:

#1 -y+1/2,x+1,z #2 y-1,-x+1/2,z #3 -x-1/2,-y+3/2,z #4 x-1/2,y-1/2,-z+1 #5 -x,-y+2,-z+1 #6 y-3/2,-x+1,-z+1 #7 -y+1,x+1/2,-z+1 #8 y-1/2,-x+1,-z+2 #9 -y+1,x+1/2,-z+2 #10 -x+1/2,-y+3/2,z

Table S13. Crystal data and structure refinement for CsBArF.

Identification code	CsBArF	
Empirical formula	C33 H14 B Cl2 Cs F24	
Formula weight	1081.06	
Temperature	100(2) K	
Wavelength	0.71073 Å	
Crystal system	Tetragonal	
Space group	P4/ncc	
Unit cell dimensions	a = 13.7562(4) Å	α= 90°.
	b = 13.7562(4) Å	β= 90°.
	c = 19.0303(7) Å	γ = 90°.
Volume	3601.2(2) Å^3	
Z	4	
Density (calculated)	1.994 Mg/m^3	
Absorption coefficient	1.329 mm^{-1}	
F(000)	2088	
Crystal size	0.300 x 0.200 x 0.050 mm^3	
Theta range for data collection	2.094 to 30.176°.	
Index ranges	-10<=h<=18, -12<=k<=19, -26<=l<=13	
Reflections collected	9316	
Independent reflections	2386 [R(int) = 0.0254]	
Completeness to theta =	25.242° 99.5 %	
Absorption correction	Empirical	
Refinement method	Full-matrix least-squares on F^2	
Data / restraints / parameters	2386 / 362 / 296	
Goodness-of-fit on F^2	1.134	
Final R indices [I>2sigma(I)]	R1 = 0.0421, wR2 = 0.1263	
R indices (all data)	R1 = 0.0558, wR2 = 0.1354	
Extinction coefficient	n/a	
Largest diff. peak and hole	0.957 and -1.188 e.Å^{-3}	

Table S14. Bond lengths [Å] and angles [°] for CsBArF.

Cs(1)-F(6')#1	3.042(10)	C(7)-F(3)	1.348(7)
Cs(1)-F(6')#2	3.042(10)	C(8)-F(6)	1.334(8)
Cs(1)-F(6')#3	3.042(10)	C(8)-F(4)	1.340(7)
Cs(1)-F(6')	3.042(10)	C(8)-F(5)	1.363(7)
Cs(1)-F(2)#4	3.060(11)	F(2)-Cs(1)#11	3.060(11)
Cs(1)-F(2)#5	3.060(11)	C(1')-C(6')	1.397(6)
Cs(1)-F(2)#6	3.060(11)	C(1')-C(2')	1.399(6)
Cs(1)-F(2)#7	3.060(11)	C(2')-C(3')	1.396(6)
Cs(1)-F(3')#4	3.060(19)	C(3')-C(4')	1.390(6)
Cs(1)-F(3')#5	3.060(19)	C(3')-C(7')	1.486(7)
Cs(1)-F(3')#6	3.060(19)	C(4')-C(5')	1.385(8)
Cs(1)-F(3')#7	3.060(19)	C(5')-C(6')	1.393(6)
B(1)-C(1)#8	1.642(6)	C(5')-C(8')	1.501(6)
B(1)-C(1)#9	1.642(6)	C(7')-F(2')	1.281(8)
B(1)-C(1)#10	1.642(6)	C(7')-F(1")	1.341(9)
B(1)-C(1)	1.642(6)	C(7')-F(3")	1.342(10)
B(1)-C(1')	1.645(7)	C(7')-F(3')	1.348(9)
B(1)-C(1')#8	1.645(7)	C(7')-F(1')	1.370(8)
B(1)-C(1')#9	1.645(7)	C(7')-F(2")	1.403(9)
B(1)-C(1')#10	1.645(7)	C(7')-Cs(1)#11	3.826(8)
C(1)-C(6)	1.397(6)	C(8')-F(5')	1.328(8)
C(1)-C(2)	1.399(6)	C(8')-F(4')	1.329(8)
C(2)-C(3)	1.397(6)	C(8')-F(6')	1.341(8)
C(3)-C(4)	1.390(6)	F(1')-F(1")	0.795(15)
C(3)-C(7)	1.487(7)	F(2')-F(2")	0.618(12)
C(4)-C(5)	1.386(8)	F(2')-F(1")	1.610(13)
C(5)-C(6)	1.394(5)	F(2')-Cs(1)#11	3.480(11)
C(5)-C(8)	1.502(6)	F(3')-Cs(1)#11	3.060(19)
C(7)-F(1)	1.343(7)	F(2")-Cs(1)#11	3.221(13)
C(7)-F(2)	1.346(7)	F(3")-Cs(1)#11	3.12(3)

C(1S)-Cl(1S)	1.723(8)	F(6')-Cs(1)-F(3')#6	62.4(4)
C(1S)-Cl(1S)#1	1.723(8)	F(3')#4-Cs(1)-F(3')#6	85.99(15)
C(1S)-Cl(1S)#3	1.723(8)	F(3')#5-Cs(1)-F(3')#6	85.99(15)
C(1S)-Cl(1S)#2	1.723(8)	F(6')#1-Cs(1)-F(3')#7	92.5(4)
Cl(1S)-Cl(1S)#1	2.053(5)	F(6')#2-Cs(1)-F(3')#7	62.4(4)
Cl(1S)-Cl(1S)#3	2.053(5)	F(6')#3-Cs(1)-F(3')#7	109.7(3)
		F(6')-Cs(1)-F(3')#7	147.5(4)
F(6')#1-Cs(1)-F(6')#2	58.8(3)	F(3')#4-Cs(1)-F(3')#7	85.99(15)
F(6')#1-Cs(1)-F(6')#3	88.0(5)	F(3')#5-Cs(1)-F(3')#7	85.99(15)
F(6')#2-Cs(1)-F(6')#3	58.8(3)	F(3')#6-Cs(1)-F(3')#7	149.3(6)
F(6')#1-Cs(1)-F(6')	58.8(3)	C(1)#8-B(1)-C(1)#9	112.5(3)
F(6')#2-Cs(1)-F(6')	88.0(5)	C(1)#8-B(1)-C(1)#10	112.5(3)
F(6')#3-Cs(1)-F(6')	58.8(3)	C(1)#9-B(1)-C(1)#10	103.6(7)
F(2)#4-Cs(1)-F(2)#5	156.6(3)	C(1)#8-B(1)-C(1)	103.6(7)
F(2)#4-Cs(1)-F(2)#6	87.63(6)	C(1)#9-B(1)-C(1)	112.5(3)
F(2)#5-Cs(1)-F(2)#6	87.63(6)	C(1)#10-B(1)-C(1)	112.5(3)
F(2)#4-Cs(1)-F(2)#7	87.63(6)	C(1')-B(1)-C(1')#8	109.1(7)
F(2)#5-Cs(1)-F(2)#7	87.63(6)	C(1')-B(1)-C(1')#9	109.7(3)
F(2)#6-Cs(1)-F(2)#7	156.6(3)	C(1')#8-B(1)-C(1')#9	109.7(3)
F(6')#1-Cs(1)-F(3')#4	147.5(4)	C(1')-B(1)-C(1')#10	109.7(3)
F(6')#2-Cs(1)-F(3')#4	92.5(4)	C(1')#8-B(1)-C(1')#10	109.7(3)
F(6')#3-Cs(1)-F(3')#4	62.4(4)	C(1')#9-B(1)-C(1')#10	109.1(7)
F(6')-Cs(1)-F(3')#4	109.7(3)	C(6)-C(1)-C(2)	115.9(5)
F(6')#1-Cs(1)-F(3')#5	62.4(4)	C(6)-C(1)-B(1)	124.1(5)
F(6')#2-Cs(1)-F(3')#5	109.7(3)	C(2)-C(1)-B(1)	119.8(5)
F(6')#3-Cs(1)-F(3')#5	147.5(4)	C(3)-C(2)-C(1)	122.1(5)
F(6')-Cs(1)-F(3')#5	92.5(4)	C(4)-C(3)-C(2)	120.7(5)
F(3')#4-Cs(1)-F(3')#5	149.3(6)	C(4)-C(3)-C(7)	120.2(5)
F(6')#1-Cs(1)-F(3')#6	109.7(3)	C(2)-C(3)-C(7)	119.0(5)
F(6')#2-Cs(1)-F(3')#6	147.5(4)	C(5)-C(4)-C(3)	118.1(5)
F(6')#3-Cs(1)-F(3')#6	92.5(4)	C(4)-C(5)-C(6)	120.7(6)

C(4)-C(5)-C(8)	120.4(6)	F(2')-C(7')-F(3")	112.9(13)
C(6)-C(5)-C(8)	118.5(4)	F(1")-C(7')-F(3")	106.6(10)
C(5)-C(6)-C(1)	122.3(5)	F(2')-C(7')-F(3')	110.5(9)
F(1)-C(7)-F(2)	105.8(6)	F(1")-C(7')-F(3')	125.8(10)
F(1)-C(7)-F(3)	104.5(6)	F(3")-C(7')-F(3')	19.8(12)
F(2)-C(7)-F(3)	106.7(7)	F(2')-C(7')-F(1')	108.4(7)
F(1)-C(7)-C(3)	113.5(6)	F(1")-C(7')-F(1')	34.1(7)
F(2)-C(7)-C(3)	112.2(8)	F(3")-C(7')-F(1')	85.0(10)
F(3)-C(7)-C(3)	113.4(6)	F(3')-C(7')-F(1')	104.1(8)
F(6)-C(8)-F(4)	106.3(7)	F(2')-C(7')-F(2")	26.1(5)
F(6)-C(8)-F(5)	104.6(7)	F(1")-C(7')-F(2")	101.7(7)
F(4)-C(8)-F(5)	105.2(6)	F(3")-C(7')-F(2")	102.8(9)
F(6)-C(8)-C(5)	114.4(19)	F(3')-C(7')-F(2")	93.0(9)
F(4)-C(8)-C(5)	113.7(7)	F(1')-C(7')-F(2")	133.2(8)
F(5)-C(8)-C(5)	111.8(15)	F(2')-C(7')-C(3')	117.7(8)
C(7)-F(2)-Cs(1)#11	135.2(7)	F(1")-C(7')-C(3')	115.2(9)
C(8)-F(4)-Cs(1)	99.9(5)	F(3")-C(7')-C(3')	120.0(15)
C(8)-F(5)-Cs(1)	118.3(5)	F(3')-C(7')-C(3')	108.5(10)
C(6')-C(1')-C(2')	115.8(5)	F(1')-C(7')-C(3')	106.7(8)
C(6')-C(1')-B(1)	126.1(6)	F(2")-C(7')-C(3')	108.4(8)
C(2')-C(1')-B(1)	118.1(6)	F(2')-C(7')-Cs(1)#11	64.8(6)
C(3')-C(2')-C(1')	122.2(5)	F(1")-C(7')-Cs(1)#11	104.4(7)
C(4')-C(3')-C(2')	120.7(5)	F(3")-C(7')-Cs(1)#11	49.3(10)
C(4')-C(3')-C(7')	120.0(5)	F(3')-C(7')-Cs(1)#11	46.6(8)
C(2')-C(3')-C(7')	119.3(5)	F(1')-C(7')-Cs(1)#11	109.9(6)
C(5')-C(4')-C(3')	117.9(5)	F(2")-C(7')-Cs(1)#11	54.5(6)
C(4')-C(5')-C(6')	120.8(6)	C(3')-C(7')-Cs(1)#11	139.8(5)
C(4')-C(5')-C(8')	119.9(6)	F(5')-C(8')-F(4')	108.2(8)
C(6')-C(5')-C(8')	119.0(5)	F(5')-C(8')-F(6')	106.5(7)
C(5')-C(6')-C(1')	122.3(5)	F(4')-C(8')-F(6')	107.2(8)
F(2')-C(7')-F(1")	75.7(7)	F(5')-C(8')-C(5')	111.6(19)

F(4')-C(8')-C(5')	112.5(9)
F(6')-C(8')-C(5')	111(2)
F(1")-F(1')-C(7')	71.0(8)
F(2")-F(2')-C(7')	88.1(11)
F(2")-F(2')-F(1")	141.5(13)
C(7')-F(2')-F(1")	53.9(5)
F(2")-F(2')-Cs(1)#11	60.5(17)
C(7')-F(2')-Cs(1)#11	95.7(6)
F(1")-F(2')-Cs(1)#11	112.5(7)
C(7')-F(3')-Cs(1)#11	114.8(9)
F(1')-F(1")-C(7')	74.9(9)
F(1')-F(1")-F(2')	123.1(10)
C(7')-F(1")-F(2')	50.4(4)
F(2')-F(2")-C(7')	65.8(10)
F(2')-F(2")-Cs(1)#11	109.9(19)
C(7')-F(2")-Cs(1)#11	104.7(6)
C(7')-F(3")-Cs(1)#11	111.6(12)
C(8')-F(6')-Cs(1)	140.3(6)
Cl(1S)-C(1S)-Cl(1S)#1	73.1(4)
Cl(1S)-C(1S)-Cl(1S)#3	73.1(4)
Cl(1S)#1-C(1S)-Cl(1S)#3	114.8(8)
Cl(1S)-C(1S)-Cl(1S)#2	114.8(8)
Cl(1S)#1-C(1S)-Cl(1S)#2	73.1(4)
Cl(1S)#3-C(1S)-Cl(1S)#2	73.1(4)
C(1S)-Cl(1S)-Cl(1S)#1	53.43(19)
C(1S)-Cl(1S)-Cl(1S)#3	53.43(19)
Cl(1S)#1-Cl(1S)-Cl(1S)#3	90.000(1)
C(1S)-Cl(1S)-Cs(1)	100.2(4)
Cl(1S)#1-Cl(1S)-Cs(1)	74.37(3)
Cl(1S)#3-Cl(1S)-Cs(1)	74.37(3)

Symmetry transformations used to generate equivalent atoms:

#1 -y+3/2,x+1,z #2 -x+1/2,-y+5/2,z #3 y-1,-x+3/2,z #4 x-1/2,-y+2,-z+1/2 #5 -x+1,y+1/2,-z+1/2 #6 y-1/2,x+1/2,-z+1/2 #7 -y+1,-x+2,-z+1/2 #8 -x+1/2,-y+3/2,z #9 -y+1,x+1/2,-z+1 #10 y-1/2,-x+1,-z+1 #11 -x+1,y-1/2,-z+1/2

Table S15. Torsion angles [°] for CsBArF

C(1)#8-B(1)-C(1)-C(6)	128(3)
C(1)#9-B(1)-C(1)-C(6)	7(3)
C(1)#10-B(1)-C(1)-C(6)	-110(3)
C(1)#8-B(1)-C(1)-C(2)	-47.4(8)
C(1)#9-B(1)-C(1)-C(2)	-169.2(10)
C(1)#10-B(1)-C(1)-C(2)	74.3(8)
C(6)-C(1)-C(2)-C(3)	2(3)
B(1)-C(1)-C(2)-C(3)	178.1(9)
C(1)-C(2)-C(3)-C(4)	-0.7(17)
C(1)-C(2)-C(3)-C(7)	-175.4(11)
C(2)-C(3)-C(4)-C(5)	1(3)
C(7)-C(3)-C(4)-C(5)	176(2)
C(3)-C(4)-C(5)-C(6)	-3(5)
C(3)-C(4)-C(5)-C(8)	-175(2)
C(4)-C(5)-C(6)-C(1)	5(6)
C(8)-C(5)-C(6)-C(1)	177(4)
C(2)-C(1)-C(6)-C(5)	-4(5)
B(1)-C(1)-C(6)-C(5)	180(3)
C(4)-C(3)-C(7)-F(1)	-97.3(9)
C(2)-C(3)-C(7)-F(1)	77.5(10)
C(4)-C(3)-C(7)-F(2)	22.6(11)
C(2)-C(3)-C(7)-F(2)	-162.6(9)

C(4)-C(3)-C(7)-F(3)	143.6(9)	C(4')-C(5')-C(6')-C(1')	-5(8)
C(2)-C(3)-C(7)-F(3)	-41.6(12)	C(8')-C(5')-C(6')-C(1')	-178(4)
C(4)-C(5)-C(8)-F(6)	-118(3)	C(2')-C(1')-C(6')-C(5')	1(6)
C(6)-C(5)-C(8)-F(6)	70(4)	B(1)-C(1')-C(6')-C(5')	-178(4)
C(4)-C(5)-C(8)-F(4)	5(4)	C(4')-C(3')-C(7')-F(2')	118.9(11)
C(6)-C(5)-C(8)-F(4)	-167(3)	C(2')-C(3')-C(7')-F(2')	-59.5(14)
C(4)-C(5)-C(8)-F(5)	124(3)	C(4')-C(3')-C(7')-F(1'')	-154.6(12)
C(6)-C(5)-C(8)-F(5)	-48(4)	C(2')-C(3')-C(7')-F(1'')	27.0(15)
F(1)-C(7)-F(2)-Cs(1)#11	-113.5(7)	C(4')-C(3')-C(7')-F(3'')	-25.2(16)
F(3)-C(7)-F(2)-Cs(1)#11	-2.5(11)	C(2')-C(3')-C(7')-F(3'')	156.4(13)
C(3)-C(7)-F(2)-Cs(1)#11	122.2(9)	C(4')-C(3')-C(7')-F(3')	-7.5(14)
F(6)-C(8)-F(4)-Cs(1)	-119.6(8)	C(2')-C(3')-C(7')-F(3')	174.1(12)
F(5)-C(8)-F(4)-Cs(1)	-9.1(8)	C(4')-C(3')-C(7')-F(1')	-119.1(11)
C(5)-C(8)-F(4)-Cs(1)	114(2)	C(2')-C(3')-C(7')-F(1')	62.5(13)
F(6)-C(8)-F(5)-Cs(1)	123.1(9)	C(4')-C(3')-C(7')-F(2'')	92.3(12)
F(4)-C(8)-F(5)-Cs(1)	11.3(10)	C(2')-C(3')-C(7')-F(2'')	-86.1(12)
C(5)-C(8)-F(5)-Cs(1)	-112.5(14)	C(4')-C(3')-C(7')-Cs(1)#11	35.9(15)
C(1')#8-B(1)-C(1')-C(6')	125(3)	C(2')-C(3')-C(7')-Cs(1)#11	-142.5(9)
C(1')#9-B(1)-C(1')-C(6')	5(3)	C(4')-C(5')-C(8')-F(5')	-124(3)
C(1')#10-B(1)-C(1')-C(6')	-114(3)	C(6')-C(5')-C(8')-F(5')	49(5)
C(1')#8-B(1)-C(1')-C(2')	-53.6(9)	C(4')-C(5')-C(8')-F(4')	-2(5)
C(1')#9-B(1)-C(1')-C(2')	-173.7(11)	C(6')-C(5')-C(8')-F(4')	171(4)
C(1')#10-B(1)-C(1')-C(2')	66.6(9)	C(4')-C(5')-C(8')-F(6')	118(4)
C(6')-C(1')-C(2')-C(3')	1(3)	C(6')-C(5')-C(8')-F(6')	-69(5)
B(1)-C(1')-C(2')-C(3')	-179.7(10)	F(2')-C(7')-F(1')-F(1'')	17.4(16)
C(1')-C(2')-C(3')-C(4')	0(2)	F(3'')-C(7')-F(1')-F(1'')	129.8(17)
C(1')-C(2')-C(3')-C(7')	178.7(12)	F(3')-C(7')-F(1')-F(1'')	135.0(16)
C(2')-C(3')-C(4')-C(5')	-4(3)	F(2'')-C(7')-F(1')-F(1'')	26.9(18)
C(7')-C(3')-C(4')-C(5')	178(3)	C(3')-C(7')-F(1')-F(1'')	-110.4(15)
C(3')-C(4')-C(5')-C(6')	6(6)	Cs(1)#11-C(7')-F(1')-F(1'')	86.5(14)
C(3')-C(4')-C(5')-C(8')	179(3)	F(1'')-C(7')-F(2')-F(2'')	174(2)

F(3")-C(7')-F(2')-F(2")	72(2)	F(3')-C(7')-F(1")-F(2')	105.2(12)
F(3')-C(7')-F(2')-F(2")	51(2)	F(1')-C(7')-F(1")-F(2')	163.0(16)
F(1')-C(7')-F(2')-F(2")	164.0(18)	F(2")-C(7')-F(1")-F(2')	2.7(9)
C(3')-C(7')-F(2')-F(2")	-75(2)	C(3')-C(7')-F(1")-F(2')	-114.3(10)
Cs(1)#11-C(7')-F(2')-F(2")	60.1(17)	Cs(1)#11-C(7')-F(1")-F(2')	58.8(6)
F(3")-C(7')-F(2')-F(1")	-102.2(11)	F(2")-F(2')-F(1")-F(1')	10(4)
F(3')-C(7')-F(2')-F(1")	-123.3(11)	C(7')-F(2')-F(1")-F(1')	19.7(18)
F(1')-C(7')-F(2')-F(1")	-9.9(9)	Cs(1)#11-F(2')-F(1")-F(1')	-61(2)
F(2")-C(7')-F(2')-F(1")	-174(2)	F(2")-F(2')-F(1")-C(7')	-10(3)
C(3')-C(7')-F(2')-F(1")	111.2(10)	Cs(1)#11-F(2')-F(1")-C(7')	-80.2(7)
Cs(1)#11-C(7')-F(2')-F(1")	-113.8(8)	F(1")-F(2')-F(2")-C(7')	8(3)
F(1")-C(7')-F(2')-Cs(1)#11	113.8(8)	Cs(1)#11-F(2')-F(2")-C(7')	97.7(8)
F(3")-C(7')-F(2')-Cs(1)#11	11.6(12)	C(7')-F(2')-F(2")-Cs(1)#11	97.7(8)
F(3')-C(7')-F(2')-Cs(1)#11	-9.5(9)	F(1")-F(2')-F(2")-Cs(1)#11	90(3)
F(1')-C(7')-F(2')-Cs(1)#11	103.9(7)	F(1")-C(7')-F(2")-F(2')	6(2)
F(2")-C(7')-F(2')-Cs(1)#11	-60.1(17)	F(3")-C(7')-F(2")-F(2')	116(2)
C(3')-C(7')-F(2')-Cs(1)#11	-134.9(6)	F(3')-C(7')-F(2")-F(2')	133.5(19)
F(2')-C(7')-F(3')-Cs(1)#11	11.9(11)	F(1')-C(7')-F(2")-F(2')	21(2)
F(1")-C(7')-F(3')-Cs(1)#11	-74.9(12)	C(3')-C(7')-F(2")-F(2')	115.8(18)
F(3")-C(7')-F(3')-Cs(1)#11	-89(4)	Cs(1)#11-C(7')-F(2")-F(2')	105.5(19)
F(1')-C(7')-F(3')-Cs(1)#11	-104.2(8)	F(2')-C(7')-F(2")-Cs(1)#11	105.5(19)
F(2")-C(7')-F(3')-Cs(1)#11	31.8(9)	F(1")-C(7')-F(2")-Cs(1)#11	99.5(8)
C(3')-C(7')-F(3')-Cs(1)#11	142.4(8)	F(3")-C(7')-F(2")-Cs(1)#11	10.7(14)
C(7')-F(1')-F(1")-F(2')	-15.6(14)	F(3')-C(7')-F(2")-Cs(1)#11	28.0(10)
F(2')-C(7')-F(1")-F(1')	-163.0(16)	F(1')-C(7')-F(2")-Cs(1)#11	84.5(11)
F(3")-C(7')-F(1")-F(1')	-52.9(18)	C(3')-C(7')-F(2")-Cs(1)#11	138.7(5)
F(3')-C(7')-F(1")-F(1')	-57.8(17)	F(2')-C(7')-F(3")-Cs(1)#11	13.9(15)
F(2")-C(7')-F(1")-F(1')	-160.3(14)	F(1")-C(7')-F(3")-Cs(1)#11	95.0(11)
C(3')-C(7')-F(1")-F(1')	82.7(15)	F(3')-C(7')-F(3")-Cs(1)#11	73(4)
Cs(1)#11-C(7')-F(1")-F(1')	-104.2(13)	F(1')-C(7')-F(3")-Cs(1)#11	121.7(11)
F(3")-C(7')-F(1")-F(2')	110.1(14)	F(2")-C(7')-F(3")-Cs(1)#11	11.5(14)

C(3')-C(7')-F(3")-Cs(1)#11	131.8(11)
F(5')-C(8')-F(6')-Cs(1)	129.6(15)
F(4')-C(8')-F(6')-Cs(1)	14.1(18)
C(5')-C(8')-F(6')-Cs(1)	109.0(15)
Cl(1S)#3-C(1S)-Cl(1S)-Cl(1S)#1	123.4(5)
Cl(1S)#2-C(1S)-Cl(1S)-Cl(1S)#	61.7(3)
Cl(1S)#1-C(1S)-Cl(1S)-Cl(1S)#3	123.4(5)
Cl(1S)#2-C(1S)-Cl(1S)-Cl(1S)#3	61.7(3)
Cl(1S)#1-C(1S)-Cl(1S)-Cs(1)	61.7(3)
Cl(1S)#3-C(1S)-Cl(1S)-Cs(1)	61.7(3)
Cl(1S)#2-C(1S)-Cl(1S)-Cs(1)	0.001(1)

Symmetry transformations used to generate equivalent atoms:

#1 -y+3/2,x+1,z #2 -x+1/2,-y+5/2,z #3 y-1,-x+3/2,z #4 x-1/2,-y+2,-z+1/2 #5 -x+1,y+1/2,-z+1/2 #6 y-1/2,x+1/2,-z+1/2 #7 -y+1,-x+2,-z+1/2 #8 -x+1/2,-y+3/2,z #9 -y+1,x+1/2,-z+1 #10 y-1/2,-x+1,-z+1 #11 -x+1,y-1/2,-z+1/2

4.7. References

1) Strauss, S. H. *Chem. Rev.* **1993**, *93*, 927–942.

2) Rosenthal, M. R. *J. Chem. Educ.* **1973**, *50*, 331–335.

3) Krossing, I.; Raabe, I. *Angew. Chem., Int. Ed.* **2004**, *43*, 2066–2090.

4) (a) Massey, A. G.; Park, A. J. *J. Organomet. Chem.* **1964**, *2*, 245–250. (b) Kobayashi, H.; Sonoda, T.; Iwamoto, H.; Yoshimura, M. *Chem. Lett.* **1981**, 579–580. (c) Nishida, H.; Takada, N.; Yoshimura, M.; Sonoda, T.; Kobayashi, H. *Bull. Chem. Soc. Jpn.* **1984**, *57*, 2600–2604. (d) Fujiki, K.; Kashiwagi, M.; Miyamoto, H.; Sonoda, A. *J. Fluorine Chem.* **1992**, *57*, 307–321. (e) Seppelt, K. *Angew. Chem., Int. Ed. Engl.* **1993**, *32*, 1025–1027. (f) Golden, J. H.; Mutolo, P. F.; Lobkovsky, E. B.; DiSalvo, F. J. *Inorg. Chem.* **1994**, *33*, 5374–5375. (g) Fujiki, K.; Ichikawa, J.; Kobayashi, H.; Sonoda, A.; Sonoda, T. *J. Fluorine Chem.* **2000**, *102*, 293–300. (h) Bernhardt, E.; Henkel, G.; Willner, H.; Pawelke, G.; Burger, H. *Chem. – Eur. J.* **2001**, *7*, 4696–4705.

5) (a) Kobayashi, H.; Sonoda, T.; Iwamoto, H. *Chem. Lett.* **1982**, 1185–1186. (b) Iwamoto, H.; Yoshimura, M.; Sonoda, T.; Kobayashi, H. *Bull. Chem. Soc. Jpn.* **1983**, *56*, 796–801. (c) Jordan, R. F. *Adv. Organomet. Chem.* **1991**, *32*, 325–387.

6) Buschmann, W. E.; Miller, J. S.; Bowman-James, K.; Miller, C. N. *Inorg. Synth.* **2002**, *33*, 83–91.

7) Cullinane, J.; Jolleys, A.; Mair, F. S. *Dalton Trans.* **2013**, *42*, 11971–11975.

8) Fujiki, K.; Ikeda, S.-Y.; Kobayashi, H.; Mori, A.; Nagira, A.; Nie, J.; Sonoda, T.; Yagupolskii, Y. *Chem. Lett.* **2000**, 62–63.

9) Aldridge, S.; Jones, C.; Gans-Eichler, T.; Stasch, A.; Kays, D. L.; Coombs, N. D.; Willock, D. J. *Angew. Chem., Int. Ed.* **2006**, *45*, 6118–6122.

10) Barriere, F.; Camire, N.; Geiger, W. E.; Mueller-Westerhoff, U. T.; Sanders, R. *J. Am. Chem. Soc.* **2002**, *124*, 7262–7263.

11) Kita, F.; Sakata, H.; Sinomoto, S.; Kawakami, A.; Kamizori, H.; Sonoda, T.; Nagashima, H.; Nie, J.; Pavlenko, N. V.; Yagupolskii, Y. L. *J. Power Sources* **2000**, *90*, 27–32.

12) Boesmann, A.; Francio, G.; Janssen, E.; Solinas, M.; Leitner, W.; Wasserscheid, P. *Angew. Chem., Int. Ed.* **2001**, *40*, 2697–2699.

13) Suzuki, H.; Naganawa, H.; Tachimori, S. *Phys. Chem. Chem. Phys.* **2003**, *5*, 726–733.

14) (a) Pfaltz, A.; Blankenstein, J.; Hilgraf, R.; Hormann, E.; McIntyre, S.; Menges, F.; Schonleber, M.; Smidt, S. P.; Wustenberg, B.; Zimmermann, N. *Adv. Synth. Catal.* **2003**, *345*, 33–44.(b) Cui, X.; Burgess, K. *Chem. Rev.* **2005**, *105*, 3272–3296.

15) (a) Mon, I.; Jose, D. A.; Vidal-Ferran, A. *Chem. –Eur. J.* **2013**, *19*, 2720–2725. (b) Vidal-Ferran, A.; Mon, I.; Bauza, A.; Frontera, A.; Rovira, L. *Chem. –Eur. J.* **2015**, *21*, 11417–11426. (c) Rovira, L.; Vaquero, M.; Vidal-Ferran, A. *J. Org. Chem.* **2015**, *80*, 10397–10403. (d) Fernández-Pérez, H.; Mon, I.; Frontera, A.; Vidal-Ferran, A. *Tetrahedron* **2015**, *71*, 4490–4494. (e) Rovira, L.; Fernández-Pérez, H.; Vidal-Ferran, A. *Organometallics* **2016**, *35*, 528–533.

16) (a) Li, Y.; Ma, B.; He, Y.; Zhang, F.; Fan, Q.-H. *Chem. Asian J.* **2010**, *5*, 2454–2458. (b) Song, F.-T.; Ouyang, G.-H.; Li, Y.; He, Y.-M.; Fan, Q.-H. *Eur. J. Org. Chem.* **2014**, *2014*, 6713–6719. (c) Zhang, X.-C.; Hu, Y.-H.; Chen, C.-F.; Fang, Q.; Yang, L.-Y.; Lu, Y.-B.; Xie, L.-J.; Wu, J.; Li, S.; Fang, W. *Chem. Sci.* **2016**, DOI:10.1039/c6sc00589f.

17) Yakelis, N. A.; Bergman, R. G. *Organometallics* **2005**, *24*, 3579–3581.

18) Brookhart, M.; Grant, B.; Volpe, A. F., Jr. *Organometallics* **1992**, *11*, 3920–3922.

19) Data collection with: *APEX II* versions v2009.1-02, Bruker AXS Inc., Madison, Wisconsin, USA, 2007.

20) Data reduction with: *SAINT* versions V7.60A, Bruker AXS Inc., Madison, Wisconsin, USA, 2003/2007.

21) *SADABS*, V2008/1, Bruker AXS Inc., Madison, Wisconsin, USA, 2003/2001, see: Blessing, R. H. *Acta Crystallogr., Sect. A: Found. Crystallogr.* **1995**, *A51*, 33–38.

22) SHELXT; Sheldrick, G.M. *Acta Cryst*. **2015** A71, 3–8.

23) SHELXle; C.B. Huebschle, G.M. Sheldrick & B. Dittrich; J.Appl.Cryst. (**2011**) 44, 1281–1284.

24) SHELXL; Sheldrick, G.M. *Acta Cryst*. **2015** A71, 3–8.

Chapter 5

Conclusions

Conclusions

- A set of new bisphosphite ligands with a distal regulation site for allylic substitutions and asymmetric hydroformylations have been synthesized. These ligands contain two differentiated structural features: a polyether backbone as the distal regulation site and a catalytic site incorporating two phosphite units derived from enantiomerically pure diols at the α and ω positions of the polyether group. The key step in the synthesis of the bisphosphite ligands is an *O*-phosphorylation reaction.

  As regards supramolecular ligands with a linear polyether chain, two new types of phosphite groups derived from enantiopure diols (*i.e.* 3,3'-di-*tert*-butyl-6,6'-dimethyl-[1,1'-biphenyl]-2,2'-diol and (2,2-dimethyl-1,3-dioxolane-4,5-diyl)bis(diphenylmethanol) or TADDOL) have been satisfactorily synthesized and employed as enantioselective catalysts.

  As regards new supramolecular ligands containing an stereogenic axis in the regulation site, enantiomerically pure [1,1'-binaphthalene]-2,2'-diol (or BINOL) was chosen as the molecular fragment, from which the regulation site of new supramolecular ligands had to be constructed. The BINOL's hydroxyl groups were alkylated with polyether chains containing one or two ethyleneoxy units. The syntheses of the supramolecular ligands were completed by *O*-phosphorylation with the chlorophosphite derived from 3,3'-di-*tert*-butyl-6,6'-dimethyl-[1,1'-biphenyl]-2,2'-diol. The new supramolecular bisphosphite ligands were satisfactorily synthesized and further employed in enantioselective transformations as catalysts.

- The catalytic activity of supramolecular ligands containing four ethyleneoxy units and phosphite groups derived from enantiopure [1,1'-binaphthalene]-2,2'-diol (or BINOL), 3,3'-di-*tert*-butyl-6,6'-dimethyl-[1,1'-biphenyl]-2,2'-diol and (2,2-dimethyl-1,3-dioxolane-4,5-diyl)bis(diphenylmethanol) (or TADDOL) in palladium-mediated asymmetric allylic substitutions was studied. It was demonstrated that the combinations of the above mentioned ligands with Pd(II) precursors suitable for this chemistry ($[Pd(\mu\text{-}Cl)(\eta^3\text{-}C_3H_5)]_2$ or $[PdCl_2(cod)]$) and an array of metal salts (for both generating the required nucleophile and triggering the regulation mechanism in the supramolecular ligands) behaved as supramolecularly regulated catalysts in allylic substitutions. All supramolecular ligands assayed were very active in the stated transformation, with the exception of the TADDOL-containing supramolecular ligands. A preference for the coordination of the TADDOL-derived phosphite groups to the palladium center in a *trans*-fashion could be responsible for the lower activity of the catalysts derived from this ligand with respect to the activity of those incorporating [1,1'-binaphthalene]-2,2'-diol-derived phosphite groups, which have

a preference for the coordination of the phosphite groups to the palladium center in a *cis*-fashion (as evidenced by single crystal X-Ray analysis).

The regio- and stereo-selectivity of the allylic substitutions mediated by palladium-complexes derived from the BINOL-containing supramolecular ligands could be regulated by using several alkali metal, alkaline earth metal, or lanthanide salts as regulation agents. The results in terms of enantioselectivity were moderate (up to 65% ee in the allylic alkylation of *rac*-(*E*)-1,3-diphenylallyl acetate with dimethylmalonate). Positive increments in the enantioselectivity were achieved in the allylic substitutions of *rac*-(*E*)-1,3-diphenylallyl acetate with benzylamine employing alkaline earth metal or lanthanide salts as regulation agents (up to 46% ee). An increment in the regioselectivity of the alkylation of cinammyl acetate with dimethylmalonate was observed when a regulation agent was used (b:l ratio of the substitution products up to 17:83 with LiOAc or CsOAc as the RA).

- Supramolecular ligands with an (*R*)- or (*S*)-configured [1,1'-binaphthalene]-2,2'-diol (or BINOL) fragment and two polyether chains containing one or two ethyleneoxy units in the regulation site, and phosphite groups derived from enantiopure 3,3'-di-*tert*-butyl-6,6'-dimethyl-[1,1'-biphenyl]-2,2'-diol in the catalytic site, have been tested in Rh-mediated asymmetric hydroformylations. Challenging heterocyclic olefins were efficiently hydroformylated in terms of regio- and enantio-selectivity by rhodium complexes derived from the aforementioned supramolecular ligands. The supramolecular ligand with an (*R*)-configured BINOL fragment, four ethyleneoxy units and (*S*)-configured phosphite groups (matched combination of stereogenic elements in the supramolecular ligand) provided higher enantioselectivities in the hydroformylation of cyclic alkenes than those obtained with the supramolecular ligand containing the (*S*)-configured BINOL fragment in the regulation site (mismatched combination of stereogenic elements in the ligand). It has been demonstrated that the addition of catalytic amounts of RAs (alkali metal BArF salts) regulated the activity of the catalyst.

  A combination of the highest performing supramolecular ligand (that with an (*R*)-configured BINOL fragment and four ethyleneoxy units in the regulation site, and (*S*)-configured phosphite groups in the catalytic site), [Rh(κ^2O,O´-acac)$(CO)_2$] as the metal precursor and KBArF as the regulation agent mediated the asymmetric hydroformylation of *cis*-4,7-dihydro-1,3-dioxepine with perfect chemoselectivity and very high enantioselectivity (93% ee), which, to the best of our knowledge, is the highest reported enantioselectivity for this substrate. The outcome of the asymmetric hydroformylations of 2,3-dihydrofuran or 2,5-dihydrofuran mediated by the highest performing supramolecular ligand could be exquisitely regulated by choosing the appropriate reactions conditions and RA (*i.e.* KBArF for these substrates), with an increase in the ee, reversal of the regioselectivity or the complete suppression of C=C isomerization processes.

- A reduction in the number of ethyleneoxy units from four to two in the regulation site of ligands containing an (*R*)- or (*S*)-configured [1,1'-binaphthalene]-2,2'-diol (or BINOL) turned out to be detrimental for the catalytic activity and regulation ability of these supramolecular ligands in asymmetric hydroformylations.

- The structure of catalytically relevant species derived from the supramolecular ligands in asymmetric hydroformylations (*i.e.* [Rh(H)$(CO)_2(\kappa^2$P,P′–RA•**L**)]; where **L** indicates the supramolecular ligand) has been investigated by state-of-the-art spectroscopic techniques. In the case of the supramolecular ligands with four ethyleneoxy units in the regulation site and 3,3'-bis(trimethylsilyl)- or di-*tert*-butyl-[1,1'-biaryl]-2,2'-diol-derived phosphite groups, the *P*-ligating groups are coordinated in an equatorial–equatorial fashion to the trigonal–bipyramidal rhodium center of the [Rh(H)$(CO)_2(\kappa^2$P,P′–RA•**L**)] complexes. In the case of the supramolecular ligand with the (*R*)-configured [1,1'-binaphthalene]-2,2'-diol fragment, four ethyleneoxy units in the regulation site and 3,3'-di-*tert*-butyl-[1,1'-biphenyl]-2,2'-diol-derived phosphite groups, catalytically active [Rh(H)$(CO)_2(\kappa^2$P,P′–RA•**L**)] complexes undergo an equilibrium between four stereoisomeric hydrido-dicarbonyl derivatives with the two *P*-ligating groups coordinated in equatorial–equatorial or apical–equatorial fashion.

  Both the coordination geometry of the phosphite groups to the rhodium center (*i.e.* an apical–equatorial or equatorial–equatorial fashion) and the nature of the substituents at the 3 and 3' positions of the [1,1'-biaryl]-2,2'-diol-derived phosphite groups (*i.e.* trimethylsilyl or *tert*-butyl substituents) affect the enantioselectivity of the AHF reaction of cyclic and linear alkenes.

- The solid state structure of the alkali metal BArF salts (BArF anion = $[B(3,5\text{-}(CF_3)_2C_6H_3)_4]^-$) have been determined by single crystal X-ray diffraction analysis. The X-ray analysis of these compounds provided a framework of the spatial distribution and the distances and geometries of these salts. All the compounds crystallized as water solvates with the exception of the CsBArF salt which crystallized as a dichloromethane solvate. In all cases the BArF anion maintains a *S*4 symmetry in the solid state. The lithium and the sodium structures are isostructural and both correspond to a disordered mixture of two salt geometries (trigonal bipyramidal and octahedral metal geometries). Also the potassium and the rubidium structures are isostructural with the metal coordinated to nine surrounding atoms (eight fluorine and one oxygen atoms). The cesium salt, which differs in the solvent contained and also in the space group, shows also a similar arrangement in the crystal packing as the potassium and rubidium salts. Due to the larger size of the cesium cation, this atom is coordinated to fourteen surrounding atoms (twelve fluorine and two chlorine atoms). The distances between the metal and boron atoms show an increasing tendency with the size of the cation, nevertheless the distances in the largest cations (*i.e.* K, Rb,

Cs) are very similar. The observed distances clearly demonstrate that the boron atom is in all cases isolated from the alkali metal cation.

Resum

A la present tesi s´ha estudiat el disseny i la síntesi de lligands supramoleculars enantiopurs de tipus bisfosfit, juntament amb les propietats de coordinació d'aquests lligands amb precursors de rodi i pal·ladi. Els complexes de rodi i pal·ladi derivats d'aquests lligands supramoleculars s'han aplicat com catalitzadors a hidroformilacions i substitucions al·líliques asimètriques.

El disseny i desenvolupament de noves estratègies per a obtenir lligands supramoleculars és un tema important degut a l'àmplia aplicació d'aquests lligands en catàlisi enantioselectiva. Els lligands dissenyats a la present tesi contenen una cadena polioxietilènica, que és la responsable de la regulació a través d'interaccions supramoleculars amb els agents de regulació, i a més contenen dos grups fosfit derivats de diols enantiomèricament purs que es coordinen amb el centre metàl·lic i constitueixen el centre catalític (vegi's la Figura 1). L'activitat catalítica d'aquests lligands està controlada per un agent de regulació que interacciona amb la cadena polioxietilènica a través d'interaccions supramoleculars (per exemple ió-dipol). Aquestes interaccions apropen els dos fòsfors terminals, faciliten la coordinació de forma bidentada d´aquests grups fosforats al centre metàl·lic i constitueixen el centre catalític. La unió de l'agent de regulació indueix un canvi a la geometria del centre actiu modificant l´activitat catalítica.

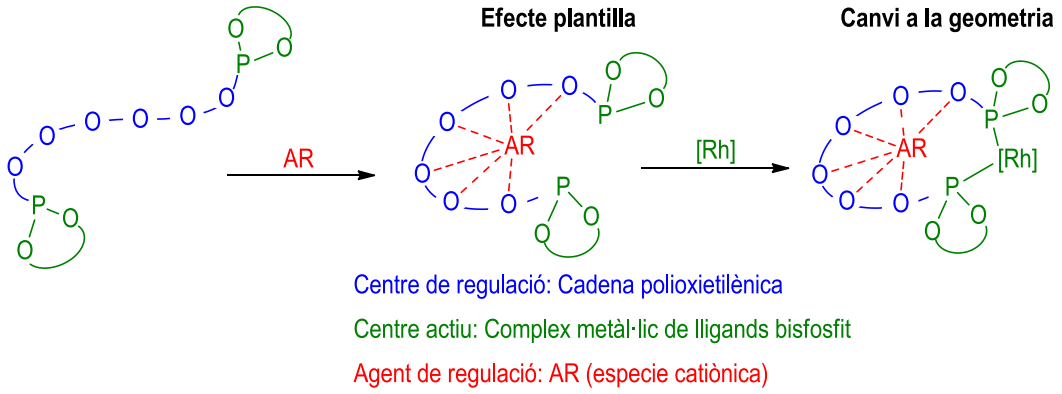

Figura 1. Estratègia supramolecular per als lligand bisfosfit amb un centre de regulació

El pas clau a la síntesi dels lligands bisfosfit correspon a una reacció d´*O*-fosforilació dels grups hidroxils terminals de la cadena polioxietilènica amb derivats electròfils de fòsfor de tipus clorofosfit en presència de quantitats estequiomètriques d'una base auxiliar. Mitjançant aquesta estratègia sintètica es va preparar la família de lligands enantiopurs amb un centre de regulació distal emprats a la present Tesi Doctoral (vegi's la Figura 2).

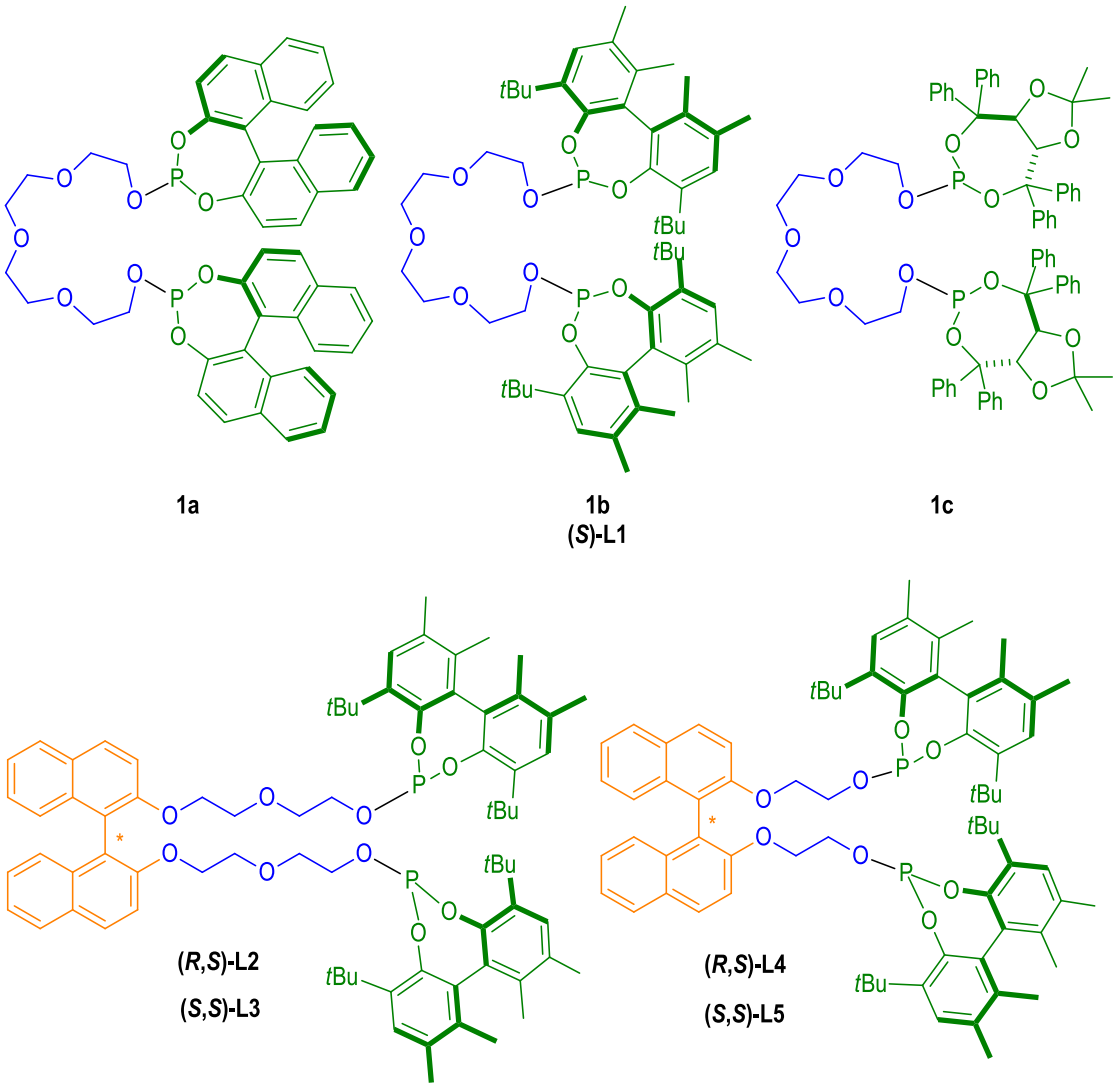

Figura 2. Família de lligands supramoleculars enantiopurs emprats a la present Tesi Doctoral

S´ha estudiat l´activitat catalítica dels lligands supramoleculars de tipus bisfosfit, **1a**–**c**, a reaccions d´alquilació al·lílica asimètrica. Es va demostrar que combinacions dels lligands esmentats anteriorment amb precursors de Pd(II) adequats per a aquesta química ($[Pd(\mu\text{-}Cl)(\eta^3\text{-}C_3H_5)]_2$ o $[PdCl_2(cod)]$) i una sèrie de sals metàl·liques (per a la generació del nucleòfil i alhora activar el mecanisme de regulació als lligands supramoleculars) es comporten com a catalitzadors supramoleculars a substitucions al·líliques asimètriques.

Tots els lligands supramoleculars estudiats per aquesta transformació resultaren ser molt actius en termes de conversió, amb l'excepció del lligand **1c** (que conté grups fosfit derivats del TADDOL). La preferència per una geometria de coordinació de tipus *trans* per part del lligand **1c** al centre de pal·ladi podria ser la responsable de la inferior reactivitat obtinguda a les reaccions de substitució al·lílica del complex derivat del lligand **1c** respecte el complex de pal·ladi derivat del lligand **1a**, que presenta una geometria de

coordinació dels grups fosfit de tipus *cis*, tal i com va evidenciar l'anàlisi de raigs-X de les estructures cristal·lines d'ambdós complexes.

La regio- i estèreo-selectivitat de les substitucions al·líliques mitjançant els complexes de pal·ladi derivats dels bisfosfits **1** va poder ser modulada utilitzant sals de metalls alcalins, alcalinoterris o lantànids com agents de regulació. Els primers estudis catalítics identificaren el lligand **1a** i $[PdCl_2(cod)]$, com el lligand i precursor de pal·ladi òptim per a les reaccions de substitució al·lílica amb l'acetat de *rac*-(*E*)-1,3-difenilal·lil (**2**) com substrat. De totes les possibilitats estudiades, la combinació de RbOAc amb el lligand **1a** i $[PdCl_2(cod)]$ com a precursor metàl·lic és la que va donar conversió completa amb un excés enantiomèric del 65%, implicant un augment del 6% a l'enantioselectivitat respecte a quan no es va emprar cap agent de regulació. Amb l´ús de benzilamina (BZA) com a nucleòfil i sals de metalls alcalinoterris o lantànids com agent de regulació es va observar un augment del 16% a l´excés enantiomèric. La reacció de substitució al·lílica de l'acetat de cinamil (**5**) amb malonat de dimetil (DMM) com a nucleòfil, també va ser regulada supramolecularment amb el lligand **1b** i $[Pd(\mu\text{-}Cl)(\eta^3\text{-}C_3H_5)]_2$ obtenint un excés enantiomèric d'un 60%, sense agent de regulació i augmentant la relació b:l en emprar $Mg(OTf)_2$ com agent de regulació.

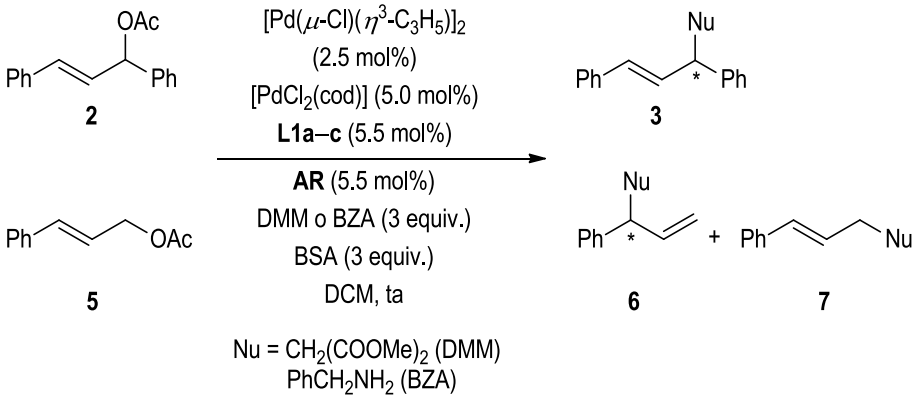

Figura 3. Alquilacions al·líliques asimètriques estudiades.

Els complexes de rodi derivats dels lligands bisfosfit (*S*)-**L1**, (*R*,*S*)-**L2,** (S,*S*)-**L3**, (*R*,*S*)-**L4** i (*S*,*S*)-**L5** van ser aplicats a la hidroformilació asimètrica de diferents olefines heterocícliques (**4**, **7** i **8**). Es va observar que aquests lligands són molt actius en aquest tipus de transformació, i que amb l'ús d'un agent de regulació adequat es pot modular satisfactòriament tant la regio- com la enantio-selectivitat.

En el cas del derivat 1,3-dioxepínic (**8**), es va observar un augment important en la conversió de fins un 76% quan s'utilitzava (*R*,*S*)-**L2** com a lligand i KBArF com agent de regulació. L'augment en el excés enantiomèric també va ser considerable, fins a un 73%, en presència de KBArF com agent de regulació. Aquests resultats suposen les condicions de hidroformilació de **8** que condueixen als excessos enantiomèrics més elevats que s'han descrit a la bibliografia fins l´actualitat. Amb aquesta estratègia

supramolecular, i adaptant les condicions de reacció per als substrats 2,5-dihidrofurà (**4**) i 2,3-dihidrofurà (**7**), es poden ajustar també els productes de la reacció, així com suprimir la formació d'un subproducte de la reacció de hidroformilació (producte d'isomerització de l'enllaç C=C (**7**)).

El sistema catalític format per els lligands (*S*)-**L1**, (*R*,*S*)-**L2** i (S,*S*)-**L3** i l'agent de regulació apropiat contribueix a un augment de l'excés enantiomèric de fins un 71% a la hidroformilació de 2,5-dihidrofurà (**4**).

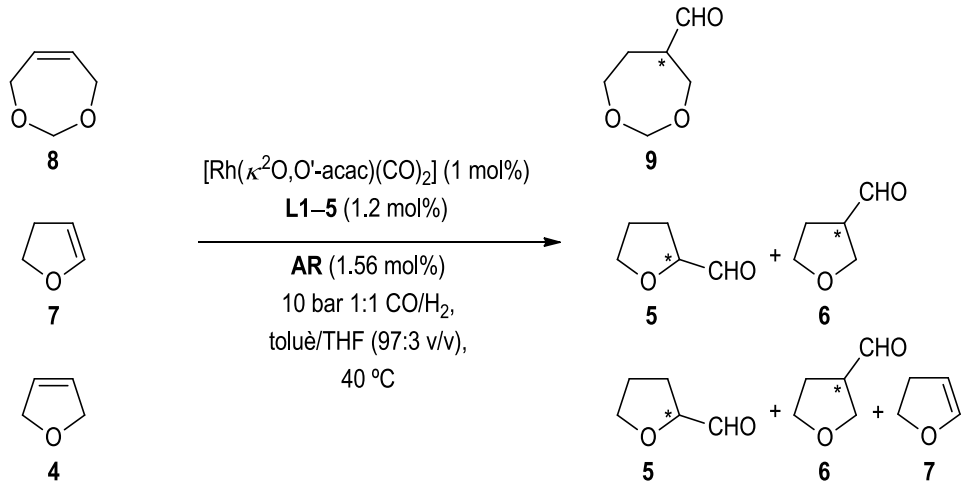

Figure 4. Hidroformilacions asimètriques estudiades.

Els estudis de complexació amb els lligands (*S*)-**L1**, (*R*)-**L6** i (*R*,*S*)-**L2**, [Rh(κ^2O,O'–acac)$(CO)_2$] com a precursor de Rh(I) a reaccions de hidroformilació, KBArF i RbBArF com agents de regulació, evidenciaren l'estructura de les especies catalítiques, mostrant diferències entre els quelats d'aquests lligands. En el cas dels lligands (*S*)-**L1**, (*R*)-**L6**, la geometria de coordinació dels dos fòsfors al centre de rodi amb geometria bipiràmide trigonal és de tipus equatorial–equatorial. D'altra banda, al quelat [Rh(H)$(CO)_2$(κ^2P,P'–KBArF•(*R*,*S*)-**L2**)], el sistema experimenta un equilibri entre quatre complexes de rodi amb els dos fòsfors coordinats de manera equatorial–equatorial o equatorial–apical al centre de rodi tipus bipiràmide trigonal.

S'ha observat que tant la geometria de coordinació dels grups fosfit al centre de rodi (tipus apical–equatorial o equatorial–equatorial), com la naturalesa dels substituents en la posició 3 i 3' del fragment [1,1-biaril]-2,2´-diol dels grups fosfit (substituents trimetilsilil- o *tert*-butil-) són factors que afecten a l'enantioselectivitat de la reacció de AHF d'alquens cíclics i lineals.

Les estructures en estat sòlid de les sals alcalines de BArF (anió BArF = $[B(3,5\text{-}(CF_3)_2C_6H_3)_4]^-$) es van estudiar mitjançant difracció de raigs-X. Aquesta tècnica espectroscòpica va proporcionar la distribució espacial dels àtoms, així com les distàncies i geometries de les espècies estudiades. Totes les estructures cristal·litzaren en forma de solvats d´aigua a excepció de la sal de CsBArF que va cristal·litzar com a solvat de diclorometà. En tots els casos l'anió de BArF manté una simetria *S*4 a l'estat sòlid. Les estructures dels cations més petits, com són el liti i sodi, són isoestructurals i totes dues tenen una barreja desordenada de dues geometries: la bipiràmide trigonal i l´octaèdrica. També són isoestructurals les estructures de les sals de potassi i rubidi, estant el metall coordinat a nou àtoms veïns (vuit àtoms de fluor i un àtom d´oxigen). L´estructura del CsBArF, que és diferent de les altres tant en el dissolvent contingut com en el grup espacial, mostra una disposició similar a la del potassi i rubidi. Degut a què el cesi és un àtom més voluminós, en aquest cas el catió està coordinat a catorze àtoms veïns (dotze àtoms de fluor i dos àtoms de clor). Les distàncies entre el metall i el centre de bor mostren una tendència creixent amb la grandària del catió, encara que les distàncies als cations més voluminosos (*i.e.* K^+, Rb^+ i Cs^+) són molt similars. Les distàncies observades mostren clarament que l´àtom de bor està en tots els casos aïllat dels àtoms corresponents als metalls alcalins.

Summary

The design and synthesis of enantiopure supramolecular bisphosphite ligands, together with their coordination properties with rhodium and palladium precursors, have been studied. Rhodium and palladium complexes derived from these supramolecular ligands have been applied as catalysts in asymmetric hydroformylations and allylic substitutions. The designed ligands contain a polyoxyethylene motif, which is the responsible for regulation through supramolecular interactions with the regulation agents, and two phosphite groups derived from enantiomerically pure diol derivatives that bind the metal center and constitute the catalytic site. The supramolecular strategy that has been followed within the present Doctoral Thesis relies on the interaction between a number of regulation agents (alkali metal, alkaline earth metal or lanthanide salts) and the polyoxyethylene motif of the ligand, which serves for the fine modification of the geometry and flexibility of the catalytic center (adaptive effect of the asymmetric catalyst). This supramolecular regulation strategy has led to high enantioselectivities in hydroformylation reactions of heterocyclic olefins and has allowed the regulation of the regioselectivity in the hydroformylation of several cyclic olefins. Furthermore, the formation of byproducts associated with the hydroformylation process has also been suppressed with the use of the above mentioned regulation agents. Supramolecularly regulated bisphosphite ligands have also been applied to asymmetric allylic substitution reactions. Noteworthy regulation effects have been achieved in this transformation, though the enantioselectivies in the allylic substitutions remained moderate.

Resum

S´ha estudiat el disseny i la síntesi de lligands supramoleculars enantiopurs de tipus bisfosfit, juntament amb les propietats de coordinació d'aquests lligands amb precursors de rodi i pal·ladi. Els complexes de rodi i pal·ladi derivats d'aquests lligands supramoleculars s'han aplicat com catalitzadors en hidroformilacions i substitucions al·líliques asimètriques. Els lligands dissenyats contenen una cadena polioxietilènica, que és la responsable de la regulació a través d'interaccions supramoleculars amb els agents de regulació, i a més contenen dos grups fosfit derivats de diols enantiomèricament purs que es coordinen amb el centre metàl·lic i constitueixen el centre catalític. L'estratègia supramolecular que s'ha emprat en la present Tesi Doctoral es basa en la interacció entre diversos agents de regulació (sals de metalls alcalins, alcalinoterris o lantànids) amb la cadena polioxietilènica del lligand, que serveix per a modificar la geometria i flexibilitat del centre catalític (efecte adaptatiu del catalitzador asimètric). L'ús d'aquesta estratègia de regulació supramolecular ha permès obtenir enantioselectivitats elevades en reaccions d´hidroformilació d'olefines heterocícliques. A més a més, s'ha pogut regular per alguns alquens heterocíclics la regioselectivitat de la reacció i s'ha pogut eliminar la formació de productes secundaris associats amb la reacció d'hidroformilació. Lligands supramoleculars regulables de tipus bisfosfit s'han aplicat també en substitucions al·líliques asimètriques. Els efectes de regulació que s'han obtingut en aquesta transformació han estat notables, tot i què les enantioselectivitats obtingudes han estat moderades.

Resumen

Se ha estudiado el diseño y la síntesis de ligandos supramoleculares enantiopuros de tipo bisfosfito, juntamente con las propiedades de coordinación de estos ligandos con precursores de rodio y paladio. Los complejos de rodio y paladio derivados de estos ligandos supramoleculares se han aplicado como catalizadores en hidroformilaciones y substituciones alílicas asimétricas. Los ligandos diseñados contienen una cadena polioxietilénica, que es la responsable de la regulación a través de interacciones supramoleculares con los agentes de regulación, y que además contienen dos grupos fosfito derivados de dioles enantioméricamente puros que se coordinan al centro metálico y constituyen el centro catalítico. La estrategia supramolecular que se ha empleado en la presente Tesis Doctoral se basa en la interacción entre agentes de regulación diversos (sales de metales alcalinos, alcalinotérreos o lantánidos) con la cadena polioxietilénica del ligando, que sirve para modificar la geometría y flexibilidad del centro catalítico (efecto adaptativo del catalizador asimétrico). El uso de esta estrategia de regulación supramolecular ha permitido obtener enantioselectividades elevadas en reacciones de hidroformilación de olefinas heterocíclicas. Además, se ha podido regular para algunos alquenos heterocíclicos la regioselectividad de la reacción y se ha podido eliminar la formación de productos de isomerización asociados con la reacción de hidroformilación. Ligandos supramoleculares de tipo bisfosfito se han aplicado también en sustituciones alílicas asimétricas. Los efectos de regulación que se han obtenido en esta transformación han sido notables, aunque las enantioselectividades obtenidas han sido moderadas.